Ionophore and Biometal Modulation of P-glycoprotein at the Blood-Brain Barrier

A thesis submitted for the degree of

Doctor of Philosophy

From the Monash Institute of Pharmaceutical Sciences

At Monash University

Mitchell Paul McInerney

Bachelor of Pharmaceutical Sciences (Honours)

2018

Drug Delivery, Disposition and Dynamics

Monash Institute of Pharmaceutical Sciences

Monash University

Melbourne, Victoria, Australia

Copyright notice

TABLE OF CONTENTS

Declaration

This thesis contains no material which has been accepted for the award of any other degree or diploma at any university or equivalent institution and that, to the best of my knowledge and belief, this thesis contains no material previously published or written by another person, except where due reference is made in the text of the thesis.

Signature: 

Print Name: Mitchell Paul McInerney

Date: 28.03.2018

Thesis-related publications:

1. MCINERNEY, M.P., SHORT, J.L. & NICOLAZZO, J.A. 2017. Neurovascular alterations in Alzheimer's disease: Transporter expression profiles and CNS drug access. *The AAPS Journal*, 19(4), 940-95

2. MCINERNEY, M.P., PAN, Y., SHORT, J.L. & NICOLAZZO, J.A. 2017. Development and validation of an in-cell western for quantifying P-glycoprotein expression in human brain endothelial (hCMEC/D3) cells. *The Journal of Pharmaceutical Sciences*, 106(9), 2614-24

3. MCINERNEY, M.P., VOLITAKIS, I., BUSH, A.I., BANKS, W.A., SHORT, J.L., & NICOLAZZO, J.A. 2018. Ionophore and biometal modulation of P-glycoprotein expression and function in human brain microvascular endothelial cells. Pharmaceutical Research, 35(4), 83.

Publications unrelated to the thesis:

1. MCINERNEY, M.P., ROBERTS, K.D., THOMPSON, P.E., LI, J., NATION, R.L., VELKOV, T. & NICOLAZZO, J.A. 2016. Quantitation of polymyxin-lipopolysaccharide interactions using an image-based fluorescent probe. *The Journal of Pharmaceutical Sciences*, 105(2),1006-10

Communications:

1. MCINERNEY, M.P., JIN, L., ROBERTS, K.D., VELKOV, T., NATION, R.L., LI, J., & NICOLAZZO, J.A. 2014. Preventing the blood-brain barrier disruptive effect of lipopolysaccharide with polymyxin analogues. *5th Federation International Pharmacy Pharmaceutical Sciences World Congress,* Melbourne, Australia.

2. MCINERNEY, M.P., SHORT, J.L. & NICOLAZZO, J.A. 2016. Clioquinol-metal ion complexes enhance P-glycoprotein expression and function at the blood-brain barrier. *Gordon Research Seminar on Barriers of the CNS, New London, New Hampshire, USA.*

3. MCINERNEY, M.P., SHORT, J.L. & NICOLAZZO, J.A. 2016. Clioquinol-metal ion complexes enhance P-glycoprotein expression and function at the blood-brain barrier. *Gordon Research Conference on Barriers of the CNS, New London, New Hampshire, USA.*

4. MCINERNEY, M.P., SHORT, J.L. & NICOLAZZO, J.A. 2017. Clioquinol modulates biometal distribution and blood-brain barrier expression of P-glycoprotein. *Cerebral Vascular Biology, Melbourne, Australia.*

Thesis including published works declaration

I hereby declare that this thesis contains no material which has been accepted for the award of any other degree or diploma at any university or equivalent institution and that, to the best of my knowledge and belief, this thesis contains no material previously published or written by another person, except where due reference is made in the text of the thesis.

This thesis includes three original papers published in peer reviewed journals and one submitted publication. The core theme of the thesis is pharmacology. The ideas, development and writing up of all the papers in the thesis were the principal responsibility of myself, the student, working within the Department of Drug Delivery, Disposition and Dynamics, under the supervision of Dr Joseph Nicolazzo and Dr Jennifer Short.

The inclusion of co-authors reflects the fact that the work came from active collaboration between researchers and acknowledges input into team-based research.

In the case of chapters two to five, my contribution to the work involved the following:

Thesis Chapt.	Publication Title	Status	Nature and % of student contribution	Co-author name(s) Nature and % of Co-author's contribution*	Student Y/N*
1	Neurovascular alterations in Alzheimer's disease: Transporter expression profiles and CNS drug access.	Published	90%. Conducted the systematic review, wrote the manuscript and critically appraised literature	1) 7% - Joseph Nicolazzo 2) 3% - Jennifer Short Critical appraisal and manuscript preparation	No No
2	Development and validation of an in-cell western for quantifying P-glycoprotein expression in human brain endothelial (hCMEC/D3) cells	Published	85%. Asserted initiative, experimental planning, technique development and validation, data processing and analysis and manuscript preparation.	1) 9% - Joseph Nicolazzo 2) 5% - Jennifer Short 3) 1% - Yijun Pan Technique development and manuscript preparation	No No Yes
3	Ionophore and biometal modulation of P-glycoprotein expression and function in human brain microvascular endothelial cells	Published	82%. Experimental planning, technique development and validation, data processing and analysis and manuscript preparation.	1) 3% - Irene Volitakis 2) 2% Ashley Bush Data acquisition 3) 2% Yijun Pan Technical assistance 4) 3% Jennifer Short 5) 1% William Banks 6) 7% Joseph Nicolazzo Technique development and manuscript preparation	No No Yes No No No

4	Effects of clioquinol on biometal distribution and P-glycoprotein expression at the brain endothelium and other peripheral tissues in mice	Soon to be submitted	82%. Experimental planning, technique development and validation, data processing and analysis and manuscript preparation.	1) 3% - Irene Volitakis 2) 2% Ashley Bush Data acquisition 3) 2% Yijun Pan Technical assistance 4) 3% Jennifer Short 5) 7% Joseph Nicolazzo Technique development and manuscript preparation	No No Yes No No

I have renumbered and modified sections of submitted or published papers in order to generate a consistent presentation within the thesis. The publications in their original form can be found in the appendix of this thesis.

Student signature: [redacted] **Date:** 28.03.2018

The undersigned hereby certify that the above declaration correctly reflects the nature and extent of the student's and co-authors' contributions to this work. In instances where I am not the responsible author I have consulted with the responsible author to agree on the respective contributions of the authors.

Main Supervisor signature: [redacted] **Date:** 23.03.2018

ACKNOWLEDGEMENTS

Completing this doctoral thesis has been the most challenging accomplishment of my life. Needless to say, it would never have been achieved without the support of the many others around me.

First and foremost, I must thank my supervisors Joseph Nicolazzo and Jennifer Short. Thank you both for constantly guiding my growth as a scientist, and for transforming me from a naïve undergraduate student into a matured scientific thinker. This must at times be painstaking work, especially since I am sometimes so disagreeable in nature. But now as I cross the finish line, I can see clearly the all the wisdom that you have both imparted upon me. You have been my academic parents, and sometimes it really does feel like a funny little family. A family which I have been very happy to be a part of. I hope that you both feel the same way and that perhaps you have both acquired some Mitchisms in the process. Thank-you both so much for your tremendous support, your contribution cannot be overstated.

I am also indebted to all the other Nicolazzo lab members whom I have had the pleasure of working with over the years. Many of you have offered me amazing technical expertise as well as incredible friendship and support throughout my whole time at Monash. Stephanie, Chris, Liang, Yijun, Danielle, Elonie and Angelo – thank you all so much for your time and for your laughter. The laughter in particular really does make it all easier to bare.

I would also like to give a big thanks Professor Ashley Bush and also to Irene Volitakis. The insight and collaboration that you provided throughout our project was totally invaluable. Your contribution is greatly appreciated, and I definitely arrived at a better destination due to your generous support.

A very special thanks must also go to Katherine. When it felt like it was all falling apart, you really helped me to get things across the line. We must have had hundreds of fantastic lunchtime conversations together, and you brightened my day each and every time. Your generous and unwavering care throughout this period have been just enormously important to me. I truly appreciate you for this. Thank you so much.

To Laure my dearest, you carried me for so far along the way. For so long you gave me the words that I needed to hear, straightened out my soul, and made me into the best possible version of myself that I could be. I am endlessly grateful for the sacrifice and support that you gave me over all of these years. Your contribution to who I have become is undeniable, and I'll never forget to acknowledge you for this.

And finally, the most special thanks goes to both of my parents, Linda and Paul McInerney. I must thank you both for the wonderful childhood and life that you managed to so gracefully provide for me. I must thank you the most, because the journey required to get to this point started a long, long time ago. It began with my inquisitive nature as a child, and was driven by the incessant desire to understand the way the world works. And there was always one person who had the time and the care to help me answer all of the questions that I had. To my father; if I can think well, it is because of you. If I can see far, it is because of you. If I make you proud, it is because of *you*. Thank-you so much for all of the intellectual nurturing that you've given me over all those years, it has definitely been worth it for me, and now hopefully, I hope that it has been worth it for you too.

The research carried out for and presented in this thesis was supported by an Australian Government Research Training Program (RTP) Scholarship.

THESIS ABSTRACT

The blood-brain barrier (BBB) is a dynamic interface which separates the brain from the systemic circulation, where the expression of transporters such as P-glycoprotein (P-gp) greatly restricts CNS exposure to xenobiotics, drugs and endogenous toxic substrates. Previously it has been shown that administration of zinc and/or copper ions can protect BBB integrity and function in both in vitro and animal models, but whether the delivery of biometals to brain endothelial cells can explicitly modify the expression or function of efflux transporters such as P-gp has not yet been examined. Clioquinol (CQ) is an ionophore compound which has been shown to traffic both zinc and copper ions across cell membranes, where these biometals can then serve as biochemical input to many cellular processes. Thus, the data produced in this thesis are centred on the hypothesis that CQ is able to deliver enhanced quantities of biometals zinc and copper into brain microvascular endothelial cells, and subsequently modify P-gp expression and function, in both in vitro and in vivo settings.

To quantify the impact of the CQ intervention on P-gp expression, two methods were developed to quantify P-gp expression in human cerebral microvascular endothelial cells (hCMEC/D3). Initially, western blotting (WB) was interrogated for P-gp quantification whereby multiple parameters were explored and optimised. Additionally, a higher-throughput in-cell western (ICW) method designed specifically for P-gp in hCMEC/D3 cells was developed and validated by correlation with other techniques such as WB and a rhodamine 123 (R123) P-gp function assay, following P-gp regulating treatments.

The limits of toxicity of the chemical agents CQ, Zn^{2+} and Cu^{2+} in hCMEC/D3 cells were then assessed individually and then in combination, via the 3-(4,5-dimethylthiazol-2-yl)-2,5-diphenyltetrazolium bromide (MTT) assay, alongside morphological assessment by microscopy. The highest concentrations tolerated by the hCMEC/D3 cells over a 24 h treatment

period of CQ, Zn^{2+} and Cu^{2+} (0.5, 0.5 and 0.1 μM respectively), were then applied via an 8-way treatment regime featuring all combinations of CQ, Zn^{2+} and Cu^{2+}, before probing the relative P-gp expression using the previously developed ICW method. Only the combination of all three components induced a significant 1.7 ± 0.3-fold (mean ± SD) upregulation in P-gp. Both WB and the R123 function assay were used to confirm this increase and concurrence was observed with a 1.8 ± 0.4-fold increase in P-gp expression (WB) and a 23 ± 5% decrease in R123 accumulation after a 1 h incubation.

To detect any altered cytosolic biometal concentrations resulting from treatment with CQ, Zn^{2+} and Cu^{2+}, hCMEC/D3 cells received the same 8-way treatment regime of CQ, Zn^{2+} and Cu^{2+} as above, before cell lysates were assessed by inductively coupled plasma mass spectrometry (ICP-MS). While zinc concentrations were found unaltered, copper concentrations were significantly affected by multiple treatment groups. hCMEC/D3 cells, when treated with 0.1 μM Cu^{2+} alone or the P-gp upregulating triple combination, raised cytosolic copper concentrations from 0.6 ± 0.2 nmol/mg of protein to 1.6 ± 0.6 nmol/mg and 3.2 ± 1 nmol/mg, respectively. A temporal investigation by ICP-MS revealed that cytosolic CQ-mediated copper levels were not higher than by treating with Cu^{2+} alone, until the 24 h time point.

To assess whether CQ treatment could affect BBB expression of P-gp in vivo, Swiss outbred mice were administered CQ by oral gavage in a suspension solution (30 mg/kg) for 11 days. Centrifugation techniques obtained microvessel enriched fractions (MEF) from the cortex of control and CQ treated mice and other tissues were also isolated (plasma, small intestine, kidney, liver and subcortical brain) for metallomic, and where appropriate, P-gp expression analysis. No changes in either copper or zinc levels, nor in the expression of P-gp were observed in the MEF of CQ-treated mice. ICP-MS revealed however, that CQ is able to alter

the distribution of sodium (25% increase in the small intestine and an 8% increase in plasma), magnesium (12% decrease in MEF), phosphorous (12% increase in the liver), potassium (10% increase In the liver), calcium (6% increase in plasma) and manganese (23% decrease in the kidney). While CQ effectively redistributed ions around the body, none of these changes were associated with altered P-gp expression in these compartments.

In order to probe for any differences in the effect of CQ/biometals in hCMEC/D3 cells in vitro versus in mice in vivo, primary mouse brain endothelial cells were isolated from Swiss outbred mice, and in separate experiments treated with a positive control rifampicin, and also with CQ, Zn^{2+} and Cu^{2+} (0.5, 0.5 and 0.1 μM), as well as CQ and Cu^{2+} (0.1 and 0.1 μM), all for 24 h, before P-gp expression was assessed via the ICW protocol. Whilst rifampicin induced a significant 1.2 ± 0.06-fold upregulation, preliminary studies suggested that the same treatment that induced a 1.7-fold upregulation in P-gp in hCMEC/D3 cells (i.e. CQ, Zn^{2+} and Cu^{2+} at 0.5, 0.5 and 0.1 μM for 24 h), showed a trend of reducing P-gp expression by 33 ± 2%, and the CQ/Cu^{2+} treatment was not effective, suggesting the possibility of a species-dependent discrepancy in treatment outcomes.

In concert, the findings of this thesis demonstrate that biometal delivery via the use of CQ can increase the expression and function of P-gp in brain endothelial cells, which is associated with increased intracellular copper concentrations, but that CQ is unable to produce this effect in mice under the dosage regimen employed. These studies open the possibility of modulating P-gp expression via the design of future ionophore drugs which specifically target the brain endothelium for copper delivery, with therapeutic applications such as modulation of CNS drug access and enhanced trafficking of endogenous P-gp substrates.

ABBREVIATIONS USED THROUGHOUT THE THESIS

AD	Alzheimer's disease
APS	Ammonium persulfate
ABC	ATP binding cassette transporter
ABCG2	Breast cancer resistance protein
ANOVA	Analysis of variance
APP	Amyloid precursor protein
ATP	Adenosine triphosphate
Aβ	Amyloid beta peptide
AβOs	Amyloid beta oligomers
BBB	Blood-brain barrier
BCA	Bicinchoninic acid
BCRP	Breast cancer resistance protein
bFGF	B-splice variant fibroblast growth factor
BMECs	Brain microvascular endothelial cells
BSA	Bovine serum albumin
CNS	Central nervous system
CQ	Clioquinol
CSF	Cerebrospinal fluid
CTR1	Copper uptake protein 1
DAPI	4',6-diamidino-2-phenylindole
DMEM	Dulbeccos's modified Eagle medium
DMSO	Dimethyl sulfoxide
DMT1	Divalent metal transporter 1
DNA	Deoxyribonucleic acid
EBM2	Endothelial basal medium 2
EDTA	Ethylenediaminetetraacetic acid

EEAT3	Excitatory amino acid transporter 3
EGF	Epidermal growth factor
FBS	Fetal bovine serum
FITC	Fluorescein isothiocyanate
FzR	Frizzled receptor
GAPDH	Glyceraldehyde 3-phosphate dehydrogenase
GLUT1	Glucose transporter 1
GSK3β	Glycogen synthase kinase 3 beta
HBSS	Hank's balanced salt solution
hCMEC/D3	Immortalised human cerebral microvascular endothelial cell line
HEPES	4-(2-hydroxyethyl)-1-piperazineethanesulfonic acid
HIV-1	Human immunodeficiency virus 1
ICP-MS	Inductively coupled plasma mass spectrometry
ICW	In-cell western
IGF	Insulin-like growth factor
IR	Infra-red
LRP1	low-density lipoprotein receptor-related protein
MBEC	Mouse brain endothelial cells
MDR	Multi drug-resistance
MDR1	Gene encoding for P-glycoprotein
MRP1	Multidrug resistance-associated protein 1
MTC8	Monocarboxylate transporter 8
MTT	3-(4,5-dimethylthiazol-2-yl)-2,5-diphenyltetrazolium bromide
MW	Molecular weight
NBD	Nucleotide binding domain
NVU	Neurovascular unit
P:C	Production to clearance ratio

PBS	Phosphate buffered saline
PBS	Phosphate buffered saline
PBS-T	Tween-20 containing phosphate buffered saline
PD	Parkinson's disease
P-gp	P-glycoprotein
pH	Potential of hydrogen
PI	Protease inhibitor
PSC833	Valspodar (P-glycoprotein inhibitor)
PXR	Pregnane X receptor
QC	Quality control
R123	Rhodamine-123
RAGE	Receptor for advanced glycation end-products
RNA	Ribonucleic acid
RXR	Retinoid X receptor
SDS	Sodium dodecyl sulfate
siRNA	Small interfering ribonucleic acid
SLC	Solute carrier superfamily
TBS	Tris buffered saline
TBST	Tween-20 containing tris buffered saline
TEMED	Tetramethylethylenediamine
Tg	Transgenic
THTR2	Thiamine transporter 2
TMD	Transmembrane domain
TR	Transfection reagent
TRIS	Tris(hydroxymethyl)aminomethane
VEGF	Vascular endothelial growth factor
WB	Western blot/western blotting

CHAPTER 1

A General Introduction

The structure and function of the blood-brain barrier

The blood-brain barrier (BBB) is anatomically defined by highly specialised brain microvascular endothelial cells (BMECs) that separate the brain parenchyma from the blood which perfuses the brain. These BMECs possess several features otherwise absent in the endothelial cells of the peripheral vasculature (2). Among these features are the presence of tight junction proteins, namely the claudin, occludin and junctional adhesion molecule proteins (4), which together establish an extracellular protein matrix that renders the paracellular route of blood-to-brain transmission impermeable to most molecules in the systemic circulation (5). Additionally, BMECs do not possess the fenestrae found in peripheral vascular endothelial cells (6), but do exhibit a larger proportion of mitochondrial structures, which facilitate the rigorously maintained energy dependent transport processes that are constantly in flux at the BBB (7). Another feature of the BBB is the large range of transporter proteins that are highly expressed at the BBB in contrast to other tissue vasculature (8). This multitude of solute specific transporters function to either permit or restrict the movement of many blood-borne solutes across the BBB, and some examples of these transporters are now described, to briefly touch upon the complexity that exists at the BBB.

Since the human brain weighs less than 2.4% of the total body weight, yet consumes ~20% of the body's glucose supply, it is fitting that glucose transporter-1 (GLUT1) is highly expressed at the BBB relative to other tissues (9). Also highly expressed at the BBB are a wide range of proteins belonging to the solute carrier superfamily (SLC). These membrane proteins selectively bind small molecule nutrients and shuttle them across the endothelial cell membrane, thus providing the CNS with its nutritional needs, without allowing unfettered access for all the remaining components of the bloodstream (10). Some examples of essential nutrients and their respective SLC transporters which are expressed at the BBB are summarised in Figure 1,

and these include: vitamin B1 which is transported by thiamine transporter 2 (THTR2; also known as SLC19A3) (11), the neurotransmitter glutamate which is transported by excitatory amino acid transporter 3 (EAAT3; also known as SLC1A1) (12), thyroid hormones which are transported by monocarboxylate transporter 8 (MTC8; also known as SLC16A2) (13), as well as biometals such as iron, zinc and copper, which are transported by divalent metal transporter 1 (DMT1; also known as SLC11A2) (14) and high affinity copper uptake protein 1 (CTR1; also known as SLC31A1) (14). The selection of transporters highlighted herein is by no means exhaustive, and the examples given are limited to small molecule transporters. Also functioning

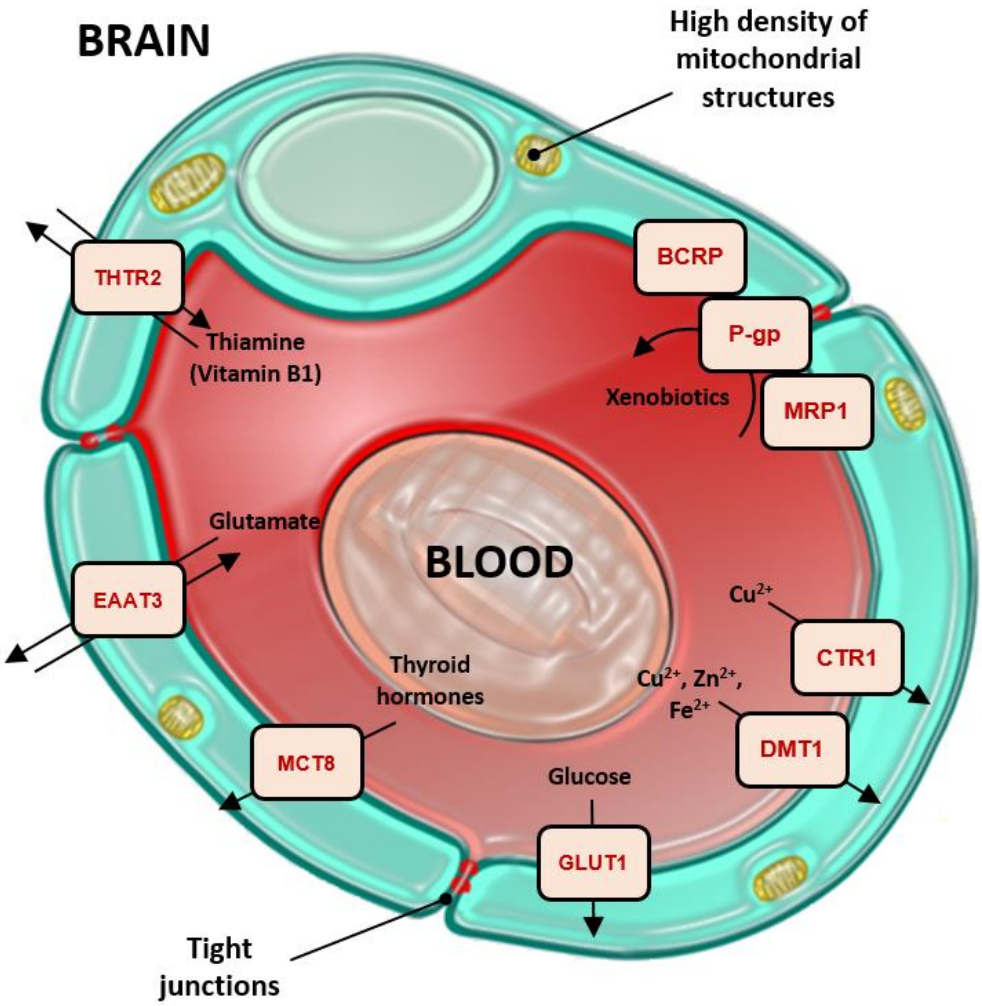

Figure 1: Schematic image of the brain endothelial cells that form the BBB, with key examples of the range of the transporter proteins which function at the BBB to regulate trafficking of the corresponding substrates, exerting direct control over molecular entry into the CNS.

at the BBB are a large range of receptor mediated transporters which are capable of trafficking much larger molecules (up to 4500 Da) (15). While all of these BBB transporter proteins are important for maintaining CNS health, one group in particular appears to play a particularly crucial role in disease states, namely the xenobiotic efflux transporters. One of the most prominent and important of these xenobiotic efflux transporters is known as P-glycoprotein (P-gp; also known as ATP binding cassette-1, abbreviated to ABCB1), and it is this protein which forms the major focus of this thesis.

P-gp acts in concert with many other important and highly expressed xenobiotic efflux transporters at the BBB, and plays a crucial role in the active efflux of a large range of substrates which might otherwise affect the CNS via toxic mechanisms (16). Breast cancer resistance protein (BCRP; also known as ABCG2) and the multidrug resistance-associated protein 1 (MRP1), alongside P-gp are considered as equally important in CNS defence, sharing significant overlap in substrate and inhibitor specificity to that of P-gp (17). Both the breadth and the overlap of substrate specificity between these three transporters indicates an element of redundancy, and therefore of the evolutionary importance of CNS protection from blood-borne xenobiotics.

When taken together, the tight junction proteins and active influx and efflux transporters constitute a formidable barrier from which the brain receives with high selectivity the substances it requires, whilst excluding those solutes which bare the potential for toxic insult. While in the past the BBB has been described as a ‘selective diffusion barrier’ that was largely static in nature, significant research in recent years has encouraged the viewpoint of the BBB as a much more dynamic and decisional interface, facilitating important communications between the peripheral circulation and the CNS (18), and it is becoming increasingly

advantageous, both physiologically and in terms of disease states, to view the brain and BBB not as separate entities, but as one multifaceted and communicative entity, known as the neurovascular unit (NVU). While concepts such as P-gp and the BBB form the major focus of this thesis, the NVU is now briefly discussed, to provide an anatomically holistic explanation of the area under study.

The neurovascular unit

Evidence accumulated over the last 20 years has indicated that the BBB is in constant communication with the various cell types surrounding it, and that the absence of one or more of those cell types results in a property-altered BBB (19, 20). Similar observations of these brain-cell interactions in other fields of inquiry prompted Lo et al, in 2004, to coin the concept of the 'neurovascular unit' (NVU) (21). As was predicted by the authors of that article (and shown in Figure 2), the concept of the NVU has gradually evolved to include not just endothelial cells, astrocytes and neurons, but also pericytes, vascular smooth muscle cells and glial cells, which together constitute a complex sensory and communicatory network. This grouping of cells act together to temporally regulate barrier permeability, nutrient supply, angiogenesis, as well as the rate of cerebral blood flow (16). Neurons themselves are able to detect minute changes in the flux of nutrient and oxygen levels available to their disposal, and accordingly react by relaying biochemical signalling to astrocytes or electrical signalling directly to the BBB endothelial cells via interneurons, with homeostatic responses resulting from such communications (22). Such signals can illicit an impressive variety of responses, including the upregulation of GLUT1 in response to glucose deprivation or hypoxia (23); release of matrix-metalloproteinases for vascular remodelling following hypoxia or injury (24); coordination of angiogenesis by stem cell factor secretion (25); brain water influx and efflux across the BBB (26); and pericyte-mediated modulation of BBB permeability (27). The flow

of information between BMECs and the remainder of the NVU is not unidirectional, with strong evidence having been provided for endothelial input into astrocyte development and differentiation (28, 29). BMECs can also affect and induce neurogenesis via secreted factors in vitro (30), further confirming the integration and co-dependency that is essential to the functional NVU.

This compilation of experiments highlighted above permits the emergence of a new way of conceptualising both the brain and the BBB. Older and more compartmentalised ways of envisioning the brain and neuronal circuitry as anatomically isolated components are gradually subsiding, instead giving way to the more integrated and networked concept of the NVU. As

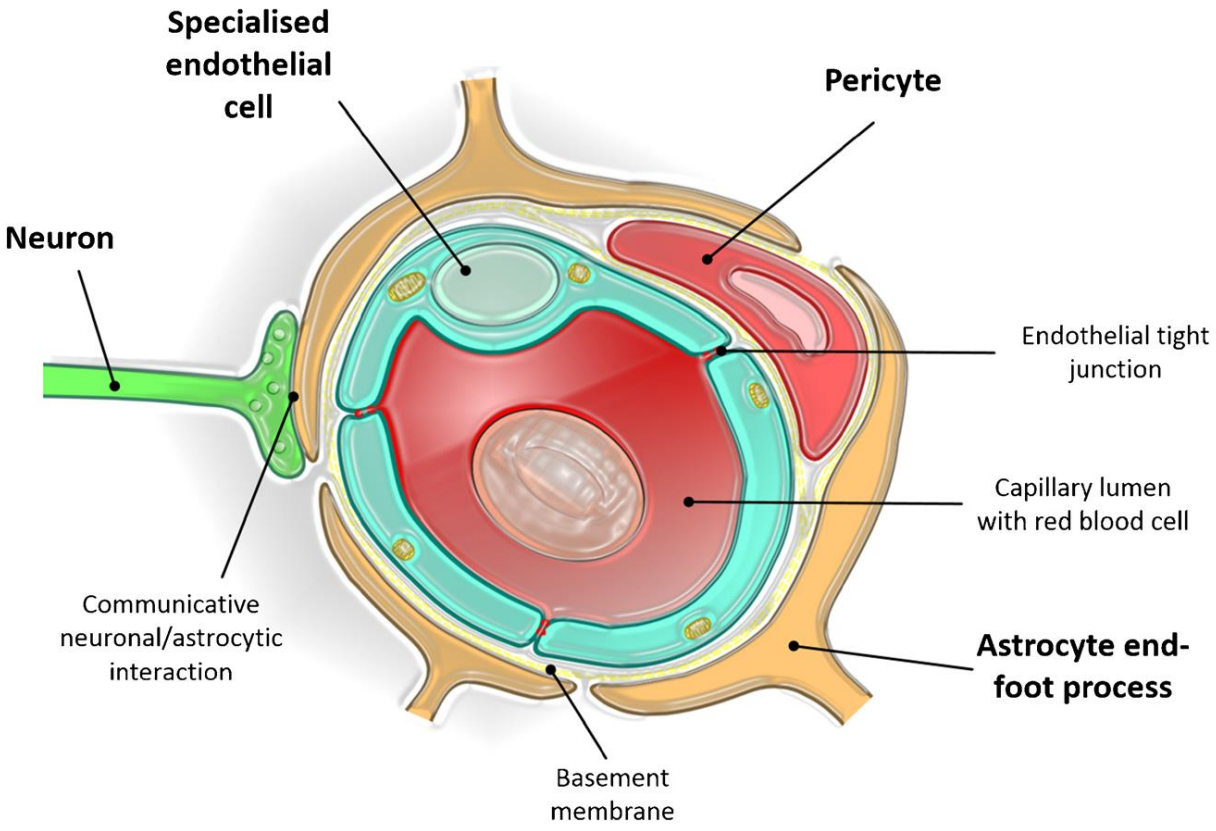

Figure 2: The neurovascular unit (NVU) and its major cell-type components (bold) and relevant features (non-bold). The NVU is composed of neurons, specialised brain endothelial cells, pericytes and astrocytes. Features include tight junction protein matrices which limit paracellular diffusion of molecules, and a collagen fibrous basement membrane providing structural support and communicative junctions between neurons and astrocytes, facilitating direct and indirect information flow between the neuronal and vascular components (3).

more and more brain diseases are discovered to involve brain vascular dysfunction (i.e. Alzheimer's disease (AD), multiple sclerosis, stroke and HIV-1 infection) (31), it becomes increasingly apparent that the disease interventions of the future will most likely have incorporated this perspective of the integrated NVU whilst resolving the currently mysterious disease states of today. From the view point of CNS health and disease progression, one of the most important aspects of the NVU and BBB is the expression and function of the ATP-binding cassette (ABC) transporters.

ABC transporters

The ABC transporters form one of the largest and oldest super-families of protein molecules, and are expressed in one form or another in all existing vertebrates (32). The ABC transporters are plasma membrane spanning proteins, usually comprised of multiple protein subunits which fit together to function as one unit (33). Broadly speaking, the full transporter units can be broken down into structurally distinct domains; the transmembrane domain (TMD) through which the solutes pass through during transport; the extracytoplasmic receptor used for extracellular substrate recognition in nutrient transporters; and the nucleotide binding domain (NBD) which facilitates the ATP hydrolysis that powers the transport mechanism (34, 35). Not all ABC transporters possess each of the described domains; for example, nutrient influx transporters usually require an extracytoplasmic receptor with specific affinity for the targeted substrate, whereas transporters which efflux xenobiotics such as P-gp, do not require receptor-mediated specificity for substrate engagement.

The name given to this super-family (ATP-binding cassette transporters) provides insight to their mechanism; ATP, the primary currency of physiological energy, is used to power the mechanism of influx or efflux of a specific substrate by an ABC transporter (36). Whilst the

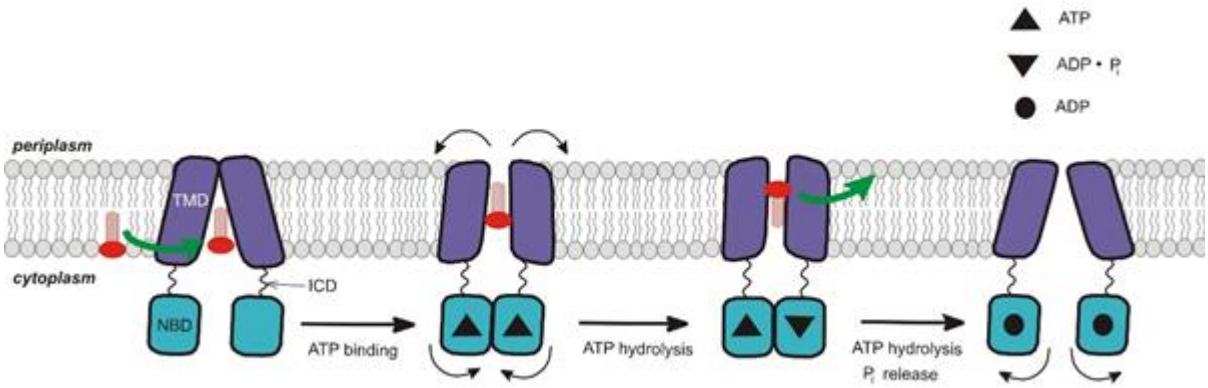

Figure 3: Schematic representation of the mechanism by which ABC efflux transporters are considered to operate (1).

mechanisms of influx and efflux transporters are different from one another and also not fully understood, it can be generally stated that the ABC transporters achieve solute transport across a membrane by manifesting conformational changes in the TMD structure, which are induced by the binding of the transporter substrate and subsequently the binding and hydrolysis of ATP, as shown in Figure 3 (36). In the inactive state, the TMD occupies a conformation which possesses a substrate binding chamber, but which is not yet permeable to the substrate. Binding of the substrate induces a conformational change in the transporter which increases the affinity for ATP to the NBD (36). Two units of ATP then cooperatively bind to the NBD, and subsequent hydrolysis of the ATP molecules alternates the conformation of the TMD, reducing the substrate/chamber affinity and allowing for the loosely bound substrate to diffuse through the created tunnel to the other side of the lipid bilayer membrane (36). The exact mechanisms of transporter subtypes are not fully understood, and may vary from the general description just provided, but most of the biochemical data produced indicates that the above mechanism is the most plausible.

The ABC transporters can be further classified into subfamilies, and those expressed at the BBB have been shown to be responsible for trafficking various nutrient molecules such as cholesterol and phospholipids (ABCA and ABCG subfamilies) (37, 38), fatty acids into

subcellular peroxisomes (ABCD subfamily) (39), and bile and steroids (ABCG subfamily) (40), into the brain endothelium, en route to the brain. While these functions have been successfully identified and ascribed to specific proteins, the current trend suggests that many more functions for the proteins within these families will be identified in the future. Aside from transporting nutrients into the brain, several members of these subfamilies play an extremely important role in protecting the brain from exposure to xenobiotics by actively effluxing such molecules out of the BBB. From a biological research perspective, a few efflux transporters in particular have received the most attention: BCRP, MRP1 and P-gp. One of the main reasons for the extended study of these proteins in particular, is their involvement in the denial of CNS access to many drug candidates (discussed in later sections). Each of these three efflux transporters possesses a diverse range of substrate specificity, and considerable overlap of substrate compatibility exists between them (41). This overlap in substrate compatibility indicates the evolutionary importance of BBB-mediated brain protection, since multiple proteins with subtly yet distinctly different structures have evolved separately on three separate occasions (42) to protect the brain from xenobiotic insults. While each of these efflux transporters are of high physiological importance, it is P-gp which is most relevant to the work described in this thesis, and therefore, P-gp accordingly forms the focus of the remaining sections.

P-glycoprotein

P-gp was first ascribed its identity in 1976 (P denoting resistance to drug Permeability), by its discoverers Juliano and Ling, who were the first to recognise this protein as a major culprit of the multi-drug resistant exhibiting phenotype presented by Chinese hamster ovary cells (43). Since this discovery a large body of research has elucidated the character of P-gp, which is now known as a very active ATP-dependent efflux pump for a broad range of substrates. P-gp is highly expressed in the liver, kidneys, small intestines, testis, uterus, ovaries, placenta, pancreas,

adrenal gland, and most pertinently to this thesis; in endothelial cells forming the BBB (44-48). The primary function of P-gp in each of these tissues is the active efflux of xenobiotics (including exogenously administered drugs alongside natural diet derived toxins or xenobiotics) from the intracellular space out into the lumen of the respective tissues (49). In the relevant case of the BBB, P-gp transports its molecular cargo from the lipid milieu of the brain endothelial cells into the blood contained within the capillary lumen. P-gp can efflux substrates ranging in size from 200-4000 Da, and ranging in polarity from fully aromatic to weakly basic or acidic ionic compounds (50). Considering the broad range of substrates that are affected by P-gp function, this transporter has a very important role in the protection of the CNS – especially with respect to human pharmacological efforts targeting the CNS – which has prompted some researchers to refer to P-gp as 'the gatekeeper' of blood-to-brain compound transport (51). However, despite this perceived importance, it should also be noted that a P-gp knockout mouse model is surprisingly non-lethal (52), an outcome subsequently shown to be due to the considerable substrate overlap shared by other members of the ABC superfamily (53). P-gp deficient mice do however exhibit the phenotypical properties of an enhanced accumulation of administered drugs within the brain, which is accompanied by an exacerbated sensitivity to the toxic profiles of those accumulated drugs (54). Altered expression and/or function of P-gp has been demonstrated to be implicated in several important disease states, including cancer, inflammatory bowel disease and AD, as well as in altering or hindering the trafficking of CNS-targeted drugs across the BBB en route to the brain. The involvement of P-gp in these areas will now be discussed.

P-gp in CNS drug access

As a greater understanding of neurodegenerative disorders accumulates, an increased proportion of new chemical entities have their pharmacological targets located within the CNS.

Compared to other pharmacological targets around the body, the protein targets within the brain present specific problems due to the presence of the BBB. The expression of tight junction proteins forms a dense extracellular matrix that largely prevents the paracellular transit of drug molecules across the BBB (55), leaving only the transcellular route available for diffusion. Solute diffusion across the transcellular route of the BBB is then further prevented by the strong expression and activity of P-gp (in combination with BCRP and MRP1) (56). P-gp in particular has been shown to be specifically involved in the powerful and continuous efflux of a large range of drugs from the brain endothelium. As shown in Table 1, many experiments have interrogated the brain uptake in P-gp null versus wild type mice, and the results are striking: this structurally diverse set of compounds exhibit up to 30-fold increases in brain exposure (58-64). This effect has been observed for many other drugs, and efforts to chemically inhibit P-gp whilst co-administering CNS therapeutics have been attempted, although with limited success (57).

P-gp is easily inhibited in an in vitro setting and initial studies using the second generation P-gp inhibitor PSC833 produced significant increases in drug exposure (65). But subsequent clinical trials involving co-administration of PSC833 with P-gp substrate drugs produced disappointing increases in CNS drug exposure, and any potential benefits were offset by unexpected pharmacokinetic interactions, as well as off target effects including inhibition of other ABC transporters and altered metabolism of the pharmacological drugs being tested (66, 67). Third generation P-gp inhibitors with nanomolar affinity and improved selectivity also failed to improve clinical outcomes, leading the field to almost totally abandon small molecule inhibition of P-gp as a strategy for improving CNS drug access, in pursuit of other strategies (68).

While on the one hand the activity of P-gp in preventing CNS drug access is normally viewed by researchers as a formidable challenge to be overcome, in another light, reduced P-gp expression or activity could also be viewed as a pathological outcome, especially in the aging brain. The integrity and permeability of the BBB begins decreasing with age (69-71), which potentially permits higher-than-optimal CNS drug concentrations in more elderly patients. The age-driven hyper-permeabilisation of the BBB may also result in increased exposure to systemically circulating xenobiotics within this cohort, and therefore an upregulation of P-gp in this context might be therapeutically desirable.

Table 1: A list of clinically used drugs which appear to be substrates of P-gp, and their brain:plasma uptake ratios in both wild-type and P-gp null mice. The brain exposure for some drugs in the list is increased by up to 30-fold in P-gp null mice, providing strong evidence for P-gp involvement in the active efflux of many drugs.

Drug	Time point of measurement	Brain:plasma ratio in wild-type mice	Brain:plasma ratio in P-gp null mice	Brain exposure increase in P-gp null mice	Reference
Cyclosporine	4 h	0.28	3.3	12	Schinkel, 1995 (58)
Digoxin	4 h	0.08	1.5	19	Schinkel, 1995 (58)
Indinavir	4 h	0.08	0.81	10	Kim, 1998 (59)
Ivermectin	24 h	0.094	2.519	26.9	Schinkel, 1994 (60)
Loperamide	4 h	0.31	2.1	6.7	Schinkel, 1996 (61)
Nelfinavir	4 h	0.09	2.65	31	Kim, 1998 (59)
Quinidine	10 min	0.17	4.64	28	Kusuhara, 1997 (62)
Saquinavir	4 h	0.13	0.88	6.67	Kim, 1998 (59)
Sparfloxacin	2 h	0.14	0.54	3.9	Tamai, 2000 (63)
Verapamil	1 h	0.42	3.3	7.9	Hendrikse, 1998 (64)
Vinblastine	4 h	1.7	18.7	11	Schinkel, 1994 (60)

From a biomedical research point of view, P-gp is involved in more areas of interest other than the denial of CNS drug access. Pathological upregulation of P-gp during tumorigenesis is a well explored phenomenon in cancer, and alterations in BBB integrity and more specifically, P-gp expression, are actually well characterised events in a range of disease states, including but not limited to AD (3), Parkinson's disease (72), epilepsy (73) and amyotrophic lateral schelrosis (74). To highlight the pivotal role for P-gp, some of these disease states shall now be discussed.

P-gp in cancer

As mentioned earlier, P-gp is not expressed in all cell types, but tends to be restricted to tissue regions which withstand heavy exposure to xenobiotic pressure, such as the epithelial layer of the liver, kidneys and small intestines, alongside the brain microvascular endothelial cells. It is usually only in these P-gp expressing cell types where P-gp mediated multi drug-resistance (MDR) to cancer therapeutics can occur, although totally analogous mechanisms can be found for both BCRP and MRP1 in cancerous MDR cell types which do not normally express P-gp (75). The mechanisms behind P-gp conferring MDR in cancerous cells is not yet fully understood, and involves a complex interplay of the many cell signalling pathways that are altered once cancer has been initiated (75). Briefly, cells become cancerous by a process of gene mutation which facilitates the escape from the normal cell cycle pathways which regulate cell senescence and apoptosis (76). The altered genetic information flow across the cell signalling network of the cancerous cell (such as constitutively increased kinase activity) can result in the activation of pathways which regulate P-gp expression (75). While this general mechanism partially explains the reduced exposure to cancer drugs that would be experienced by cancer tumours, more specific pathways probably exist which confer drug-induced MDR in cancer cells. For example, in one particular study it was shown that lung perfusion into humans

of doxorubicin (a chemotherapeutic agent used in the treatment of cancer), increased P-gp expression in cancerous lung cells dramatically and within 50 minutes of treatment, but that this effect did not occur in normal, non-cancerous lung cells (77). While the pathways involved are not fully characterised, it is evident from studies like these that cancer-altered signalling pathways are inherently geared toward upregulating self-defence machinery against pharmacological insults, in comparison to normal and healthy cells. Despite some comprehension of these mechanisms, pharmacological blockade of P-gp in cancer treatments has achieved limited success due to issues with toxicity and adverse drug reactions and further pharmacokinetic complications (64). It is for these reasons that further research aimed at full characterisation of cell signalling pathways governing P-gp expression may be desirable in informing future research. AD is another disease state for which P-gp exhibits heavy involvement, and the pathogenesis of AD is next discussed.

Alzheimer's disease – a general introduction

Much evidence has mounted that waning P-gp expression plays an integral role in AD disease progression, and that AD might actually represent one of the most relevant applications for the P-gp modulation set out in this thesis. As such, an extensive introduction into the pathophysiology of AD and the importance of P-gp in the disease progression, particularly with respect to the role of P-gp in the BBB clearance of the major toxin accumulating in the AD brain, is discussed in detail over the next sections.

The biomedical revolution of the last century afforded a steady increase in the average life expectancy in most of the western world (78). Since the greatest risk factor for AD is aging (79), a rise in AD diagnosis and mortality has accompanied the rise in life expectancy. According to the 2015 World Alzheimer Report, the prevalence of AD has been projected to

increase exponentially, with diagnoses approximately doubling every twenty years, before reaching a figure as high as 131 million individuals across the world by 2050 (80). These estimations place AD as one of the world's most central health concerns.

AD manifests as a rapid progression of a broad spectrum of cognitive symptoms, including but not limited to; short and long term memory deficits (81), cognitive decline (82), loss of verbal fluency (83, 84) and a lack of awareness of the subjects disease state (anosognosia) (85). Symptoms of AD appear only subtly at first, complicating an early diagnosis by blurring the distinction between AD and the mild cognitive decline that can be seen in the elderly in general (10). In addition to the array of symptoms just described, AD also places a large burden on the family and caregivers of people with AD. During the late stage of the disease's progression, individuals are unable to complete or execute the most pedestrian of tasks without aid, including locating essential objects, visiting the bathroom, bathing and dressing, and patients can require much care to navigate daily living (86).

The manifestation of AD can be classified into one of two types; familial or sporadic, also known as autosomal dominant AD and late-onset AD, respectively. Untangling the genetic components and resulting phenotypes of AD is difficult, but currently familial AD is thought to represent between 1-5% of total AD cases (87). Familial AD has been demonstrated to involve specific genetic mutations, which precipitate AD symptoms much earlier in life (average age of onset is 46.2 years (88, 89)). Sporadic AD however, represents the remaining majority of cases, and symptoms occur much later in life, with an average age of symptom onset of 72 years (88, 89). Whilst the root causes and temporal unfolding of the two types of AD are quite different, the histochemical changes and resulting psychiatric phenotypes remain similar enough that both types are generally comprehended in unison. At a histochemical level,

AD is known to involve multiple well-characterised pathogenic events, and has been described as having a 'robust histological signature' that allows for straightforward post-mortem diagnosis (90). One of the main histological features (illustrated in Figure 4) is the formation of extra-neuronal senile plaques of which insoluble amyloid-beta (Aβ) peptides are the major component (91-93), as well as elevated levels of soluble Aβ oligomers (AβOs) (94, 95). Aβ peptides are defined as short peptides of 37-49 amino acids in length which are derived from proteolytic processing of the physiologically active parent protein, amyloid precursor protein (96). The two most abundant and pathologically relevant isoforms have been identified as $A\beta_{40}$ and $A\beta_{42}$, and these species constitute 90% and 5-10%, respectively, of the total Aβ produced in a non-AD human brain (97), and it is currently thought that the accumulation of these soluble oligomeric forms of the two peptides is one of the main drivers of AD disease progression, due to strong correlation between AβO concentrations with synaptic loss and cognitive decline in human AD (94, 95, 98). Other hallmark features include the presence of neurofibrillary tangles (illustrated in Figure 4) composed primarily of the hyper-phosphorylated tau protein (99-101); as well as inflamed cerebral blood vessels also associated with Aβ deposits (102, 103), elevated

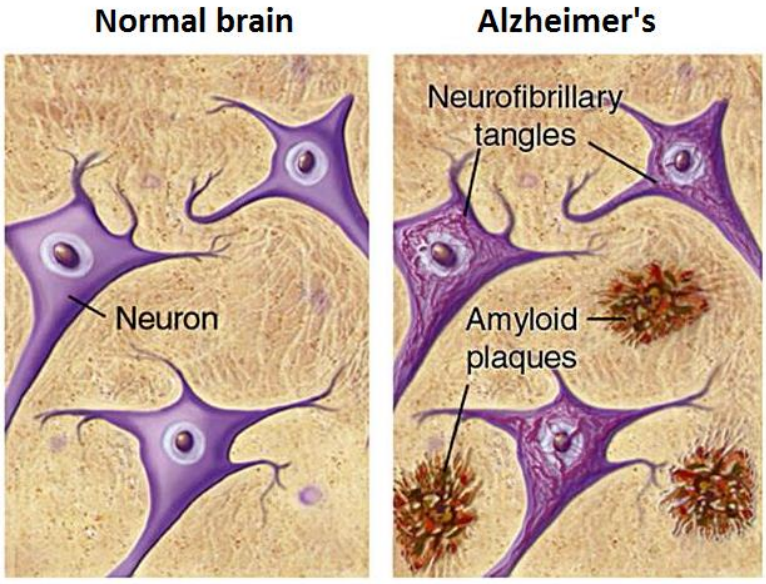

Figure 4: Schematic representation of normal healthy neurons versus neurons afflicted by neurofibrillary tangles and amyloid plaques which are seen in AD. Image by the BrightFocus Foundation, 2000.

brain levels of soluble AβOs (104), increased oxidative stress within the brain (105), reduced cholinergic neuronal transmission (106), and a significantly reduced brain weight compared to healthy age-matched controls (107). Whilst much progress has been made in the biochemical characterisation of these events individually, the causative interplay between each, and how each fits within the wider temporal pathogenesis of AD, remains largely enigmatic. Of all the pathogenic events described above, probably the most widely implicated and well-characterised is the accumulation of the Aβ peptide in the brain, and a detailed analysis of the unique properties of Aβ and the clearance thereof, is presented in the next section.

Aβ clearance and the neurovascular hypothesis of AD

The neurovascular hypothesis of AD was first put forward by Zlokovic et al in 2005. Briefly, it stated that a causative link between cerebrovascular dysregulation and brain Aβ accumulation may exist, and may even be the root cause of Aβ accumulation in the CNS, and therefore of sporadic AD (108). This hypothesis has made available the possibility of influencing new specific neurovascular targets via pharmacological intervention or other means, as a strategy for preventing Aβ accumulation early in the disease, or enhancing Aβ efflux and thus Aβ pool dissociation later in the disease – both as potential options for treating AD (108). While the pathogenesis of AD is likely to arise from increased concentrations of Aβ in the CNS, this increase likely manifests as a result of one or more of three key processes relating to the neurovasculature; 1) diminished or faulty degradation of Aβ species within the CNS, 2) impaired clearance of Aβ species from the CNS to the periphery or 3) enhanced influx of peripheral Aβ species across the BBB. Substantial evidence supporting the neurovascular hypothesis has accumulated since 2005. In 2010, a landmark study was provided by Mawuenyega et al, where the production-to-clearance ratios (P:C) of $A\beta_{40}$ and $A\beta_{42}$ were measured in 12 individuals suffering from sporadic AD and 12 healthy controls. Whilst the

study reported near identical Aβ production rates for $A\beta_{40}$ and $A\beta_{42}$, the authors found significantly altered clearance rates of both Aβ species between the two groups ($A\beta_{42}$: 7.6 %/h for non-AD and 5.3 %/h for AD individuals; and $A\beta_{40}$: 7.0 %/h for non-AD and 5.2 %/h for AD individuals) (109). Considering the Aβ production rate was found to be approximately 6.7 %/h for both AD and control groups, these results imply that the AD individuals in this study exhibited a P:C ratio of 1.35, compared to a P:C ratio of 0.95 for non-AD participants (109). This study provided substantial evidence of a reduced capacity for clearance of the Aβ peptides in the human AD brain, which likely contributes to the accumulation of Aβ within the CNS, and indeed the wider pathogenesis of AD. Subsequent investigations have identified multiple endogenous Aβ clearance mechanisms which are summarised schematically in Figure 5, including astrocyte mediated enzymatic degradation (110), Aβ removal via bulk flow of cerebrospinal fluid (CSF) (111), and active efflux across the BBB. The relative contributions

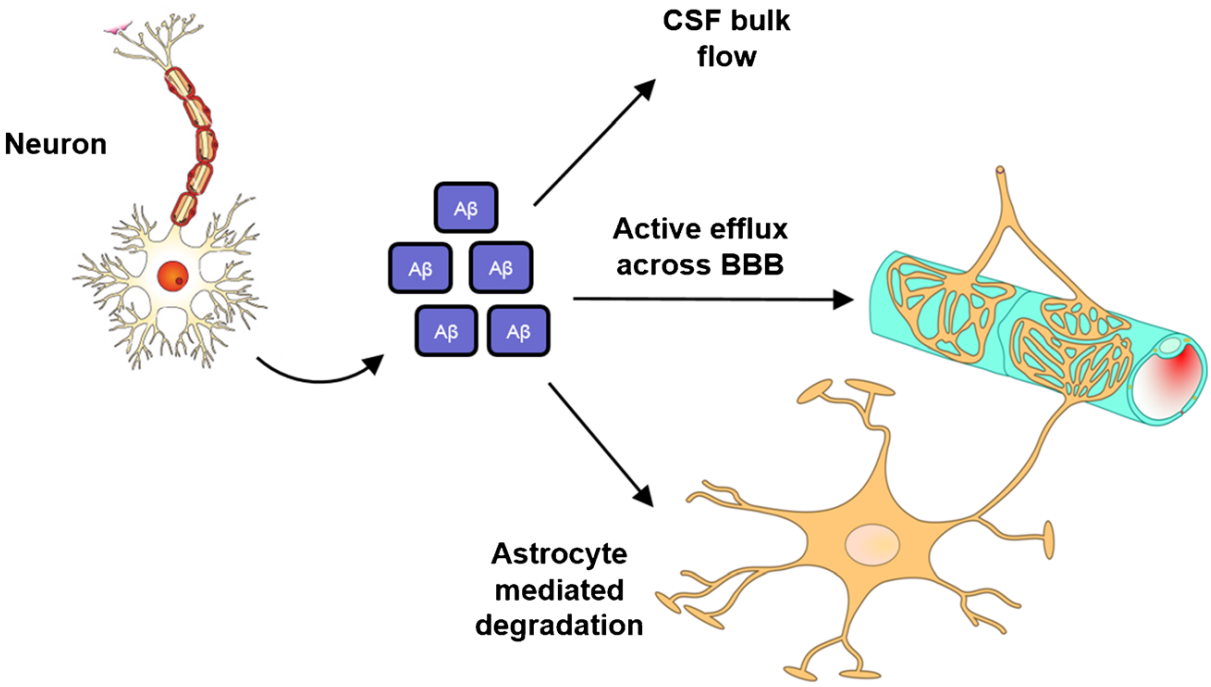

Figure 5: Identified routes of clearance for the Aβ peptide. Aβ is continually cleaved from neurons and released into interstitial space, where it is cleared by several identified mechanisms: removal via the bulk flow of the cerebrospinal fluid (CSF), active efflux across the blood-brain barrier (BBB) via transport proteins and astrocyte-mediated enzymatic degradation (3).

of each of the described mechanisms are still under debate, but it has been estimated that active efflux of the Aβ peptide across the BBB is one of the main routes of clearance, and the evidence for this statement is discussed in the following sections.

Evidence for blood-brain barrier mediated clearance of Aβ

As described earlier, strong evidence has indicated that it is Aβ clearance and not production which has gone awry in sporadic AD. While it has been long understood that the Aβ peptide is cleared by efflux across the BBB, the relative contribution of this mechanism to total Aβ clearance has only recently been estimated. Using three separate Aβ assays to quantify venous to arterial ratios of endogenous Aβ peptides in cognitively healthy subjects, Roberts et al concluded that approximately 25% of brain-derived Aβ peptides are cleared via BBB transit (112). Shibata et al attempted to quantify the same relative contributions in wildtype C57BL/6 mice. Using fractional clearance rates of iodinated Aβ, after 60 nM cannula injections and at various time points, the authors estimated that 74% of Aβ clearance was BBB mediated in this mouse model. A more recent study by Qosa et al attempted to quantify Aβ clearance mechanisms, also using C57BL/6 mice. The authors found that of the total $A\beta_{40}$ cleared from the brain over the 30 minute interval measured, approximately 38% was degraded within the CNS and that the remaining 62% was effluxed across the BBB (113). The apparent disparity between these results (25% of brain Aβ cleared across the BBB in humans versus 62-74% in mice) underscores inherent differences in Aβ trafficking between these two species and demonstrates the inherent variability between mice and humans for assessing Aβ trafficking and many other aspects of human disease. In any case, a large effort attempting to identify and characterise the specific transporters involved in BBB-mediated trafficking of the Aβ peptide has ensued over the last decade, and P-gp has emerged as an important mediator of Aβ clearance.

P-gp and other transporters traffic Aβ at the BBB

The role of P-gp in brain-to-blood transport of the Aβ peptide has been thoroughly explored, yielding mostly concordant conclusions. Lam et al were the first to demonstrate that pharmacological blockade of P-gp in P-gp-transfected human embryonic kidney cells resulted in reduced Aβ secretion, and that Aβ was able to compete for binding and efflux against other known P-gp substrates (29). Cirrito et al used a P-gp deficient mouse model to demonstrate a reduction in brain clearance of exogenously-administered $A\beta_{42}$ from 16% in wild-type mice to 6% in P-gp-null mice. Additionally, the same study showed an enhanced accumulation of exogenously administered Aβ in the mouse hippocampus, and an elevated concentration of endogenous Aβ in the brain interstitial fluid of wild-type mice dosed with a P-gp inhibitor (108). Kuhnke et al provided additional evidence for a role for P-gp mediated Aβ transport in MDR-1 gene transfected porcine epithelial cells and inverted membrane vesicles (114). These authors demonstrated that Aβ transport was in competition with the known P-gp substrate rhodamine -123, and that Aβ transport could also be inhibited by using P-gp specific inhibitors (114). More recently, Wang et al have shown that P-gp deficient mice exhibit greater radiolabelled-Aβ accumulation after intravenous administration compared to wild-type counterparts, and that after these mice were cross-bred with Tg2576 APP mice, a similar accumulation of (endogenously produced) Aβ was observed (115). In tandem, these findings indicate a role for P-gp in facilitating both brain-to-blood Aβ efflux, as well as the prevention of blood-to-brain transit of the same peptide. P-gp however is not the only BBB transporter that appears to be engaged in Aβ transport, and the involvement of other proteins is now briefly discussed.

Among the transport proteins expressed at the BBB, of particular relevance to AD is low-density lipoprotein receptor-related protein (LRP-1). Alongside other processes, LRP-1 participates in the active transcytosis of Aβ across the BBB (20, 116, 117). The receptor for

advanced glycation end-products (RAGE) has been shown to play a role in blood-to-brain re-uptake of Aβ species (118). RAGE is upregulated in the AD brain and can mediate Aβ deposition into the cell membranes of neurons and microglia, thus allowing Aβ to bypass normal physiological antioxidant mechanisms and inflict oxidative damage upon those cells (119). Krohn et al engineered several mouse strains with alternative ABC transporter knockouts (other than P-gp). They found six month old mice lacking the gene encoding for MRP1 also appeared to exhibit an almost 13-fold higher accumulation of Aβ species in the brain (120). Tai et al were the first to show that BCRP may also be involved in the prevention of apical to basolateral BBB transmission of Aβ (121). Whilst this study was suggestive, several other groups attempted to confirm the findings in subsequent years. The general trend seems to be that BCRP is playing a minor role in Aβ efflux, which may become more important when P-gp is knocked down under experimental conditions (122). These findings, summarised in Figure 6, illustrate the complex and dynamic nature of proteostasis amongst the BBB transporters, and highlight the difficulty in identifying the key variations between normal brain and AD brain Aβ trafficking.

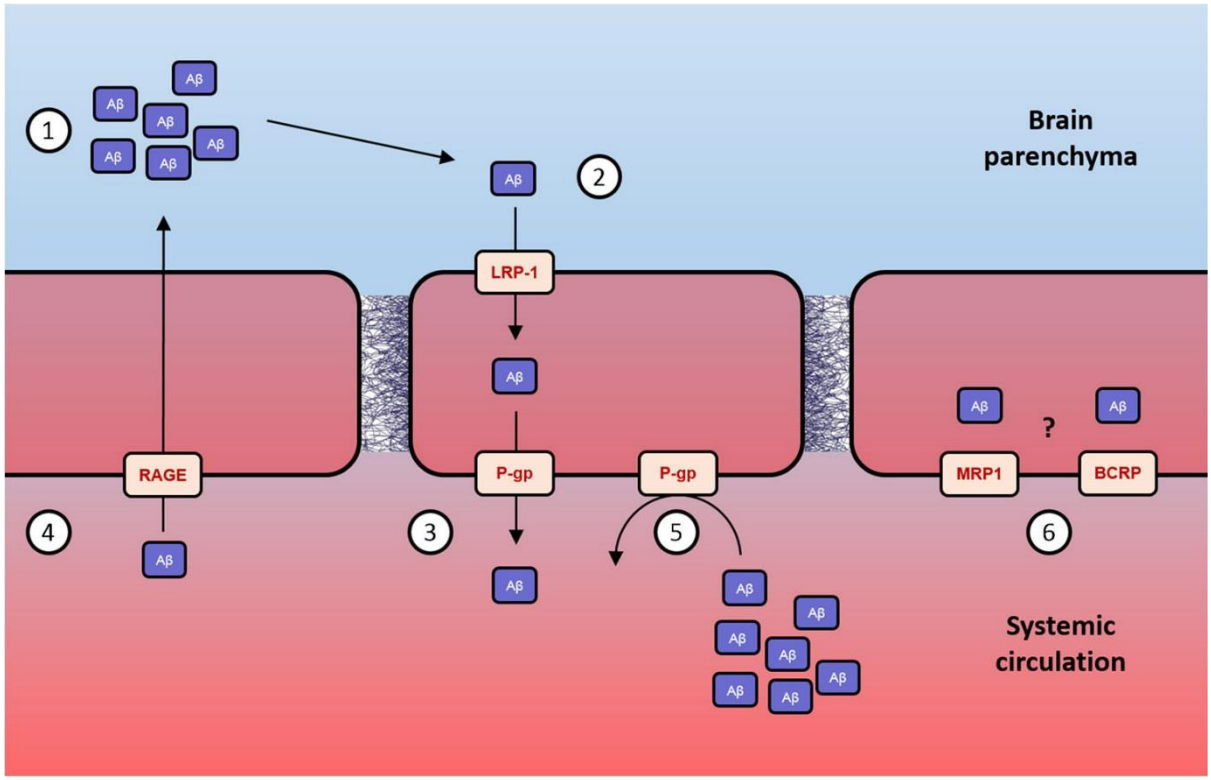

Figure 6: Clearance mechanisms currently predicted to be involved in Aβ trafficking across the BBB: (1) dissociated pool of oligomeric Aβ in the interstitial fluid of the brain, which accumulates to toxic levels in AD, (2) LRP-1 traffics Aβ peptides from dissociated pool into brain endothelium, (3) P-gp effluxes Aβ peptides from endothelial lipid-bilayer membrane into systemic circulation, (4) RAGE facilitates receptor-mediated endocytosis of blood-borne Aβ peptides, back into the brain interstitial fluid, (5) P-gp prevents the relatively higher concentrated (compared to brain ISF) blood-borne Aβ from crossing the BBB by active efflux from the lipid bilayer membrane and (6) the possible involvement of MRP1 and/or BCRP in Aβ efflux under either normal conditions or potentially in later stages of AD or AD mouse models (3).

Blood-brain barrier function in preventing apical to basolateral diffusion of Aβ

With regard to BBB implication in the pathogenesis of AD, most of the research focus has been on impaired clearance mechanisms which normally traffic Aβ in the brain-to-blood direction. This focus follows a logical trajectory, since the most AD-relevant pathological changes occur within the brain. In recent times however, much evidence has suggested that there may be also be a protective role for the BBB in preventing blood-borne Aβ from entering the brain, and that this mechanism may also be impaired in the early stages of the AD progression. This concept has been explored with various models, yielding perhaps unsurprisingly, differing conclusions.

Clifford et al showed that FITC-conjugated $A\beta_{40-42}$ are unable to cross a healthy mouse brain endothelium, until those animals are pretreated with pertussis toxin, a known instigator of BBB breakdown, after which the noxious peptides begin to accumulate in neurons of AD-associated brain regions (123). Tai et al used a human cerebromicrovascular endothelial cell line (hCMEC/D3) to show that inhibition of P-gp (and BCRP) increased apical-to-basolateral but not basolateral-to-apical permeability of iodinated-Aβ (I-$A\beta_{40}$), concluding that both proteins may function in preventing blood-borne Aβ from traversing the BBB (121).

Conversely, Banks et al demonstrated that I-$A\beta_{42}$ can penetrate the mouse BBB when administered peripherally (124), and that pre-complexing the peptide with aluminium, which has been shown to be associated with AD (125), enhances this uptake (126). Similar experiments have confirmed apical-to-basolateral diffusion of I-$A\beta_{42}$ in other laboratories (127), a process which is apparently exacerbated by induced cerebral ischemia, which has been suggested (128) and elaborated upon (129) as a causative risk factor for AD in the past. Some of the discrepancies arising from these studies may be partially explained by the type of labelling used in the experiments, for example, it may be possible that FITC-conjugated Aβ cannot traverse the BBB of a live animal due to substrate recognition of the FITC moiety by an efflux transporter, or by altering the confirmation and thus polar interactions between the Aβ peptide and brain endothelial membranes.

In line with the findings of Lue et al (1999) and Sotolongo-Grau et al (2014), it may be that Aβ concentrations in the periphery are higher than that of soluble and freely available Aβ in the brain parenchyma, which suggests that a concentration gradient would promote both receptor mediated uptake and passive diffusion of the Aβ peptide in the blood-to-brain direction. If such a gradient does indeed exist, then the roles for P-gp, RAGE, BCRP and MRP1 in Aβ trafficking

or the prevention thereof, become even more prominent in the pathogenesis of and prevention of AD acquisition. Much evidence has emerged in the last 5-10 years of research that P-gp and possibly other AD-related transporters are in fact downregulated in AD, and this body of work shall now be discussed.

P-glycoprotein and other Aβ transporters are downregulated in AD

The first solid evidence for P-gp involvement in human and sporadic AD was provided by Vogelgesang et al, in 2002. This group analysed the apparent expression levels of P-gp in 243 deceased human subjects via semi-quantitative immunohistochemistry, and found an inverse correlation between P-gp status and the frequency of Aβ deposition in the medial temporal lobe (130). This study suggested that an absence or reduction of normal P-gp production, by whatever causal means, may permit the inefficient clearance of Aβ peptides from brain-to-blood in humans diagnosed with AD. More recently, a smaller but similar study by Chiu et al has provided concordant evidence to that of Vogelgesang et al, by showing a decrease in P-gp expression as a function of age in both normal and AD-diagnosed brains (69). Another study by Wijesura et al also appeared to confirm the above findings, whereby immunohistochemistry on human brain slices revealed a reduced abundance of P-gp, but not BCRP or MRP4, in those samples associated with diagnosed AD (131). Finally, another recent study demonstrating the likely role for P-gp in AD used a radiolabelled P-gp substrate (^{11}C-verapamil) to demonstrate reduced P-gp functionality (as opposed to post-mortem expression analysis), in living humans diagnosed with mild-AD, when compared to age matched controls (132). This latter study appears as particularly convincing with regards to altered P-gp expression potentially representing a causal or contributing factor for AD. The authors identified that P-gp activity was significantly reduced in all brain regions associated with AD (parietotemporal, frontal, and posterior cingulate cortices alongside the hippocampus) (132). This observation provides

strong evidence that the modulation (upregulation) of P-gp at the BBB of those brain regions affected by the disease may well prove a viable strategy in the treatment of AD.

Similar findings of reduced P-gp have also been demonstrated in mouse models of AD. Hartz et al employed freshly isolated mouse brain capillaries, and upon administering fluorescently labelled Aβ followed by quantitative fluorescence detection analysis, found that administration of either P-gp or LRP-1 inhibitors reduced transport of fluorescent Aβ to approximately 50% of those capillaries that were untreated (133). This same group also used a fluorescent marker of P-gp activity to demonstrate a 70% decrease in P-gp activity, and western blotting to show a 60% decrease in P-gp expression, in an APP transgenic (Tg) mouse model of AD (133). This latter finding prompted the questioning of a straightforward causal relationship between reduced P-gp expression and reduced brain-to-blood Aβ transport, and it was hypothesised that mild elevations of Aβ concentrations can inhibit P-gp expression, setting off a degenerative cycle of peptide accumulation and a reduced capacity for removal of that peptide. In the more complex triple transgenic AD mouse model (referred to as 3xTG AD mice in the literature), Mehta et al also observed reduced P-gp expression in isolated brain microvessel (42%), fortifying the findings outlined above (134). In the same study however, brain uptake of P-gp substrate drug molecules was also measured, and found to be equally matched to wild-type controls (134). The authors proposed that an AD-driven thickening of the BBB basement membrane (a fibrous tissue which separates the endothelial layer of the NVU from the various surrounding cell types), may have compensated for the reduced P-gp abundance regarding CNS access of the drugs tested in the study (134).

If the experiments described above and in previous sections regarding the observed reduction in P-gp abundance in the human AD brain represent an accurate reflection of the pathogenesis

of AD, it can be logically deduced that Aβ accumulation within the brain may be at least partially caused by a loss of abundance of P-gp. The fortification of the BBB via the intentional upregulation of P-gp (amongst other BBB transporters such as LRP1 if possible), may represent an intelligent and feasible strategy for the treatment of AD. The positive effects of upregulating P-gp to physiological levels which existed before the manifestation of the disease may potentially include; an increase in brain-to-blood trafficking of Aβ, a reduction in brain penetration of blood-borne Aβ, and resultantly, a restored balance of Aβ production to clearance within the human brain, such that the progression of AD is dramatically slowed or halted altogether. The intentional modulation of P-gp abundance or function, may also find application in future CNS drug efflux considerations. Pharmacological modulation of the signalling pathways which govern P-gp expression may be the best approach for such an aim, and those signalling pathways shall now be discussed.

Cell signalling pathways regulating P-gp expression

Since P-gp plays such a central role in xenobiotic efflux and thus cellular protection, it is unsurprising that the expression of this protein is governed by multiple signalling pathways, each of which are triggered by a variety of inputs. Whilst the experimental evidence demonstrates the potential for an enormous range of biochemical mediators stimulating P-gp regulation, only a few key pathways have been fully contextualised. These pathways will now be briefly summarised.

Firstly, P-gp expression can modulated by direct binding to the DNA promotor regions for P-gp by the promiscuous transcriptional factors p53 (135), hypoxia inducible factor 1 α (136), Y box protein 1 (137) and nuclear factor κ B (138). Whilst these factors can be secreted as a part of many pathways, two specific pathways modulating P-gp production have been thoroughly

characterised. The pregnane X receptor (PXR) is a nuclear receptor system which responds to perceived xenobiotic insult (foreign toxic substrates) by inducing the upregulation of multiple proteins involved in cellular defence of such situations (139). Since the primary role of P-gp is in preventing xenobiotics from penetrating important tissues, it is unsurprising that P-gp is upregulated by stimulation of this receptor (140, 141). The PXR system is expressed abundantly in the liver, intestine and BBB, and moderately in other peripheral tissues such as the kidney and lungs (140). In the absence of an agonist in the binding site, PXR is normally found in complex with co-repressor proteins named nuclear co-repressor 1 and 2 (140). When ligands bind to PXR, conformational changes are induced such that affinity to the co-repressor proteins is diverted to co-activator proteins instead. The new complex then binds with the heterodimer partner receptor known as the retinoid X receptor (RXR), which facilitates this large complex's ability to depart from the nuclear membrane (139). The PXR/RXR complex is then free in the nucleus to bind to the promoter regions of DNA which transcribe for proteins involved in xenobiotic defence mechanisms, including but not limited to, P-gp and BCRP and cytochrome P450 (139, 141). Interestingly, a huge number of P-gp substrates are also substrates for PXR, which indicates that both defence mechanisms seemed to have co-evolved. In this way P-gp can be thought of as a short term first line of xenobiotic defence, and PXR activation being a slower albeit fortifying cellular response to xenobiotic stress.

The second of these pathways is the Wnt/β-catenin signalling system. The Wnt/β-catenin pathway is a major driving pathway for tight junction expression during development and maintenance of the BBB (142-145) as well as CNS specific angiogenesis (142), among many other important processes of BBB development. Central to the Wnt/β-catenin pathway is the highly promiscuous kinase protein known as glycogen synthase kinase-3-β (GSK3β). When Wnt ligands are bound to FzRs, the GSK3β/destruction complex possesses an affinity for the

FzR, whereby it becomes phosphorylated and thereby deactivated, and β-catenin is permitted to accumulate within the cytosol (146, 147). Once β-catenin has reached high enough concentrations to occupy each of its cytosolic binding domains, it is permitted access to the nucleus, where it acts as a necessary co-factor for the transcription of a variety of proteins (146). When no Wnt ligand is present however, the GSK3β/destruction complex assumes a dephosphorylated state, and thereby has a preferred affinity for β-catenin, catalysing its ubiquitination (146). This tags β-catenin for proteasome mediated degradation, preventing its accumulation and thus transcription of the proteins which it regulates (146). The expression of BBB transporters P-gp and GLUT-1 are both regulated by the Wnt/β-catenin pathway (142, 148, 149). Since GSK3β has been shown to be generally hyperactive in the AD brain (150), pharmacological strategies implemented to reduce its activity may indeed be beneficial for treatment of the AD state as a whole. In the pursuit of modifying CNS drug access or Aβ efflux for AD therapy, one potentially viable strategy for inhibiting GSK3β and thus upregulating P-gp at the brain endothelium, could be the delivery of biometals to the BBB. The basis for this claim is now briefly discussed.

Biometals and the BBB

Whilst the concept has not been extensively pursued, some studies have assessed the influence of the biometals zinc and copper on the brain endothelium. Song et al demonstrated that administration of zinc to rats had positive effects on BBB function, including reduced Evan's blue brain penetration, and increased tight junction protein expression, and that the presence of zinc also inhibited the adverse effects exhibited by aluminium on BBB ultrastructure (151). Another study by Hennig et al probed the presence of zinc in cell culture medium on porcine BBB endothelial cells. The authors found that when zinc was removed from the media by the omission of the fetal bovine serum (FBS) component, albumin transit across the endothelial

monolayer (a proxy measure for permeability) was greatly increased, but that addition of zinc to the serum depleted media restored the monolayer permeability to healthy serum-treated control levels (152). The authors also showed by use of a zinc chelating agent, that serum treated cells reverted to possessing the increased albumin transport across a monolayer, indicating strongly that zinc is required for integral endothelial monolayer formation (152).

In more recent times, the effects of copper on brain endothelial function have also been studied. Li et al isolated the thoracic aortas from rats and cultured sections of this vascular tissue for eight days, in the presence or absence of increasing concentrations of copper. At optimal concentrations it was found that copper stimulated angiogenesis of the aortic rings, but only cooperatively when in the presence of vascular endothelial growth factor (VEGF) (153). The observed copper-mediated angiogenic effects were abolished when either a VEGF antibody or a copper chelating agent were present, indicating some interplay between VEGF and copper as cofactors of the same signalling pathways (153). Similarly, Wang et al have shown that copper administration to cultured primary rat brain endothelial cells also has positive effects regarding barrier properties. Their results indicated that optimal copper concentrations are required for barrier health, with lower concentrations having no effect, middle concentrations increasing cell viability, proliferation and the expression of tight junction proteins claudin-1,3,5 and 12, while higher concentrations induced apoptosis in these cells (154).

As mentioned earlier, GSK3β represents an important signalling node in the Wnt/β-catenin pathway which governs BBB development and maintenance, including P-gp expression. GSK3β requires magnesium as an activating cofactor, and some evidence suggests that the magnesium ions can be displaced by biometals such as calcium (155), beryllium (156), lithium (156, 157), zinc (158) and copper (158), although these findings have been shown in non-BBB

cell types such as neurones. Thus whether or not these biometals can inhibit GSK3β in brain endothelial cells and affect pathways which upregulate P-gp at the BBB is an area yet to be explored. While each of these results above represents progress towards understanding biometal involvement in BBB health, the ground covered above is quite limited, and whether or not biometal concentrations within endothelial cells can affect the expression and/or activity of important transporter proteins such as P-gp has not yet been examined, and thus represents a potential arm of research. Furthermore, even if it could be shown that biometals such as zinc and/or copper were to have positive effects on P-gp expression and function, how to manifest such changes in vivo is not obvious, and whether or not pharmacological targeting of biometal delivery to the BBB is a feasible enterprise is also unexplored. One such strategy for enhancing the delivery of biometals to certain biological compartments could be the use of the recently developed ionophore drugs, and a brief history of the development and application of ionophore drugs is outlined in the next section.

Ionophore drugs as tools for increasing cytosolic zinc and copper

A class of drug molecules which have received much attention in the last decade are the metal ionophores. Ionophores are drugs which bind to metal ions, but possess two key differences to metal ion chelators. Chelators are generally thought of as metal sequesterers, and upon binding to metal ions, tend to effectively remove the bound ions from biological participation (159). Ionophores however, do not have as extreme an affinity to their ions as do chelators, and are also able to cross biological membranes, shuttling bound metals across in the process. As a simple example, the logged binding affinity constant, $\log(K_m)$, for the well-known metal chelator EDTA for Cu^{2+} ions, has been observed to be 18.8 (160). Clioquinol (CQ), an emerging metal ionophore, possesses a log(Km) for Cu^{2+} of only 10.1 (161), representing a difference in affinity of over eight orders of magnitude. Thus it can be seen that this large

difference in affinity for metal ions might allow for CQ to bind and subsequently let go of metal ions much more readily than is possible with metal chelators like EDTA. The small molecule ionophore CQ, which is of great interest to this thesis, was one of the first used ionophores. A member of the hydroxyquinolone family, CQ possesses the two electron withdrawing groups (N and OH) which facilitate its metal binding properties (Figure 7A and B). CQ forms binding complexes with common biometals (such as but not limited to zinc and copper), and subsequently shields their polarity to facilitate the crossing of biological membranes, a process for which the metal ions would normally possess too much polarity to accomplish without electric shielding.

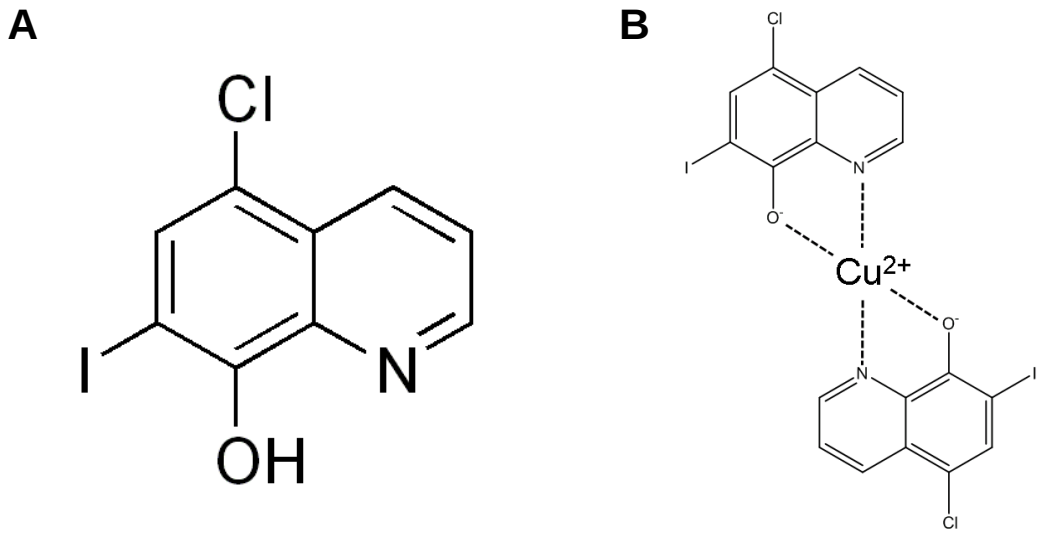

Figure 7: A) Chemical structure of Clioquinol (CQ) featuring electronegative hydroxyl and pyridine nitrogen groups which facilitates chelation to metal ions Zn^{2+} and Cu^{2+} among others. B) CQ in chelation complex with Cu^{2+}.

CQ found its original use back in 1934, where it was prescribed as an antiamebicide agent, and was also used later in treating acrodermatitis enteropathica, an intestinal zinc uptake disorder (162). In both uses, the therapeutic mechanism was found to be based upon the shuttling of metal ions zinc and copper across biological membranes (162).

Since that time however, CQ has been shown to elicit positive outcomes with regards to AD mouse models. A nine week treatment with CQ on APP2576 transgenic mice (an AD mouse model that overexpresses a mutant form of amyloid precursor protein, resulting in elevated levels of Aβ and eventually Aβ plaques), produced remarkably, a 49% reduction in Aβ brain deposition (163). The same study also demonstrated that CQ was able to block H_2O_2 production in vitro, prevent precipitation of Aβ by Zn^{2+} and Cu^{2+}, and was able to dissolve Aβ from post-mortem AD brain samples (163). This initial positive outcome utilizing CQ in the treatment of AD has gained popular momentum, with many studies attempting to elucidate the exact mechanisms of CQ and the concept of ionophores in general. Later studies showed that CQ and its sister compound PBT2 can transport extracellular Zn^{2+} and Cu^{2+} ions across cell membranes into the interior of neurones, where they are then free to interact with cell signalling pathways such as those involving GSK3β (158). This work however has been executed in neurons, and whether similar mechanisms are feasible in brain endothelial cells has not yet been explored.

Since CQ has been demonstrated to successfully increase intracellular metal ion levels in several cell types, and since it has been shown elsewhere that increasing biometal exposure in brain endothelial cells increases empirical measures of BBB integrity in both in vitro and in vivo settings, whether or not enhanced biometal delivery to the brain endothelium can affect the expression or function of BBB transporters such as P-gp, represents an opening in the literature which may be feasibly explored. This exploration forms the basis of the work carried out in this thesis and is expressed in the form of specific hypotheses and aims in the following section.

OVERVIEW OF RESEARCH PROJECT

Hypotheses of the project:

The overarching hypothesis of this project is that CQ in combination with biometals can enhance the delivery of copper or zinc ions to the cytosol of brain endothelial cells, where these ions may, either alone or complexed with CQ, modulate P-gp expression and function in both in vitro and in vivo settings.

Specific hypotheses of the research project:

1. That CQ is able to deliver enhanced quantities of zinc and/or copper ions to the cytosol of human brain endothelial cells

2. That CQ and metal ion treatments increase the expression of P-gp in brain endothelial cells

3. That the observed CQ/metal ion-mediated upregulation of P-gp will lead to enhanced P-gp activity

4. That administration of CQ to mice will lead to increased BBB expression of P-gp in vivo

Aims of the research project:

1. To develop and optimise a western blot procedure for accurate quantitation of P-gp derived from hCMEC/D3 cells and in vivo tissue lysates

2. To develop and validate a higher-throughput immunohistochemistry-based method for the quantitative assessment of relative P-gp abundance derived from hCMEC/D3 cells

3. To identify appropriate concentrations of CQ, Zn^{2+} and Cu^{2+} that can be tolerated by hCMEC/D3 cells

4. To use both of the P-gp quantitation methods described above to assess any alterations in P-gp expression and function in vitro, following CQ, Zn^{2+} and Cu^{2+} administration

5. To measure altered metal ion concentrations in the cytosol of brain endothelial cells after treatment with CQ and the biometals Zn^{2+} and Cu^{2+}

6. To observe differences in brain endothelial transporter expression profiles resulting from CQ treatment in vivo

7. To characterise changes in metal ion concentrations in barrier tissues in vivo, following CQ administration

Overall significance of project:

By addressing the aims of this project, improved insight into the role of biometals in the regulation of a biologically important transporter will be achieved. Such insights could lead to pharmacological approaches for modulating P-gp expression in vivo, with potential applications in CNS drug access, and possibly for the clearance of the Aβ peptide from the AD-afflicted brain. Furthermore, a better understanding of the pharmacological mechanisms of action of the clinically used drug CQ will be developed, and may influence future drug discovery. The capabilities of ionophore drugs and biometals with regards to the neurovasculature and within the context of neurodegenerative disorders will also be identified, and will inform future work with ionophore drugs, as well as confirm the importance of biometals in endothelial transporter expression profiles.

Organisation of the thesis:

Chapter 1 – Introduction and literature review, with excerpts from a published review: "*Neurovascular alterations in Alzheimer's disease: transporter expression profiles and CNS drug access*"

Chapter 2 - Optimisation of western blotting for P-glycoprotein quantification

Chapter 3 - Published work: "*Development and validation of an in-cell western for quantifying P-glycoprotein expression in human brain microvascular endothelial (hCMEC/D3) cells*"

Chapter 4 - Published work: "*Ionophore and biometal modulation of P-glycoprotein expression and function in human brain microvascular endothelial cells*"

Chapter 5 - Work being prepared for submission: "*Effects of clioquinol on biometal distribution and P-glycoprotein expression in various tissues in mice*"

Chapter 6 - Summary and future directions

REFERENCES

1. Dong J, Yang G, McHaourab HS. Structural basis of energy transduction in the transport cycle of MsbA. Science. 2005;308(5724):1023-1028.
2. Hawkins BT, Davis TP. The blood-brain barrier/neurovascular unit in health and disease. Pharmacol Rev. 2005;57(2):173-185.
3. McInerney MP, Short JL, Nicolazzo JA. Neurovascular alterations in Alzheimer's disease: transporter expression profiles and CNS drug access. AAPS J. 2017;19(4):940-956.
4. Kniesel U, Wolburg H. Tight junctions of the blood-brain barrier. Cell Mol Neurobiol. 2000;20(1):57-76.
5. Nicolazzo JA, Charman SA, Charman WN. Methods to assess drug permeability across the blood-brain barrier. J Pharm Pharmacol. 2006;58(3):281-293.
6. Fenstermacher J, Gross P, Sposito N, Acuff V, Pettersen S, Gruber K. Structural and functional variations in capillary systems within the brain. Ann N Y Acad Sci. 1988;529:21-30.
7. Oldendorf WH, Cornford ME, Brown WJ. The large apparent work capability of the blood-brain barrier: a study of the mitochondrial content of capillary endothelial cells in brain and other tissues of the rat. Ann Neurol. 1977;1(5):409-417.
8. Shawahna R, Decleves X, Scherrmann JM. Hurdles with using in vitro models to predict human blood-brain barrier drug permeability: a special focus on transporters and metabolizing enzymes. Curr Drug Metab. 2013;14(1):120-136.
9. Erickson MA, Banks WA. Blood-brain barrier dysfunction as a cause and consequence of Alzheimer's disease. J Cereb Blood Flow Metab. 2013;33(10):1500-1513.

10. Campos-Bedolla P, Walter FR, Veszelka S, Deli MA. Role of the blood-brain barrier in the nutrition of the central nervous system. Arch Med Res. 2014;45(8):610-638.

11. Spector R, Johanson CE. Vitamin transport and homeostasis in mammalian brain: focus on Vitamins B and E. J Neurochem. 2007;103(2):425-438.

12. O'Kane RL, Martinez-Lopez I, DeJoseph MR, Vina JR, Hawkins RA. Na(+)-dependent glutamate transporters (EAAT1, EAAT2, and EAAT3) of the blood-brain barrier. A mechanism for glutamate removal. J Biol Chem. 1999;274(45):31891-31895.

13. Morris ME, Rodriguez-Cruz V, Felmlee MA. SLC and ABC transporters: expression, localization, and species differences at the blood-brain and the blood-cerebrospinal fluid barriers. AAPS J. 2017;19(5):1317-1331.

14. Zheng W, Monnot AD. Regulation of brain iron and copper homeostasis by brain barrier systems: implication in neurodegenerative diseases. Pharmacol Ther. 2012;133(2):177-188.

15. Ueno M, Nakagawa T, Wu B, Onodera M, Huang CL, Kusaka T, Araki N, Sakamoto H. Transporters in the brain endothelial barrier. Curr Med Chem. 2010;17(12):1125-1138.

16. Winkler EA, Bell RD, Zlokovic BV. Central nervous system pericytes in health and disease. Nat Neurosci. 2011;14(11):1398-1405.

17. Matsson P, Pedersen JM, Norinder U, Bergstrom CA, Artursson P. Identification of novel specific and general inhibitors of the three major human ATP-binding cassette transporters P-gp, BCRP and MRP2 among registered drugs. Pharm Res. 2009;26(8):1816-1831.

18. Banks WA. Brain meets body: the blood-brain barrier as an endocrine interface. Endocrinology. 2012;153(9):4111-4119.

19. Beuckmann CT, Dernbach K, Hakvoort A, Galla HJ. A new astrocytic cell line which is able to induce a blood-brain barrier property in cultured brain capillary endothelial cells. Cytotechnology. 1997;24(1):11-17.

20. Deane R, Sagare A, Hamm K, Parisi M, Lane S, Finn MB, Holtzman DM, Zlokovic BV. ApoE isoform-specific disruption of amyloid beta peptide clearance from mouse brain. J Clin Invest. 2008;118(12):4002-4013.

21. Atwood CS, Perry G, Zeng H, Kato Y, Jones WD, Ling KQ, Huang X, Moir RD, Wang D, Sayre LM, Smith MA, Chen SG, Bush AI. Copper mediates dityrosine cross-linking of Alzheimer's amyloid-beta. Biochemistry. 2004;43(2):560-568.

22. Muoio V, Persson PB, Sendeski MM. The neurovascular unit - concept review. Acta Physiol (Oxf). 2014;210(4):790-798.

23. Boado RJ, Pardridge WM. Glucose deprivation and hypoxia increase the expression of the GLUT1 glucose transporter via a specific mRNA cis-acting regulatory element. J Neurochem. 2002;80(3):552-554.

24. Boroujerdi A, Welser-Alves JV, Milner R. Matrix metalloproteinase-9 mediates post-hypoxic vascular pruning of cerebral blood vessels by degrading laminin and claudin-5. Angiogenesis. 2015;18(3):255-264.

25. Sun L, Hui AM, Su Q, Vortmeyer A, Kotliarov Y, Pastorino S, Passaniti A, Menon J, Walling J, Bailey R, Rosenblum M, Mikkelsen T, Fine HA. Neuronal and glioma-derived stem cell factor induces angiogenesis within the brain. Cancer Cell. 2006;9(4):287-300.

26. Mae M, Armulik A, Betsholtz C. Getting to know the cast - cellular interactions and signaling at the neurovascular unit. Curr Pharm Des. 2011;17(26):2750-2754.

27. Thanabalasundaram G, Pieper C, Lischper M, Galla HJ. Regulation of the blood-brain barrier integrity by pericytes via matrix metalloproteinases mediated activation of vascular endothelial growth factor in vitro. Brain Res. 2010;1347:1-10.

28. Estrada C, Bready JV, Berliner JA, Pardridge WM, Cancilla PA. Astrocyte growth stimulation by a soluble factor produced by cerebral endothelial cells in vitro. J Neuropathol Exp Neurol. 1990;49(6):539-549.

29. Ali A, Hoeflich KP, Woodgett JR. Glycogen synthase kinase-3: properties, functions, and regulation. Chem Rev. 2001;101(8):2527-2540.

30. Plane JM, Andjelkovic AV, Keep RF, Parent JM. Intact and injured endothelial cells differentially modulate postnatal murine forebrain neural stem cells. Neurobiol Dis. 2010;37(1):218-227.

31. Karamanos Y, Gosselet F, Dehouck MP, Cecchelli R. Blood-brain barrier proteomics: towards the understanding of neurodegenerative diseases. Arch Med Res. 2014;45(8):730-737.

32. Jones PM, George AM. The ABC transporter structure and mechanism: perspectives on recent research. Cell Mol Life Sci. 2004;61(6):682-699.

33. ter Beek J, Guskov A, Slotboom DJ. Structural diversity of ABC transporters. J Gen Physiol. 2014;143(4):419-435.

34. Hollenstein K, Dawson RJ, Locher KP. Structure and mechanism of ABC transporter proteins. Curr Opin Struct Biol. 2007;17(4):412-418.

35. Hollenstein K, Frei DC, Locher KP. Structure of an ABC transporter in complex with its binding protein. Nature. 2007;446(7132):213-216.

36. Holland IB. ABC transporters, mechanisms and biology: an overview. Essays Biochem. 2011;50(1):1-17.

37. Quazi F, Molday RS. Differential phospholipid substrates and directional transport by ATP-binding cassette proteins ABCA1, ABCA7, and ABCA4 and disease-causing mutants. J Biol Chem. 2013;288(48):34414-34426.

38. Tarr PT, Tarling EJ, Bojanic DD, Edwards PA, Baldan A. Emerging new paradigms for ABCG transporters. Biochim Biophys Acta. 2009;1791(7):584-593.

39. Baker A, Carrier DJ, Schaedler T, Waterham HR, van Roermund CW, Theodoulou FL. Peroxisomal ABC transporters: functions and mechanism. Biochem Soc Trans. 2015;43(5):959-965.

40. Moitra K, Silverton L, Limpert K, Im K, Dean M. Moving out: from sterol transport to drug resistance - the ABCG subfamily of efflux pumps. Drug Metabol Drug Interact. 2011;26(3):105-111.

41. Marquez B, Van Bambeke F. ABC multidrug transporters: target for modulation of drug pharmacokinetics and drug-drug interactions. Curr Drug Targets. 2011;12(5):600-620.

42. Wang B, Dukarevich M, Sun EI, Yen MR, Saier MH, Jr. Membrane porters of ATP-binding cassette transport systems are polyphyletic. J Membr Biol. 2009;231(1):1-10.

43. Juliano RL, Ling V. A surface glycoprotein modulating drug permeability in Chinese hamster ovary cell mutants. Biochim Biophys Acta. 1976;455(1):152-162.

44. Cordon-Cardo C, O'Brien JP, Casals D, Rittman-Grauer L, Biedler JL, Melamed MR, Bertino JR. Multidrug-resistance gene (P-glycoprotein) is expressed by endothelial cells at blood-brain barrier sites. Proc Natl Acad Sci U S A. 1989;86(2):695-698.

45. Chin JE, Soffir R, Noonan KE, Choi K, Roninson IB. Structure and expression of the human MDR (P-glycoprotein) gene family. Mol Cell Biol. 1989;9(9):3808-3820.

46. Thiebaut F, Tsuruo T, Hamada H, Gottesman MM, Pastan I, Willingham MC. Cellular localization of the multidrug-resistance gene product P-glycoprotein in normal human tissues. Proc Natl Acad Sci U S A. 1987;84(21):7735-7738.

47. Thorgeirsson SS, Huber BE, Sorrell S, Fojo A, Pastan I, Gottesman MM. Expression of the multidrug-resistant gene in hepatocarcinogenesis and regenerating rat liver. Science. 1987;236(4805):1120-1122.

48. Silva R, Vilas-Boas V, Carmo H, Dinis-Oliveira RJ, Carvalho F, de Lourdes Bastos M, Remiao F. Modulation of P-glycoprotein efflux pump: induction and activation as a therapeutic strategy. Pharmacol Ther. 2015;149:1-123.

49. Callaghan R. Providing a molecular mechanism for P-glycoprotein; why would I bother? Biochem Soc Trans. 2015;43(5):995-1002.

50. Bugde P, Biswas R, Merien F, Lu J, Liu DX, Chen M, Zhou S, Li Y. The therapeutic potential of targeting ABC transporters to combat multi-drug resistance. Expert Opin Ther Targets. 2017;21(5):511-530.

51. Nicolazzo JA, Banks WA. Decreased blood-brain barrier expression of P-glycoprotein in Alzheimer's disease: impact on pathogenesis and brain access of therapeutic agents. Ther Deliv. 2011;2(7):841-844.

52. Schinkel AH, Mol CA, Wagenaar E, van Deemter L, Smit JJ, Borst P. Multidrug resistance and the role of P-glycoprotein knockout mice. Eur J Cancer. 1995;31A(7-8):1295-1298.

53. Lagas JS, Vlaming ML, Schinkel AH. Pharmacokinetic assessment of multiple ATP-binding cassette transporters: the power of combination knockout mice. Mol Interv. 2009;9(3):136-145.

54. Borst P, Schinkel AH. P-glycoprotein ABCB1: a major player in drug handling by mammals. J Clin Invest. 2013;123(10):4131-4133.

55. Ma SC, Li Q, Peng JY, Zhouwen JL, Diao JF, Niu JX, Wang X, Guan XD, Jia W, Jiang WG. Claudin-5 regulates blood-brain barrier permeability by modifying brain microvascular endothelial cell proliferation, migration, and adhesion to prevent lung cancer metastasis. CNS Neurosci Ther. 2017;23(12):947-960.

56. Nicolazzo JA, Katneni K. Drug transport across the blood-brain barrier and the impact of breast cancer resistance protein (ABCG2). Curr Top Med Chem. 2009;9(2):130-147.

57. Callaghan R, Luk F, Bebawy M. Inhibition of the multidrug resistance P-glycoprotein: time for a change of strategy? Drug Metab Dispos. 2014;42(4):623-631.

58. Schinkel AH, Wagenaar E, van Deemter L, Mol CA, Borst P. Absence of the MDR1a P-Glycoprotein in mice affects tissue distribution and pharmacokinetics of dexamethasone, digoxin, and cyclosporin A. J Clin Invest. 1995;96(4):1698-1705.

59. Kim RB, Fromm MF, Wandel C, Leake B, Wood AJ, Roden DM, Wilkinson GR. The drug transporter P-glycoprotein limits oral absorption and brain entry of HIV-1 protease inhibitors. J Clin Invest. 1998;101(2):289-294.

60. Schinkel AH, Smit JJ, van Tellingen O, Beijnen JH, Wagenaar E, van Deemter L, Mol CA, van der Valk MA, Robanus-Maandag EC, te Riele HP, et al. Disruption of the mouse MDR1a P-glycoprotein gene leads to a deficiency in the blood-brain barrier and to increased sensitivity to drugs. Cell. 1994;77(4):491-502.

61. Schinkel AH, Wagenaar E, Mol CA, van Deemter L. P-glycoprotein in the blood-brain barrier of mice influences the brain penetration and pharmacological activity of many drugs. J Clin Invest. 1996;97(11):2517-2524.

62. Kusuhara H, Suzuki H, Terasaki T, Kakee A, Lemaire M, Sugiyama Y. P-Glycoprotein mediates the efflux of quinidine across the blood-brain barrier. J Pharmacol Exp Ther. 1997;283(2):574-580.

63. Tamai I, Yamashita J, Kido Y, Ohnari A, Sai Y, Shima Y, Naruhashi K, Koizumi S, Tsuji A. Limited distribution of new quinolone antibacterial agents into brain caused by multiple efflux transporters at the blood-brain barrier. J Pharmacol Exp Ther. 2000;295(1):146-152.

64. Hendrikse NH, Schinkel AH, de Vries EG, Fluks E, Van der Graaf WT, Willemsen AT, Vaalburg W, Franssen EJ. Complete in vivo reversal of P-glycoprotein pump function in the blood-brain barrier visualized with positron emission tomography. Br J Pharmacol. 1998;124(7):1413-1418.

65. Atadja P, Watanabe T, Xu H, Cohen D. PSC-833, a frontier in modulation of P-glycoprotein mediated multidrug resistance. Cancer Metastasis Rev. 1998;17(2):163-168.

66. Davis TP, Sanchez-Covarubias L, Tome ME. P-glycoprotein trafficking as a therapeutic target to optimize CNS drug delivery. Adv Pharmacol. 2014;71:25-44.

67. Thomas H, Coley HM. Overcoming multidrug resistance in cancer: an update on the clinical strategy of inhibiting p-glycoprotein. Cancer Control. 2003;10(2):159-165.

68. Palmeira A, Sousa E, Vasconcelos MH, Pinto MM. Three decades of P-gp inhibitors: skimming through several generations and scaffolds. Curr Med Chem. 2012;19(13):1946-2025.

69. Chiu C, Miller MC, Monahan R, Osgood DP, Stopa EG, Silverberg GD. P-glycoprotein expression and amyloid accumulation in human aging and Alzheimer's disease: preliminary observations. Neurobiol Aging. 2015;36(9):2475-2482.

70. Montagne A, Barnes SR, Sweeney MD, Halliday MR, Sagare AP, Zhao Z, Toga AW, Jacobs RE, Liu CY, Amezcua L, Harrington MG, Chui HC, Law M, Zlokovic BV. Blood-brain barrier breakdown in the aging human hippocampus. Neuron. 2015;85(2):296-302.

71. Ueno M, Akiguchi I, Hosokawa M, Shinnou M, Sakamoto H, Takemura M, Higuchi K. Age-related changes in barrier function in mouse brain II. Accumulation of serum albumin in the olfactory bulb of SAM mice increased with aging. Arch Gerontol Geriatr. 1997;25(3):321-331.

72. Vautier S, Fernandez C. ABCB1: the role in Parkinson's disease and pharmacokinetics of antiparkinsonian drugs. Expert Opin Drug Metab Toxicol. 2009;5(11):1349-1358.

73. Feldmann M, Asselin MC, Liu J, Wang S, McMahon A, Anton-Rodriguez J, Walker M, Symms M, Brown G, Hinz R, Matthews J, Bauer M, Langer O, Thom M, Jones T, Vollmar C, Duncan JS, Sisodiya SM, Koepp MJ. P-glycoprotein expression and function in patients with temporal lobe epilepsy: a case-control study. Lancet Neurol. 2013;12(8):777-785.

74. Qosa H, Lichter J, Sarlo M, Markandaiah SS, McAvoy K, Richard JP, Jablonski MR, Maragakis NJ, Pasinelli P, Trotti D. Astrocytes drive upregulation of the multidrug resistance transporter ABCB1 (P-Glycoprotein) in endothelial cells of the blood-brain barrier in mutant superoxide dismutase 1-linked amyotrophic lateral sclerosis. Glia. 2016;64(8):1298-1313.

75. Housman G, Byler S, Heerboth S, Lapinska K, Longacre M, Snyder N, Sarkar S. Drug resistance in cancer: an overview. Cancers (Basel). 2014;6(3):1769-1792.

76. Williams GH, Stoeber K. The cell cycle and cancer. J Pathol. 2012;226(2):352-364.

77. Abolhoda A, Wilson AE, Ross H, Danenberg PV, Burt M, Scotto KW. Rapid activation of MDR1 gene expression in human metastatic sarcoma after in vivo exposure to doxorubicin. Clin Cancer Res. 1999;5(11):3352-3356.

78. Vaupel JW. Biodemography of human ageing. Nature. 2010;464(7288):536-542.

79. Guerreiro R, Bras J. The age factor in Alzheimer's disease. Genome Med. 2015;7:106.

80. Prince M, Wimo A, Guerchet M, Ali GC, Wu YT, M P. World Alzheimer report 2015, the global impact of dementia: an analysis of prevalence, incidence, cost and trends. In.: Global observatory for ageing and dementia care - King's college London; 2015.

81. Becker JT. Working memory and secondary memory deficits in Alzheimer's disease. J Clin Exp Neuropsychol. 1988;10(6):739-753.

82. Folstein MF, Whitehouse PJ. Cognitive impairment of Alzheimer disease. Neurotoxicol Teratol. 1983;5(6):631-634.

83. Henry JD, Crawford JR, Phillips LH. Verbal fluency performance in dementia of the Alzheimer's type: a meta-analysis. Neuropsychologia. 2004;42(9):1212-1222.

84. Verma M, Howard RJ. Semantic memory and language dysfunction in early Alzheimer's disease: a review. Int J Geriatr Psychiatry. 2012;27(12):1209-1217.

85. Galeone F, Pappalardo S, Chieffi S, Iavarone A, Carlomagno S. Anosognosia for memory deficit in amnestic mild cognitive impairment and Alzheimer's disease. Int J Geriatr Psychiatry. 2011;26(7):695-701.

86. Dr Henry Cutler DC, Rebecca McKibbin, Simone Cheung and Lynne Pezzullo. Caring places: planning for aged care and dementia 2010-2050. . In.: Access Economics Pty Limited for Alzheimer's Australia; 2010.

87. Strobel G. What is early onset familial Alzheimer disease (eFAD). Alzforum. 2017 Available from: http://www.alzforum.org/early-onset-familial-ad/overview/what-early-onset-familial-alzheimer-disease-efad.

88. Waring SC, Doody RS, Pavlik VN, Massman PJ, Chan W. Survival among patients with dementia from a large multi-ethnic population. Alzheimer Dis Assoc Disord. 2005;19(4):178-183.

89. Ryman DC, Acosta-Baena N, Aisen PS, Bird T, Danek A, Fox NC, Goate A, Frommelt P, Ghetti B, Langbaum JB, Lopera F, Martins R, Masters CL, Mayeux RP, McDade E,

Moreno S, Reiman EM, Ringman JM, Salloway S, Schofield PR, Sperling R, Tariot PN, Xiong C, Morris JC, Bateman RJ. Symptom onset in autosomal dominant Alzheimer disease: a systematic review and meta-analysis. Neurology. 2014;83(3):253-260.

90. Jin M, Shepardson N, Yang T, Chen G, Walsh D, Selkoe DJ. Soluble amyloid beta-protein dimers isolated from Alzheimer cortex directly induce Tau hyperphosphorylation and neuritic degeneration. Proc Natl Acad Sci U S A. 2011;108(14):5819-5824.

91. Alzhiemer A. Über einen eigenartigen schweren Erkrankungsprozeß der Hirnrinde. Neurologisches Centralblatt. 1906;23:1129-1136.

92. Glenner GG, Wong CW. Alzheimer's disease: Initial report of the purification and characterization of a novel cerebrovascular amyloid protein. Biochem Biophys Res Commun. 1984;120(3):885-890.

93. Colin L. Masters GS, Nicola A. Weinman, Gerd Multhaup, Brian L. Mcdonald, And Konrad Beyreuther Amyloid plaque core protein in Alzheimer disease and Down syndrome. Proc Natl Acad Sci U S A. 1985;82:4245-4249.

94. Lue LF, Kuo YM, Roher AE, Brachova L, Shen Y, Sue L, Beach T, Kurth JH, Rydel RE, Rogers J. Soluble amyloid beta peptide concentration as a predictor of synaptic change in Alzheimer's disease. Am J Pathol. 1999;155(3):853-862.

95. McLean CA, Cherny RA, Fraser FW, Fuller SJ, Smith MJ, Beyreuther K, Bush AI, Masters CL. Soluble pool of Abeta amyloid as a determinant of severity of neurodegeneration in Alzheimer's disease. Ann Neurol. 1999;46(6):860-866.

96. Hartmann T, Bieger SC, Bruhl B, Tienari PJ, Ida N, Allsop D, Roberts GW, Masters CL, Dotti CG, Unsicker K, Beyreuther K. Distinct sites of intracellular production for Alzheimer's disease abeta40/42 amyloid peptides. Nat Med. 1997;3(9):1016-1020.

97. Walsh DM, Selkoe DJ. A beta oligomers - a decade of discovery. J Neurochem. 2007;101(5):1172-1184.

98. Wang J, Dickson DW, Trojanowski JQ, Lee VM. The levels of soluble versus insoluble brain abeta distinguish Alzheimer's disease from normal and pathologic aging. Exp Neurol. 1999;158(2):328-337.

99. Nukina N, Ihara Y. One of the antigenic determinants of paired helical filaments is related to tau protein. J Biochem. 1986;99(5):1541-1544.

100. Kenneth S. Kosik CLJ, and Dennis J. Selkoe. Microtubule-associated protein tau is a major antigenic component of paired helical filaments in Alzheimer disease. Proc Natl Acad Sci U S A. 1986;83:4044-4048.

101. Inge Grundke-Iqbal KI, Yunn-Chyn Tung, Maureen Quinlan, Henryk M. Wisniewski, And Lester I. Binder. Abnormal phosphorylation of the microtubule-associated protein Tau in Alzhiermer cytoskeletal pathology. Proc Natl Acad Sci U S A. 1986;83:4913-4917.

102. Akiyama H, Barger S, Barnum S, Bradt B, Bauer J, Cole GM, Cooper NR, Eikelenboom P, Emmerling M, Fiebich BL, Finch CE, Frautschy S, Griffin WS, Hampel H, Hull M, Landreth G, Lue L, Mrak R, Mackenzie IR, McGeer PL, O'Banion MK, Pachter J, Pasinetti G, Plata-Salaman C, Rogers J, Rydel R, Shen Y, Streit W, Strohmeyer R, Tooyoma I, Van Muiswinkel FL, Veerhuis R, Walker D, Webster S, Wegrzyniak B, Wenk G, Wyss-Coray T. Inflammation and Alzheimer's disease. Neurobiol Aging. 2000;21(3):383-421.

103. Swardfager W, Lanctot K, Rothenburg L, Wong A, Cappell J, Herrmann N. A meta-analysis of cytokines in Alzheimer's disease. Biol Psychiatry. 2010;68(10):930-941.

104. Cherny RA, Legg JT, McLean CA, Fairlie DP, Huang X, Atwood CS, Beyreuther K, Tanzi RE, Masters CL, Bush AI. Aqueous dissolution of Alzheimer's disease Abeta amyloid deposits by biometal depletion. J Biol Chem. 1999;274(33):23223-23228.

105. Markesbery WR. Oxidative stress hypothesis in Alzheimer's disease. Free Radic Biol Med. 1997;23(1):134-147.

106. Nilsson L, Nordberg A, Hardy J, Wester P, Winblad B. Physostigmine restores 3H-acetylcholine efflux from Alzheimer brain slices to normal level. J Neural Transmission. 1986;67(3-4):275-285.

107. Uylings HBM, de Brabander JM. Neuronal changes in normal human aging and Alzheimer's disease. Brain Cogn. 2002;49(3):268-276.

108. Cirrito JR, Deane R, Fagan AM, Spinner ML, Parsadanian M, Finn MB, Jiang H, Prior JL, Sagare A, Bales KR, Paul SM, Zlokovic BV, Piwnica-Worms D, Holtzman DM. P-glycoprotein deficiency at the blood-brain barrier increases amyloid-beta deposition in an Alzheimer disease mouse model. J Clin Invest. 2005;115(11):3285-3290.

109. Mawuenyega KG, Sigurdson W, Ovod V, Munsell L, Kasten T, Morris JC, Yarasheski KE, Bateman RJ. Decreased clearance of CNS -amyloid in Alzheimer's disease. Science. 2010;330(6012):1774-1774.

110. SanMartín CD, Paula-Lima AC, Hidalgo C, Núñez MT. Sub-lethal levels of amyloid β-peptide oligomers decrease non-transferrin-bound iron uptake and do not potentiate iron toxicity in primary hippocampal neurons. BioMetals. 2012;25(4):805-813.

111. Iliff JJ, Wang M, Liao Y, Plogg BA, Peng W, Gundersen GA, Benveniste H, Vates GE, Deane R, Goldman SA, Nagelhus EA, Nedergaard M. A paravascular pathway facilitates CSF flow through the brain parenchyma and the clearance of interstitial solutes, including amyloid beta. Sci Transl Med. 2012;4(147):147ra111.

112. Rembach A, Faux NG, Watt AD, Pertile KK, Rumble RL, Trounson BO, Fowler CJ, Roberts BR, Perez KA, Li QX, Laws SM, Taddei K, Rainey-Smith S, Robertson JS, Vandijck M, Vanderstichele H, Barnham KJ, Ellis KA, Szoeke C, Macaulay L, Rowe CC, Villemagne VL, Ames D, Martins RN, Bush AI, Masters CL. Changes in plasma amyloid beta in a longitudinal study of aging and Alzheimer's disease. Alzheimers Dement. 2014;10(1):53-61.

113. Qosa H, Abuasal BS, Romero IA, Weksler B, Couraud PO, Keller JN, Kaddoumi A. Differences in amyloid-beta clearance across mouse and human blood-brain barrier models: Kinetic analysis and mechanistic modeling. Neuropharmacol. 2014;79C:668-678.

114. Kuhnke D, Jedlitschky G, Grube M, Krohn M, Jucker M, Mosyagin I, Cascorbi I, Walker LC, Kroemer HK, Warzok RW, Vogelgesang S. MDR1-P-Glycoprotein (ABCB1) Mediates Transport of Alzheimer's amyloid-beta peptides--implications for the mechanisms of Abeta clearance at the blood-brain barrier. Brain Pathol. 2007;17(4):347-353.

115. Wang W, Bodles-Brakhop AM, Barger SW. A role for P-glycoprotein in clearance of Alzheimer amyloid beta -peptide from the Brain. Curr Alzheimer Res. 2016;13(6):615-620.

116. Shibata M, Yamada S, Kumar SR, Calero M, Bading J, Frangione B, Holtzman DM, Miller CA, Strickland DK, Ghiso J, Zlokovic BV. Clearance of Alzheimer's amyloid-ss(1-40) peptide from brain by LDL receptor-related protein-1 at the blood-brain barrier. J Clin Invest. 2000;106(12):1489-1499.

117. Deane R, Wu Z, Sagare A, Davis J, Du Yan S, Hamm K, Xu F, Parisi M, LaRue B, Hu HW, Spijkers P, Guo H, Song X, Lenting PJ, Van Nostrand WE, Zlokovic BV.

LRP/amyloid β-peptide interaction mediates differential brain efflux of Aβ isoforms. Neuron. 2004;43(3):333-344.

118. Deane R, Du Yan S, Submamaryan RK, LaRue B, Jovanovic S, Hogg E, Welch D, Manness L, Lin C, Yu J, Zhu H, Ghiso J, Frangione B, Stern A, Schmidt AM, Armstrong DL, Arnold B, Liliensiek B, Nawroth P, Hofman F, Kindy M, Stern D, Zlokovic B. RAGE mediates amyloid-beta peptide transport across the blood-brain barrier and accumulation in brain. Nat Med. 2003;9(7):907-913.

119. Yan SD, Chen X, Fu J, Chen M, Zhu H, Roher A, Slattery T, Zhao L, Nagashima M, Morser J, Migheli A, Nawroth P, Stern D, Schmidt AM. RAGE and amyloid-beta peptide neurotoxicity in Alzheimer's disease. Nature. 1996;382(6593):685-691.

120. Krohn M, Lange C, Hofrichter J, Scheffler K, Stenzel J, Steffen J, Schumacher T, Bruning T, Plath AS, Alfen F, Schmidt A, Winter F, Rateitschak K, Wree A, Gsponer J, Walker LC, Pahnke J. Cerebral amyloid-beta proteostasis is regulated by the membrane transport protein ABCC1 in mice. J Clin Invest. 2011;121(10):3924-3931.

121. Tai LM, Loughlin AJ, Male DK, Romero IA. P-glycoprotein and breast cancer resistance protein restrict apical-to-basolateral permeability of human brain endothelium to amyloid-beta. J Cereb Blood Flow Metab. 2009;29(6):1079-1083.

122. Abuznait AH, Kaddoumi A. Role of ABC transporters in the pathogenesis of Alzheimer's disease. ACS Chem Neurosci. 2012;3(11):820-831.

123. Clifford PM, Zarrabi S, Siu G, Kinsler KJ, Kosciuk MC, Venkataraman V, D'Andrea MR, Dinsmore S, Nagele RG. Abeta peptides can enter the brain through a defective blood-brain barrier and bind selectively to neurons. Brain Res. 2007;1142:223-236.

124. Maness LM, Banks WA, Podlisny MB, Selkoe DJ, Kastin AJ. Passage of human amyloid beta-protein 1-40 across the murine blood-brain barrier. Life Sci. 1994;55(21):1643-1650.

125. Martyn CN, Barker DJ, Osmond C, Harris EC, Edwardson JA, Lacey RF. Geographical relation between Alzheimer's disease and aluminum in drinking water. Lancet. 1989;1(8629):59-62.

126. Banks WA, Niehoff ML, Drago D, Zatta P. Aluminum complexing enhances amyloid beta protein penetration of blood-brain barrier. Brain Res. 2006;1116(1):215-221.

127. Pluta R, Barcikowska M, Januszewski S, Misicka A, Lipkowski AW. Evidence of blood-brain barrier permeability/leakage for circulating human Alzheimer's beta-amyloid-(1-42)-peptide. Neuroreport. 1996;7(7):1261-1265.

128. Kalaria RN. The role of cerebral ischemia in Alzheimer's disease. Neurobiol Aging. 2000;21(2):321-330.

129. Pluta R, Jablonski M, Ulamek-Koziol M, Kocki J, Brzozowska J, Januszewski S, Furmaga-Jablonska W, Bogucka-Kocka A, Maciejewski R, Czuczwar SJ. Sporadic Alzheimer's disease begins as episodes of brain ischemia and ischemically dysregulated Alzheimer's disease genes. Mol Neurobiol. 2013;48(3):500-515.

130. Vogelgesang S, Cascorbi I, Schroeder E, Pahnke J, Kroemer HK, Siegmund W, Kunert-Keil C, Walker LC, Warzok RW. Deposition of Alzheimer's beta-amyloid is inversely correlated with P-glycoprotein expression in the brains of elderly non-demented humans. Pharmacogenetics. 2002;12(7):535-541.

131. Wijesuriya HC, Bullock JY, Faull RL, Hladky SB, Barrand MA. ABC efflux transporters in brain vasculature of Alzheimer's subjects. Brain Res. 2010;1358:228-238.

132. Deo AK, Borson S, Link JM, Domino K, Eary JF, Ke B, Richards TL, Mankoff DA, Minoshima S, O'Sullivan F, Eyal S, Hsiao P, Maravilla K, Unadkat JD. Activity of P-glycoprotein, a beta-amyloid transporter at the blood-brain barrier, is compromised in patients with mild Alzheimer disease. J Nucl Med. 2014;55(7):1106-1111.

133. Hartz AM, Miller DS, Bauer B. Restoring blood-brain barrier P-glycoprotein reduces brain amyloid-beta in a mouse model of Alzheimer's disease. Mol Pharmacol. 2010;77(5):715-723.

134. Mehta DC, Short JL, Nicolazzo JA. Altered brain uptake of therapeutics in a triple transgenic mouse model of Alzheimer's disease. Pharm Res. 2013;30(11):2868-2879.

135. Goldsmith ME, Gudas JM, Schneider E, Cowan KH. Wild type p53 stimulates expression from the human multidrug resistance promoter in a p53-negative cell line. J Biol Chem. 1995;270(4):1894-1898.

136. Chen J, Ding Z, Peng Y, Pan F, Li J, Zou L, Zhang Y, Liang H. HIF-1alpha inhibition reverses multidrug resistance in colon cancer cells via downregulation of MDR1/P-glycoprotein. PLoS One. 2014;9(6):e98882.

137. Bargou RC, Jurchott K, Wagener C, Bergmann S, Metzner S, Bommert K, Mapara MY, Winzer KJ, Dietel M, Dorken B, Royer HD. Nuclear localization and increased levels of transcription factor YB-1 in primary human breast cancers are associated with intrinsic MDR1 gene expression. Nat Med. 1997;3(4):447-450.

138. Zhou G, Kuo MT. NF-kappaB-mediated induction of MDR1b expression by insulin in rat hepatoma cells. J Biol Chem. 1997;272(24):15174-15183.

139. Kliewer SA, Goodwin B, Willson TM. The nuclear pregnane X receptor: a key regulator of xenobiotic metabolism. Endocr Rev. 2002;23(5):687-702.

140. Jain S, Rathod V, Prajapati R, Nandekar PP, Sangamwar AT. Pregnane X receptor and P-glycoprotein: a connexion for Alzheimer's disease management. Mol Divers. 2014;18(4):895-909.

141. Lemmen J, Tozakidis IE, Galla HJ. Pregnane X receptor upregulates ABC-transporter ABCG2 and ABCB1 at the blood-brain barrier. Brain Res. 2013;1491:1-13.

142. Daneman R, Agalliu D, Zhou L, Kuhnert F, Kuo CJ, Barres BA. Wnt/beta-catenin signaling is required for CNS, but not non-CNS, angiogenesis. Proc Natl Acad Sci U S A. 2009;106(2):641-646.

143. Lammert E. Developmental biology. Brain Wnts for blood vessels. Science. 2008;322(5905):1195-1196.

144. Liebner S, Corada M, Bangsow T, Babbage J, Taddei A, Czupalla CJ, Reis M, Felici A, Wolburg H, Fruttiger M, Taketo MM, von Melchner H, Plate KH, Gerhardt H, Dejana E. Wnt/beta-catenin signaling controls development of the blood-brain barrier. J Cell Biol. 2008;183(3):409-417.

145. Polakis P. Formation of the blood-brain barrier: Wnt signaling seals the deal. J Cell Biol. 2008;183(3):371-373.

146. MacDonald BT, Tamai K, He X. Wnt/β-catenin signaling: components, mechanisms, and diseases. Developmental Cell. 2009;17(1):9-26.

147. Komiya Y, Habas R. Wnt signal transduction pathways. Organogenesis. 2008;4(2):68-75.

148. Harati R, Benech H, Villegier AS, Mabondzo A. P-glycoprotein, breast cancer resistance protein, organic anion transporter 3, and transporting peptide 1a4 during blood-brain barrier maturation: involvement of Wnt/beta-catenin and endothelin-1 signaling. Mol Pharm. 2013;10(5):1566-1580.

149. Shen DY, Zhang W, Zeng X, Liu CQ. Inhibition of Wnt/beta-catenin signaling downregulates P-glycoprotein and reverses multi-drug resistance of cholangiocarcinoma. Cancer Sci. 2013;104(10):1303-1308.

150. Ma T. GSK3 in Alzheimer's disease: mind the isoforms. J Alzheimers Dis. 2014;39(4):707-710.

151. Song Y, Xue Y, Liu X, Wang P, Liu L. Effects of acute exposure to aluminum on blood-brain barrier and the protection of zinc. Neurosci Lett. 2008;445(1):42-46.

152. Hennig B, Wang Y, Ramasamy S, McClain CJ. Zinc deficiency alters barrier function of cultured porcine endothelial cells. J Nutr. 1992;122(6):1242-1247.

153. Li QF, Ding XQ, Kang YJ. Copper promotion of angiogenesis in isolated rat aortic ring: role of vascular endothelial growth factor. J Nutr Biochem. 2014;25(1):44-49.

154. Wang J, Chen J, Tang Z, Li Y, Hu L, Pan J. The effects of copper on brain microvascular endothelial cells and claudin via apoptosis and oxidative stress. Biol Trace Elem Res. 2016;174(1):132-141.

155. Lu SY, Huang ZM, Huang WK, Liu XY, Chen YY, Shi T, Zhang J. How calcium inhibits the magnesium-dependent kinase GSK3beta: a molecular simulation study. Proteins. 2013;81(5):740-753.

156. Ryves WJ, Dajani R, Pearl L, Harwood AJ. Glycogen synthase kinase-3 inhibition by lithium and beryllium suggests the presence of two magnesium binding sites. Biochem Biophys Res Commun. 2002;290(3):967-972.

157. Ryves WJ, Harwood AJ. Lithium inhibits glycogen synthase kinase-3 by competition for magnesium. Biochem Biophys Res Commun. 2001;280(3):720-725.

158. Crouch PJ, Savva MS, Hung LW, Donnelly PS, Mot AI, Parker SJ, Greenough MA, Volitakis I, Adlard PA, Cherny RA, Masters CL, Bush AI, Barnham KJ, White AR. The Alzheimer's therapeutic PBT2 promotes amyloid-beta degradation and GSK3 phosphorylation via a metal chaperone activity. J Neurochem. 2011;119(1):220-230.

159. Ding WQ, Lind SE. Metal ionophores - an emerging class of anticancer drugs. IUBMB Life. 2009;61(11):1013-1018.

160. Harris DC. Quantitative chemical analysis. New York, NY: W.H. Freeman and Co.; 2007.

161. Ferrada E, Arancibia V, Loeb B, Norambuena E, Olea-Azar C, Huidobro-Toro JP. Stoichiometry and conditional stability constants of Cu(II) or Zn(II) clioquinol complexes; implications for Alzheimer's and Huntington's disease therapy. Neurotoxicology. 2007;28(3):445-449.

162. Bareggi SR, Cornelli U. Clioquinol: review of its mechanisms of action and clinical uses in neurodegenerative disorders. CNS Neurosci Ther. 2012;18(1):41-46.

163. Cherny RA, Atwood CS, Xilinas ME, Gray DN, Jones WD, McLean CA, Barnham KJ, Volitakis I, Fraser FW, Kim Y, Huang X, Goldstein LE, Moir RD, Lim JT, Beyreuther K, Zheng H, Tanzi RE, Masters CL, Bush AI. Treatment with a copper-zinc chelator markedly and rapidly inhibits beta-amyloid accumulation in Alzheimer's disease transgenic mice. Neuron. 2001;30(3):665-676.

Chapter 2

Western blot optimisation for P-glycoprotein

ABSTRACT

Before western blotting (WB) can be used to quantify relative changes in protein expression, a protocol must be successfully developed that is capable of detecting and reporting such changes accurately. Although WB protocols for specific proteins of interest may already be reported, differential access to WB materials, and subsequently the existence of significant lab to lab variability, necessitates an in-house interrogation of the protocol at hand. Starting with a semi-developed protocol for immortalised human cerebral microvascular endothelial cell lysates, in this chapter multiple variables within the WB workflow were interrogated, including lysis buffer composition, blocking buffer selection, membrane selection and transfer buffer composition, with the aim of producing a standardised and robust protocol for the quantification of P-glycoprotein (P-gp) in hCMEC/D3 cells. The resulting protocol was assessed by linear regression of the linear dynamic range for P-gp signal, and an R^2 value of 0.95 was produced, indicating a sufficiently responsive method for P-gp quantification. Equally important to optimised WB technique are protein concentration assays, which serve as numeric input to the WB workflow to ensure equal protein loading in adjacent lanes of a WB. As such, the BCA protein assay kit was also interrogated for accuracy and precision, yielding satisfactory results (R^2 of standard curve = 0.99), and thus confidence in this method. The protocols developed and assessed herein, namely the western blot for P-gp and the BCA protein concentration assay, were judged as adequately developed techniques for use in all future experiments within the remainder of this thesis.

INTRODUCTION

The independent development of the western blotting (WB) method by the three scientists Towbin, Stark and Burnette in 1979, could be considered as a significant milestone in the development of modern biology (1-3). The need to quantify relative protein expression levels in both 1979 and in the modern era is near ubiquitous in all of the life sciences. The combination of both the apparent simplicity and the relative inexpensiveness of the WB technique, established WB early on as the preferred or most widely-used method of protein quantification for decades to come. The advent of this method allowed for a rapid expansion of data accumulation throughout the 1980s and 90s, greatly enhancing knowledge and understanding of cellular signalling, communication, metabolism, transport and structure. Particularly pertinent to this thesis, is the ability of WB to measure changes in protein expression resulting from pharmacological intervention in cell lines. The employment of WB to answer such research questions is extremely widespread within the biological sciences, but before these questions can be answered, it is essential for the WB protocol to be optimised to provide robust and valid data. The mass of proteins probed via WB can vary enormously in size, abundance, hydrophobicity, temperature stability, water solubility and membrane binding affinity, and so the conditions required for proper quantification of any given protein must first be identified. This thesis is primarily concerned with the relative abundance of P-glycoprotein (P-gp) in the human cerebral microvascular endothelial cell line (hCMEC/D3) and the regulation thereof, and as such this chapter outlines the brief optimisation process that was completed to establish a WB protocol that would yield valid and robust results. P-glycoprotein is a large (170 kDa) and hydrophobic transmembrane protein (4), which provides specific challenges during optimisation. Typically, larger proteins migrate more slowly during electrophoretic transfer, and transmembrane proteins being naturally hydrophobic by virtue of being located natively in

the lipid milieu of the plasma membrane, can also suffer from solubility and membrane binding issues (5).

For accurate, precise and meaningful interpretation of WB protein expression levels, uniform quantities of proteins from the various cell treatment samples must be loaded onto the gel. Without such uniform loading, any observed variance in protein quantities could not be deduced to result from the intended cell treatment strategies, but rather represent artefacts of sub-standard laboratory technique. Therefore the total protein concentration from each cell treatment being analysed must be determined before a WB can be reliably executed. For this purpose, the colourimetric bicinchoninic acid (BCA) assay was used to quantify protein concentrations within cellular lysates. In turn, the BCA assay itself must be validated as accurate and precise, as an extra measure of control over WB analyses. Therefore, the experimental section of this chapter opens with a brief validation of the BCA protein quantification assay, before presentation of the WB optimisation process for P-gp in hCMEC/D3 cells.

MATERIALS

Tween-20, sodium chloride, potassium chloride, disodium phosphate and potassium phosphate were all purchased from Sigma Aldrich (St Louis, MO). TRIS buffer salt (TRIZMA base), sodium dodecyl sulphate (SDS), ammonium persulfate, N,N,N',N'-tetramethylethylenediamine (TEMED), trypan blue, glycerol, Hank's balanced salt solution (HBSS), trypsin-EDTA solution 0.25% in HBSS and Dulbecco's sterile phosphate buffered saline (PBS) were all purchased from Sigma Life Sciences (St Louis, MO). 40% Acrylamide/bis solution and *Dual Xtra Precision Plus Protein Prestained Standards* was purchased from Bio-Rad Laboratories (Hercules, CA). *Licor Odyssey blocking buffer* and the

IR dye 800CW goat anti-mouse IgG antibody were both purchased from Millennium Science (Mulgrave, Victoria, Australia). *cOmplete Tablets Mini EASY pack* protease inhibitors were purchased from Roche Diagnostics GmbH (Mannheim, Germany). Nitrocellulose membrane (0.2 µm pore-sized) was purchased from GE Life Sciences (Rydalmere, New South Wales, Australia). The C219 P-gp antibody was purchased from Australian Biosearch (Balcatta, Western Australia, Australia). Corning Costar transparent 96 well plates were purchased from Invitro (Noble Park North, Victoria, Australia). The *Pierce BCA protein assay kit* and *Pierce IP lysis buffer* were purchased from Thermo Fisher Scientific (Scoresby, Victoria, Australia). The hCMEC/D3 cells were generously provided by Dr Pierre-Olivier Couraud (INSERM, Paris, France). Both Clonetics EBM-2 basal media and Clonetics EGM-2 single quots growth factor kits were purchased from Lonza (Walkersville, MD). Collagen type I was purchased from Corning Discovery Labware (Bedford, MD). Sterile cell-culture treated 6-well plates were purchased from Corning Incorporated (Corning, NY). T75 Greiner Cellstar flasks were purchased from Interpath (Heidelberg West, Victoria, Australia).

METHODS

Culturing of hCMEC/D3 cells

Vials of the hCMEC/D3 cell line were kept cryogenically frozen in liquid nitrogen in a solution comprised of 5% (v/v) DMSO in heat inactivated FBS solution. Before defrosting cells, T75 flasks were pre-coated with 3 mL of a 0.1 mg/mL solution of collagen type I and incubated for 1 h, before being washed with 10 mL of PBS, to remove any excess collagen. Vials containing ~2 million cells in 1 mL of the above described cryo-storage solution were dispensed into T75 flasks containing 14 mL of EBM2 media. Following a 2 h wait after seeding, the EBM2 media was aspirated off and replaced with freshly warmed media EBM2 media to remove trace DMSO from the cryo-storage solution. As per the manufacturer's instructions (Lonza), EBM2

was supplemented with the following: 0.01% (v/v) ascorbic acid, 0.01% (v/v) gentamicin/amphotericin, 0.01% (v/v) hydrocortisone, 0.025% (v/v) epidermal growth factor (EGF), 0.025% (v/v) insulin-like growth factor (IGF), 0.025% (v/v) vascular endothelial growth factor (VEGF), 0.1% (v/v), b-splice variant fibroblast growth factor (bFGF), 10 mM HEPES, 1% (v/v) penicillin/streptomycin and 2.5% (v/v) fetal bovine serum. Cells were left to grow in an *HERA cell 150* (Heraeus, Thermofisher Scientific, Scoresby, Victoria, Australia) incubation chamber that was kept at 37°C, with an air composition of 95% O_2 and 5% CO_2, and the media was changed every two days until the flasks reached approximately 90-100% confluency (~4 days), at which point they were split into new flasks or plates for subsequent experiments. All experiments performed using the hCMEC/D3 cell line occurred between passages 30 to 35, for both optimisation procedures and all remaining studies presented within this thesis. All cell culture work was carried out in either a *Topsafe 1.2 ABC* model biosafety cabinet from Bioair (Siziano, Italy) or a *BH2000 series* biosafety cabinet from Clyde-Apac (Minto, NSW, Australia) and all materials, solutions and working hands were kept sterile.

Splitting of hCMEC/D3 cells

Flasks were, depending on the experiment, routinely split into 6 or 96-well plates which had been pre-coated with collagen as described above (0.5 mL per 6-well plate well and 75 µL per 96-well plate well). The cells in the T75 flasks were rinsed twice with 10 mL of PBS after spent media removal, before being treated with 4 mL of trypsin/EDTA solution, and incubated for 4 min. Immediately after the 4 min period, 11 mL of a solution containing 2.5% (v/v) FBS in PBS was dispensed into the flask to halt the trypsinisation process. The flask was then tapped to mechanically remove additional cells from the flask surface, and after microscopic inspection to ensure adequate cell detachment, the solution was then withdrawn and transferred to a 50 mL Falcon tube. The solution was homogenised to break up formed cell particles which

would perturb accurate cell counts, by stripetting the solution up and down 20 times using a 5 mL stripette. An 80 µL aliquot of the cell suspension solution was then transferred to an Eppendorf tube and combined with 20 µL of trypan blue staining solution, mixed briefly and allowed to rest for 2 min. The resulting solution was transferred by pipette to a haemocytometer and the cell concentration was calculated following the manufacturer's instructions. The Falcon tube containing the cell suspension was transferred to an *Eppendorf 5810R* centrifuge chamber and centrifuged at 1000 rcf at 37°C for 10 min. The supernatant was then aspirated off, and cells pelleted at the bottom of the Falcon tube were redistributed and homogenised in an appropriate volume of pre-warmed EBM2 media, such that the volume to be transferred to any plate used throughout the thesis would correspond to a cell seeding density of 30,000 cells cm^{-2}. The working volumes and surface areas utilised in all cell culture experiments throughout this thesis are summarised in Table 1. The appropriate volume of cell-containing EBM2 was then dispensed slowly alongside gentle agitation of the plate to ensure accurate pipetting and uniform cell distribution into wells. Plates were then left on a non-vibratory benchtop for 30 min before being transferred to the incubation chamber to prevent any the vibration induced edge effects of cell adherence. Finally, the plates were transferred to the incubation chamber where they remained until the time of experiment or lysis, with media being refreshed every two days.

Lysis of hCMEC/D3 cells for WB

Typically, all BCA assay validation and WB optimisation experiments were performed on lysates that were derived from either full T75 flasks or cells that had been seeded onto 6-well plates. To each well, 200 µL (or 2 mL in the case of a whole flask) of a solution containing a 6:1 ratio of *Pierce IP lysis buffer* and a 7x concentrated solution of cOmplete protease inhibitor (PI) cocktail, respectively, was added to each well. Cells were then lysed in this solution for 15 min at 4°C, after which each well was scraped to ensure full detachment of cells. The solution

from each well was transferred to a pre-cooled Eppendorf tube and spun at 14,000 rcf for 5 min before supernatant collection and protein content analysis via the Pierce BCA protein assay kit, using bovine serum albumin (BSA) as a standard.

Table 1: Specifications of cell culture plate sizes, related solution volumes and cell seeding densities that were used for optimisation of P-gp WB and throughout the duration of the thesis.

Parameter	**6-well plate**	**24-well plate**	**96-well plate**	**T-75 flask**
Surface area (cm^{-2})	9.6	1.9	0.32	75
Working volume (mL)	2	0.5	0.15	14
Volume of 0.1 mg/mL collagen solution (mL)	0.25	0.25	0.075	3
Seeding density	30,000	30,000	30,000	n/a
Approx No. cells per well upon seeding	290,000	60,000	9600	1-2 million

Validation of BCA assay accuracy and precision:

To validate the precision and accuracy of the BCA assay, a series of linearly spaced BSA concentrations were prepared in the same diluent solution used for cell lysis, consisting of *Pierce IP lysis buffer* and a cocktail of protease inhibitors (see cell lysis method for exact ingredients). The BSA concentrations used ranged from 25 to 2000 μg/mL, and constituted the known concentrations appearing on the standard curve, against which quality control (QC) protein samples would be compared for accuracy and precision. Three replicates of 20 μL volumes of each standard were pipetted into a 96 well plate, followed by 200 μL of the *Pierce BCA protein assay kit* working reagent. The working reagent contains two components which are mixed immediately prior to assay execution, of which the active chemicals are $CuSO_4$ and BCA. The reaction which then proceeds (shown in Figure 1), involves the protein derived

peptide bonds reducing the available Cu^{2+} ions, forming Cu^{+} ions which chelate two BCA molecules, and resultantly produce a purple coloured solution. Since the quantity of Cu(I) produced is proportional to the quantity of peptide bonds present in the sample, the colour produced by the chelation reaction is also proportional to the quantity of protein available for copper reduction in the sample being analysed. The plate was then protected from light with aluminium foil, gently stirred for 30 sec, followed by incubation at 37°C for 30 min. The plate was then allowed to cool to room temperature for 5 min, before being applied to the *Emstar* from *Perkin Elmer* (Glen Waverly, Victoria, Australia), where absorbance measurements were read at a wavelength of 562 nm. Three replicates of blank diluent solutions were also processed this way, of which an average was taken and subtracted from the absorbance of all other samples. The averages of the standard solutions were calculated and plotted as a function of their concentrations, before performing linear regression to generate a standard curve using the *Prism Graphpad* software. Additionally, to analyse the precision and accuracy of the standard

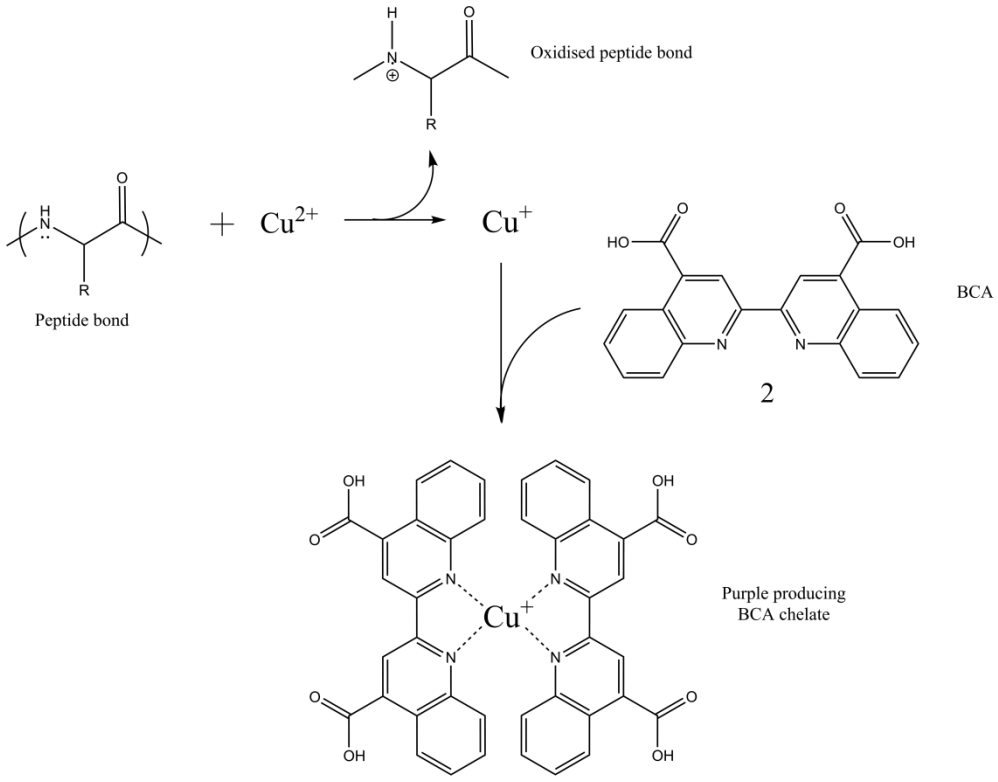

Figure 1: Schematic representation of the colour producing BCA/copper/peptide reaction validated for accuracy and precision.

curve as a means of calculating unknown protein content as a function of its absorbance in this assay, three replicates of low (125 μg/mL), medium (750 μg/mL) and high (1500 μg/mL) QC BSA solutions were prepared and analysed on a separate 96-well plate. These recorded absorbance values were processed as described previously, and the protein concentration was calculated therefrom. The predetermined limitations of precision and accuracy for the assays performance to be considered accurate and robust were for the QCs averages to fall within ± 20% for the lower QC sample and ± 10% for the high and medium QCs. The accuracy and precision of the QC samples was assessed using the equations below:

$$Accuracy = \frac{measured\ concentration}{known\ concentration} \times 100$$

$$Precision = \frac{mean + \delta}{mean} \times 100$$

Where δ = standard deviation.

General protocol of WB optimisation for P-gp:

Acrylamide gel preparation:

All polyacrylamide gels were hand-casted with a non-gradient 10% polyacrylamide concentration separating gel, and using the following composition: separating gel: 25.1% (v/v) of 40% acrylamide (final concentration = 10%), 25.1% (v/v) 1.5 M TRIS buffer (pH = 8.8, final [TRIS] = 0.38 M), 0.1% (w/v) sodium dodecyl sulphate (SDS), 0.1% (w/v) of ammonium persulfate (APS), and 0.1% (v/v) N,N,N',N'-tetramethylethylenediamine (TEMED), all in milliQ filtered H_2O; stacking gel: 10% (v/v) of 40% acrylamide (final = 4%), 25.2% (v/v) 0.5 M TRIS buffer (pH = 6.8, final [TRIS] = 0.13 M), 0.1% (w/v) SDS, 0.1% (w/v) of APS, and 0.1% (v/v) TEMED, all in milliQ filtered H_2O.

Electrophoresis:

After the total concentration of protein within the cell lysate samples had been determined, the appropriate volume corresponding to 10 μg of protein (except in the case of increasing protein load for P-gp signal linearity) was combined and mixed by vortex with loading (*Laemmli*) buffer (20% (w/w) glycerol, 0.125 M Tris H-Cl buffer, 10% (v/v) sodium dodecyl sulphate (SDS), 0.5% (v/v) bromophenol blue in milliQ water), in a ratio of 5:1, before being left to stand at room temperature for 30 min, all within a microfuge tube. This step is essential for protein denaturation, with the loading buffer containing β-mercaptoethanol, a reagent responsible for breaking any disulphide bonds which might otherwise prevent protein denaturation. The samples were then pipetted from the microfuge tubes into the lane wells of a previously prepared hand-cast polyacrylamide gel. Additionally, 5 μL of the *Dual Xtra Precision Plus Protein Prestained Standards* ladder solution was loaded into the first well, to aid in correct protein identification by comparison of molecular weight (MW). The gel was lowered into a buffer dam, where electrophoresis was then applied, using *Bio-Rad mini protean tetra cell* (Hercules, CA), at 100 V for 10 min (to facilitate gentle protein transfer from stacking gel to separating gel), and 150 V for the following h (to facilitate satisfactory resolution in protein separation), with both phases having 0.05 amps and thus 5 then 7.5 watts of power applied. The gel and buffer dam apparatus was submerged in running buffer (composition: 25 mM Tris base, 190 mM glycine and 0.1% (w/v) SDS in milliQ water) which was buffered to a pH of 8.2.

Protein transfer:

After the proteins had been sufficiently separated via electrophoresis as recognised by the spreading of the labelled DNA ladder in lane well 1, the gel was removed from the buffer dam/electrophoresis apparatus and soaked in transfer buffer (25 mM Tris buffer, 190 mM

glycine and a variable % of methanol) for 30 min. This soak facilitates the removal of the various salts and surfactants that were used in the electrophoretic phase. The nitrocellulose and blotting paper to be used in the transfer stage were also soaked in transfer buffer, in a separate vessel, to facilitate adequate electrical transmission. Next the protein gel contents were transferred onto a nitrocellulose membrane using the *Bio-Rad Trans-Blot Turbo transfer system* (Hercules, CA). Briefly, the transfer step involved the construction of an electrophoretic sandwich, with the order of contents being; anode, blotting paper, nitrocellulose membrane, gel, blotting paper and lastly cathode, described from the bottom up. The transfer was then run for 40 min at 25 V and 1.0 A. Once the transfer had reached completion, the nitrocellulose membrane was rinsed three times with tris-buffered saline (TBS) containing 0.1% (v/v) Tween 20 (TBST).

Membrane blocking and antibody application:

The membrane then needed to be blocked from non-specific antibody interaction, and was done so with either *Odyssey Blocking Buffer* or 5% (w/v) skim milk in TBST at room temperature for one h. The membrane was then rinsed free of skim milk solution three times by TBST. Primary antibodies specific for both β-actin (normalising protein) and P-gp were diluted into 10 mL of TBST by a factor of 2,500-10,000 and 100-500 respectively (varied throughout the optimisation process), and added to a vessel containing the protein-transferred membrane, and left to react at 4°C under gentle agitation overnight. Again the membranes were washed in TBST 5 times for 5 min each, before the secondary goat-anti-mouse antibody was applied. The fluorophore containing secondary antibody was also diluted in 10 mL of TBST but by a factor of 10,000, with 1% skim milk also being present in this solution. The membrane was incubated in this solution for 1-3 h at room temperature. After secondary antibody incubation was complete, the membranes were washed in TBST 5 times for 5 min each, before being

transported in a light protective vessel to the imaging instrument. Imaging was completed using the *LI-COR Odyssey scanner* (Lincoln, NE). Some experiments were assessed qualitatively whilst others received quantification, which was carried out using the Image J software, where determination of the relative protein abundances was assessed by densiometric analysis. Briefly, quantification of pixel intensity was measured by the software, which in theory is directly proportional to the quantity of fluorescing secondary antibody, which again should be directly proportional to the quantity of the protein of interest. For quantitative experiments, an average and standard deviation of the cell lysate samples that received the same treatment were calculated, and normalised against the house keeping protein β-actin, to account for loading, transfer and well-to-well biological variability.

Lysis buffer selection: RIPA vs Pierce IP lysis buffer

Since P-gp is a transmembrane protein, the likelihood of high water solubility without the addition of solubility-enhancing chemical agents is low. Therefore, two different lysis buffer solutions were trialled. To test the difference in P-gp amenability between these buffers, hCMEC/D3 cells from 6-well plates were lysed following the protocol outlined above, using either a simplified RIPA buffer or the proprietary *Pierce IP lysis buffer* as the sole variable, and the remainder of the WB protocol was followed as described. The composition of the two buffers was; RIPA buffer: 150 mM NaCl, 1.0% (v/v) Triton X-100, 0.5% (w/v) sodium deoxycholate, 0.1% (w/v) SDS and 50 mM Tris, pH 8.0; *Pierce IP lysis buffer*: 25 mM Tris•HCl pH 7.4, 150 mM NaCl, 1% (v/v) NP-40, 1 mM EDTA and 5% (v/v) glycerol. The results were assessed qualitatively for the superior choice.

Blocking buffer selection: skim milk vs Odyssey blocking buffer solution

The blocking buffer used to block the non-protein bound space within a WB transferred membrane can have profound effects on protein quantification. This effect can be due to specific interactions between the blocking buffer components and the protein of interest, which can sometimes physically hinder antibody/protein of interest interactions. Whilst skim milk is a common laboratory solution to blocking membrane binding of secondary antibody, an alternative was trialled for use within this protocol. To test the *Odyssey blocking buffer*, an experiment was performed whereby lysate samples from hCMEC/D3 cells were subjected to the WB method developed above, but where the membrane was cut into two separate pieces which were incubated for 1 h in either 5% skim milk in TBST or *Odyss*ey blocking buffer. The results were then qualitatively assessed.

Membrane selection: nitrocellulose vs PVDF

Generally speaking, two variants of protein blotting membrane are commercially available for use with WB, nitrocellulose and PVDF. Specific proteins will bind with higher affinity to one or the other type of membrane depending on their size, hydrophobicity and subsequently their specific interactions with the chemical functional groups presented by the membrane. Therefore an experiment was conducted whereby hCMEC/D3 cells lysed using the *Pierce IP lysis buffer* (judged as superior from the results of the previous section) were blotted in equal quantities onto two different membranes; nitrocellulose and PDF, as the only variable, while the remainder of the WB protocol was followed. The results were qualitatively assessed for superiority.

Percentage of methanol in transfer buffer

Methanol is generally required as a component of the transfer buffer within the WB method. Whilst methanol aids in transferring protein from the gel to the membrane, it has been observed that too high a concentration can hinder the transfer of larger proteins. P-gp is a large protein with a MW of 170 kDa, and the transfer thereof is likely affected by the concentration of methanol present in the transfer buffer. In regard of this knowledge, a simple experiment assessing the transfer of heavy proteins from electrophoresed gels to nitrocellulose membranes using varying concentrations of methanol within the transfer buffer (0, 10 and 20% v/v) was performed. Using lysed samples from the hCMEC/D3 cells, the WB protocol was followed until the end of the transfer step, at which point the resultant membranes were stained with Ponceau red solution (0.1% (w/v) Ponceau red in a 5% (v/v) acetic acid in milliQ water) for one h, followed by three successive 10 sec rinses in MilliQ water. The membranes were then scanned using a *Canon* flat-bed scanner at 600 dpi and resulting images were stored as tiff files. All protein stained by Ponceau above the arbitrarily set heavy protein cut-off of 75 kDa was assessed densiometrically via the ImageJ software. The observed density of protein stain above 75 kDa was then statistically evaluated using the Prism Graphpad software.

Antibody concentration and linear dynamic range of P-gp signal

Whilst being one of the most widely used antibodies within the field, the C219 P-gp antibody used in all WB experiments executed thus far was diluted at a relatively high ratio of 1:100 during WB incubations. After it had been determined that the use of the *Odyssey blocking buffer* presented an increase of the P-gp signal magnitude, and in consideration of the cost of future experiments, the P-gp antibody concentration was subjected to change. As the final iteration explored during WB protocol development, a lower dilution of the C219 antibody was assessed (changed from 1:100 to 1:500) while the remainder of the WB protocol was followed

as described earlier, using lysates of the hCMEC/D3 cells. Whilst these results were interpreted qualitatively, the final choice of 1:500 as an adequate and cost effective antibody concentration, was interrogated in a final experiment assessing the linear dynamic range of the P-gp signal. In this final experiment, three replicates of increasing quantities of protein content (5-40 μg) were loaded into adjacent lane wells of a gels and the WB protocol hitherto developed was carried out as described above. P-gp signal was quantified as described earlier and plotted as a function of protein load, before being assessed for linear regression using the *Prism Graphpad* software.

RESULTS

BCA assay validation

Before WB can be considered a semi-quantitative technique, it must be established that accurate and known quantities of total lysate proteins can be loaded into the polyacrylamide gel. Therefore the signal magnitude from the BCA protein concentration assay was assessed for precision and accuracy against three QC sample concentrations of BSA (low, medium and high). The standard curve generated by colourimetric reaction of the BCA working reagent against increasing concentrations of BSA is shown below in Figure 2. Linear regression produced an R^2 value of 0.99, indicating a high degree of signal linearity by this assay.

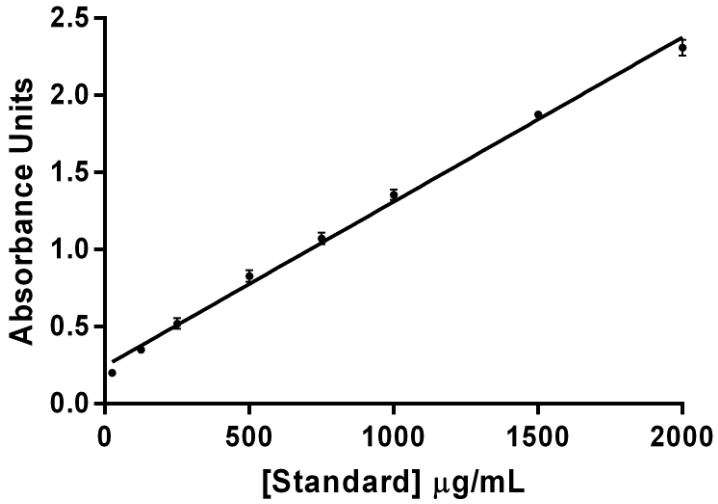

Figure 2: Standard curve with linear regression produced from absorbance readings of known and increasing BSA concentrations. Each data point represents the mean ± SD, where n = 3.

When assessed by the assay, the three QC samples presented protein concentrations of 111 ± 3.5, 787 ± 25 and 1532 ± 40 μg/mL, as low, medium and high, respectively. Shown in table 2 are the calculated accuracy and precision values of the derived protein concentrations from the three BSA QC samples (high, medium and low). The criterion of both precision and accuracy falling between ± 10% for the high and medium samples, and ± 20 % for the low samples was satisfied and thus it was concluded that the Pierce BCA protein assay kit is a relatively accurate and precise method for calculating protein quantities within future hCMEC/D3 cell lysate samples.

Table 2: Accuracy and precision of the three QC BSA solutions assessed for protein concentration using the BCA protein assay kit.

QC sample (μg/mL)	Accuracy (%)	Precision (%)	Criteria satisfied
1500 (high)	102.1	102.6	Y
750 (medium)	104.9	103.2	Y
125 (low)	89.1	103.1	Y

Western blot optimisation

Pierce IP lysis buffer is superior for P-gp solubilisation

At the commencement of WB optimisation for P-gp, a standard RIPA buffer was used for hCMEC/D3 cell lysis. When WB was carried out for P-gp using this RIPA buffer recipe however, no P-gp signal was observed, indicating that this large transmembrane protein may not be adequately solubilised during lysis. After some investigation, it was revealed that using the *Pierce IP lysis buffer* which contained the key component of glycerol, P-gp was observable (data not shown). Thus all further experiments employing WB for the detection of P-gp involved the use of the glycerol-containing *Pierce IP lysis buffer* for lysing hCMEC/D3 cells.

Odyssey blocking buffer is superior to skim milk

As a part of the WB optimisation process, two different blocking buffers were assessed within the WB workflow for P-gp. Whilst significant P-gp signal had been observed in preliminary experiments using 5% (w/v) skim-milk in TBS, the signal appeared relatively weak and exhibited inconsistencies across different blots. The use of milk also caused darker and more inconsistent background staining, which may have become problematic for straightforward densiometric analysis in future WB experiments. Therefore a proprietary product (*Odyssey blocking buffer*) was tested for use in membrane blocking alongside skim milk during optimisation. The results are shown in Figure 3, with *Odyssey blocking buffer* (3B) facilitating superior detection of P-gp and β-actin in comparison to the use of skim milk in TBS (Figure 3A). Due to the stark difference between the two blots, and to ensure that protein had been adequately transferred to the membrane blocked with skim milk, the Ponceau red staining procedure was used. Figures 3C and D confirmed that adequate and similar protein loads for both blots had been achieved, validating the above finding of *Odyssey blocking buffer* as

superior. This experiment allowed for the designation of *Odyssey blocking buffer* as the blocking buffer of choice in all future WB experiments.

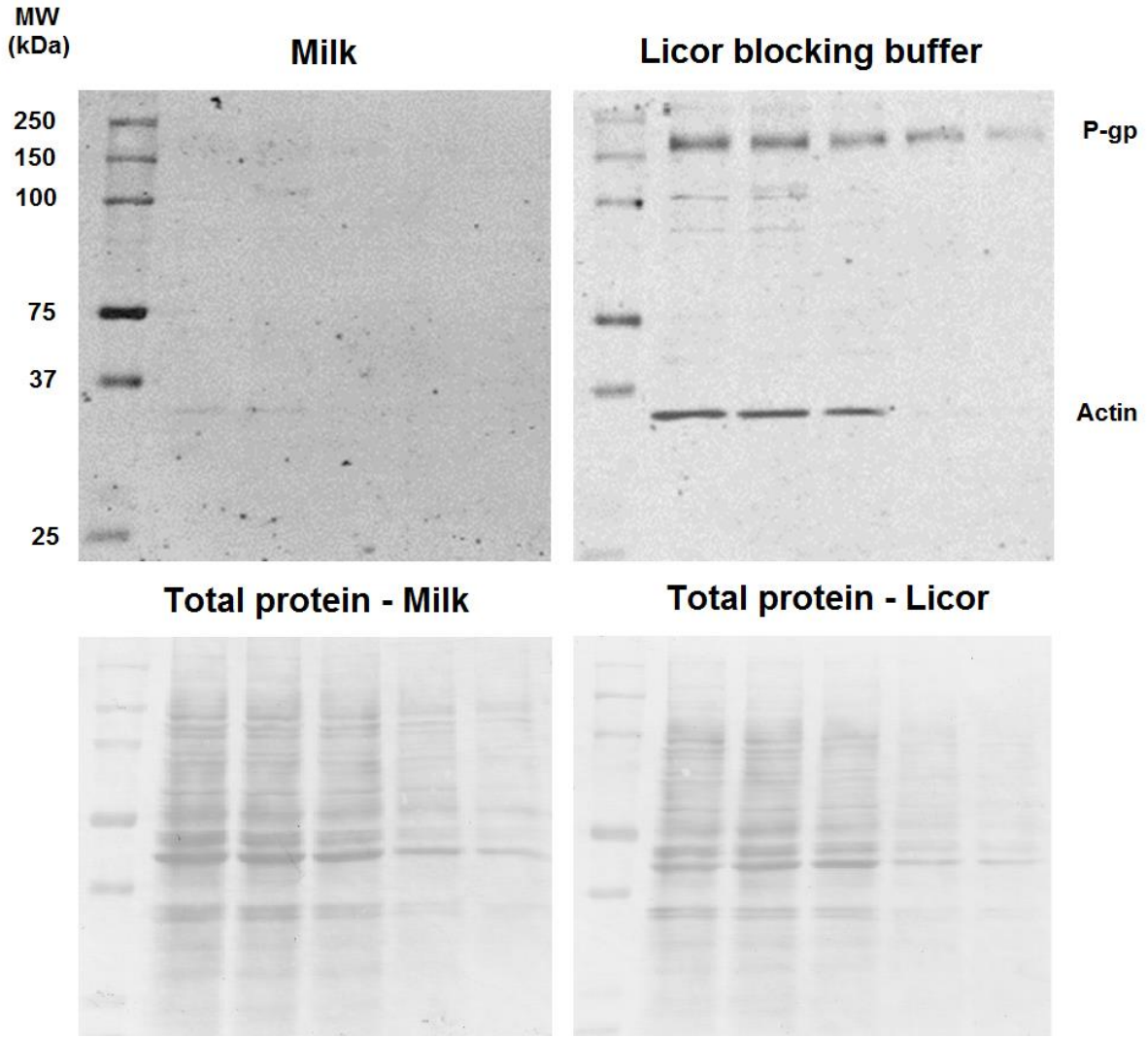

Figure 3: Assessment of two different blocking buffers within the WB workflow being developed for P-gp in hCMEC/D3 samples, with decreasing protein load from left to right (40 to 5 µg): A) 5% skim milk in TBS and B) Odyssey blocking buffer. Images C & D are Ponceau red total protein stains from the same blots as above, and indicate similar protein loads between the two membranes.

Nitrocellulose is a superior membrane choice compared to PVDF for P-gp presentation

Whilst the initial WB experiments for P-gp were assessed on nitrocellulose membranes, the alternative choice of PVDF was also investigated, in light of the possibility that it may have provided superior conditions for P-gp quantitation. Shown in Figure 4 below, the results clearly indicate that lysates derived from the brain endothelial (hCMEC/D3) cell line bind with higher affinity, or are able to better interact with antibodies, on nitrocellulose membranes when compared to that of PVDF, within the working WB protocol. Thus nitrocellulose was chosen for all further WB experiments probing P-gp concentrations.

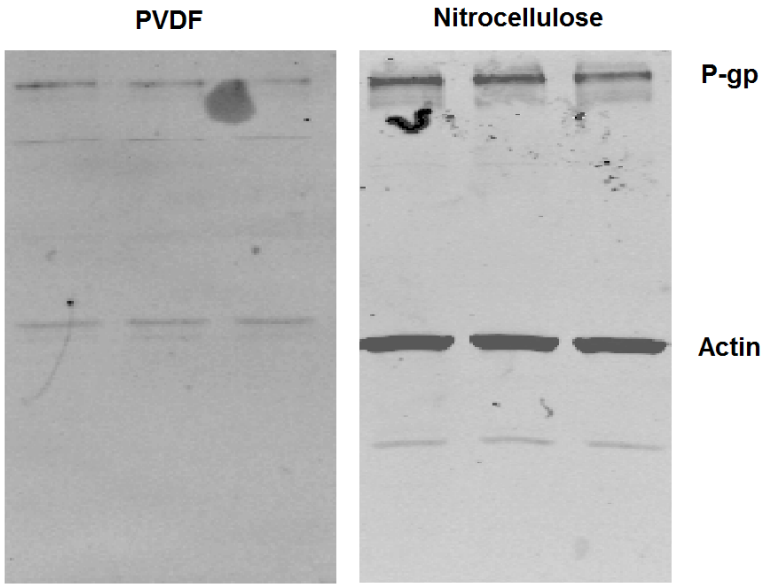

Figure 4: hCMEC/D3 lysates assessed qualitatively for P-gp and β-actin signals when blotted onto PVDF (left) or nitrocellulose (right) membranes. The three lanes in each gel represent lysates from three different biological samples.

Optimisation of methanol content in transfer buffer

The presence of methanol within the transfer buffer can enhance membrane protein transfer during incubation and the transfer process, but the optimal concentration needs to be determined for the specific protein of interest. Thus the ability of methanol to enhance the transfer of heavy molecular weight proteins (as a surrogate measure for P-gp) was assessed on

three separate gels, each of which were exposed to a different methanol concentrations during transfer to membranes within the WB workflow. As shown in Figures 5A and B, a lower concentration of methanol present in the transfer buffer enhanced high MW protein transfer when using hCMEC/D3 cell lysates. Whilst no significant difference was detected between the AUC signal magnitudes of the 0 and 10% methanol groups, the presence of 20% methanol approximately halved the transfer of high MW proteins. Since the 0% methanol gel exhibited significant swelling during the incubation with transfer buffer (data not shown), 10% methanol was selected as the optimal concentration and represents what was used for all future WB experiments.

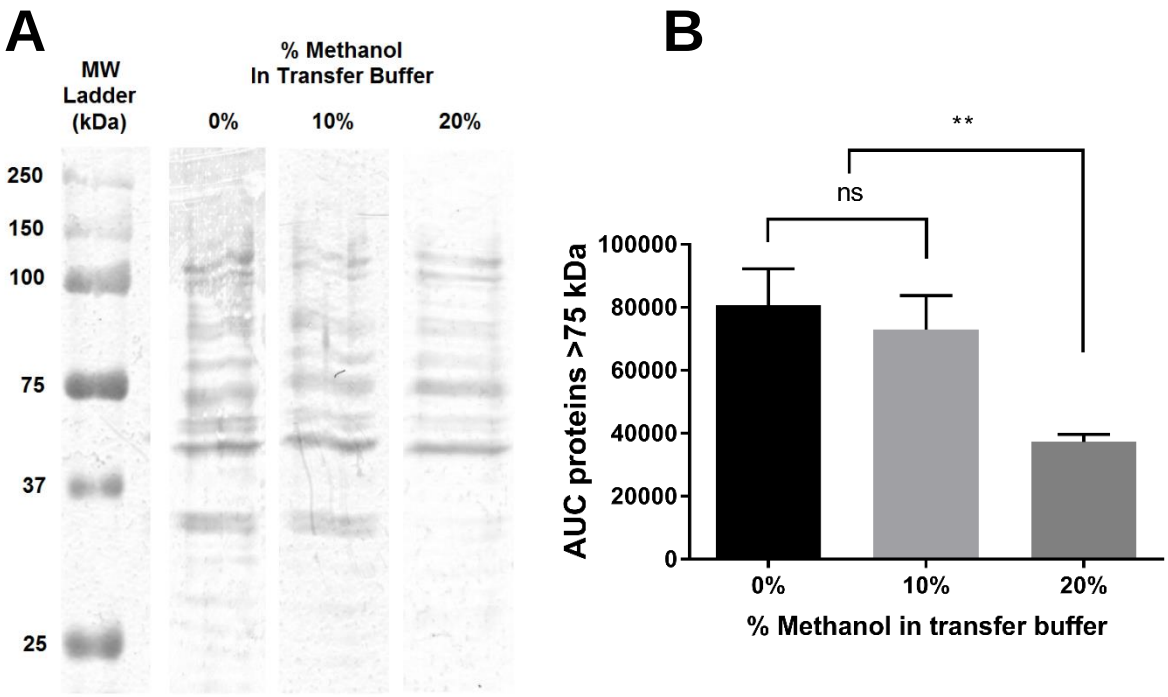

*Figure 5: Assessment of the influence of methanol concentration in the transfer buffer on heavy MW proteins derived from hCMEC/D3 cells: A) Representative image of WB lanes stained with Ponceau red with varying methanol concentrations in the transfer buffer during separate gel transfers and B) quantitation of heavy proteins (arbitrarily set to protein > 75 kDa) as assessed by the total protein stain in A, where the horizontal lines represent mean ± SD where n = 3, ns denotes no significance and ** = $p < 0.01$.*

Antibody dilution and linear dynamic range of P-gp signal

Prior to this final WB optimisation experiment, the C219 P-gp antibody was used at a relatively high and expensive concentration (1:100 dilution). In consideration of the affordability of future experiments, and since the P-gp signal magnitude had been increased with successive protocol improvements, a new C219 dilution (1:500) was used in an experiment assessing the linear dynamic range of P-gp in the developed protocol. The results, shown in Figure 6, indicated that a 1:500 dilution of the C219 antibody still provided adequate P-gp signal. Linear regression of the P-gp signal magnitude plotted against total protein load gave an R^2 value of 0.95, providing evidence that the developed WB protocol for P-gp was able to accurately reflect increasing quantities of total protein load, which was used here as a proxy measure for increasing P-gp load.

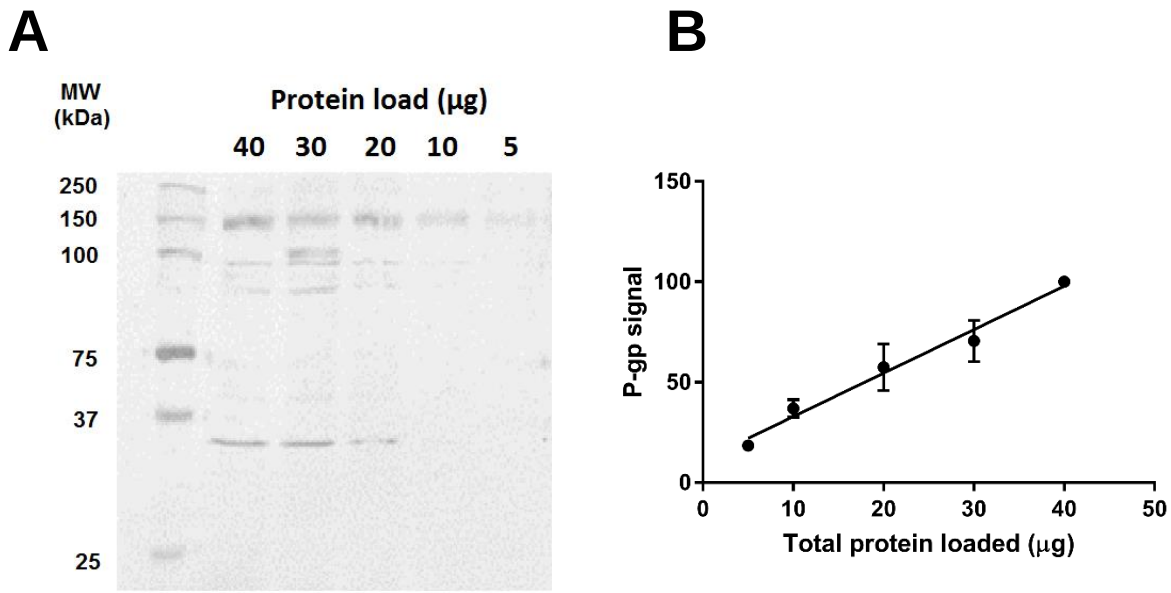

Figure 6: Assessment of the linear dynamic range of P-gp signal with a C219 antibody dilution of 1:500. A) Representative blot showing decreasing P-gp signal corresponding to decreasing protein load from left to right and B) Graphical assessment and linear regression of densiometric analysis of A.

DISCUSSION

Of the scientific techniques explored within this thesis, protein quantification, or more specifically, quantification of P-gp in hCMEC/D3 cells, was of central importance. Currently within the life sciences, WB is the technique most widely employed to facilitate this aim. Before accurate results can be obtained by WB however, the protocol must be specifically developed for the protein of interest (P-gp), and the linear dynamic range of the protocol must be assessed for responsiveness to increased levels of the protein of interest. This thesis chapter was primarily concerned with further developing an already established WB protocol for P-gp, for specific use within our laboratory. To address this concern, multiple parameters of the WB protocol for P-gp were explored and ideal conditions were identified for further use.

Other experiments presented herein guided protocol development, and these included; the use of the *Odyssey blocking buffer* to provide an unsmothered signal, a medium concentration of methanol within the transfer buffer to facilitate transfer of higher MW proteins, nitrocellulose as a superior membrane type for P-gp specifically, and the Pierce IP lysis buffer as being required to solubilise P-gp during the lysis of hCMEC/D3 cells. Each of these findings is in line with observations made in the literature, again instilling confidence in the decisions and choices made during optimisation. For example, it has been shown previously that glycerol is often a required component within lysis buffers for the solubilisation of transmembrane proteins (5, 6), and that while methanol is a near universal component of transfer buffers, lower concentrations of methanol are generally desired for electrophoretic transfer of larger proteins from gel to membrane (7).

The most important experiment described herein was the apparent linearity of P-gp signal in the optimised WB protocol for P-gp. As shown in Figure 6B, when increasing quantities of

total protein were loaded into adjacent WB lanes, a high degree of linearity was observed between the quantity loaded and the P-gp signal output ($R^2 = 0.95$). This observation alongside the experience gained during the optimisation process, provided confidence in the ability of both the protocol and the user to provide accurate results in future experiments probing P-gp modulation.

Whilst a WB protocol for P-gp was successfully developed, we found that the technique itself was labour intensive and low-throughput. With this experience in mind alongside the consideration of life science fields moving increasingly toward higher throughput methods as newer technologies emerge, an alternative method known as the in-cell western was explored for use in P-gp quantification, and these findings are presented in the next chapter.

CONCLUSION

A WB protocol for quantification of the important efflux transporter P-gp was successfully developed in hCMEC/D3 cells, and the linear dynamic range was assessed as satisfactory. The developed protocol was considered sufficient for use in future WB experiments aimed at quantifying relative changes in P-gp expression following pharmacological manipulation, and was also used to compare and validate results from alternative techniques such as the in-cell western, which is outlined in the next chapter.

REFERENCES

1. Burnette WN. "Western blotting": electrophoretic transfer of proteins from sodium dodecyl sulfate--polyacrylamide gels to unmodified nitrocellulose and radiographic detection with antibody and radioiodinated protein A. Anal Biochem. 1981;112(2):195-203.
2. Renart J, Reiser J, Stark GR. Transfer of proteins from gels to diazobenzyloxymethyl-paper and detection with antisera: a method for studying antibody specificity and antigen structure. Proc Natl Acad Sci U S A. 1979;76(7):3116-3120.
3. Towbin H, Staehelin T, Gordon J. Electrophoretic transfer of proteins from polyacrylamide gels to nitrocellulose sheets: procedure and some applications. 1979. Biotechnology. 1992;24:145-149.
4. Sharom FJ. The P-glycoprotein multidrug transporter. Essays Biochem. 2011;50(1):161-178.
5. Farnum M, Zukoski C. Effect of glycerol on the interactions and solubility of bovine pancreatic trypsin inhibitor. Biophys J. 1999;76(5):2716-2726.
6. Gutmann DA, Mizohata E, Newstead S, Ferrandon S, Postis V, Xia X, Henderson PJ, van Veen HW, Byrne B. A high-throughput method for membrane protein solubility screening: the ultracentrifugation dispersity sedimentation assay. Protein Sci. 2007;16(7):1422-1428.
7. Jacobson G, Karsnas P. Important parameters in semi-dry electrophoretic transfer. Electrophoresis. 1990;11(1):46-52.

Chapter 3:

Development and validation of an in-cell western for quantifying P-glycoprotein expression in human brain microvascular endothelial (hCMEC/D3) cells

ABSTRACT

An in-cell western (ICW) protocol detecting the relative expression of P-gp in human cerebro-microvascular endothelial cells (hCMEC/D3) was developed and optimised, with the intention of improving throughput relative to western blotting (WB). For validation of the ICW protocol, hCMEC/D3 cells were incubated with known P-gp upregulators (10 μM rifampicin and 5 μM SR12813) and treated with siRNA targeted against MDR1, before measuring changes in P-gp expression, using both ICW and WB in parallel. To confirm a relationship between the detected P-gp expression and function, the uptake of the P-gp substrate rhodamine-123 was assessed following SR12813 treatment. Rifampicin and SR12813 significantly upregulated P-gp expression (1.5 and 1.9-fold, respectively) compared to control, as assessed by the ICW protocol. WB analysis of the same treatments revealed 1.4 and 1.5 fold upregulations. MDR1 siRNA reduced P-gp abundance by 20% and 35% when assessed by ICW and WB, respectively. SR12813 treatment reduced rhodamine-123 uptake by 18%, indicating that the observed changes in P-gp expression by ICW were associated with comparable functional changes. The correlation of P-gp upregulation by WB, rhodamine-123 uptake and the ICW protocol, provide validation of a new ICW method as an alternative approach for the quantification of P-gp in hCMEC/D3 cells.

INTRODUCTION

P-glycoprotein (P-gp) is a physiologically important efflux pump responsible for protecting many cell types and organs from the excessive accumulation of a broad spectrum of potentially harmful xenobiotics (1). P-gp is expressed at relatively low levels in most mammalian tissues, but it appears most abundantly in intestinal epithelial cells; kidney proximal tubules; liver bile ductules and the brain endothelial cells that line the cerebro-vasculature and comprise the blood-brain barrier (BBB) (2-5). Within the aforementioned tissues, the prominent presence of P-gp is considered integral to the maintenance of normal physiological function (2-5). In cancerous cells however, the expression of P-gp is often highly upregulated in response to previous exposure to cytotoxic treatments, and the resulting cells are characterised as multi-drug resistant, by virtue of the enhanced P-gp mediated efflux activity, which effectively limits the access of drugs to their intracellular targets (6). Within cancer research, this upregulated function has engendered a status for P-gp as a formidable barrier to delivering cytotoxic drugs to their sites of action in vivo (7).

P-gp is also considered a hindrance for drugs targeting the central nervous system (CNS) (8, 9). P-gp, sometimes referred to as 'the gatekeeper' of the brain (10), greatly limits the access of many CNS-acting drugs to their therapeutic targets, through the active efflux of a wide range of drugs from the lipid membrane of brain endothelial cells, back into the systemic circulation (11). Thus the modulation of P-gp expression and function has been a strategy considered for enhancing the CNS delivery of drugs which are P-gp substrates, although with only limited success achieved thus far (7, 12). To further highlight the importance of P-gp, it is becoming increasingly apparent that P-gp expression and function may play an important role in several neurological disease states, including Alzheimer's disease (13-16) and Parkinson's disease (17, 18), among others (19). Therefore, methods for assessing the relative quantities of P-gp which

might result from physiological or pathological processes, or after pharmacological interventions, are of great use to many research areas that focus on the BBB. Currently, the method most commonly employed for quantifying P-gp abundance is western blotting (WB). WB as a method of protein quantification has been indispensable to the life sciences since its inception in 1979. The combination of both the apparent simplicity and the relative inexpensiveness of the technique quickly established the role of WB as the preferred or most widely-used method of protein quantification. Certainly this method facilitated the rapid expansion of data accumulated throughout the 1980s and 90s, greatly enhancing knowledge and understanding of the processes underlying cellular signalling, communication, metabolism, transport, and structure. Particularly pertinent to the pharmaceutical sciences is the ability of WB to measure changes in protein expression resulting from pharmacological interventions in various cell types. The employment of WB to answer such research questions is extremely useful and widespread, yet despite this ubiquity, WB possesses several key drawbacks. The most pertinent of these drawbacks is that WB may be considered a low throughput method. The need to generally harvest > 10 μg of protein for analysis often necessitates the use of 6-well plates, and the average two day processing time delays the researcher's ability to optimise experimental protocols and proceed with experiments whose parameters rely on the results from previous experiments. These factors may also limit the set of experimental conditions that are explored, i.e. one to two time points and/or concentrations of pharmacological intervention are often tested, since the labour time required to investigate alternatives increases linearly with each extra data point desired.

An alternative method known as the in-cell western (ICW) is beginning to occupy a place within the literature. The ICW protocol is based on the same principles as WB; primary and secondary antibodies are still used to signal and quantify the protein of interest, but the

antibodies bind to the target of interest in its native form (not sodium dodecyl sulfate treated) and in situ (within cellular matrices in 96 well plates). Most importantly, the ICW protocol can be performed on 96 well plates, a format which provides moderate but still significant benefits, when compared to WB. The smaller scale of ICW reduces the quantity of consumables used within an experiment, and also enhances the throughput and therefore the effective rate of a researcher's investigations.

The aim of this study was to develop and validate an ICW western protocol for the relative quantification of P-gp, as a moderately improved alternative to WB, in immortalised human cerebral microvascular endothelial cells (hCMEC/D3), a cell line which closely models the human BBB.(20) As a part of the validation process, the autofluorescent capacities of several 96-well plate types were assessed, to aid appropriate plate selection and thus minimise the impact of experimental artifacts. Next, the linearity of the P-gp signal and DAPI nuclear stain (to be later used for normalisation of the P-gp signal) were assessed as a function of increasing cell density. For further validation of the responsiveness of the P-gp ICW, hCMEC/D3 cells were exposed to two known upregulators of P-gp (rifampicin, SR12813) as well as siRNA against MDR1 (the gene encoding P-gp), and P-gp expression was assessed by the new ICW protocol and WB in parallel. Lastly, to confirm the link between ICW-measured changes in P-gp, and apparent P-gp functionality at the cellular membrane, cellular accumulation of the P-gp specific substrate rhodamine-123 (R123) was assessed after exposure to one of the treatments used in this study, SR12813.

MATERIALS

4',6-Diamidino-2-phenylindole (DAPI), triton X-100, Tween-20, paraformaldehyde, sodium chloride, potassium chloride, disodium phosphate, rhodamine-123 (R123), SR12813,

rifampicin, potassium phosphate and Corning black polystyrene TC-treated 96 well plates were all purchased from Sigma Aldrich (St Louis, MO). TRIS buffer salt (TRIZMA base), sodium dodecyl sulphate (SDS), ammonium persulfate, N,N,N',N'-tetramethylethylenediamine (TEMED), trypan blue, glycerol, Hank's balanced salt solution (HBSS), trypsin-EDTA solution 0.25% in HBSS and Dulbecco's sterile phosphate buffered saline (PBS) were all purchased from Sigma Life Sciences (St Louis, MO). 40% acrylamide/bis solution was purchased from Bio-Rad Laboratories (Hercules, CA). Valspodar (PSC833) was a gift from Novartis (Basel, Switzerland). Odyssey blocking buffer and the IR dye 800CW goat anti-mouse IgG antibody were both purchased from Millennium Science (Mulgrave, Victoria, Australia). cOmplete Tablets Mini EASY pack protease inhibitors were purchased from Roche Diagnostics GmbH (Mannheim, Germany). 0.2 µm pore-sized nitrocellulose membrane roll was purchased from GE Life Sciences (Rydalmere, New South Wales, Australia). The C219 P-gp antibody was purchased from Australian Biosearch (Balcatta, Western Australia, Australia). Corning Costar transparent 96 well plates were purchased from Invitro (Noble Park North, Victoria, Australia). Fluorescein goat anti-mouse IgM antibody was purchased from Vector Laboratories (Burlingame, USA). Black polystyrene ViewPlateR-96 F TC 96-well plates were purchased from Perkin Elmer, and Pierce BCA protein assay kit and Pierce IP lysis buffer were purchased from Thermo Fisher Scientific (Scoresby, Victoria, Australia). The hCMEC/D3 cells were generously provided by Dr Pierre-Olivier Couraud (INSERM, Paris, France). Both Clonetics EBM-2 basal media and Clonetics EGM-2 single quots growth factor kits were purchased from Lonza (Walkersville, MD). Collagen type I was purchased from Corning Discovery Labware (Bedford, MD). Normal transparent 6 and 96-well plates were purchased from Corning Incorporated (Corning, NY). HiPerfect transfection reagent, 4 x GeneSolution siRNA for ABCB1 (SI03040156, SI03028116, SI00018732 and SI00018718),

AllStars Negative Control siRNA (SI03650318) and the RNeasy Plus mini kit were purchased from Qiagen (Hilden, Germany).

METHODS

Selection of appropriate 96 well plate for ICW

Inherent properties of 96 well plates can greatly influence the values produced by certain assays. Edge effects as well as auto-fluorescence (a concept which can be applied to infra-red (IR) and other light sources as well) occur to varying degrees with different plate types, and the type of plastic used can also influence the spread of light to and from adjacent wells. The type of plate used in any one assay is crucial and should always be thoroughly explored in the planned experimental context before commencing studies. Therefore, an experiment was conducted whereby three different plate types (Corning, Costar and Perkin Elmer) containing no reagents were scanned on the Licor Odyssey IR imager, without reagents but using the same settings under which the experimental data would later be analysed. Briefly, all three plate types were thoroughly wiped clean with 80% (v/v) ethanol, as well as the glass surface of the Odyssey imager. The plates were then individually placed within the imager, and the imager software was set to the microplate2 setting with a 3.0 mm focus offset, a medium image quality with 169 μm resolution, and the light intensity from the 800 nm channel was set to 10. The entire plate was scanned and a 96 well plate ICW grid was applied to the constructed image, with care taken to align the grid such that only light emanating from the individual wells was integrated. The integrated intensity of IR light from each well was exported from the Odyssey software, and plotted as a function of its row position within the 96 well plate.

Seeding/splitting of hCMEC/D3 cells

Vials of the hCMEC/D3 cell line were kept cryogenically frozen in liquid nitrogen in a solution comprised of 5% (v/v) DMSO in heat inactivated FBS solution. One mL vials containing ~2 million cells were dispensed into T-75 flasks containing 14 mL of EBM2 media, which had been pre-coated with 3 mL of a 0.1 mg/mL solution of collagen type I and incubated for 1 h, before being washed with 10 mL of PBS to remove excess collagen. Two h after seeding, the DMSO containing EBM2 media was removed and replaced with freshly warmed media. EBM2 was supplemented with the following: 0.01% (v/v) ascorbic acid, 0.01% (v/v) gentamicin/amphotericin, 0.01% (v/v) hydrocortisone, 0.025% (v/v) epidermal growth factor (EGF), 0.025% (v/v) insulin-like growth factor (IGF), 0.025% (v/v) vascular endothelial growth factor (VEGF), 0.1% (v/v), b-splice variant fibroblast growth factor (bFGF), 10 mM HEPES, 1% (v/v) penicillin/streptomycin and 2.5% (v/v) fetal bovine serum.

Signal to noise ratio optimisation

Once it had become apparent that the initially observed signal to noise ratio was far from optimal, several iterations of the initially trialled ICW protocol were executed. hCMEC/D3 cells were plated onto a *Corning* black 96-well plate at 35,000 cells cm^{-2} and left to grow for 48 h (to mimic future experimental conditions), at which point they were 80-90% confluent. Whilst the above conditions remained the same throughout the iterative process, the following variables were explored with the intent of optimisation: varying primary and secondary antibody concentrations; time of primary and secondary antibody incubation; intensity of light source within the *Licor Odyssey* IR scanner; presence and concentration of surfactants to lower non-specific antibody binding; and the addition of extra rinse steps at the very end of the protocol. Each of these variables was fine-tuned to generate an optimal signal to noise ratio, and the final protocol is described in the next section.

Construction of standard curves for infra-red P-gp and cell number signals

The first ICW experiments were designed to assess the construction of the standard curves of both the infra-red P-gp signal derived from hCMEC/D3 cells and the fluorescent nuclear stain DAPI, the latter to be used to normalise the data to the total number of cells. To construct the standard curves, hCMEC/D3 cells (passage 30 to 35) were seeded onto collagen type I-coated Corning 96-well plates at varying seeding densities, ranging from 5,000 to 35,000 cells *per well* (to facilitate observation of a standard curve). Cells were allowed to settle for either two h before commencing the ICW protocol such that no cell growth had occurred and thus the linearity of the seeding density was preserved, or for 24 h to assess the ability of the DAPI stain to respond to cell growth. After the appropriate time interval, the ICW protocol was applied. As shown in Figure 2a, the initial P-gp ICW trial yielded data of poor quality and a signal of low magnitude. As such, the protocol was iteratively improved, to reach the final protocol described herein. EBM2 media was removed from all wells and the cells were briefly rinsed with 150 µL of PBS. The PBS was discarded and replaced with 150 µL of fixing solution (4% (w/v) paraformaldehyde in PBS), and the plate was left to stand without agitation at room temperature for 20 min. After 20 min, the fixing solution was discarded and the cells were permeabilised by four consecutive 5 min rinses with 200 µL of cell permeabilisation solution (0.1% triton X-100 in PBS) under moderate shaking at room temperature. A final rinse using 210 µL of PBS was included to remove any residual surfactant. A 150 µL aliquot of Licor PBS blocking buffer ™ was applied to each well and the plate was left on gentle agitation for 1 h at room temperature. The blocking buffer was then discarded, and replaced with 50 µL of the same blocking buffer, now containing a 1:50 dilution of the C219 P-gp antibody or blocking buffer alone (to be used as secondary antibody controls). The plate was then left under gentle shaking overnight in a cool room (4°C). All wells were then subjected to four consecutive 200 µL washes under gentle shaking with PBS-T (0.1% (v/v) Tween-20 in PBS). After the fourth

rinse, each well was incubated with 50 μL of blocking buffer containing 0.5% (v/v) Tween-20, 1 μg/mL DAPI, and Licor goat-anti-mouse (secondary) antibody (1:2000). Immediately after application of the secondary antibody, the plate was wrapped in aluminium foil and placed on gentle agitation at room temperature for 1 h. Finally, after DAPI/secondary antibody incubation, the plate was subjected to five more 5 min rinses with 200 μL of PBS-T at room temperature, followed by two final rinses with PBS (in place of PBS-T) to remove residual surfactant (the increased number of final rinses greatly reduces non-specific secondary antibody binding). The plate was then carefully aligned on the Odyssey imager (such that only light emanating from the individual wells was recorded) and scanned using the settings previously described.

To remove the intrinsic IR auto-fluorescence associated with the plates, an average of the IR signal was calculated from cell-free wells, and this average was subtracted from all other cell-containing wells. Next an average of control wells that had undergone incubation with secondary antibody only (primary antibody omitted) was calculated, and this value was also subtracted from all remaining data points, to account for non-specific binding of the secondary antibody. These two subtractions were performed as separate steps, to facilitate the calculation of the percentage contributions from both specific and non-specific secondary antibody binding to P-gp, after the exclusion of plate-intrinsic IR auto-fluorescence.

The plate was then scanned in a *Perkin Elmer* fluorescence spectrophotometer with an excitation wavelength of 495 nm and emission wavelength of 515 nm, and the scan mode was set to well area scan mode with 100 flashes spaced 0.72 mm apart, round scan mode and fluorescence emission measurements occurring at the bottom of the wells. The plates always included wells which contained only collagen, and an average of these wells was subtracted

from all other fluorescent data points to remove any non-specific fluorescence not associated with DAPI staining. For experiments where P-gp expression was measured following exposure to a known modulator of P-gp expression, the data were expressed as a fold-change in comparison to the average of control wells, according to Equation 1:

Equation 1: $$Fold\ change = \frac{\frac{IR_t - IR_b}{F_t - F_b}}{\frac{\sum_{i=1}^{n}\left(\frac{IR_c - IR_b}{F_c - F_b}\right)}{n}}$$

Where IR_t = the infra-red signal from treatment wells; IR_b = the infra-red signal from control wells treated with secondary antibody only (P-gp signal background subtraction); F_t = the fluorescent signal from treatment wells F_b = the fluorescent signal from empty wells containing collagen only (DAPI background subtraction); IR_c = the infra-red signal from control wells; F_c = the fluorescent signal from control wells and n = the number of control replicates.

Imaging of IR antibody signal origin

Due to the generally hydrophobic nature of many antibodies and proteins, non-specific binding between the antibodies utilised in this protocol and serum proteins used in blocking buffers must be assessed, in order to determine an appropriate signal origin. In short, close range visualisation of the signal being measured at the cellular level would be desirable to build confidence that the future data generated was indeed a reflection of P-gp abundance, rather than experimental artifact. Therefore, an imaging experiment was conducted to visualise hCMEC/D3 cells at the cellular level, to observe the signal origin, using the following experimental protocol. Briefly, untreated hCMEC/D3 cells were cultured in a 96 well plate until reaching ~90% confluency, at which point the media was removed, and the cells were rinsed with 200 µL of PBS followed by fixation in paraformaldehyde as described above. Next, the ICW protocol was followed as described above, except for the secondary antibody

incubation. To facilitate imaging by confocal fluorescence microscopy, the IR-conjugated secondary antibody was replaced in this experiment with a goat-anti-mouse secondary antibody conjugated to fluorescein isothiocyanate (FITC), at a concentration of 20 μg/mL. All other parameters of the ICW protocol remained the same. Images were captured on a *Perkin Elmer* Operetta high throughput imager using Harmony version 3.5.2 and a 20x UPlanApo NA0.8 objective. DAPI fluorescence was collected using a 380/40 excitation and 445/70 emission filter, and fluorescein fluorescence using a 475/30 excitation and 525/50 emission filter.

Validation of P-gp ICW by comparison to WB following treatment with P-gp regulators

Once the changeable parameters of the ICW protocol were optimised and a desirable signal to noise ratio had been achieved, the impact of known modulators of P-gp expression were compared using the novel ICW protocol and a traditional WB technique. hCMEC/D3 cells were seeded at 35,000 cells cm^{-2} onto collagenated 6 (WB) or black Corning 96 (ICW) well plates. Approximately 24 h after seeding, when cells had reached 30-50% confluency, the media was removed and replaced with treatment media containing either 0.1% DMSO (control), 10 μM rifampicin or 5 μM SR12813, all as separate experiments. In each of these experiments cells were incubated in treatment media for 72 h, at which point the treatment media was removed and cells were briefly rinsed in 2 mL or 200 μL of PBS (6 or 96 well plate) and then immediately either lysed for WB analysis or fixed with 4% paraformaldehyde for 20 min, as per the ICW protocol. The remainder of the ICW protocol was then carried out as described in the previous sections, and the WB analysis was executed using the technique described below. To each well, 200 μL of a solution containing a 6:1 ratio of *Pierce IP* lysis buffer and a seven times concentrated solution of cOmplete protease inhibitor (PI) cocktail, respectively, was added to each well. Cells were then lysed in this solution for 15 min at 4°C, after which each well was scraped to ensure full detachment of cells. The solution from each

well was transferred to a pre-cooled Eppendorf tube and spun at 14,000 rcf for 5 min before supernatant collection and protein content analysis via the *Pierce* BCA protein assay kit using bovine serum albumin as a standard. WB was carried out by loading a 10% acrylamide 1 mm hand-cast gel with varying volumes of lysate/Laemlli (5:1 ratio) buffer resulting in 15 μg of protein being loaded into each lane. Electrophoresis was executed at 60 V for 30 min followed by 1.5 h at 150 V. Electrophoresed gels along with extra thick blot paper and 0.2 μm pore-sized nitrocellulose membranes were allowed to equilibrate in transfer buffer containing 10% (v/v) methanol for 30 min before transfer. Transfer was executed using semi-dry consumables and the Turbo-blot transfer system (*Bio-rad*, Gladesville, New South Wales, Australia) set to 40 min at 25 V and 1.0 A. Transfer membranes were then rinsed briefly in TBS-T and then incubated in ~20 mL of *Licor* ™ blocking buffer at room temperature for 1 h. Membranes were again rinsed briefly in TBS-T and then incubated with a 1:500 dilution of the C219 antibody in TBS-T overnight. The β-actin antibody was added to incubation solution for only the final 20 min of the overnight primary antibody incubation step, to avoid saturation of the actin signal at a dilution of 1:10,000. Following 4 x 10 min membrane washes in TBS-T, the membranes were incubated in *Licor* ™ goat-anti-mouse secondary antibodies for two h at room temperature followed by the same washing regime as above. Membranes were scanned on the *Licor Odyssey* IR imaging instrument, and densitometric analysis was executed via the *ImageJ* software. Data was normalised to β-actin signal and expressed as fold-changes compared to controls.

P-gp knock-down by siRNA transfection

To confirm that the ICW was able to detect changes in P-gp abundance, the hCMEC/D3 cell line was treated with siRNA against MDR1. Briefly, cells were seeded at densities of 35,000 cells cm^{-2} on collagenated plastic, and left to grow for 48 h. On the day of transfection (48 h

after seeding) a solution containing four separate 5 nM siRNA complexes (with the target sequences; ACCGGACATCCCAGTGCTTCA, AACATTCGCTATGGCCGTGAA, GACAGAAAGCTTAGTACCAAA and ATCGAGTCACTGCCTAATAAA) was mixed with 3% (v/v) HiPerfect Transfection reagent in serum free EBM2 media, and allowed to incubate at room temperature for 10 min to allow siRNA transfection complexes to form. These solutions were then delivered to the cells dropwise (200 or 20 µL per well for 6 and 96 well plates respectively), and the cells were left to incubate with these complexes for eight min. After eight min, each well received 1.8 or 0.18 mL of serum-containing EBM2 media (6 or 96-well plates), and then left to incubate at 37 °C for 48 h. After this 48 h siRNA incubation period, cells were either fixed for ICW or lysed for PCR or WB analysis. Additional wells were treated with a scrambled siRNA sequence for use as a negative control, against which the statistical comparisons were made. Before assessing the above siRNA protocol for P-gp knockdown, identical procedures were executed on 96-well plates for cell viability analysis via the MTT assay. The MTT assay included four groups; 1) control, 2) transfection reagent alone, 3) P-gp siRNA + transfection reagent and 4) scrambled siRNA + transfection reagent, and was executed as follows. After the 48 h transfection complex incubation period, all treatment/media solutions were discarded, and the cells were washed twice with 150 µL of warm PBS. All wells were then treated with 160 µL of FBS free EBM2 media which contained 6.25% (v/v) of an 8 mg/mL MTT reagent solution. The plates were then wrapped in aluminium foil and left to incubate for a further four h. After the four h incubation with the MTT reagent, the solution was discarded, and 150 µL of DMSO was added to each well. The plates were then briefly shaken and incubated with DMSO for a further 30 min to dissolve the MTT crystals. Once more the plates were briefly shaken, and then absorbance at 540 nm was recorded. Blank wells which had undergone all the above procedures except in the absence of cells were also present on the plate, an average of which was taken and subtracted from each individual reading

recorded. The absorbances were then normalized against the average of the control values, to be expressed comparatively as % viability when compared to the control group.

Verification of MDR1 gene down regulation by PCR

Total RNA from mock and siRNA transfected hCMEC/D3 cells was isolated using an RNeasy Plus Mini Kit (Qiagen, Hilden, Germany). Each PCR reaction mixture (25 µL) contained 12.5 µL iScript™ 2X probes RT-PCR reaction mix, 0.5 µL iScript™ reverse transcriptase, 0.695 µL of Taqman® primer/probe, 100 ng of RNA (in 5 µL) and 6.305 µL nuclease-free water. Measurement of gene expression by quantitative analysis was carried out in a CFX96 system (Bio-Rad, Hercules, CA). Thermocycling was performed at 50 ºC for 10 min, 95 ºC for 5 min, followed by 50 cycles of 95 ºC for 15 sec and 60 ºC for 30 sec. The threshold cycles (Ct) were calculated automatically using the CFX manager software. To determine relative gene expression between scrambled siRNA and P-gp-directed siRNA transfected cells, the-fold change method (2-ΔΔCt) was employed using Equations 2 and 3, with glyceraldehyde 3-phosphate dehydrogenase (GAPDH) and β-actin employed as reference genes. The geometric mean of the Ct values for the two reference genes (Ct reference) were used in the calculation:

$$\Delta Ct = Ct_{(P\text{-}gp)} - Ct_{(reference)} \qquad \textit{Equation 2}$$

$$\Delta\Delta Ct = \Delta Ct_{(siRNA\ transfected\ cells)} - \Delta Ct_{(scrambled\ siRNA\ cells)} \qquad \textit{Equation 3}$$

Verification of P-gp upregulation by functional P-gp assay

For assessment of functional upregulation of P-gp, hCMEC/D3 cells were seeded onto 24-well plates at a density of 35,000 cells cm^{-2}. Approximately 24 h later, when cells had reached 30-50% confluency, the media was removed and replaced with 500 µL of media with 0.1% DMSO

(control), or media containing the known P-gp upregulator, SR12813 (5 μM), before being left to incubate for 72 h. The relatively higher increase in P-gp expression observed by SR12813 (relative to rifampicin), guided the selection of this molecule for functional analysis. After the 72 h growth period, the accumulation experimental protocol was commenced, based on the protocol developed by Tai et al (15). Initially, the drug solutions were removed and all wells were rinsed twice with 500 μL of pre-warmed PBS, before being re-incubated for 15 min on a shaker platform in transport buffer (10 mM HEPES in HBSS, pH = 7.40) again containing 0.1% (v/v) DMSO or 5 μM SR12813. In addition, a subset of control and drug treated cells were incubated with 5 μM PSC833 (a P-gp inhibitor). After 15 min the wells were then rinsed once more with 500 μL/well of transport buffer, which was then replaced with 500 μL of transport buffer containing 5 μM of the known P-gp substrate R123, in addition to the 5 μM SR12813 ± 5 μM PSC833. Cells were then left on gentle shaking inside an incubator for 60 min. After 60 min, each well was rinsed three times with 500 μL per well of ice-cold transport buffer, before being immediately lysed with ice-cold lysis solution (1% Triton X-100 in milliQ water), for 15 min with gentle agitation at 4°C. After 15 min, the fluorescence of R123 in each individual well was measured using an Enspire fluorescence spectrophotometer (PerkinElmer, Waltham, MA, USA), with an excitation wavelength of 511 nm and an emission wavelength of 534 nm. The unknown concentrations of R123 were determined by comparison to standard solutions of known concentrations of R123 which were prepared in the same matrix (1% Triton X-100 in milliQ) and on the same day as the accumulation experiment and pipetted into and scanned in a 24-well plate. Immediately after fluorescence was measured, two 20 μL aliquots from each well were removed and dispensed onto a non-sterile 96 well plate for protein content analysis. This new 96-well plate was then processed and compared to a freshly prepared standard curve for protein quantification using the BCA protein kit and bovine serum albumin

as a standard. The accumulation of R123 was then expressed as nmol of R123 per μg of total protein per well.

Statistical analysis

All statistical analyses were executed using the *GraphPad Prism* 6 software. All data are presented as mean ± SD and the number of biological replicates is in most cases conveyed by representation by individual data points on each graph. For experiments comparing differences between two groups only, a Student's t-test was used, and for all experiments considering three or more groups, statistical differences were assessed by a one-way ANOVA, using a post-hoc Tukey's test, unless otherwise stated.

RESULTS

Selection of appropriate 96 well plate for ICW

The first experiment assessed the magnitude and consistency of light interference and plate autofluorescence in several plate types to help guide plate selection. As shown in Figure 1, the row to row variation in inherent signal magnitude was surprisingly marked in both Perkin Elmer and Costar plates, highlighting their incompatibility with the assay. The Corning plates appeared to provide superior properties and thus this plate type was selected for further use in the development and optimisation of the ICW protocol.

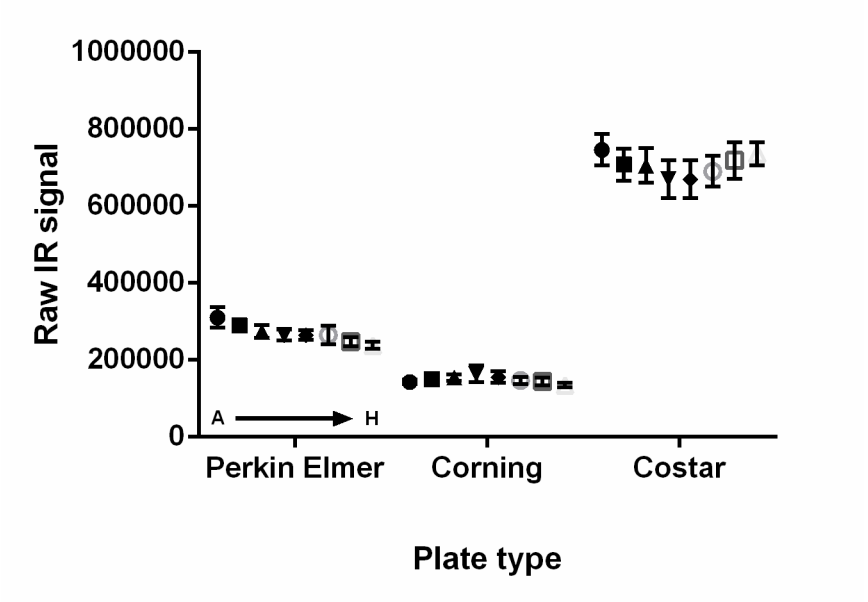

Figure 1: IR signal from 8 rows (A to H) of three different plate types when scanned on the Licor Odyssey imager with the same scanning settings used in all subsequent experiments (microplate2 setting, 3 mm focus offset, scan intensity = 10). Left: Black polystyrene ViewPlateR-96 F TC (Perkin Elmer); middle: Black TC-treated, clear flat bottom wells (Corning); right: transparent, clear flat bottom 96 well plates, sterile but untreated (Costar). The Corning plate exhibited superior inter-row consistency and low autofluorescence amongst the plate types tested. Data are presented as mean ± SD (n = 12 wells per row).

Construction of standard curves for infra-red P-gp and cell number signals and signal to noise ratio optimisation

The new ICW assay was trialled for signal detection for both the IR P-gp signal and the normalising DAPI signal. Figures 2A-B show a standard curve of the IR P-gp signal as a function of increasing cell density in the initial trial (Figure 2A) and then after a series of incremental changes in experimental protocol (Figure 2B), including alterations in primary and secondary antibody concentrations, the addition of surfactant during secondary antibody incubation, the temporal extension of primary antibody incubation, alteration of light intensity settings, and the addition of multiple rinsing steps at the end of the protocol. In the initial trial experiment, the signal contribution to overall IR light was found to be only 10%, but after the optimisation process this ratio reached > 98%. Also improved was the linearity of the standard curve, which was initially calculated to have an R^2 of 0.64 (Fig 2A), but which reached 0.98 in

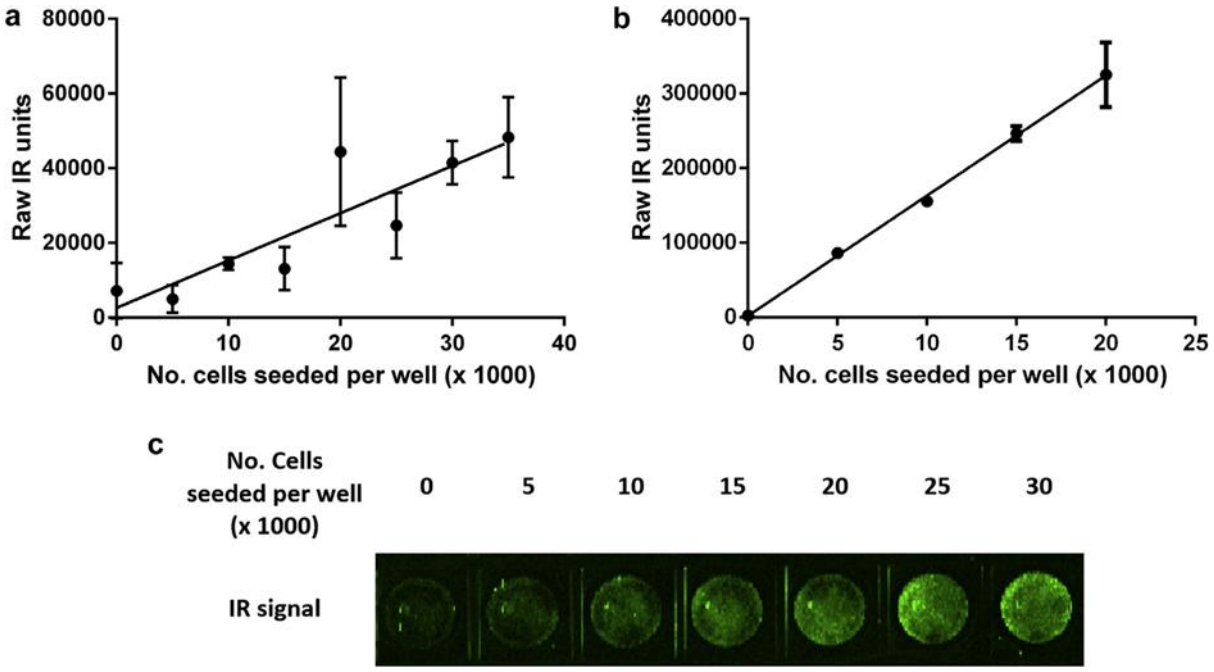

Figure 2: Iterative improvement of experimental protocol of ICW for P-gp in hCMEC/D3 cells: IR signal from P-gp as a function of known number of hCMEC/D3 cells seeded in A) initial trial with signal:noise of only 10% and an R^2 = 0.64 and B) final protocol with a signal:noise ratio of 98% and an R^2 of 0.98. Data are mean ± SD where n = 3. C) Representative image of P-gp signal generated with increasing number of hCMEC/D3 cells by this developed and optimised ICW protocol.

the final protocol (Figure 2B), indicating a high degree of linearity. As shown on the y-axis of figures 2A-B, signal magnitude was also enhanced approximately 8-fold, in the centre of the final linear dynamic range, as a result of the optimisation process. Figure 2C exemplifies the typical IR signal readout, where a fairly homogenous distribution of light emanates from each well, in this case increasing with cell density from left to right. The same iterative process described above was applied simultaneously to the DAPI signal intended for use to normalise the P-gp signal to the number of cells in each well. The DAPI signal appeared to be quite consistent and robust in the first iteration, and did not require any further optimisation. Figures 3A-B show the DAPI signal plotted as a function of increasing number of cells seeded into individual wells, either immediately after the completion of cell plating (4 h post plating) or after allowing for significant cell growth (24 h post plating). The difference between the profiles shown here (linear versus exponential/sigmoidal) demonstrates an aspect of sensitivity in the assay. Figure 3A indicates that the DAPI signal reflects the intended linear increase in the number of cells with increasing cell density, and Figure 3B indicates that a relatively low cell density can retard cellular proliferation, due to the lower concentration of cell signalling factors within the growth setting, as has been demonstrated previously (21). Figure 3C shows a DAPI heat map where increasingly red colours represent increasing cell density as detected by DAPI fluorescence.

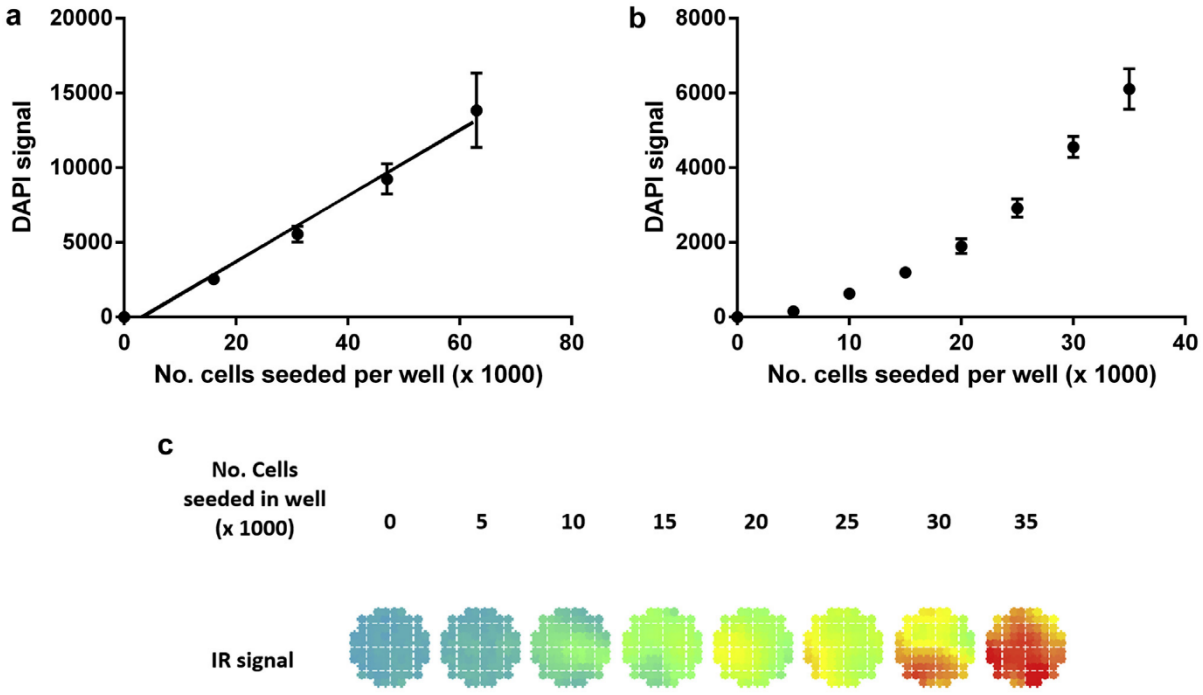

Figure 3: Linearity of DAPI signal as a function of number of hCMEC/D3 cells seeded. A) Linear signal obtained when cells are fixed 4 h post seeding (R^2 = 0.94), B) exponential signal obtained when cells are fixed 24 h after seeding, at which point significant cell growth reveals differences in proliferation rates for different seeding densities. Data are mean ± SD where n = 3. C) Representative image of DAPI heat map with increasing number of hCMEC/D3 cells generated by Perkin Elmer software.

Imaging of IR antibody signal origin in hCMEC/D3 cells

Once satisfactory standard curves relating hCMEC/D3 seeding density to the P-gp and DAPI signals had been obtained, it was necessary to confirm that the signal associated with both P-gp and DAPI was arising from the appropriate cellular origins. Therefore an experiment utilising the now established ICW protocol was executed with the IR emitting secondary antibody being substituted for the fluorescent FITC-conjugated secondary antibody to facilitate visualisation by confocal fluorescence microscopy. As can be seen in Figure 4A, the green channel (FITC) displays an appreciable P-gp signal dispersed amongst the cell surface, and some trans-golgi apparatus and endoplasmic reticulum staining, all above a visibly present but low background stain. The DAPI signal, shown in blue, correlated spatially with the FITC signal in an expected manner. Figure 4B shows an image taken under the same conditions but

in the absence of primary antibody incubation. The very low level of green fluorescence in this image demonstrates the requirement of the P-gp antibody, supporting antibody specificity under the conditions of this assay.

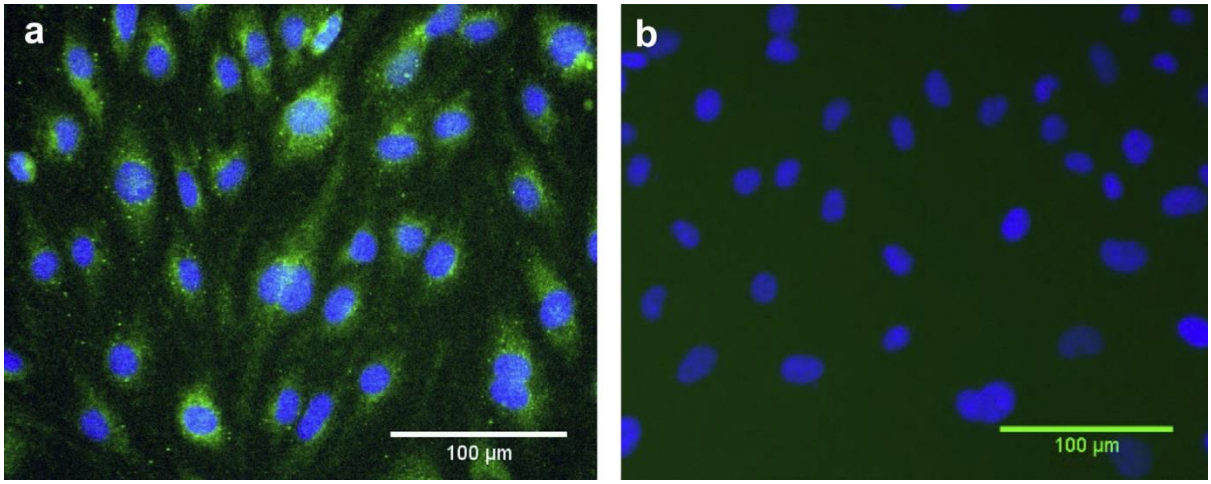

Figure 4: A) hCMEC/D3 cells stained with FITC conjugated to C219 antibody for P-gp (green) and DAPI binding to DNA in cell nucleus (blue), B) image generated same as above but in the absence of C219 P-gp antibody, showing vastly reduced green channel signal. Images demonstrate that the majority of the FITC signal originates from cell surfaces and organelles rather than inter-cell background regions and that non-specific secondary antibody binding is largely absent when the P-gp primary antibody is omitted from the protocol.

Validation of P-gp ICW by comparison to WB using known P-gp regulators

The next phase of the ICW validation involved treating hCMEC/D3 cells with compounds which were shown previously in the literature to cause an upregulation in P-gp expression and to compare these results to those obtained using the traditional WB procedure. Figures 5A-B show the increased expression of P-gp by 1.4 and 1.5-fold after a 72 h treatment with rifampicin, when assessed by WB and ICW respectively. Figure 5C illustrates a representative blot from this experiment, and 5D represents the raw IR signal from one control well and one rifampicin treated well. Figures 6A-B show a 1.5 and 1.9-fold upregulation of P-gp following a 72 h SR12813 treatment, as assessed by WB and ICW respectively. Representative examples of the WB and ICW results are depicted in Figures 6C-D respectively, where the intensity of

the IR signal is visibly enhanced upon treatment of the hCMEC/D3 cell line with 5 μM SR12813. This close approximation to WB analysis by the new ICW protocol indicated that the latter assay was able to detect similar fold-changes in P-gp expression as the traditional WB approach, but with the potential for improvements in throughput.

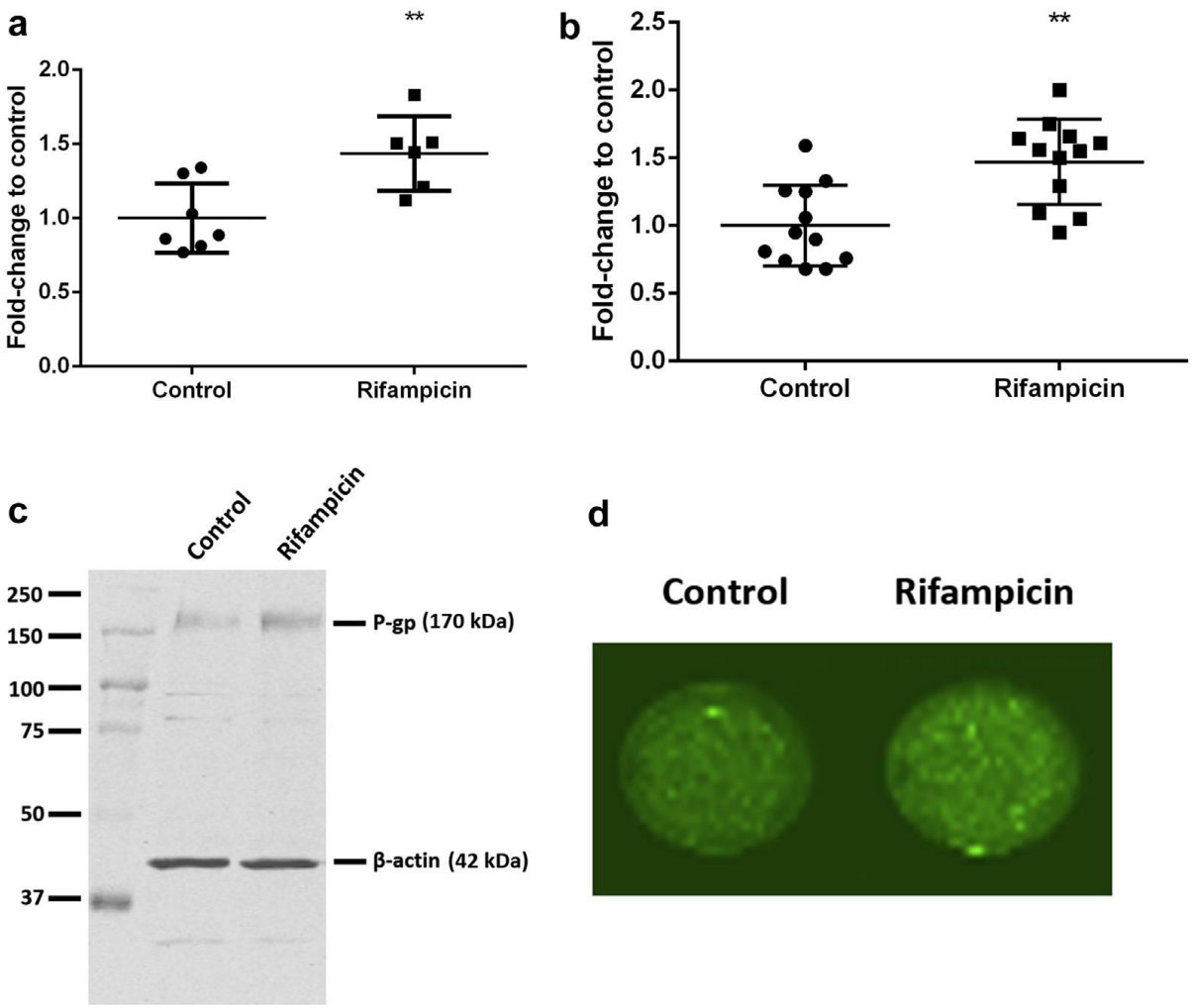

*Figure 5: Use of known P-gp upregulator rifampicin for validation of P-gp ICW protocol. A) 72 h treatment with 10 μM rifampicin led to a 1.4 fold upregulation when assessed by WB (n = 6 - 7); B) The same treatment as above led to a 1.5-fold upregulation when assessed by ICW (n = 12), C) Representative western blot and D) Representative image of IR P-gp signal from control well (left) and 10 μM rifampicin. Data shown are mean ± SD where ** = p < 0.01, when compared to control via an unpaired t-test.*

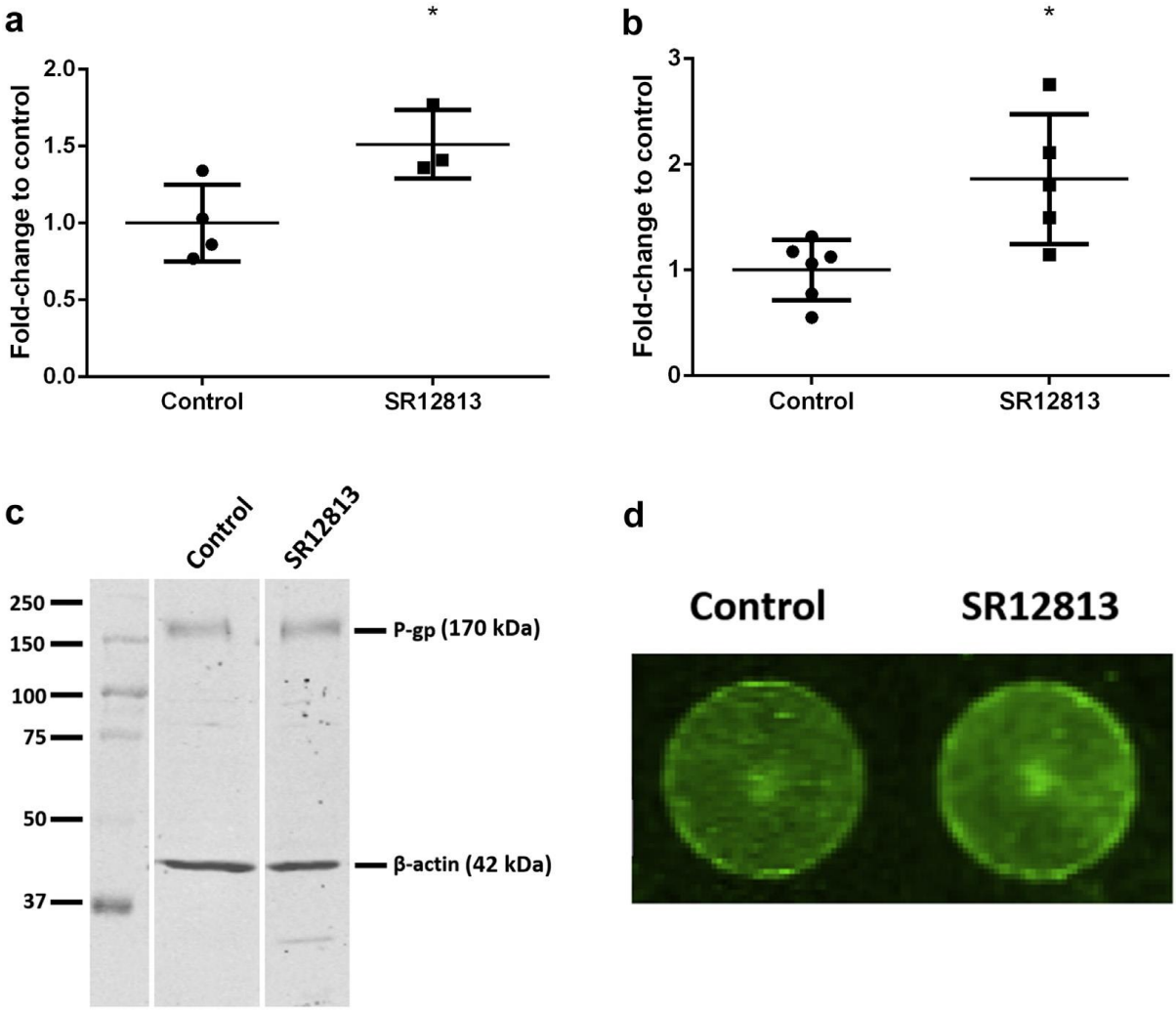

*Figure 6: Use of known P-gp upregulator SR12813 for validation of P-gp ICW protocol. A) 72 h treatment with 5 μM SR12813 led to a 1.5-fold upregulation as assessed by WB (n = 3-4); B) 72 h treatment with 5 μM SR12813 led to a 1.9-fold upregulation as assessed by ICW (n = 5-6). C) Representative western blot and D) Representative image of IR P-gp signal from control well (left) and well treated with 5 μM SR12813 (right). Data shown are mean ± SD where * = $p < 0.05$, when compared to control via an unpaired t-test.*

P-gp knockdown by siRNA transfection

As an extra measure of confirmation that the ICW IR signal originated with P-gp, siRNA directed against P-gp was transfected into the hCMEC/D3 cell line. Initially a cell viability assay (MTT) was utilised to ensure that the transfection reagents and siRNA samples did not interfere with cellular density and metabolism. The MTT results, shown in Figure 7A, indicate that the transfection regime used herein did not appear to harm the normal functioning of the

cells. As shown in Figure 7B, treating immortalised human brain endothelial cells with four separate siRNA target sequences resulted in a 55% reduction in available MDR1 mRNA, as assessed by PCR. When cells were treated with a non-specific target sequence, no significant alterations in MDR1 mRNA were found (Figure 7B). This alteration in MDR1 mRNA by siRNA transfection was next analysed via ICW. The P-gp siRNA transfection treatment produced a 20% reduction in P-gp expression when compared to the scrambled siRNA transfected control (Figure 7C). The same experiment performed in 6-well plates to allow for WB analysis showed a 35% decrease in P-gp abundance in the siRNA mediated knock-down group alone, compared to the scrambled siRNA sequence (Figure 7D).

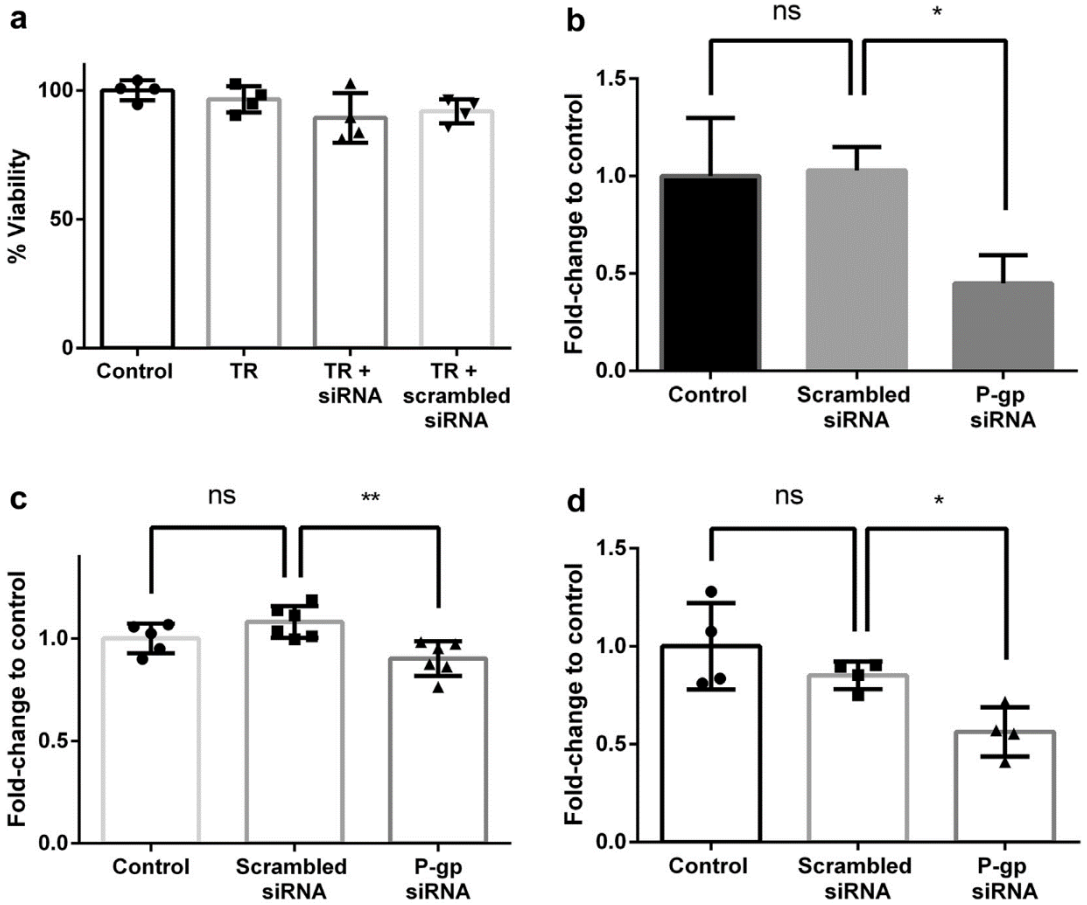

Figure 7: Resulting cell viability, and P-gp gene and protein knock-down after 48 h treatment with transfection reagent (TR) + MDR1 siRNA or scrambled siRNA: A) Cell viability assay demonstrating no significant differences in MTT metabolism between control, TR, TR + P-gp siRNA or TR + scrambled siRNA; B) PCR shows a 55% reduction in MDR1 expression between scrambled and P-gp siRNA treated groups (n = 3); C) ICW assessment shows a 20% reduction in P-gp expression relative to scrambled siRNA control and D) WB assessment shows a 35% reduction in P-gp expression relative to the scrambled siRNA control (all data expressed as mean ± SD and assessed by one-way ANOVA with a post-hoc Tukey's test.

Verification of P-gp upregulation by functional P-gp assay

In order to confirm that the observed upregulation of P-gp by ICW correlated appropriately with enhanced P-gp functionality, SR12813, the treatment shown to produce the largest alteration in P-gp abundance was selected for use in a follow-up experiment. As shown in Figure 8, treatment of the hCMEC/D3 cell line with 5 μM SR12813 decreased R123 accumulation by 18%, whilst the negative control subset of cells incubated with the P-gp inhibitor PSC833 increased R123 accumulation by 80%.

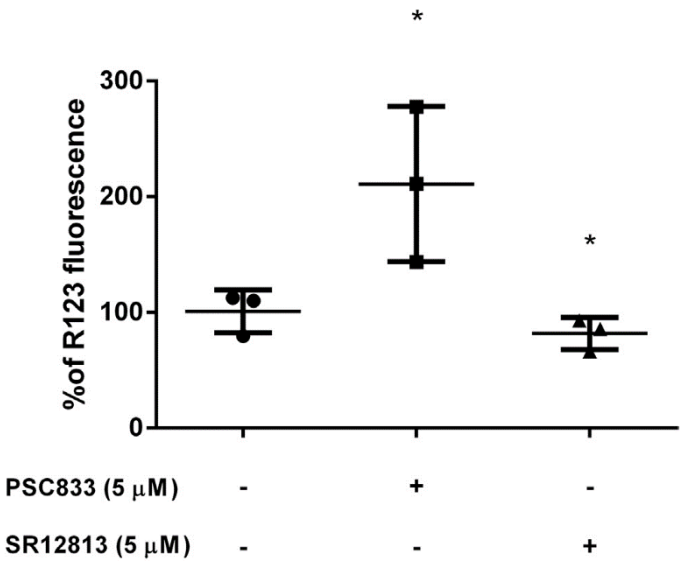

Figure 8: Accumulated R123 fluorescence normalised by mg of protein and expressed as a % relative to the control after 72 h treatment with SR12813. Accumulation during incubation with PSC833 (P-gp inhibitor) causes an 80% increase in accumulated R123, relative to control (positive control) and pre-incubation with SR12813 for 72 h reduced accumulation of R123 by 18% ($p < 0.05$, all data were expressed as mean ± SD and assessed by one-way ANOVA with a post-hoc Tukey's test).*

DISCUSSION

The WB protocol is a very useful method for protein quantification, but at times it can restrain the researcher's rate of decision making and scope of inquiry, by necessitating increased labour per each extra data point desired. Here we attempt to demonstrate the validity of a different method (ICW), with the aim of moderately increasing throughput. Before confidence in this

new method could be experienced, the method needed first to be trialled, developed and validated as an accurate and sensitive method for measuring P-gp abundance using hCMEC/D3 cells as a model of human brain endothelial cells, cells which express P-gp at a similar magnitude to human brain microvessel (22).

During the development phase of assay preparation, multiple parameters were altered in an effort to improve the signal-to-noise ratio and magnitude. Primary and secondary antibody concentrations were altered to find an optimal balance between signal magnitude and the cost-effectiveness of the assay. Initially (first iteration), the primary and secondary antibody dilutions were set to an arbitrary starting point of 1:50 and 1:200, respectively, which yielded a poor signal-to-noise ratio of only 10% (Figure 2A). An antibody optimisation experiment indicated that the signal-to-noise ratio improved to 67%, when the primary and secondary dilutions were instead set to 1:20 and 1:2000, indicating that much of the noise in the initial iteration was due to non-specific binding of the concentrated secondary antibody. In another effort to reduce the initially high background, which is often caused by non-specific binding of secondary antibody, the concentration of Tween-20 in the secondary antibody buffer was increased from 0.1 to 0.5 % (v/v). This increase in surfactant concentration reduced the background level of IR detection and increased the signal-to-noise ratio to 87%, indicating that the provision of a hydrophobic alternative to that of the cellular matrix improved the signal to noise ratio by absorbing much of the non-specific secondary antibody binding. The final improvement in background reduction involved the addition of multiple extra rinsing steps after secondary antibody incubation. The initial trial (Figure 2A) included only three post-secondary antibody rinses with PBS-T. Toward the end of the development process the protocol was updated to five consecutive rinses in 200 μL of PBS-T, followed by two additional rinses with PBS to remove any residual surfactant which might interfere with light transmission.

The addition of these final rinse steps increased the signal-to-noise ratio to its final value of 98%, which was considered satisfactory. The standard curves of both the IR P-gp signal and the DAPI nuclear stain (Figures 2B and 3A respectively) produced by using the final iteration of the ICW protocol showed a high degree of linearity with R^2 values of 0.94 and 0.98, respectively, over the range tested (5000 to 20,000 cells per well). Therefore we define the detection limits of this assay between these seeding densities, which do capture the normal working densities for hCMEC/D3 cells. A typical cell seeding density for hCMEC/D3 cells into 96 well plates would approximate between 10,000 and 15,000 cells per well. When looking at the standard curves of both these signals, such seeding densities are well within the linear dynamic range of both the IR P-gp and DAPI standard curves. Future experiments utilising the new ICW however, would presumably interrogate P-gp regulation between 2-5 days after seeding, where cell density may have increased by a factor of 2-3 by that point in time. Producing linear standard curves under such conditions (after 2-5 days of growth) is however not possible, due to nature of in vitro cell culture, where cell growth and expansion are hindered by the physical space of the wells. Therefore the standard curves here served to show that both the P-gp and DAPI signals were in fact able to respond to increasing abundances of P-gp and nuclei, and that those signals were not saturable under as near as possible to future experimental conditions.

During the development phase, we intentionally chose to use the nuclear DAPI stain for P-gp normalisation rather than a 'housekeeping protein', in order to avoid some of the apparent issues associated with this practice. It has been well reported in the literature that house-keeping protein expression levels fluctuate more than was previously understood, and that their high expression levels lead to saturated signals (23-26). Since each cell can possess only one nucleus, DAPI reflects quite accurately the number of nuclei and therefore the number of cells

within a given well, which ultimately is the intended purpose of normalisation. It is this rationale, combined with the robust and highly linear response from the DAPI molecule which validate this choice.

One of the main concerns when validating a new ICW is genuine signal origin. Unlike WB, there is no attached information about the size of the protein signal in the ICW result. Additionally, unwanted interactions between secondary antibody and the experimental reagents (blocking buffer, collagen, plastic, etc.) may occur and contribute to the observed signal, where the researcher may be unaware of such effects. To investigate the potential for these issues, cellular imaging in both the presence and absence of primary P-gp antibody was performed after execution of the final ICW protocol. In the hCMEC/D3 cell line, expression of matured P-gp should be observed at the cellular and lysosomal membranes (27), as well as P-gp undergoing intracellular trafficking at the trans-golgi apparatus and the endoplasmic reticulum (27). Although the widefield imaging system used in this study was not powerful enough to distinguish accurately between these various localisations and relative magnitudes of P-gp expression, it was successfully demonstrated that the signal obtained after ICW protocol did originate from the hCMEC/D3 cell body and not from intercellular space, with a high concentration green channel light emphasising the spindle like shape of endothelial cells, over a much lower and homogenously distributed background stain (Figures 4A). Furthermore, when a similar image was generated with an identical protocol but in the absence of the C219 P-gp primary antibody (Figure 4B), the previously observed cell body staining was absent, above the same homogenous but low background. Therefore these images served to build confidence that the observed signal was mostly genuine and specific for P-gp.

Once a seemingly satisfactory protocol had been developed, it was necessary to determine whether it was able to detect changes in P-gp expression resulting from pharmacological intervention, assessed side by side with the current standard technique of WB. Several treatments shown to alter P-gp expression in other laboratories were identified in the literature, and replication of these results was undertaken as evidence that the new assay was able to detect changes in P-gp abundance at a similar level of confidence to that of WB. Bendayan et al. have worked extensively with P-gp inhibitors and upregulators, using WB to observe changes in P-gp expression. Bendayan et al. had shown previously that known agonists of human pregnane X receptor (hPXR) were able to initiate an upregulation in P-gp abundance in hCMEC/D3 cells, as assessed by WB. A 2013 publication by this group showed that 72 h treatment with rifampicin or SR12813 caused a 1.9 and 2.2-fold increase in P-gp abundance, respectively, as assessed by WB (28). When the studies were replicated via the ICW protocol, increases in P-gp abundance were indeed observed, albeit sometimes to a more modest degree. For each of the treatments trialled (rifampicin, SR12813 and siRNA targeted against MDR1), both methods produced approximately the same fold-changes between WB and ICW, indicating that the ICW is able to produce results in concordance with those obtained using WB, whether those fold-changes reflect increases or decreases in P-gp abundance.

It can be useful for researchers to distinguish between total cellular P-gp regulation, and the portion of membrane-bound P-gp pertaining to cellular efflux specifically. Within this framework, the ICW is intended not as a standalone tool, but rather to be employed in parallel with functional R123 experiments to better understand the nature and relationship of the detected alterations. It is important to note however, that the changes in P-gp abundance measured by either WB or ICW, are not expected to correlate linearly with functional changes in P-gp by the R123 assay, for which there are several reasons. Firstly, changes measured by

WB or ICW represent total P-gp in the whole cell, whereas the functional R123 assay measures the activity of only the membrane component of cellular P-gp. Additionally, P-gp activity may be at or near the point of saturation when presented with the R123 concentrations typically used in P-gp function experiments, a feature which is necessary to achieve satisfactory R123 signal detection levels. Furthermore, R123 has been shown to be effluxed by transporters other than P-gp (29), further hindering a straightforward relationship between P-gp expression and apparent function. Therefore the 1.9-fold upregulation of P-gp by SR12813 corresponding to an 18% reduction of R123 accumulation appears as expected and appropriate, within the context of routine findings in our laboratory among others (28, 30), as well as confirming a link between observed P-gp expression by ICW and functional enhancement of P-gp activity.

In total, the validation process in this study included comparisons of pharmacologically treated samples between ICW and WB; siRNA knock-down of P-gp gene transcription; fluorescent images indicating appropriate P-gp signal origin and lastly; correlation of observed P-gp expression by ICW with functional upregulation, as demonstrated by the fluorescent P-gp substrate R123. Taken together, the findings of this newly developed ICW protocol appear to provide a valid alternative for the detection of relative P-gp abundance in hCMEC/D3 cells. The 96-well plate format may allow researchers to assess the impact of interventions at multiple time points, or perform multiple experiments in parallel within the one plate, whilst requiring no additional labour time than is required by the processing of one WB. Therefore the ICW method for assessing P-gp expression presented herein represents a viable alternative to WB, which can offer a modest but useful improvement in the rate of progress for researchers probing P-gp regulation and abundance.

CONCLUSION

This study has developed and validated a new ICW method for quantifying the expression of P-gp in hCMEC/D3 cells. The method facilitates an improvement in throughput when compared to WB, and can occupy a place within standard protocols of the laboratories focused on P-gp regulation.

REFERENCES

1. Silva R, Vilas-Boas V, Carmo H, Dinis-Oliveira RJ, Carvalho F, de Lourdes Bastos M, Remiao F. Modulation of P-glycoprotein efflux pump: induction and activation as a therapeutic strategy. Pharmacol Ther. 2015;149:1-123.
2. Cordon-Cardo C, O'Brien JP, Casals D, Rittman-Grauer L, Biedler JL, Melamed MR, Bertino JR. Multidrug-resistance gene (P-glycoprotein) is expressed by endothelial cells at blood-brain barrier sites. Proc Natl Acad Sci U S A. 1989;86(2):695-698.
3. Chin JE, Soffir R, Noonan KE, Choi K, Roninson IB. Structure and expression of the human MDR (P-glycoprotein) gene family. Mol Cell Biol. 1989;9(9):3808-3820.
4. Thiebaut F, Tsuruo T, Hamada H, Gottesman MM, Pastan I, Willingham MC. Cellular localization of the multidrug-resistance gene product P-glycoprotein in normal human tissues. Proc Natl Acad Sci U S A. 1987;84(21):7735-7738.
5. Fojo AT, Ueda K, Slamon DJ, Poplack DG, Gottesman MM, Pastan I. Expression of a multidrug-resistance gene in human tumors and tissues. Proc Natl Acad Sci U S A. 1987;84(1):265-269.
6. Ambudkar SV, Dey S, Hrycyna CA, Ramachandra M, Pastan I, Gottesman MM. Biochemical, cellular, and pharmacological aspects of the multidrug transporter. Annu Rev Pharmacol Toxicol. 1999;39:361-398.

7. Binkhathlan Z, Lavasanifar A. P-glycoprotein inhibition as a therapeutic approach for overcoming multidrug resistance in cancer: current status and future perspectives. Curr Cancer Drug Targets. 2013;13(3):326-346.

8. Davis TP, Sanchez-Covarubias L, Tome ME. P-glycoprotein trafficking as a therapeutic target to optimize CNS drug delivery. Adv Pharmacol. 2014;71:25-44.

9. McCaffrey G, Davis TP. Physiology and pathophysiology of the blood-brain barrier: P-glycoprotein and occludin trafficking as therapeutic targets to optimize central nervous system drug delivery. J Investig Med. 2012;60(8):1131-1140.

10. Schinkel AH. P-Glycoprotein, a gatekeeper in the blood-brain barrier. Adv Drug Deliv Rev. 1999;36(2-3):179-194.

11. Callaghan R. Providing a molecular mechanism for P-glycoprotein; why would I bother? Biochem Soc Trans. 2015;43(5):995-1002.

12. Miller DS, Bauer B, Hartz AM. Modulation of P-glycoprotein at the blood-brain barrier: opportunities to improve central nervous system pharmacotherapy. Pharmacol Rev. 2008;60(2):196-209.

13. Kuhnke D, Jedlitschky G, Grube M, Krohn M, Jucker M, Mosyagin I, Cascorbi I, Walker LC, Kroemer HK, Warzok RW, Vogelgesang S. MDR1-P-Glycoprotein (ABCB1) Mediates Transport of Alzheimer's amyloid-beta peptides--implications for the mechanisms of Abeta clearance at the blood-brain barrier. Brain Pathol. 2007;17(4):347-353.

14. Lam FC, Liu R, Lu P, Shapiro AB, Renoir JM, Sharom FJ, Reiner PB. beta-amyloid efflux mediated by p-glycoprotein. J Neurochem. 2001;76(4):1121-1128.

15. Tai LM, Loughlin AJ, Male DK, Romero IA. P-glycoprotein and breast cancer resistance protein restrict apical-to-basolateral permeability of human brain endothelium to amyloid-beta. J Cereb Blood Flow Metab. 2009;29(6):1079-1083.

16. Vogelgesang S, Cascorbi I, Schroeder E, Pahnke J, Kroemer HK, Siegmund W, Kunert-Keil C, Walker LC, Warzok RW. Deposition of Alzheimer's beta-amyloid is inversely correlated with P-glycoprotein expression in the brains of elderly non-demented humans. Pharmacogenetics. 2002;12(7):535-541.

17. Liu X, Ma T, Qu B, Ji Y, Liu Z. Pesticide-induced gene mutations and Parkinson disease risk: a meta-analysis. Genet Test Mol Biomarkers. 2013;17(11):826-832.

18. Westerlund M, Belin AC, Olson L, Galter D. Expression of multi-drug resistance 1 mRNA in human and rodent tissues: reduced levels in Parkinson patients. Cell Tissue Res. 2008;334(2):179-185.

19. Qosa H, Miller DS, Pasinelli P, Trotti D. Regulation of ABC efflux transporters at blood-brain barrier in health and neurological disorders. Brain Res. 2015;1628(Pt B):298-316.

20. Weksler BB, Subileau EA, Perriere N, Charneau P, Holloway K, Leveque M, Tricoire-Leignel H, Nicotra A, Bourdoulous S, Turowski P, Male DK, Roux F, Greenwood J, Romero IA, Couraud PO. Blood-brain barrier-specific properties of a human adult brain endothelial cell line. FASEB J. 2005;19(13):1872-1874.

21. Todaro GJ, Green H. Quantitative studies of the growth of mouse embryo cells in culture and their development into established lines. J Cell Biol. 1963;17:299-313.

22. Ohtsuki S, Ikeda C, Uchida Y, Sakamoto Y, Miller F, Glacial F, Decleves X, Scherrmann JM, Couraud PO, Kubo Y, Tachikawa M, Terasaki T. Quantitative targeted absolute proteomic analysis of transporters, receptors and junction proteins for validation of human cerebral microvascular endothelial cell line hCMEC/D3 as a human blood-brain barrier model. Mol Pharm. 2013;10(1):289-296.

23. Ferguson RE, Carroll HP, Harris A, Maher ER, Selby PJ, Banks RE. Housekeeping proteins: a preliminary study illustrating some limitations as useful references in protein expression studies. Proteomics. 2005;5(2):566-571.

24. Gorr TA, Vogel J. Western blotting revisited: critical perusal of underappreciated technical issues. Proteomics Clin Appl. 2015;9(3-4):396-405.

25. Welinder C, Ekblad L. Coomassie staining as loading control in western blot analysis. J Proteome Res. 2011;10(3):1416-1419.

26. Li R, Shen Y. An old method facing a new challenge: re-visiting housekeeping proteins as internal reference control for neuroscience research. Life Sci. 2013;92(13):747-751.

27. Fu D, Arias IM. Intracellular trafficking of P-glycoprotein. Int J Biochem Cell Biol. 2012;44(3):461-464.

28. Chan GN, Patel R, Cummins CL, Bendayan R. Induction of P-glycoprotein by antiretroviral drugs in human brain microvessel endothelial cells. Antimicrob Agents Chemother. 2013;57(9):4481-4488.

29. van der Sandt IC, Blom-Roosemalen MC, de Boer AG, Breimer DD. Specificity of doxorubicin versus rhodamine-123 in assessing P-glycoprotein functionality in the LLC-PK1, LLC-PK1:MDR1 and Caco-2 cell lines. Eur J Pharm Sci. 2000;11(3):207-214.

30. Tai LM, Reddy PS, Lopez-Ramirez MA, Davies HA, Male DK, Loughlin AJ, Romero IA. Polarized P-glycoprotein expression by the immortalised human brain endothelial cell line, hCMEC/D3, restricts apical-to-basolateral permeability to rhodamine 123. Brain Res. 2009;1292:14-24.

Chapter 4:

Ionophore and biometal modulation of P-glycoprotein expression and function in human brain microvascular endothelial cells

ABSTRACT

Biometals such as zinc and copper have been shown to affect tight junction expression and subsequently blood-brain barrier (BBB) integrity. Whether these biometals also influence the expression and function of BBB transporters such as P-glycoprotein (P-gp) however is currently unknown. Using the immortalised human cerebral microvascular endothelial (hCMEC/D3) cell line, an in-cell western assay (alongside western blotting) assessed relative P-gp expression after treatment with the metal ionophore clioquinol and biometals zinc and copper. The fluorescent P-gp substrate rhodamine-123 was employed to observe functional modulation, and inductively coupled plasma mass spectrometry (ICP-MS) provided information on biometal trafficking. A 24-h treatment with clioquinol, zinc and copper (0.5, 0.5 and 0.1 μM) induced a significant upregulation of P-gp (1.7-fold) assessed by in-cell western and this was confirmed with western blotting (1.8-fold increase). This same treatment resulted in a 23% decrease in rhodamine-123 accumulation over a 1 h incubation. ICP-MS demonstrated that while this combination treatment had no effect on intracellular zinc concentrations, the treatment significantly enhanced bioavailable copper (4.6-fold). Enhanced delivery of copper to human brain microvascular endothelial cells is associated with enhanced expression and function of the important efflux pump P-gp, which may provide therapeutic opportunities for P-gp modulation.

INTRODUCTION

The blood-brain barrier (BBB) is a dynamic interface which separates the brain parenchyma from the systemic circulation, and serves to protect the brain from xenobiotic insult, whilst simultaneously permitting a high influx of central nervous system (CNS)-essential nutrients (1). To facilitate these needs, a large range of transporter proteins are expressed within the specialised endothelial cells that line the lumen of the BBB (2). Over decades of transporter characterisation research, one of these transporters, P-glycoprotein (P-gp), has emerged as of particular interest in both drug discovery efforts and the pathophysiology of some disease states. P-gp is expressed on the luminal face of the brain endothelium (3), where from the lipid milieu of plasma membrane bilayer it actively effluxes xenobiotics (4), pharmaceuticals and endogenously produced substrates. The existence of P-gp at the BBB has hindered the success of many attempts at brain-targeted drug discovery, whereby many otherwise pharmacologically sound molecular entities are denied CNS access, by virtue of P-gp activity (5). P-gp is also associated with a pathological role in tumorigenesis, where sustained upregulation of P-gp can be a key defensive feature, preventing cellular access of chemotherapeutic agents (6).

It is also becoming increasingly apparent that P-gp plays a pivotal role in the prevention of some disease states, such as that of Alzheimer's disease (AD) (7). In AD, the noxious amyloid-beta (Aβ) which is thought to be responsible for downstream neurodegeneration, is steadily produced by neurons, and cleared from the brain by several mechanisms to prevent accumulation (8). Active efflux of Aβ across blood-brain barrier (BBB) represents one of the main clearance mechanisms of Aβ from the brain parenchyma (9-11), and P-gp appears to play a role in both brain-to-blood efflux of Aβ, as well as in preventing blood-borne Aβ from diffusing or endocytosing back into the brain (12, 13). Although the timelines and causes of

the observed reductions are not yet fully understood (7), waning P-gp expression has been observed within the pathophysiological cascade of AD, which likely corresponds to a reduced capacity for healthy Aβ trafficking (14, 15). Thus it has been suggested that approaches to increase the expression or activity of P-gp by pharmacological means may aid in the treatment of AD, by restoring BBB efflux mechanisms of Aβ trafficking, and subsequently halting the accumulation of Aβ within the CNS (16, 17).

Since P-gp activity is of such interest to CNS-drug access, oncology and AD research, understanding the various biological inputs for P-gp expression is of importance. One potential mechanism for upregulating P-gp is the redistribution of biometals within brain endothelial cells, which has been shown previously to contribute to BBB integrity in a positive manner. Whilst this area is relatively unexplored, some encouraging studies have been conducted. Zinc ions have been shown for example to protect BBB diffusion integrity in juvenile rats (18), and elsewhere Zn^{2+} was demonstrated as essential in maintaining cultured porcine endothelial barrier function (19). More recently, additional studies have also shown that in primary brain microvascular endothelial cells (BMECs), copper at low concentrations increases cell viability and proliferation (20), and that copper alongside vascular endothelial growth factor is a stimulatory driver of angiogenesis in the rat vascular endothelium (21). Thus it was hypothesised that enhanced delivery of zinc or copper ions to human BMECs might facilitate the upregulation of the key AD-related efflux transporter, P-gp.

A set of pharmacological tools available for enhancing the delivery of biometals to cell interiors are a class of drugs known as the ionophores. One of the early ionophores, clioquinol (CQ), has been shown previously to enhance the delivery of both copper and zinc ions across cell membranes and into the cytosol of neurons, where these ions are then freed to influence cell

signalling pathways in a positive manner, with respect to AD (22). Additionally, a nine week treatment of CQ in APP2576 transgenic mice (a mouse model of familial AD that overexpresses a mutant form of amyloid precursor protein, resulting in elevated levels of both soluble and plaque entombed Aβ), produced a 49% reduction in Aβ brain deposition (23). Since CQ was able to ameliorate the AD phenotype in this mouse model via the redistribution of metal ions within the brain, it is possible that CQ may have the potential to traffic plasma-bound biometals in or out of the brain endothelium en route to the brain, with the potential of influencing BBB transporter expression profiles along the way. Therefore, it was hypothesised that by enhancing brain endothelial cell levels of Cu^{2+} and Zn^{2+}, CQ may be able to upregulate P-gp expression and function at the BBB. Herein we used a recently developed and validated in-cell western (ICW) approach, which provides higher throughput and is less labour and consumable intensive than other methods such as western blotting (24), to assess whether CQ can shuttle metal ions into immortalised human cerebral microvascular endothelial cells (hCMEC/D3), resulting in upregulation of P-gp expression and function. The outcomes of these studies have the potential to provide insight into fundamental mechanisms governing the regulation of the important BBB efflux transporter P-gp, with implications for both CNS drug delivery and Aβ clearance from the brain.

MATERIALS

4',6-diamidino-2-phenylindole (DAPI), 3-(4,5-dimethylthiazol-2-yl)-2,5-diphenyltetrazolium bromide (MTT reagent), triton X-100, Tween-20, paraformaldehyde, sodium chloride, potassium chloride, disodium phosphate, rhodamine-123 (R123), potassium phosphate and Corning black polystyrene TC-treated 96 well plates were all purchased from Sigma Aldrich (St Louis, MO). TRIS buffer salt (TRIZMA base), sodium dodecyl sulphate (SDS), ammonium persulfate (APS), N,N,N',N'-tetramethylethylenediamine (TEMED), trypan blue, glycerol,

Trypsin-ethylenediaminetetraacetic acid (EDTA) solution 0.25% in Hank's balanced saline solution (HBSS) and phosphate buffered saline (PBS) were all purchased from Sigma Life Sciences (St Louis, MO). 40% acrylamide/bis solution was purchased from Bio-Rad Laboratories (Hercules, CA). PSC833 was a gift from Novartis (Basel, Switzerland). Odyssey PBS blocking buffer and the goat-anti-mouse secondary antibody were both purchased from Millennium Science (Mulgrave, Victoria, Australia). cOmplete Tablets Mini EASY pack protease inhibitors were purchased from Roche Diagnostics GmbH (Mannheim, Germany). Nitrocellulose membrane (0.2 μm pore-sized) was purchased from GE Life Sciences (Rydalmere, New South Wales, Australia). The C219 P-glycoprotein antibody was purchased from Australian Biosearch (Balcatta, Western Australia, Australia). Corning Costar transparent 96 well plates were purchased from Invitro (Noble Park North, Victoria, Australia). Fluorescein was purchased from Vector laboratories (Burlingame, CA). Black polystyrene ViewPlateR-96 F TC from Perkin Elmer, the Pierce IP lysis buffer and the BCA protein assay kit were all purchased from Thermo Fisher Scientific (Scoresby, VIC, Australia). Both Clonetics EBM-2 basal media and Clonetics EGM-2 single quots growth factor kits were purchased from Lonza (Walkersville, MD). Collagen type I was purchased from Corning Discovery Labware (Bedford, MD). Heat inactivated fetal bovine serum (FBS) was purchased from Life Technologies (Mulgrave, Victoria, Australia). 6 and 96-well plates were purchased from Corning Incorporated (Corning, NY). The purified water used in all experiments was obtained from a Millipore unit and filtered through a Q-pod fitted with a 0.22 μm membrane filter.

METHODS

Seeding/splitting of hCMEC/D3 cells

The immortalized human brain microvascular endothelial cell line (hCMEC/D3) was generously provided by Dr Pierre-Olivier Couraud (INSERM, Paris, France). The EBM2

media which was used for all cell culture experiments, was prepared by supplementation with the following prior to commencement of the studies: 0.01% (v/v) ascorbic acid, 0.01% (v/v) gentamicin/amphotericin, 0.01% (v/v) hydrocortisone, 0.025% (v/v) epidermal growth factor, 0.025% (v/v) insulin-like growth factor, 0.025% (v/v) vascular endothelial growth factor, 0.1% (v/v), b-splice variant fibroblast growth factor, 10 mM HEPES, and 1% (v/v) penicillin/streptomycin and 2.5% (v/v) FBS. Vials of the hCMEC/D3 cell line were kept cryogenically frozen in liquid nitrogen in a solution comprised of 5% (v/v) DMSO in FBS solution. 1 mL vials containing approximately 2 million cells were dispensed into T-75 flasks containing 14 mL of EBM2 media, which had been pre-coated with 3 mL of a 0.1 mg/mL solution of Collagen type I and incubated for 1 h, before being washed with 10 mL of PBS to remove excess collagen. 2 h after seeding of the hCMEC/D3 cells, the initial media was aspirated off and the cells washed twice with warm PBS, before being replaced with fresh and warm EBM2 media. The media was then changed every 2 days until the flasks reached approximately 90 – 100% confluency, at which point they were split into new flasks or plates for subsequent experiments. All experiments involving cells being treated with CQ and/or metal ions Zn^{2+} and Cu^{2+}, involved the following preparation: cells were left to grow in EBM2 growth media until they had reached 70-80% confluency. At the commencement of treatment, in order to remove trace FBS from wells and thus prevent extensive protein binding by CQ, the media was always removed and the cells were rinsed twice with PBS, before the addition of FBS-free EBM2 media with or without CQ and/or Zn^{2+} and Cu^{2+}, in which the cells were incubated until the experimental endpoint. The cells were always stored in an incubator that was kept continuously at 37°C, with an air composition of 95% O_2 and 5% CO_2. All experiments performed using the hCMEC/D3 cell line occurred between passage 30 to 35.

Identification of combinatorial CQ/Zn^{2+}/Cu^{2+} toxicity in hCMEC/D3 cells via morphological assessment and cell viability (MTT) assay

hCMEC/D3 cells were seeded onto 96 well plates, at a density of 30,000 cells cm^{-2} and allowed to grow until reaching approximately 70-80 % confluency. Cells were then washed twice with 150 uL of PBS and then re-nourished with 150 µL of FBS-free EBM2 media containing CQ, $ZnCl_2$ and $CuCl_2$ at increasing concentrations first individually, and in subsequent experiments, in combination. The 96-well plates were then returned to the incubator for 24 h, after which, the plates were transported to a temperature and humidity controlled chamber housing a microscope and camera for morphological assessment. The microscope used was the Nikon Ti-E from Nikon, Japan. The camera used to generate the images was a Photometrics Coolsnap Myo from Photometrics, USA. The 10 x objective lens used was Version 3.22 from Nikon. One image per treatment well was captured before all treatment/media solutions were discarded, and the cells were washed twice with 160 µL of warm PBS. All wells were then treated with 160 µL of FBS free EBM2 media which additionally contained 6.25% (v/v) of an 8 mg/mL MTT reagent solution and then re-incubated for a further 4 h. After the 4 h incubation with the MTT reagent, the solution was aspirated off and 150 µL of DMSO was added to each well. The plates were then agitated for 30 sec and then incubated with DMSO for a further 30 min. Again the plates were shaken for 30 sec, and then absorbance at 540 nm was recorded on a Perkin Elmer absorbance spectrophotometer (Waltham, MA). Blank samples which had undergone all the above procedures except in the absence of cells were also present on the plate, an average of which was taken and subtracted from each individual reading recorded. The absorbance values were then normalized against the average of the control values, to be expressed comparatively as % viability when compared to the control group. Statistical comparisons of the datasets was performed using Dunnett's multiple comparisons test.

Influence of CQ/Zn^{2+}/Cu^{2+}combinations on P-gp expression using an in-cell western approach

hCMEC/D3 cells were seeded onto 96-well collagen-coated plates at a density of 30,000 cells/cm^2 and left to grow in 150 µL of EBM2 growth media until they had reached 70-80% confluency. Cells were then treated with individual and combinatorial treatments of CQ, $ZnCl_2$ and $CuCl_2$ in FBS free media for 24 h, after which the treatment solutions were discarded, and the expression of P-gp quantified by the previously reported ICW technique (24). Briefly, 150 µL of fixing solution (4% (w/v) paraformaldehyde in PBS) was transferred to each well, and the plate was left at room temperature for 20 min. The fixing solution was then discarded and cells were rinsed four times with 200 µL of cell permeabilisation solution (0.1% w/v Triton X-100 in PBS) under mild shaking. A final rinse using 210 µL of PBS was included to remove the detergent. Next, 150 µL of *Licor* PBS blocking buffer was added to each well and the plate was left to stir for 1 h at room temperature. The PBS blocking buffer solution was then removed, and 50 µL of PBS blocking buffer solution containing either a 1:50 dilution of the C219 P-gp antibody or no additional reagents (to be later used as secondary antibody controls) was added. The plate was then left overnight on gentle agitation at 4°C. The following day, each well was rinsed again four times with 200 µL of Tween washing solution (0.1% (v/v) Tween-20 in PBS, (PBS-T)). After removal of the last rinse, each well received 50 µL of PBS blocking buffer containing 0.5% (v/v) Tween-20, 1 µg/mL DAPI, and a 1:2000 dilution of *Licor* goat-anti-mouse (secondary) antibody. During secondary antibody incubation the plate was wrapped in aluminium foil and agitated gently at room temperature for 1 h. After this final incubation the plate was subjected to seven more 5 min rinses with 200 µL of PBS-T in each well, and the final two of these rinses using PBS to remove residual surfactant. The plate was then scanned on an *Odyssey* imager using the 'microplate2' setting with a 3 mm focus offset and the scan intensity of the 800 channel set to 5. After scanning, an ICW grid was applied to the obtained image within the *Odyssey* software, and the integrated intensity of IR signal from

each well was then exported. The average of the IR signal of control wells that had not received P-gp primary antibody incubation was calculated and subtracted from all sample wells, to remove signal coming from non-specific binding of secondary antibody. The plate was then scanned in a *Perkin Elmer* fluorescence spectrophotometer with an excitation/emission wavelengths of 358 and 461 nm respectively. Wells treated only with collagen were used to calculate fluorescent background and subtracted from all other wells to discount any non-specific fluorescence. The remaining P-gp signal of treatment wells was then divided by the remaining DAPI signal, and finally expressed as fold change compared to the average of the control wells (not dissimilar to WB), according to Equation 1:

Equation 1: $$Fold\ change = \frac{\frac{IR_t - IR_b}{F_t - F_b}}{\frac{\sum_{i=1}^{n}\left(\frac{IR_c - IR_b}{F_c - F_b}\right)}{n}}$$

where IR_t = the IR signal from treatment wells; IR_b = the infra-red signal from control wells treated with secondary antibody only (P-gp signal background subtraction); F_t = the fluorescence signal from treatment wells; F_b = the fluorescence signal from empty wells containing collagen only (DAPI background subtraction); IR_c = the IR signal from control wells; F_c = the fluorescence signal from control wells and n = the number of control replicates.

Confirmation of CQ/Zn^{2+}/Cu^{2+}mediated upregulation of P-gp using western blotting

hCMEC/D3 cells were seeded onto 6-well collagen-coated plates at a density of 30,000 cells/cm^2 and left to grow in 2 mL of EBM2 growth media until they had reached 70-80% confluency. Cells were then treated with CQ, $ZnCl_2$ and $CuCl_2$ (0.5, 0.5 and 0.1 μM) in FBS free media for 24 h. Immediately after the 24 h incubation period, treatment solutions were discarded and to each well, 200 μL of a solution containing a 6:1 ratio of *Pierce IP* lysis buffer and a 7x-concentrated solution of cOmplete Tablets Mini EASY pack protease inhibitors, was

dispensed into each well. Cells were then lysed in this solution for 15 min at 4°C, after which each well was scraped to ensure full detachment of cells. The solution from each well was transferred to a pre-cooled Eppendorf tube and spun at 14,000 rcf for 5 min before supernatant collection and protein content analysis via the *Pierce* BCA protein assay kit using bovine serum albumin (BSA) as a standard. Western blotting was carried out by loading a 10% acrylamide 1 mm hand-cast gel with varying volumes of lysate/Laemlli (5:1 ratio) buffer resulting in 15 μg of total cellular protein being loaded into each lane. Electrophoresis was executed at 60 V for 30 min followed by 1.5 h at 150 V. Electrophoresed gels along with extra thick blot paper and 0.2 μm pore-sized nitrocellulose membranes were allowed to equilibrate in transfer buffer containing 20% (v/v) methanol for 30 min before transfer. Transfer was executed using semi-dry consumables and the Turbo-blot transfer system (*Bio-rad*, Gladesville, New South Wales, Australia) set to 40 min at 25 V and 1.0 A. Transfer membranes were then rinsed briefly in TBS-T and then incubated in ~20 mL of *Licor* blocking buffer at room temperature for 1 h. Membranes were again rinsed briefly in TBS-T and then incubated with a 1:500 dilution of the C219 antibody in TBS-T overnight. The β-actin antibody was added to the incubation solution for only the final 20 min of the overnight primary antibody incubation step, to avoid saturation of the actin signal at a dilution of 1:10,000. Following 4 x 10 min membrane washes in TBS-T, the membranes were incubated in *Licor* goat-anti-mouse secondary antibodies for 2 h at room temperature followed by the same washing regime as above. Membranes were scanned on the *Licor Odyssey* imaging instrument, and densitometric analysis was executed via the *ImageJ* software. Densitometric P-gp signals were normalised to β-actin signals and expressed as relative fold-changes to controls.

Influence of CQ/Zn^{2+}/Cu^{2+} on P-gp function assessed by R123 trafficking

hCMEC/D3 cells were seeded onto two separate 24-well collagen-coated plates at a density of 30,000 cells/cm^2 and left to grow in 500 µL of EBM2 growth media until they had reached 70-80% confluency. Plate 1 was used for the analysis of R123 uptake and plate 2, processed in parallel until the final 10 min of experimentation, was used for the determination of R123 efflux. Upon reaching 70-80% confluency, cells were treated with either (1) no treatment (control) or (2) 0.5 µM CQ, 0.1 µM Zn^{2+} and 0.1 µM Cu^{2+}. Each of these treatment conditions contained 0.1% DMSO and each were administered in an identical fashion to replicates occurring on both plates. After a 24 h incubation, the uptake/efflux experimental protocol was commenced; all solutions were removed and the wells were rinsed twice with 500 µL of pre-warmed PBS. Following rinsing, the cells were then re-incubated in transport buffer (10 mM HEPES in HBSS, pH = 7.40), or transport buffer containing 5 µM PSC833 (a known P-gp inhibitor), for 15 min on a shaker platform. After 15 min the wells were rinsed once with 500 µL/well of transport buffer (± 5 µM PSC833), which was then replaced with 500 µL of transport buffer (± 5 µM PSC833), or 500 µL of transport buffer (± 5 µM PSC833) with the addition of 5 µM of the known P-gp substrate R123. Both plates (still effectively identical at this stage) were then left on gentle shaking inside an incubator for 60 min. After 60 min, the experimental processing of the two plates diverged; plate 1 (R123 uptake) was rinsed three times with 500 µL per well of ice-cold transport buffer before being immediately lysed with ice-cold transport lysis solution (1% v/v Triton X-100 in MilliQ water), for 20 min and on gentle agitation at 4°C. After 20 min, the fluorescence of R123 in each individual well was measured using an *Enspire* fluorescence spectrophotometer (PerkinElmer, Waltham, MA), with an excitation wavelength of 511 nm and an emission wavelength of 534 nm. The unknown concentrations of R123 were determined by comparison to standard solutions of known R123 concentrations which were prepared in the same matrix (1% v/v Triton X-100 in milliQ water) on the day of the uptake

experiments. Immediately after the fluorescence was measured, two 20 μL aliquots from each well were removed and dispensed onto a non-sterile 96 well plate for protein content analysis. This new 96-well plate was then processed and compared to a freshly prepared standard curve for protein quantification using a BCA protein kit and BSA dissolved in the same matrix used as standards, and these values were later used to normalise R123 content in individual wells. The wells in plate 2 (R123 efflux) were then also rinsed three times with 500 μL per well of ice-cold transport buffer, before being re-incubated in transport buffer (± 5 μM PSC833) for a further 10 min, again on gentle agitation. After this 10 min period, all wells in the plate were subjected to the same lysing protocol as described for plate 1, before the measurement of R123 fluorescence and determination of protein content (described above). The experiment was executed in such a way that both plates 1 and 2 received identical treatments with respect to time, excluding the 10 min efflux phase (plate 2 only). The R123 fluorescence values from the accumulation plates were first normalised by well specific protein content, and then expressed as a percentage relative to the control replicates. The data from the efflux plates were expressed as the percentage of R123 remaining after efflux, relative to the accumulation control wells.

Assessment of hCMEC/D3 cellular translocation of Zn^{2+} and Cu^{2+} by CQ treatment

To identify whether treatment of hCMEC/D3 cells with CQ and different metal combinations resulted in enhanced cellular uptake of metals, the concentrations of Cu and Zn were measured by inductively coupled plasma mass spectrometry (ICP-MS). hCMEC/D3 cells were seeded onto two separate 24-well collagen-coated plates at a density of 30,000 cells/cm^2 and left to grow in 500 μL of EBM2 growth media until they had reached 70-80% confluency. Cells were then treated with the same treatment regime as was used for assessing P-gp expression above (individual and combinatorial treatments of CQ, Zn^{2+} and Cu^{2+}) in FBS free media for 24 h. After 24 h of treatment (or alternative time points as illustrated in results figures), the media

was removed and cells were rinsed twice with sterile PBS to wash out any plastic-bound metal ions, before the addition of 250 μL per well of 1% Triton X-100 in PBS. Lysis was carried out exactly as was described for western blotting (including protein quantification for normalisation), except for the omission of the cellular-debris removing centrifuge step, but including the removal of a 20 μL aliquot for protein quantification by the BCA assay, to later be used for normalising data against well-to-well variability in cell density. Samples were stored at -80°C until analysis by ICP-MS. After freeze-drying the samples, each lyophilised cell crude extract was resuspended by adding 30 μL of concentrated nitric acid 65% (Suprapur Merck, Darmstadt, Germany) and allowed to digest for 6 h at room temperature. The samples were heated at 90°C for 20 min using a heating block to complete the digestion. The reduced volume after digestion was ~20 μL. Each sample was made up to 1.150 mL by the addition of 1.130 mL of 1% (v/v) of nitric acid diluent. Measurements were made with an Agilent 7700 series ICP-MS instrument (Agilent Technologies, Santa Clara, CA) under routine multi-element operating conditions using a Helium Reaction Gas Cell. The instrument was calibrated using 0, 5, 10, 50, 100 and 500 ppb of certified multi-element ICP-MS standard calibration solutions (ICP-MS-CAL2-1, ICP-MS-CAL-3 and ICP-MS-CAL-4, AccuStandard, New Haven, CT) for a range of elements. A certified internal standard solution containing 200 ppb of Yttrium (Y89) as an internal control (ICP-MS-IS-MIX1-1, Accustandard, New Haven, CT) was used for internal calibration. For each individual treatment tested, wells containing no cells were also incubated in treatment solutions, and underwent the same procedure as just described, such that background signal caused by treatment/plastic contamination was quantified, and averages of these controls were subtracted from actual experimental metal concentrations. The remaining metal concentrations were then multiplied by the lysis volume (230 μL) to reach a molar quantity of metal ions, and then normalised by the protein content of each well measured during lysis, and resultantly expressed as nmol (metal)/mg of protein, according to Equation 2:

Equation 2: $$Normalised\ [metal] = \frac{([cellular\ metal] - [blank\ metal]) \times V}{protein}$$

where [cellular metal] = the metal concentrations in treated cell samples determined by ICP-MS, [blank metal] = the metal concentrations in samples derived from wells which received treatment but contained no cells, V = the volume of lysis buffer after the removal of protein content sample (0.00023 L), and protein = protein mass per well determined by the BCA assay, used here to normalise against well-to-well variability in cell density.

Statistical analysis

All data were visualised and statistically analysed using the Prism Graphpad Version 7 software. All comparisons between two groups were assessed by Student's t-test, whilst all experiments involving more than two groups, were assessed by one-way analysis of variance (ANOVA), with multiple comparisons assessed by Dunnett's test, or Tukey's test in the case of ICP-MS. Differences between groups were considered significant if the generated p values fell below 0.05.

RESULTS

Identification of combinatorial CQ/Zn^{2+}/Cu^{2+}limits of toxicity in hCMEC/D3 cells

Before the chemical agents CQ/Zn^{2+}/Cu^{2+} could be assessed for modulation of P-gp, the toxicity of each agent individually and in combination against the hCMEC/D3 cell line had to first be assessed, so as to not unintentionally deliver toxic concentrations and induce P-gp upregulation by generic cellular defence mechanisms. Toxicity in this regard was assessed via the use of the MTT reagent alongside morphological assessment of the cells via microscopy. Each component of CQ, Zn^{2+} and Cu^{2+} was assessed over the concentration range of 0.1 to 10 μM. As shown in Figures 1A and C, low concentrations of both CQ (0.1 and 0.5 μM) and Cu^{2+} (0.1 μM) actually stimulated metabolism of the MTT reagent (proxy for cell viability), causing

36 and 23% increases in formazan production, respectively. On these same figures it is observed that the highest concentrations of CQ and Cu^{2+} which did not induce detectable toxicity were 0.5 and 1 μM respectively. Figure 1B shows cell viability following Zn^{2+} treatment, and indicates that the cells tolerated the addition of Zn^{2+} up to a concentration of 1 μM.

Representative images from the morphological assessment are shown in Figures 1D, E and F and are concordant with the results generated by the MTT assay, whereby cells treated with 0.5 μM of CQ (Figure 1E) appear as normal compared to control cells, but in contrast those treated with 10 μM of CQ (Figure 1F) exhibit visible pathological morphology. The same procedures were executed for treatment combinations of all three chemical agents ($CQ/Zn^{2+}/Cu^{2+}$), and the highest concentrations tolerated by the hCMEC/D3 cell line were 0.5, 0.5 and 0.1 μM for $CQ/Zn^{2+}/Cu^{2+}$ in combination, respectively. Therefore these concentrations were chosen for the further experiments below regarding P-gp regulation, function and biometal trafficking.

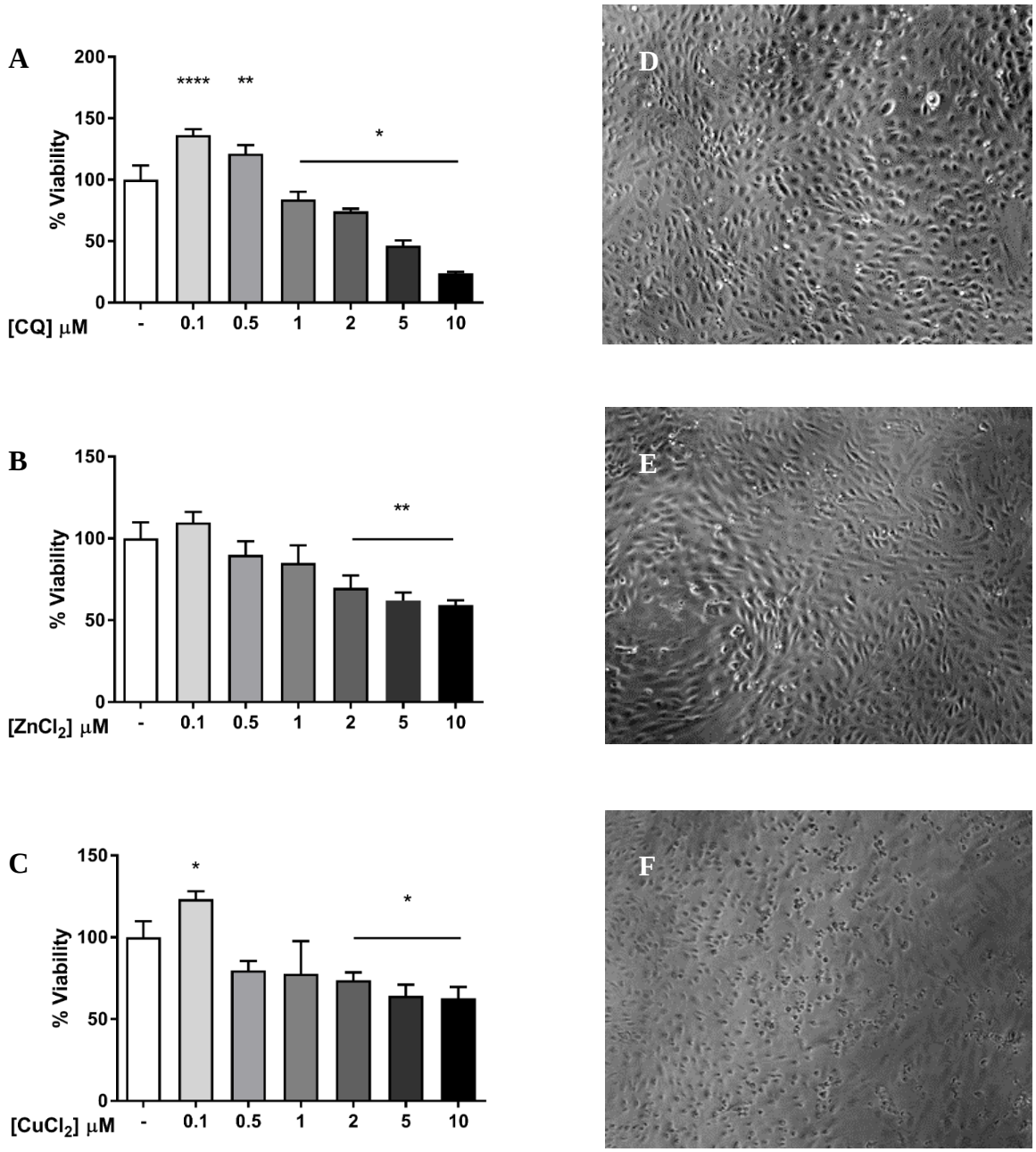

*Figure 1: Cell viability as assessed by cellular metabolism of the MTT reagent following treatment of hCMEC/D3 cells with increasing concentrations of the chemical agents CQ (1A), Zn^{2+} (1B) and Cu^{2+} (1C). Lower concentrations of CQ and Cu^{2+} (0.5 and 0.1 μM respectively) increase cell viability whilst higher concentrations induce decreases in cell viability. Figures 1D-F are microscopic images of hCMEC/D3 cells used for morphological assessments of the following treatments D) control indicating benchmark for normal morphology, E) 0.5 μM CQ - normal morphology and thus indicating no toxicity and F) 10 μM CQ - altered morphology indicating toxicity of treatment. All data shown were assessed by Dunnett's test, and bars represent mean ± SD where n = 3 and * denotes p < 0.05.*

P-gp expression in hCMEC/D3 cells is increased with exposure to CQ/Zn^{2+}/Cu^{2+} combination

A recently developed ICW protocol (24) was implemented to first assess whether CQ and the metal ions Zn^{2+} and Cu^{2+}, alone or in combination, were able to enhance P-gp expression in hCMEC/D3 cells. The highest non-toxic concentrations that were tolerated by the hCMEC/D3 cell line (both alone and in combination) were identified as 0.5 μM CQ, 0.5 μM Zn^{2+} and 0.1 μM Cu^{2+} via the MTT assay and morphological assessment. As shown in Figures 2A and B, the only treatment group to significantly increase P-gp expression relative to control group after analysis via a Dunnett's one-way ANOVA, was the combination of all three components: CQ (0.5 μM), Zn^{2+} (0.5 μM) and Cu^{2+} (0.1 μM), which produced a 1.7-fold increase in P-gp abundance ($p = 0.0045$). Since each of the components (CQ, Zn^{2+} and Cu^{2+}) when tested alone had no significant effect on P-gp expression, this result indicated that the presence of CQ and both metal ions may be required for significant upregulation of P-gp. The influence of this treatment group on P-gp expression was then assessed by western blotting, to confirm the observed upregulation, and as shown in Figures 2C and D, this combination produced a significant 1.8-fold upregulation of P-gp abundance ($p = 0.043$), similar to that observed with the ICW approach. All further studies assessing the influence of CQ/Zn^{2+}/Cu^{2+}on hCMEC/D3 dynamics were undertaken with this particular combination.

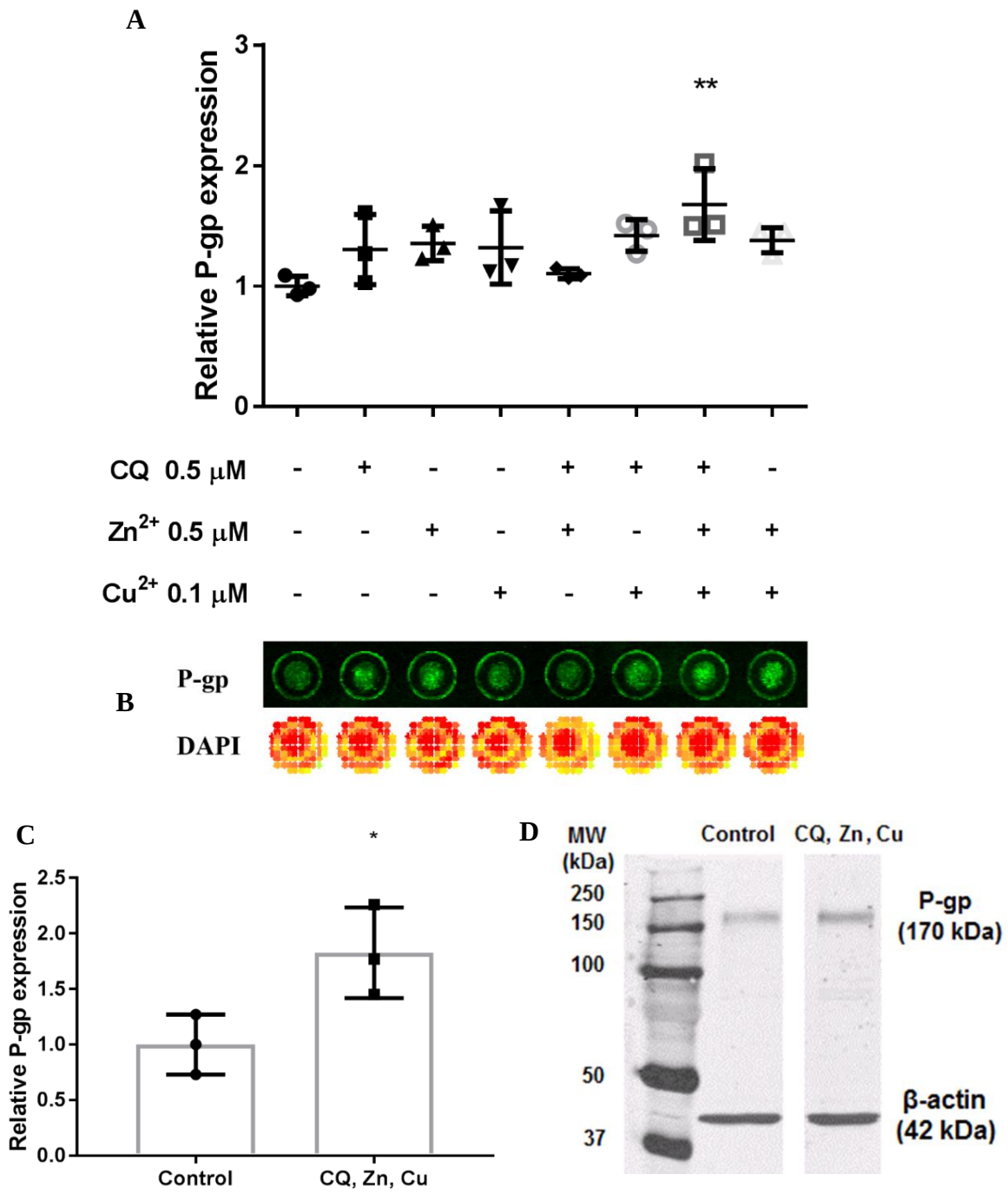

*Figure 2: Combinatorial assessment of P-gp upregulation after 24 h treatment with the chemical agents CQ (0.5 μM), Zn2+ (0.5 μM) and Cu2+ (0.1 μM). A) Quantification of relative P-gp expression as assessed by the recently developed ICW protocol. Statistical significance was assessed by a two-way ANOVA (Dunnett's test where n = 3 and ** denotes p < 0.01). B) Representative image of ICW results showing raw infrared P-gp signal (above) and cell number normalising DAPI heat map (below), indicating differential P-gp expression above homogenous inter-well cell distribution. C) Quantification of relative P-gp expression between control and ICW-validated combination of CQ, Zn2+ and Cu2+ as assessed by western blotting. Statistical significance was assessed by a Students t-test (where n = 3 and * denotes p < 0.05). D) Representative western blot for P-gp and β-actin of control versus combination of CQ, Zn2+ and Cu2+. All data shown are individually plotted data points with bars representing mean ± SD.*

Functional trafficking of the P-gp substrate R123 is enhanced following CQ/Zn^{2+}/Cu^{2+} treatment

Since P-gp is expressed and subsequently localised in two distinct regions of brain endothelial cells, namely, the outer cell membrane and the lysosomal membrane (25), an assay utilising the known P-gp substrate R123 was used concomitantly, to ensure that any increase in P-gp expression resulted in increased cellular efflux capacity. Figure 3A illustrates the relative cytosolic accumulation of R123 after a 1 h incubation with the substrate in the presence or absence of the known P-gp inhibitor PSC833. The presence of PSC833 induced a 36% increase in R123 accumulation, whilst pre-incubation for 24 h with CQ (0.5 μM), Zn^{2+} (0.5 μM) and Cu^{2+} (0.1 μM) produced a 23% decrease in R123 accumulation. The inhibitory effect of PSC833 on R123 accumulation was offset by pre-incubation with CQ (0.5 μM), Zn^{2+} (0.5 μM) and Cu^{2+} (0.1 μM). After the accumulation phase, cells were presented with empty transport buffer (± PSC833) and allowed to efflux the substrate for 10 min before additional measurements were made, to demonstrate substrate flux in a bidirectional capacity. As shown in Figure 3B, 32% of the initial R123 load remained in control cells, whilst PSC833 incubated cells retained 56% of the initial substrate load due to P-gp inhibition. The cells pre-treated with the CQ/Zn^{2+}/Cu^{2+} combination however, retained significantly less R123 than control cells (23%), signifying a functional enhancement of P-gp activity in both reducing cellular accumulation of and increased efflux capacity of the R123 substrate. These findings indicate that the induction of P-gp was effective in a bidirectional capacity.

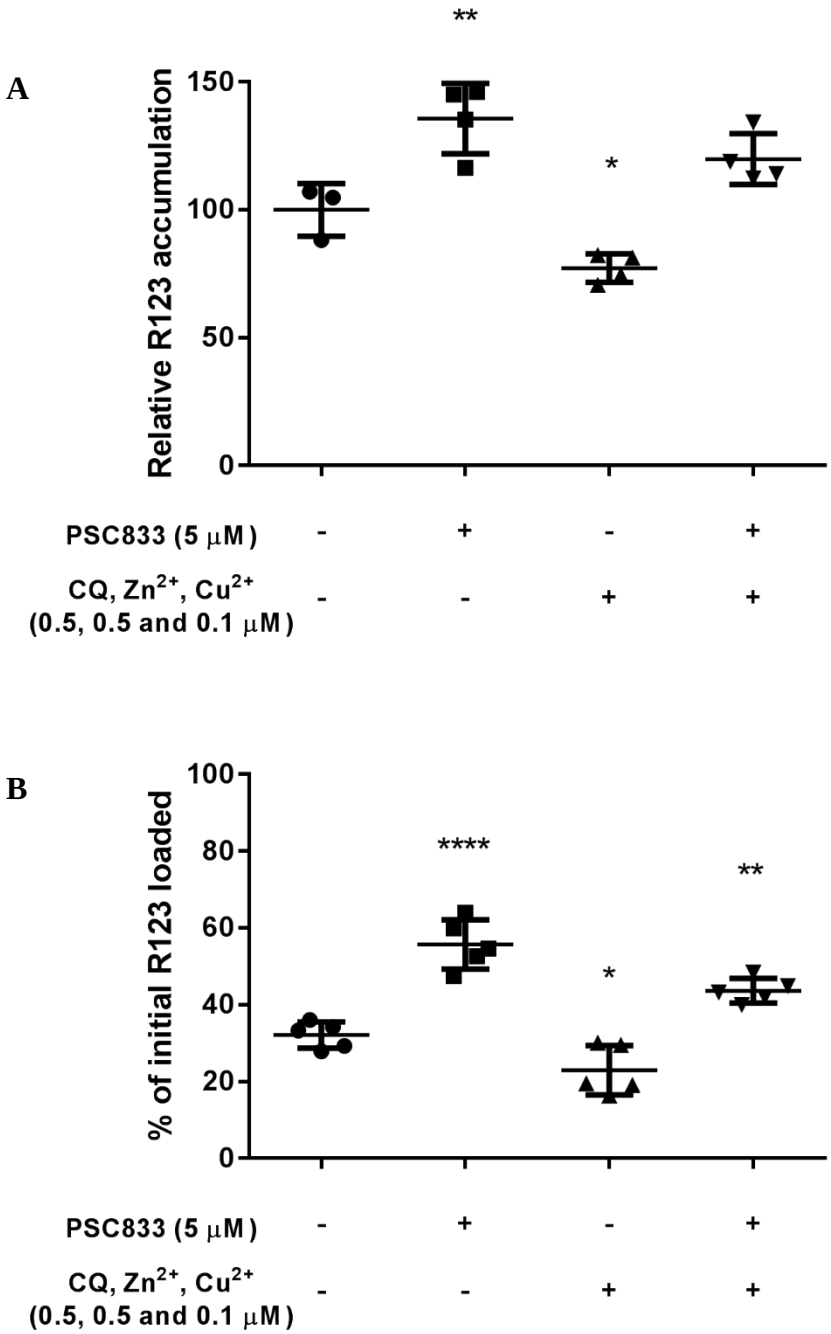

*Figure 3: Functional P-gp upregulation assessed by use of the known fluorescent P-gp substrate Rhodamine-123 (R123), normalised to well protein content via BCA protein assay. A) Relative R123 accumulation is significantly increased (+36%) by assay co-incubation with the known P-gp inhibitor PSC833, and significantly decreased (-23%) after 24 h preincubation with the chemical agents CQ (0.5 μM), Zn2+ (0.5 μM) and Cu2+ (0.1 μM), assessed by two-way ANOVA (Dunnett's test where n = 3-4, * denotes p < 0.05 and ** denotes p < 0.01). B) Percentage of initial R123 loaded remaining after 10 min of substrate efflux. Control cells retained 36%, cells coincubated with PSC833 retained significantly more R123 (56%, where **** denotes p < 0.0001) and cells receiving 24 h preincubation with the chemical agents CQ (0.5 μM), Zn2+ (0.5 μM) and Cu2+ (0.1 μM) retained significantly less R123 (23%), as assessed by two-way ANOVA (Dunnett's test where n = 5). All data shown are individually plotted data points with bars representing mean ± SD.*

CQ increases intracellular copper but not zinc, measured by inductively-coupled plasma mass spectrometry

As a part of identifying the mechanism by which CQ and metal ions were able to facilitate upregulation of P-gp, ICP-MS was employed to measure changes in cellular metal levels (zinc and copper) resulting from the same treatment regime as was assessed for P-gp upregulation above. Despite the complex experimental design and notable intra-treatment noise, three treatment groups (Cu^{2+}, CQ/Cu^{2+} and $CQ/Zn^{2+}/Cu^{2+}$) produced significant increases in cytosolic copper levels when compared to the control group via Tukey's test (Figure 4A). No significant differences between the Cu^{2+} treatment and the P-gp upregulating combination ($CQ/Zn^{2+}/Cu^{2+}$) treatment groups were determined (p = 0.12, bars 4 and 7), however this

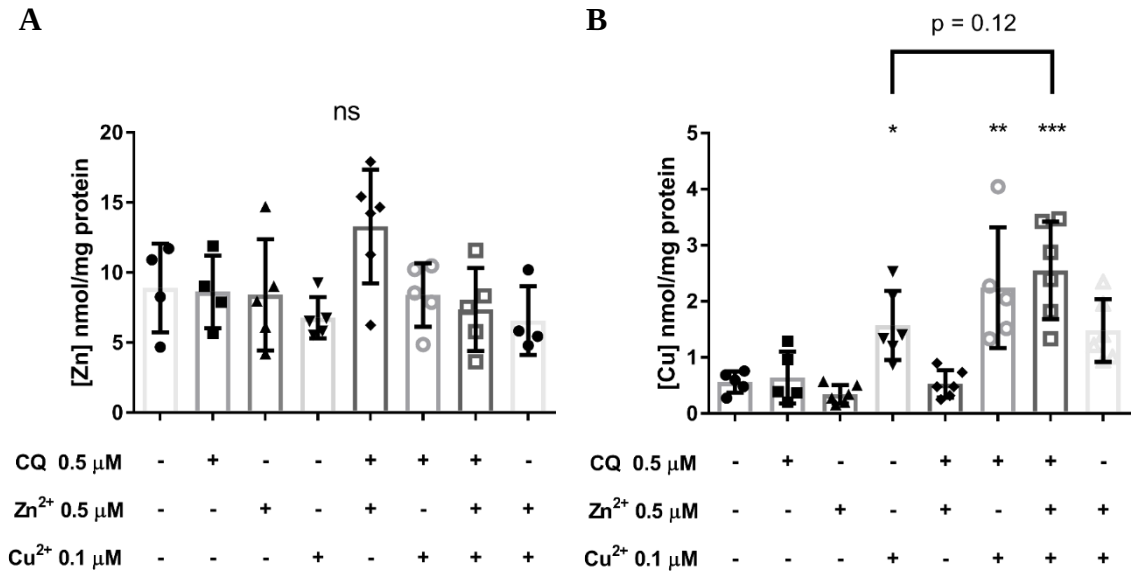

*Figure 4: Combinatorial assessment of metal ion accumulation assessed by inductively coupled plasma mass spectrometry, normalised to well protein content via BCA protein assay, after 24 h treatment by the chemical agents CQ (0.5 μM), Zn2+ (0.5 μM) and Cu2+ (0.1 μM). A) Intracellular Cu levels are significantly increased by 0.1 μM Cu in isolation (bar 4 where * denotes p < 0.05), or by combination with CQ (bar 6 where ** denotes p < 0.01) or by combination with CQ and Zn (bar 7 where *** denotes p < 0.001), as assessed by two-way ANOVA (Dunnett's test where n = 5-6). Additional two-way ANOVA analysis via Tukey's test indicates near significant difference (p = 0.12) between treatment groups with Cu^{2+} alone (bar 4) and in combination with CQ and Zn^{2+} (bar 7), indicating that CQ may enhance Cu uptake. B) All treatment groups failed to increase intracellular Zn levels including CQ + Zn^{2+} group (bar 5 where p = 0.15) as assessed by two-way ANOVA (Dunnett's test where n = 5-6). All data shown are individually plotted data points with bars representing mean ± SD.*

comparison was hindered by the large study design, and was resolved in subsequent experiments. The same ICP-MS analyses albeit for zinc is depicted in Figure 4B. None of the eight treatment groups were able to significantly increase cytosolic zinc levels, suggesting that the observed effects of the CQ/Zn^{2+}/Cu^{2+} enhancing P-gp expression and function, are unlikely to be mediated by effects by Zn^{2+}, but rather by Cu^{2+}.

To gain further insight into CQ-mediated mechanisms of P-gp upregulation, the kinetics of free versus CQ-mediated copper uptake into hCMEC/D3 cells were assessed in parallel. Figure 5 shows free copper (in blue) increasing marginally over time, whilst CQ-mediated copper uptake (shown in red) resulted in a significantly larger copper increase, but only the final time point assessed (24 h). Taken together, this set of ICP-MS experiments indicate that whilst endogenous copper uptake mechanisms are apparent in hCMEC/D3 cells, CQ administered in combination with copper can enhance the delivery of copper to intracellular regions, as was

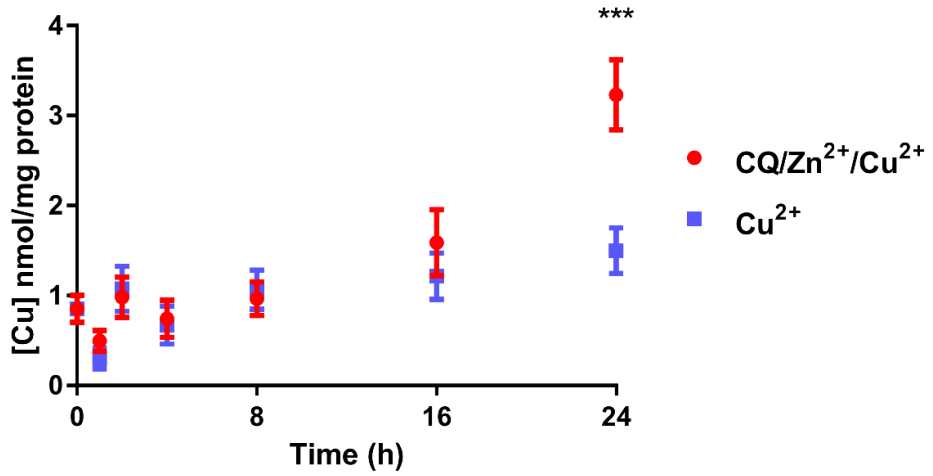

*Figure 5: Time-dependent assessment of intracellular Cu levels via inductively coupled plasma mass spectrometry, normalised to well protein content via BCA protein assay, after 1, 2, 4, 8, 16 or 24 h treatment with the chemical agents Cu^{2+} (0.1 μM) alone (shown in blue) or with combination shown to induce P-gp upregulation: CQ (0.5 μM), Zn^{2+} (0.5 μM) and Cu^{2+} (0.1 μM) (shown in red). No significant differences in copper accumulation between the two treatment groups are resolved until the final time-point of 24 h, (where *** denotes $p < 0.001$). Statistical comparisons were made between time matched groups via Student's t-test, and all data shown represent mean ± SEM where n = 3-6.*

hypothesised, presumably via the metal ionophore activity described above, although the significant increases of cytosolic copper mediated by CQ are only visible after 24 h.

DISCUSSION

P-gp plays an important role in many life science applications and disease states, and understanding the biological inputs modulating the expression and activity of P-gp is a valuable endeavour. Whilst it has been shown that biometals such as zinc and copper can influence the barrier like properties of the endothelium (18-21), the effects of metal ions on barrier transporter proteins such as P-gp are relatively unknown. This study attempted to identify whether enhanced uptake of either of the biometals zinc or copper by ionophoric delivery via the use of CQ could result in modulation of P-gp expression and/or activity.

To investigate this aim, the relative expression of P-gp was measured in an ICW assay, performed in the immortalised hCMEC/D3 cell line. This ICW approach has been validated previously by comparing modulated P-gp expression results with those derived from WB, after treatment with several known P-gp regulating compounds (24). The results from the ICW in this study indicated that only the combination of CQ, Zn^{2+} and Cu^{2+} (0.5, 0.5 and 0.1 μM) produced a statistically significant upregulation (1.7-fold) of P-gp expression. Use of the fluorescent P-gp substrate R123 showed that treating hCMEC/D3 cells for 24 h with the combination just described induced a reduction in R123 accumulation, and an increase in post-R123-loading efflux, indicating that the activity of P-gp had been functionally enhanced. This effect of P-gp functional enhancement was negated when cells were co-treated with the known P-gp inhibitor PSC833, indicating specific modulation of P-gp. These results were also confirmed by WB, which indicated a concordant 1.8-fold increase in P-gp expression. Previous studies have demonstrated links between biometal treatment and BBB integrity, barrier

function, endothelial viability and angiogenesis in both *in vitro*, as well as murine and porcine *in vivo* systems (18-21). Since it has been shown elsewhere that tight junction proteins essential for barrier formation and function, and the expression for transporters like P-gp are both under the influence of similar signalling pathways (26, 27), these findings of enhanced expression and function of P-gp via biometal delivery are consistent with the other experimental evidence available.

Investigation of biometal uptake into the endothelial cell line by ICP-MS revealed that despite the combination of CQ/Zn^{2+}/Cu^{2+} being required to achieve significant upregulation of P-gp, cytosolic zinc levels were not affected in the experimental paradigm used (Figure 4B), indicating that zinc may not play a major role in the observed endothelial upregulation of P-gp. Treatment with copper alone (0.1 μM $CuCl_2$) was able to significantly increase levels of cytosolic copper from approximately 0.6 ± 0.2 nmol/mg of protein to 1.6 ± 0.6 nmol/mg of protein (Figure 4A), but this increase did not appear to drive an increase in P-gp expression in the experimental paradigm that was explored (Figure 1A). Under normal physiological conditions, BBB uptake of zinc and copper are mediated and regulated by endogenous biometal transporter proteins, divalent metal transporter 1 (DMT1; both zinc and copper) (28), and copper transporter 1 (CTR1; copper only) (28). The rate and extent of copper uptake however, is mediated by CTR1 expression, which has been shown to become downregulated by endothelial cells in the presence of relatively higher extracellular concentrations of copper, by a process of internalisation and recycling of the CTR1 transporter (29). Cytosolic protein-mediated copper storage mechanisms also function within cells, to limit the biologically available copper and thus prevent toxicity (30). Therefore, therapeutically enhanced delivery of copper to cellular interiors might be required to drive the desired copper-mediated protein signalling and expression, such as the upregulation of P-gp. The use of the ionophore

compound CQ appears to have achieved this aim. As assessed by ICP-MS, treatment of hCMEC/D3 cells with CQ/Cu^{2+} and CQ/Zn^{2+}/Cu^{2+} increased cytosolic copper to 2.2 ± 1.1 and 2.6 ± 0.9 nmol/mg of protein respectively (Figure 4A). Whilst these average increases (compared to the 0.1 μM Cu^{2+} treatment group value of 1.6 ± 0.6 nmol/mg of protein) did not reach statistical significance due to the large study design, subsequent experiments were able to resolve this difference. When time-dependent copper uptake in hCMEC/D3 cells was measured in a separate experiment as shown in Figure 5, CQ-mediated copper delivery was observed as significantly enhanced at the 24-h time point when compared to uptake of free copper alone, but not in earlier time-point measurements (3.2 ± 1 vs 1.5 ± 0.6 nmol/mg of protein respectively). This experiment demonstrates that while endogenous endothelial copper uptake is rate and extent limited, copper delivery to cell interiors can be enhanced by the use of biometal ionophores such as CQ.

Whilst encouraging, the data presented herein are subject to some limitations. Firstly, due to the high proportion of protein binding (31), it was required for CQ to be administered to cells in serum free media, which represents a divergence from physiological conditions, where proteins appear ubiquitously in all biological fluids and will most likely interact with CQ *in vivo*. Additionally, the lysis protocol used for the generation of the ICP-MS data was designed intentionally to leave the cells largely intact, and thus to observe and quantify only cytosolic and cytosolically protein-bound biometals in our analysis. As a result, any biometals that were taken up by the cells and immediately utilised for cellular processes such as incorporation into plasma membrane bound proteins, etc. may not have been measured in our experiments, potentially leading to an underestimation of biometal uptake, in the case of both endogenous and CQ-mediated copper uptake.

Despite these limitations, we find that the data presented in this study provides firm ground upon which to base further experiments. Most obvious is the need to identify the mechanism by which increased intracellular copper is able to drive P-gp expression. Copper interacts with a host of cell proteins (32), some of which may be upstream of P-gp expression signalling mechanisms. Cu^{2+} has also been shown to inhibit glycogen synthase kinase 3 (22), a signalling molecule which has been demonstrated to be an integral part of the Wnt/β-catenin signalling pathway that serves as one input for P-gp expression (33, 34), and which has been reported to be functional in hCMEC/D3 cells (34). Another possibility is the stabilisation of P-gp at the plasma membrane. Normally, P-gp exhibits the presence of a divalent magnesium ion, the concentration of which influences marginal control over P-gp stability and activity, but which is not essential for P-gp activity (35). An increase of Cu^{2+} ion influx through the plasma membrane might have the potential to displace Mg^{2+} ions, subsequently stabilising P-gp at the plasma membrane. Studies to elucidate the mechanism of CQ/Cu^{2+} mediated upregulation of P-gp are currently underway, alongside investigations in animal models, to interrogate the broader context of the *in vitro* findings observed within this study.

These studies have highlighted that CQ together with biometals, can increase the expression and function of P-gp in BBB phenotypical cells. It is possible, therefore, that part of the Aβ-lowering effects of CQ reported previously (23, 36) may result from increased BBB efflux of Aβ, since Aβ is a substrate of P-gp, although further studies to confirm this hypothesis are required to be undertaken. Furthermore, this study has revealed a potential role of Cu^{2+} in regulating the expression and function of P-gp at the BBB, which is a novel finding. Given that P-gp is a major hindrance to the CNS entry of many therapeutic agents intended to reach the brain, it is possible that intentional manipulation of brain endothelial cell Cu^{2+} levels could be exploited to reduce P-gp expression and enhance CNS delivery of drugs which are substrates

of P-gp. In addition, drugs such as CQ which modulate the brain endothelial cell levels of Cu^{2+} have the potential to result in interactions with drugs which are substrates with P-gp, as the enhanced P-gp expression mediated by CQ could reduce the CNS entry of drugs with high affinity to P-gp.

CONCLUSION

When co-administered with copper at nanomolar concentrations, CQ is able to produce significant upregulation of P-gp, in an immortalised human cerebral microvascular endothelial cell line. Enhanced P-gp expression appears to be associated with increased intracellular copper uptake, and future studies will interrogate the mechanism mediating the increase of this important efflux transporter, along with the biological relevance of these findings within *in vivo* systems.

REFERENCES

1. Hawkins BT, Davis TP. The blood-brain barrier/neurovascular unit in health and disease. Pharmacol Rev. 2005;57(2):173-185.
2. Zlokovic BV. Neurovascular pathways to neurodegeneration in Alzheimer's disease and other disorders. Nat Rev Neurosci. 2011;12(12):723-738.
3. Tatsuta T, Naito M, Oh-hara T, Sugawara I, Tsuruo T. Functional involvement of P-glycoprotein in blood-brain barrier. J Biol Chem. 1992;267(28):20383-20391.
4. Callaghan R. Providing a molecular mechanism for P-glycoprotein; why would I bother? Biochem Soc Trans. 2015;43(5):995-1002.
5. Punitha AD, Srivastava AK. CNS drug targeting: have we travelled in right path? J Drug Target. 2013;21(9):787-800.

6. Fletcher JI, Williams RT, Henderson MJ, Norris MD, Haber M. ABC transporters as mediators of drug resistance and contributors to cancer cell biology. Drug Resist Updat. 2016;26:1-9.

7. McInerney MP, Short JL, Nicolazzo JA. Neurovascular alterations in Alzheimer's disease: transporter expression profiles and CNS drug access. AAPS J. 2017;19(4):940-956.

8. Selkoe DJ. Alzheimer's Disease. Cold Spring Harb Perspect Biol. 2011;3(7):a004457-a004457.

9. Roberts KF, Elbert DL, Kasten TP, Patterson BW, Sigurdson WC, Connors RE, Ovod V, Munsell LY, Mawuenyega KG, Miller-Thomas MM, Moran CJ, Cross DT, 3rd, Derdeyn CP, Bateman RJ. Amyloid-beta efflux from the central nervous system into the plasma. Ann Neurol. 2014;76(6):837-844.

10. Shibata M, Yamada S, Kumar SR, Calero M, Bading J, Frangione B, Holtzman DM, Miller CA, Strickland DK, Ghiso J, Zlokovic BV. Clearance of Alzheimer's amyloid-ss(1-40) peptide from brain by LDL receptor-related protein-1 at the blood-brain barrier. J Clin Invest. 2000;106(12):1489-1499.

11. Qosa H, Abuasal BS, Romero IA, Weksler B, Couraud PO, Keller JN, Kaddoumi A. Differences in amyloid-beta clearance across mouse and human blood-brain barrier models: Kinetic analysis and mechanistic modeling. Neuropharmacology. 2014;79C:668-678.

12. Cirrito JR, Deane R, Fagan AM, Spinner ML, Parsadanian M, Finn MB, Jiang H, Prior JL, Sagare A, Bales KR, Paul SM, Zlokovic BV, Piwnica-Worms D, Holtzman DM. P-glycoprotein deficiency at the blood-brain barrier increases amyloid-beta deposition in an Alzheimer disease mouse model. J Clin Invest. 2005;115(11):3285-3290.

13. Wang W, Bodles-Brakhop AM, Barger SW. A role for P-glycoprotein in clearance of Alzheimer amyloid beta-peptide from the brain. Curr Alzheimer Res. 2016;13(6):615-620.

14. Vogelgesang S, Cascorbi I, Schroeder E, Pahnke J, Kroemer HK, Siegmund W, Kunert-Keil C, Walker LC, Warzok RW. Deposition of Alzheimer's beta-amyloid is inversely correlated with P-glycoprotein expression in the brains of elderly non-demented humans. Pharmacogenetics. 2002;12(7):535-541.

15. Deo AK, Borson S, Link JM, Domino K, Eary JF, Ke B, Richards TL, Mankoff DA, Minoshima S, O'Sullivan F, Eyal S, Hsiao P, Maravilla K, Unadkat JD. Activity of P-glycoprotein, a beta-Amyloid transporter at the blood-brain barrier, is compromised in patients with mild Alzheimer disease. J Nucl Med. 2014;55(7):1106-1111.

16. Miller DS, Bauer B, Hartz AM. Modulation of P-glycoprotein at the blood-brain barrier: opportunities to improve central nervous system pharmacotherapy. Pharmacol Rev. 2008;60(2):196-209.

17. Abuznait AH, Kaddoumi A. Role of ABC transporters in the pathogenesis of Alzheimer's disease. ACS Chem Neurosci. 2012;3(11):820-831.

18. Song Y, Xue Y, Liu X, Wang P, Liu L. Effects of acute exposure to aluminum on blood-brain barrier and the protection of zinc. Neurosci Lett. 2008;445(1):42-46.

19. Hennig B, Wang Y, Ramasamy S, McClain CJ. Zinc deficiency alters barrier function of cultured porcine endothelial cells. J Nutr. 1992;122(6):1242-1247.

20. Wang J, Chen J, Tang Z, Li Y, Hu L, Pan J. The Effects of Copper on Brain Microvascular Endothelial Cells and Claudin Via Apoptosis and Oxidative Stress. Biol Trace Elem Res. 2016;174(1):132-141.

21. Li QF, Ding XQ, Kang YJ. Copper promotion of angiogenesis in isolated rat aortic ring: role of vascular endothelial growth factor. J Nutr Biochem. 2014;25(1):44-49.

22. Crouch PJ, Savva MS, Hung LW, Donnelly PS, Mot AI, Parker SJ, Greenough MA, Volitakis I, Adlard PA, Cherny RA, Masters CL, Bush AI, Barnham KJ, White AR. The Alzheimer's therapeutic PBT2 promotes amyloid-beta degradation and GSK3 phosphorylation via a metal chaperone activity. J Neurochem. 2011;119(1):220-230.

23. Cherny RA, Atwood CS, Xilinas ME, Gray DN, Jones WD, McLean CA, Barnham KJ, Volitakis I, Fraser FW, Kim Y, Huang X, Goldstein LE, Moir RD, Lim JT, Beyreuther K, Zheng H, Tanzi RE, Masters CL, Bush AI. Treatment with a copper-zinc chelator markedly and rapidly inhibits beta-amyloid accumulation in Alzheimer's disease transgenic mice. Neuron. 2001;30(3):665-676.

24. McInerney MP, Pan Y, Short JL, Nicolazzo JA. Development and validation of an in-cell western for quantifying P-glycoprotein expression in human brain microvascular endothelial (hCMEC/D3) Cells. J Pharm Sci. 2017;106(9):2614-2624.

25. Fu D, Arias IM. Intracellular trafficking of P-glycoprotein. Int J Biochem Cell Biol. 2012;44(3):461-464.

26. Liebner S, Corada M, Bangsow T, Babbage J, Taddei A, Czupalla CJ, Reis M, Felici A, Wolburg H, Fruttiger M, Taketo MM, von Melchner H, Plate KH, Gerhardt H, Dejana E. Wnt/beta-catenin signaling controls development of the blood-brain barrier. J Cell Biol. 2008;183(3):409-417.

27. Tran KA, Zhang X, Predescu D, Huang X, Machado RF, Gothert JR, Malik AB, Valyi-Nagy T, Zhao YY. Endothelial beta-catenin signaling is required for maintaining adult blood-brain barrier integrity and central nervous system homeostasis. Circulation. 2016;133(2):177-186.

28. Zheng W, Monnot AD. Regulation of brain iron and copper homeostasis by brain barrier systems: implication in neurodegenerative diseases. Pharmacol Ther. 2012;133(2):177-188.

29. Clifford RJ, Maryon EB, Kaplan JH. Dynamic internalization and recycling of a metal ion transporter: Cu homeostasis and CTR1, the human Cu(+) uptake system. J Cell Sci. 2016;129(8):1711-1721.

30. Tapiero H, Townsend DM, Tew KD. Trace elements in human physiology and pathology. Copper. Biomed Pharmacother. 2003;57(9):386-398.

31. Adlard PA, Cherny RA, Finkelstein DI, Gautier E, Robb E, Cortes M, Volitakis I, Liu X, Smith JP, Perez K, Laughton K, Li QX, Charman SA, Nicolazzo JA, Wilkins S, Deleva K, Lynch T, Kok G, Ritchie CW, Tanzi RE, Cappai R, Masters CL, Barnham KJ, Bush AI. Rapid restoration of cognition in Alzheimer's transgenic mice with 8-hydroxy quinoline analogs is associated with decreased interstitial Abeta. Neuron. 2008;59(1):43-55.

32. Hordyjewska A, Popiolek L, Kocot J. The many "faces" of copper in medicine and treatment. BioMetals. 2014;27(4):611-621.

33. Shen DY, Zhang W, Zeng X, Liu CQ. Inhibition of Wnt/beta-catenin signaling downregulates P-glycoprotein and reverses multi-drug resistance of cholangiocarcinoma. Cancer Sci. 2013;104(10):1303-1308.

34. Lim JC, Kania KD, Wijesuriya H, Chawla S, Sethi JK, Pulaski L, Romero IA, Couraud PO, Weksler BB, Hladky SB, Barrand MA. Activation of beta-catenin signalling by GSK-3 inhibition increases P-glycoprotein expression in brain endothelial cells. J Neurochem. 2008;106(4):1855-1865.

35. Urbatsch IL, Gimi K, Wilke-Mounts S, Senior AE. Investigation of the role of glutamine-471 and glutamine-1114 in the two catalytic sites of P-glycoprotein. Biochemistry. 2000;39(39):11921-11927.

36. Grossi C, Francese S, Casini A, Rosi MC, Luccarini I, Fiorentini A, Gabbiani C, Messori L, Moneti G, Casamenti F. Clioquinol decreases amyloid-beta burden and

reduces working memory impairment in a transgenic mouse model of Alzheimer's disease. J Alzheimers Dis. 2009;17(2):423-440.

Chapter 5:

Effects of clioquinol on biometal distribution and P-glycoprotein expression at the brain endothelium and other peripheral tissues in mice

ABSTRACT

The work presented in the previous chapters of this thesis has indicated that the ionophore drug clioquinol (CQ), in conjunction with copper and zinc, increases the expression of the AD relevant xenobiotic efflux transporter, P-glycoprotein (P-gp), in the immortalised human cerebral microvascular endothelial cell line. This result, however, was observed under the idealised conditions of in vitro cell culture, and whether the effect would manifest within an in vivo system was yet to be assessed. In this chapter, work testing the hypothesis of this thesis in an in vivo model is presented. Swiss outbred mice received an 11 day treatment of CQ (30 mg/kg) by oral gavage, after which organs were obtained for metallomic and AD-related transporter expression analysis. From the mouse brain cortices, microvessel enriched fractions (MEF) were extracted, and to facilitate a holistic approach, other tissue compartments (subcortical brain, plasma, liver, small intestines and kidneys) were also isolated for analysis. All isolated tissues were assessed for CQ-induced redistribution of metals, by inductively coupled plasma mass spectrometry, and the liver, kidneys and MEF were assessed for the expression of amyloid trafficking proteins P-gp and low density lipoprotein receptor-related protein 1 (LRP1). No changes in copper/zinc levels, nor in P-gp or LRP1 abundances were observed in the MEF, however many other significant observations were detected in alternative regions of the body. Metallomic analysis revealed that CQ is able to effectively alter the distribution of sodium, magnesium, phosphorous, potassium, calcium and manganese in many compartments of the murine body, although this was not associated with altered P-gp or LRP1 expression. This study demonstrates that the ionophoric effects of CQ are not restricted to the brain, and that CQ is able to modify metal ion levels in many tissue compartments of the body.

INTRODUCTION

Ionophores are a class of molecules which, by virtue of their balanced physicochemical properties and amenable functionality, are able to shuttle metal ions across biological membranes (1). Ionophores achieve this mechanism by reversibly binding to metal ions, shielding their polarity and thus facilitating movement across lipophilic barriers to which the charged metal ions would otherwise be impermeable. An initial interpretation of such a mechanism with regard to pharmaceutical interventions, might seem highly undesirable due to the naturally tight homeostatic control over the distribution of metal ions normally exhibited within biological systems. Strong evidence has emerged however, that neurological disease states such as Alzheimer's disease (AD), Parkinson's disease (PD) and amyotrophic lateral sclerosis, exhibit well defined elements of metal ion dyshomeostasis which demonstrably contribute to the disease pathogenesis (2). In AD, both zinc and copper ions are co-precipitated with the β-amyloid (Aβ) plaques, forming abnormally high extracellular concentrations within the neuropil, accompanied by low neuronal intracellular concentrations of these metals (3, 4). PD has been associated with increased iron and decreased copper within the substantia nigra, along with elevated copper levels in the systemic circulation (5). Whilst the causes for the maldistribution of metal ions in these disease states are not fully understood, it is understandable that ionophore drug approaches have been considered, explored and implemented for such disease states, since the biological consequences of a metal ion maldistribution would likely be numerous, diverse and networked.

Metal ionophores, by their ability to enhance the biological availability of metal ions to the intracellular interactome, are able to influence cell signalling pathways for which the metal ions being chaperoned would normally operate within, as either cofactors for signalling processes or as essential components of functional proteins. Copper for example is required as

a co-factor for enzymatic processes as diverse as oxygen activation during carbohydrate catabolism (galactose oxidase) (6), mitochondrial energy production (cytochrome-C oxidase) (7), free radical scavenging (superoxide dismutase) (8), iron transport and oxidation (ceruloplasmin) (9) and extracellular matrix protein cross-linking (protein-lysine-6-oxidase) (10). Multiple mechanisms exist to keep copper concentrations at physiologically optimal levels (glutathione, metallothionein among others), highlighting the evolutionary importance of such control (7). Thus, the apparent metal ion dyshomeostasis observed in AD and other neurological disorders might be beneficially approached by the use of ionophores, which may have the ability to restore dysfunctional metal ion equilibria within biological systems.

The ionophore drug clioquinol (CQ) presents a pertinent example of ionophore activity demonstrably influencing cell signalling pathways. CQ and the structurally related compound PBT2, are able to shuttle extracellular zinc and copper inside neurons, and subsequently influence cell signalling pathway outputs via inhibition of glycogen synthase kinase 3-beta (GSK3β) (11), a central signalling kinase that operates within many information pathways (12). GSK3β is also a key mediator of the Wnt/β-catenin signalling pathway, which is highly implicated in the development and maintenance of the blood-brain barrier (BBB), including regulation of the important efflux pump transporter protein, P-glycoprotein (P-gp) (13-15). It has also been shown previously that CQ, when administered to transgenic mice that express the human variant of the amyloid-beta peptide (Aβ), was able to lower the total brain Aβ load (16, 17), potentially via multiple proposed mechanisms, although the identity of the main driving mechanism is not entirely clear. These observations led to the hypothesis that CQ and copper ions when co-administered, may have an appreciable and disease modifying effect with regards to AD, on the expression profile of BBB transporter proteins. Both P-gp and low-density lipoprotein related receptor (LRP1) have been implicated as important efflux pumps of

the Aβ peptide in the human and murine brains, where they have been shown to be involved in either the prevention of apical-to-basolateral transit and basolateral-to-apical trafficking, or both, of the Aβ peptide (18).

Our laboratory has recently demonstrated a potentially novel mechanism for CQ, whereby we have shown that CQ is indeed able to shuttle copper ions inside the in vitro human cerebral microvascular endothelial (hCMEC/D3) cell line, and subsequently induce an upregulation in the expression of P-gp (19). These observed effects however, were produced under the ideal conditions of in vitro cell culture, and whether or not they would manifest within an in vivo system is yet to be determined. The main aim of this study then, was to observe any alterations in metal ion distribution across the brain endothelium, measured in microvessel enriched fractions (MEF) obtained from Swiss outbred mice that had been dosed with CQ for 11 days (the treatment period shown previously to lower brain Aβ) and assess AD-related BBB transporter (P-gp and LRP1) expression levels. Though no link between CQ/biometals and LRP1 had yet been established, the expression of LRP1 was still assessed in these tissues, given its importance with respect to AD, and the availability of tools to probe LRP1 abundance in parallel to that of P-gp.

P-gp and LRP1 are not expressed only at the BBB, but are also present in other anatomical regions of barrier formation around the body, such as the kidneys, the small intestines and the liver. Since the efforts to determine the ionophoric effects of CQ have focused mainly on the CNS, it would be of clinical interest to identify any ionophoric activity of CQ that may occur in other organs of the body, which may or may not affect transporter expression levels in any tissues subjected to metal ion input. For these reasons, in the current study the redistribution of metal ions in the plasma, brain microvessels, subcortical brain tissue, liver, kidney and small

intestine was also assessed, as well as the relative expression levels of P-gp and LRP1 in a subset of transporter related tissues, ie the brain microvessels, kidneys and liver, all following oral administration of CQ to mice. Finally, to confirm that any effects of CQ in vivo were similar to those found with human brain endothelial cells as in Chapter 4, primary mouse brain endothelial cells (MBECs) were isolated and the effects of similar treatments as was performed on hCMEC/D3s (rifampicin and the CQ/Zn^{2+}/Cu^{2+} combination), were also undertaken on MBECs.

MATERIALS

Tween-80, sodium chloride, and sodium carboxymethyl cellulose were all purchased from Sigma Aldrich, USA. TRIS buffer salt (TRIZMA base), sodium dodecyl sulphate (SDS), ammonium persulfate (APS) and N,N,N',N'-tetramethylethylenediamine (TEMED) were all purchased from Sigma Life Sciences (St Louis, MO). 40% acrylamide/bis solution was purchased from Bio-Rad Laboratories (Hercules, CA). Benzyl alcohol was purchased from Chem-Supply (Gillman, South Australia, Australia). *Odyssey blocking buffer*, donkey-anti-rabbit secondary antibody and the goat-anti-mouse secondary antibody were all purchased from Millennium Science (Mulgrave, Victoria, Australia). cOmplete Tablets Mini EASY pack protease inhibitors were purchased from Roche Diagnostics (GmbH, Mannheim, Germany). Nitrocellulose membrane roll (0.2 µm pore-sized) was purchased from GE Life Sciences (Rydalmere, New South Wales, Australia). Dulbecco's modified Eagle medium (DMEM), Collagenase type II powder and DNase I were purchased from Life Technologies (Mulgrave, Victoria, Australia). Both Clonetics EBM-2 basal media and Clonetics EGM-2 single quots growth factor kits were purchased from Lonza (Walkersville, MD), and combined as per the manufacturer's instructions to produce EBM2-MV media for primary cells. Bovine serum albumin (BSA), rat tail collagen solution and Hyclone Hank's Balanced Saline Solution

(HBSS) were purchased from In Vitro Technologies (Noble Park North, Victoria, Australia). Puromycin hydrochloride was purchased from Astral Scientific (Tarren Point, New South Whales, Australia). The C219 P-glycoprotein antibody was purchased from Australian Biosearch (Balcatta, Western Australia, Australia) and the EPR3724 LRP1 and the β-actin antibodies was purchased from Abcam (Cambridge, MA).

METHODS

Oral gavage of mice with CQ

All animal experiments were approved by the Monash Institute of Pharmaceutical Sciences Animal Ethics Committee and performed in accordance with the National Health and Medical Research Council Guidelines for the care and use of animals for scientific purposes. To facilitate sufficient collection of pooled MEF for both ICP-MS and WB, a total of 46 male Swiss outbred mice were used. Before CQ or vehicle dosing, mice were housed and acclimatized in a holding room on a 12:12 h reverse light-dark cycle (lights on 7:00 P.M.) with water and food ad libitum for seven days. Mice were split randomly into two groups (23 mice per group) and were dosed daily for 11 days by oral gavage (200 μL), with a suspension vehicle (0.9% (w/w) NaCl, 0.5% (w/w) Na-carboxymethylcellulose, 0.5% (v/v) benzyl alcohol and 0.4% (v/v) Tween-80) with or without CQ, such that treated mice received 30 mg/kg of CQ. After 11 days, the mice were humanely killed to remove various organs for metallomic and biochemical analysis.

Brain microvessel enriched fraction isolation and organ harvesting

To obtain a sufficient protein yield for western blotting (WB), the MEF of 4-5 mice were pooled, and with 23 mice it was therefore possible to obtain 5-6 replicates for both WB and inductively coupled plasma mass spectrometry (ICP-MS) analysis. Obtaining brain MEF was

performed as previously reported by Pan et al (20), albeit with a slightly modified protocol. Briefly, the cortex was separated from the rest of the subcortical brain and placed in an ice-cold Dounce homogenizer (the subcortical brain was snap frozen in liquid nitrogen and stored for later use). The cortices were homogenized (10 strokes) in Dulbecco's Modified Eagle's Medium. BSA was added to the homogenate to achieve a final concentration of 15% (w/v) and the homogenate was centrifuged at 2000 × g for 30 min at 4°C. The resulting supernatant (brain parenchymal fraction) and pellet (capillary fraction) were separated. The excessive BSA was removed by rinsing the capillary pellet with Dulbecco's Modified Eagle's Medium twice and the final mixture was filtered through a 70-μm nylon mesh (BD Biosciences, Franklin Lakes, NJ) to remove large blood vessels. The flow-through was pelleted and stored at −80°C until further use. Small intestines, kidneys and livers were dissected and placed in microfuge tubes, before being snap frozen in liquid nitrogen and stored at -80°C until further use. Blood samples were obtained via cardiac puncture and transferred to microfuge tubes containing 5 μL of heparin, which were centrifuged at 15,000 rcf for 15 min before the supernatant (plasma) was collected and stored at -80°C until further use.

ICP-MS of brain microvessel enriched fractions and organ homogenates

Plasma samples (50 μL) were diluted 10-fold with 450 μL of 1% (v/v) nitric acid diluent prior to ICP-MS analysis. All other tissue samples were dissected and aliquoted to the following approximate wet weights with the actual sample weight recorded before being freeze dried; subcortical brain hemispheres ~100 mg, livers ~200 mg, kidneys ~270 mg and small intestines ~150 mg. To the lyophilised samples, 150 μL (or 300 μL for liver samples) of nitric acid (HNO_3) (65% Suprapur, Merck) was added to each sample microfuge tube and allowed to digest overnight. Samples were then further digested at 90°C for 20 min using a heating block. Samples were then removed from the heating block and an equivalent volume of 30 μL

hydrogen peroxide 30% (v/v) (Aristar, BDH) was added to each sample. Samples were allowed to stop effervescing (digesting) for 30 min, before being heating again for a further 15 mins at 70°C. The average reduced volume was determined and the samples were further diluted with 1% HNO_3 (v/v).

ICP-MS measurements were made using an Agilent 7700 series ICP-MS instrument under routine multi-element operating conditions using a Helium Reaction Gas Cell. The instrument was calibrated using 0, 5, 10, 50, 100 and 500 ppb of certified multi-element ICP-MS standard calibration solutions (ICP-MS-CAL2-1, ICP-MS-CAL-3 and ICP-MS-CAL-4, Accustandard, New Haven) for a range of elements. Additionally, a certified internal standard solution containing 200 ppb of Yttrium (Y89) was used as an internal control (ICP-MS-IS-MIX1-1, Accustandard). Each of the following metals were assessed; sodium, magnesium, phosphorous, calcium, manganese, iron, cobalt, nickel, copper, zinc, selenium and rubidium, and any elements that recorded abundances at or below detection limits were excluded from the data analysis.

Western blotting of brain microvessel enriched fractions and organ homogenates

The pooled MEF pellets were homogenised by the addition of 300 µL of Pierce IP lysis buffer mixed with a 7 x concentrated protease inhibitor solution (1:6 ratio) followed by thorough pipetting, before being left on agitation at 4°C for 45 min. The lysates were then centrifuged for 10 min at 14,000 rcf, and the supernatant was collected and aliquoted for protein content analysis via the BCA protein assay, before stored immediately at -80°C until further use with WB. The liver and kidney tissues were homogenised as follows: approximately 20 mg of wet weight tissue was dissected from each main sample, and placed into a 4 mL homogenisation tube containing 0.5 mL of Pierce IP lysis buffer and 7 x concentrated protease inhibitor solution

(1:6 ratio). Tissues were then homogenised very briefly due to the small tissue weight (10 sec per tube) using an IKA T25 digital ULTRA-TURRAX tissue homogeniser (Lab Gear Australia, Milton, Queensland, Australia), set at 4,000/min. Each sample was then left to sit on ice for 30 min, before centrifugation at 15,000 rcf for 15 min. The supernatant was collected and aliquoted for protein content analysis via the BCA protein assay, and then stored in -80°C until further use.

After protein quantification, all tissue lysates were thawed and mixed with 6 x Laemmli buffer (in a 5:1 ratio) and left to incubate with gentle mixing at room temperature for 30 min. Due to the differential abundances of P-gp and LRP1 in the various tissues, protein quantities loaded for electrophoresis were as follows (P-gp and LRP1 respectively): Microvessels: 10 μg and 10 μg; liver: 50 μg and 5 μg; and kidneys: 50 μg for P-gp (LRP1 not expressed). WB was carried out on 10% acrylamide 1 mm hand-cast gels, electrophoresed at executed at 60 V for 30 min followed by 1.5 h at 150 V. Electrophoresed gels along with extra thick blot paper and 0.2 μm pore-sized nitrocellulose membranes were allowed to equilibrate in transfer buffer containing 20% (v/v) methanol for 30 min before transfer. Transfer was executed using semi-dry consumables and the Turbo-blot transfer system (*Bio-rad*, Gladesville, New South Wales, Australia) set to 40 min at 25 V and 1.0 A. Transfer membranes were then rinsed briefly in 5% (v/v) tween-20 in tris buffered saline (TBS-T) and then incubated in ~20 mL of *Odyssey blocking buffer* at room temperature for 1 h. Membranes were again rinsed briefly in TBS-T and then incubated with either a 1:500 dilution of the C219 antibody (P-gp) or 1:5000 dilution of the LRP1 antibody in blocking buffer overnight. The β-actin antibody was added to incubation solution for only the final 20 min of the overnight primary antibody incubation step, to avoid saturation of the actin signal, at a dilution of 1:10,000. Following 4 x 10 min membrane washes in TBS-T, the membranes were incubated in *Licor* ™ goat-anti-mouse secondary

antibodies (P-gp 1:10,000) or donkey-anti-rabbit (LRP1 1:10,000) for 2 h at room temperature followed by the same washing regime as above. Membranes were scanned on the *Licor Odyssey* IR imaging instrument, and densitometric analysis was executed via the *ImageJ* software. Data was normalised to β-actin signal and expressed as relative fold-changes compared to controls.

Primary mouse brain endothelial cell isolation

To observe if any species specific (human versus mouse) differential responses to CQ/biometal treatment existed, it was decided to administer CQ/biometal treatments to primary MBECs, with the intention of comparing the results with those from Chapter 4. To isolate primary mouse brain endothelial cells, the following method was used, which has been validated in other laboratories previously as a technique for isolating a near pure population of endothelial cells: A black corning TC-treated 96-well plate was incubated at 37°C overnight with 75 μL of rat tail collagen solution (0.1 mg/mL in PBS), before two rinses with 150 μL of PBS to remove any excess collagen. The plate was then re-incubated with 75 μL of EBM2-MV media (EBM2 media supplemented as per manufacturer's instructions but with the addition of 50 U/mL of penicillin and 50 μg/mL of streptomycin) at 37°C until later use with isolated primary cells. Swiss outbred mice were sacrificed by cervical dislocation and submerged in 80% (v/v) ethanol in water for 4 min. In a sterile cabinet, the mouse brains were then dissected out and transferred to 60 mm petri dishes holding ice-cold HBSS. The brains were then blotted on sterile paper to remove the meninges and large blood vessels before isolation of the cortices. Isolated cortices were stored and rinsed in separate petri dishes containing DMEM. The rinsing DMEM was then removed and replaced with 5 mL of a solution containing 0.1% (w/v) collagenase type II and 0.13% (v/v) DNase I in DMEM. In this solution the cortices were cut into successively smaller pieces until the solution could be homogenised by a 5 mL pipette. The homogenate

was then transferred to an incubator (37°C, air composition: 95% O_2 and 5% CO_2) for 1.5 h with gentle stirring applied twice throughout the incubation. Towards the end of the incubation, 15 mL Falcon tubes were pre-coated with 20% (w/v) BSA in PBS, and after 1.5 h incubation the mixtures were transferred to these tubes, and centrifuged at 1000 rcf for 8 min at 4°C. The supernatant was then discarded, and 5 mL of 20% (w/v) BSA in PBS was then used to resuspend the remaining pellet by pipetting. The mixture was again centrifuged at 1000 rcf for 20 min (4°C), to separate astrocytes, myelin and neurons, which formed a floating pellet that was removed, along with the BSA solution layer, post-centrifuge. Next, the remaining pellet was resuspended in 5 mL of DMEM, before being centrifuged once more at 1000 rcf for 5 min at room temperature. Again the supernatant was removed, and this last step was repeated once more to ensure the complete removal of any remaining BSA or myelin. The resulting endothelial enriched pellet was then resuspended in 5 mL of EBM2-MV, and transferred to the prepared 96-well plate as 75 μL aliquots (resulting in 150 μL cell suspensions in each well), before being left to incubate overnight. On the following day, the media was removed and replaced with 150 μL of fresh EBM2-MV containing 3 μg/mL of the toxic P-gp substrate puromycin, and then left to incubate for the following three days. After the three-day puromycin treatment (designed to inhibit the growth of pericytes and astrocytes which express less P-gp than endothelial cells), the media was removed, the wells were rinsed twice with 160 μL of PBS and replaced with fresh EMB2-MV containing no puromycin. The primary brain endothelial enriched cells were then cultured for a further six days (media changed every second day), until they had reached 70-80% confluency. Two separate experiments were performed on these isolated primary cells. First, as a positive control, cells were treated with 50 μM rifampicin for 24 h in serum containing EBM2-MV media. Secondly, to treat the cells with CQ and metal ions, EBM2-MV was removed and the wells were carefully rinsed twice with 160 μL of PBS to ensure the removal of serum proteins in the media, before being replaced

with 150 µL of serum free EBM2-MV containing either CQ, Zn^{2+} and Cu^{2+} (0.5, 0.5 and 0.1 µM respectively), or CQ and Cu^{2+} (both at 0.1 µM). After 24 h of treatment, the media was removed, and the in-cell western protocol outlined in Chapter 3 was then applied to the plate, to assess relative P-gp expression.

Statistical analysis

All data were visualised and statistically analysed using the Prism Graphpad Version 7 software. All comparisons between two groups were assessed by Student's t-test, whilst all experiments involving more than two groups were assessed by one-way analysis of variance (ANOVA), with multiple comparisons assessed by Dunnett's test. Differences between groups were considered significant if the p value fell below 0.05.

RESULTS

CQ redistributes metal ions in murine organs

To assess whether CQ treatment altered the distribution of metal ions in brain MEF and other transporter related organs, ICP-MS was performed on homogenised organ samples. The central hypothesis of these experiments was that ionophoric activity of CQ may increase the barrier tissue concentrations of some biometals (for which copper, zinc and iron were of most interest due to their emerging roles in AD), and this may result in altered expression of transporter proteins that are partially regulated by biometal input (Chapter 4 of this thesis). All metallic elements for which the biological concentrations were above the limits of detection were analysed. The results indicated that CQ was able to affect metal ions in some of these tissues, in subtle yet numerous ways.

In brain MEF, copper and zinc levels were left unchanged by CQ treatment (Figures 1A and B), however other minor changes were observed. As shown in Figure 1C, orally gavaged CQ induced a 12% reduction in magnesium and a 19% reduction in potassium (Figure 1D) in the murine brain MEF. All other metals tested in MEF including sodium, phosphorous, calcium, manganese, iron, zinc and rubidium were left unchanged, and are summarised in Table 1.

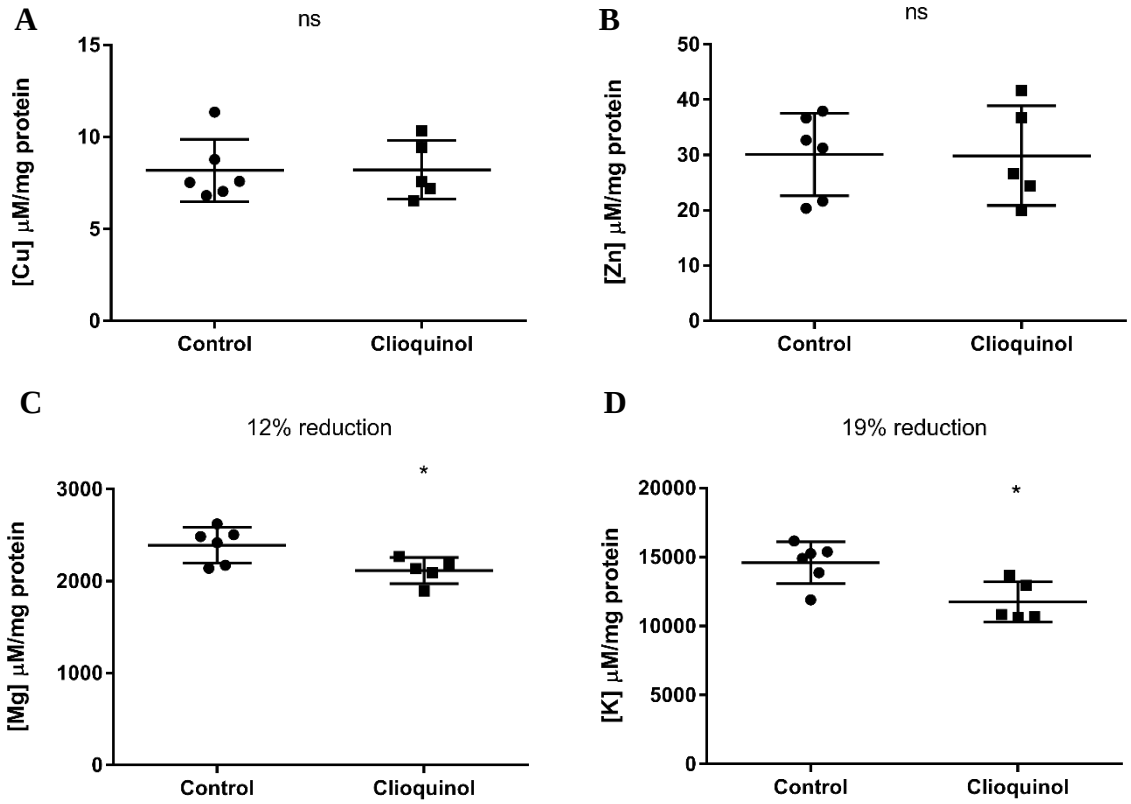

*Figure 1: Inductively coupled plasma mass spectrometry (ICP-MS) analyses of various metallic elements in the microvessel enriched fractions of vehicle treated versus clioquinol-treated Swiss outbred mice (30 mg/kg once per day for 11 days). A) Copper; B) Zinc; C) Magnesium and D) Potassium. Significance assessed by Students t-test (where n = 5-6, ns denotes no statistical significance, and * denotes p < 0.05). All data shown are individually plotted data points, with horizontal lines representing mean ± SD.*

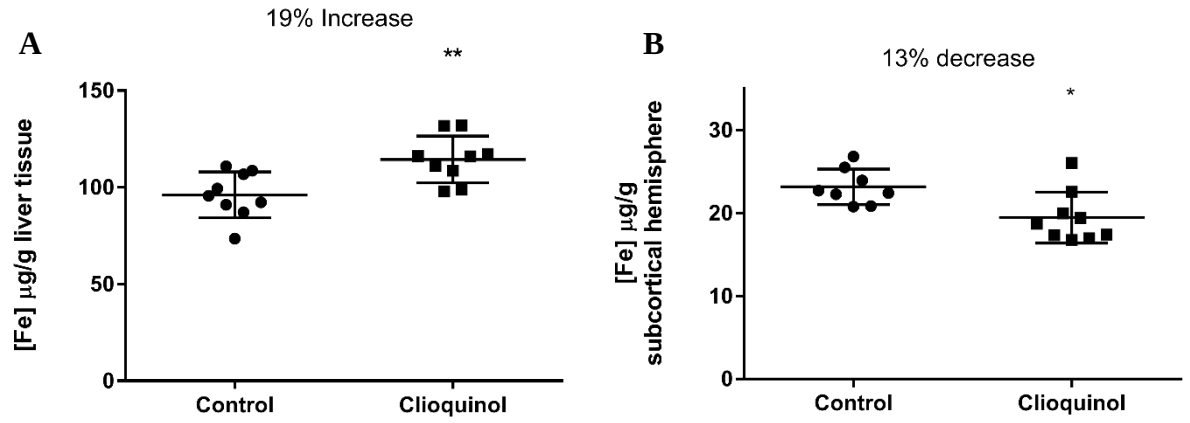

*Figure 2: Inductively coupled plasma mass spectrometry (ICP-MS) analyses of iron content in the A) liver and B) subcortical brain hemisphere of vehicle treated versus CQ-treated mice (30 mg/kg once per day for 11 days). Significance assessed by Students t-test (where n = 8 - 9, * denotes p < 0.05 and ** denotes p < 0.01). All data shown are individually plotted data points, with horizontal lines representing mean ± SD.*

The effects of CQ administration on the level of metals in the kidneys of Swiss Outbred mice were minor, with no change detected for all of the metals tested, except for a significant 23% reduction in manganese (Table 2). Similar results were obtained for the metal ion levels in the small intestines of CQ-treated mice. No changes were detected in any of the metals tested, except for a 25% increase in sodium (Table 3).

The compartment that exhibited the most numerous significant changes in metal concentration following CQ administration was the mouse plasma, where four of the eight metals that could be analysed at concentrations above the limits of detection registered modest yet statistically significant differences. In mouse plasma, CQ induced an 8% increase in sodium, a 12% increase in phosphorous, a 6% increase in calcium, and a 24% increase in zinc (Table 4). No significant differences were detected for magnesium, potassium, iron or copper.

In the mouse liver, treatment with CQ induced a significant 12% increase in phosphorous (Table 5), a 10% increase in potassium (Table 5) and most significantly, a 19% increase in iron

Table 1: Concentrations of metal ions (µg/mg of protein) in the microvessel enriched fractions of Swiss outbred mice treated with control vehicle or CQ (30 mg/kg) by oral gavage for 11 days. Data are presented as mean ± SEM, with p-value determined via Students t-test.

Microvessel enriched fraction				
Element	**Control** (n = 6)	**CQ** (n = 5)	**P-value**	**% Change from control** (if significant)
Sodium	130061 ± 18314	131948 ± 20067	0.95	
Magnesium	2395 ± 79	2116 ± 63	0.03	- 12%
Phosphorous	14032 ± 869	13243 ± 654	0.50	
Potassium	14588 ± 618	11752 ± 652	0.01	- 19%
Calcium	1345 ± 127	1280 ± 177	0.77	
Manganese	1.48 ± 0.14	1.42 ± 0.14	0.79	
Iron	206 ± 28	178 ± 32	0.52	
Copper	8.19 ± 0.69	8.22 ± 0.72	0.97	
Zinc	30.1 ± 3.1	29.9 ± 4.0	0.96	
Rubidium	1.63 ± 0.19	1.53 ± 0.23	0.73	

levels (Figure 2A). No changes were detected for sodium, magnesium, calcium, copper or zinc (Table 5), and manganese and rubidium levels were below the limits of detection in this organ. Because of the requirement to sacrifice the mouse cortex in order to obtain the MEF, cortical brain regions could not be assessed for CQ induced metal changes. One hemisphere of the subcortical brain however was analysed by ICP-MS, in order to track any CQ induced changes in this brain region. As shown in Table 6, no significant changes for the metals above the limits of detection within this tissue reached significance (sodium, magnesium, potassium, phosphorous, calcium, copper and zinc), except for iron, for which a 13% reduction in subcortical brain iron load was observed (Figure 2B).

Table 2: Concentrations of metal ions (μg/g of tissue) in the kidneys of Swiss outbred mice treated with control vehicle or CQ (30 mg/kg) by oral gavage for 11 days. Data are presented as mean ± SEM, with p-value determined via Students t-test.

Kidney				
Element	**Control conc.** (n = 9)	**CQ conc.** (n = 8)	**P-value**	**% Change from control** (if significant)
Sodium	1484 ± 45	1527 ± 44	0.50	
Magnesium	206.9 ± 3.0	200.8 ± 5.5	0.33	
Phosphorous	4067 ± 69	3997 ± 97	0.55	
Potassium	3110 ± 96	3023 ± 96	0.45	
Calcium	52.0 ± 1.6	50.3 ± 2.2	0.54	
Manganese	1.51 ± 0.04	1.35 ± 0.05	0.02	- 23%
Iron	75.8 ± 2.8	70.6 ± 3.6	0.26	
Copper	3.63 ± 0.06	3.47 ± 0.07	0.12	
Zinc	18.2 ± 0.3	18.1 ± 0.46	0.81	
Cobalt	0.089 ± 0.008	0.076 ± 0.005	0.18	
Nickel	0.0124 ± 0.0009	0.01438 ± 0.0013	0.24	
Selenium	1.66 ± 0.04	1.58 ± 0.05	0.23	
Rubidium	9.64 ± 0.42	9.14 ± 0.34	0.38	

Table 3: Concentrations of metal ions (μg/mg protein) in the small intestines of Swiss outbred mice treated with control vehicle or CQ (30 mg/kg) by oral gavage for 11 days. Data are presented as mean ± SEM, with p-value determined via Students t-test.

Small intestine				
Element	**Control conc.** (n = 9)	**CQ conc.** (n = 9)	**P-value**	**% Change from control** (if significant)
Sodium	1475 ± 62	1837 ± 114	0.01	+ 25%
Magnesium	403 ± 32	332 ± 60	0.31	
Phosphorous	3508 ± 217	3425 ± 216	0.79	
Potassium	2465 ± 138	2685 ± 173	0.34	
Calcium	1524 ± 181	1024 ± 355	0.23	
Manganese	20.5 ± 2.4	15.9 ± 5.2	0.43	
Iron	32.3 ± 2.8	29.0 ± 2.5	0.39	
Copper	3.27 ± 0.34	2.91 ± 0.33	0.47	
Zinc	28.6 ± 1.9	27.5 ± 2.7	0.75	
Cobalt	0.12 ± 0.01	0.08 ± 0.02	0.14	
Nickel	0.45 ± 0.06	0.37 ± 0.12 (n = 8)	0.55	
Selenium	0.37 ± 0.03	0.41 ± 0.05	0.50	
Rubidium	6.47 ± 0.39	6.90 ± 0.47	0.49	

Table 4: Concentrations of metal ions (μM) in the plasma of Swiss outbred mice treated with control vehicle or CQ (30 mg/kg) by oral gavage for 11 days. Data are presented as mean ± SEM, with p-value determined via Students t-test.

Plasma				
Element	**Control conc.** (n = 9)	**CQ conc.** (n = 9)	**P-value**	**% Change from control** (if significant)
Sodium	154622 ± 1540	167159 ± 3757	0.007	+ 8%
Magnesium	849 ± 33	867 ± 34	0.71	
Phosphorous	6433 ± 186 (n = 8)	7078 ± 134	0.01	+ 12%
Potassium	6479 ± 225	6095 ± 220	0.24	
Calcium	2174 ± 7 (n = 8)	2281 ± 12 (n = 8)	< 0.0001	+ 6%
Iron	84.2 ± 10.5	78.0 ± 7.8	0.64	
Copper	7.45 ± 0.79	7.29 ± 0.36	0.85	
Zinc	10.8 ± 0.4	13.4 ± 0.9	0.02	+ 24%

Table 5: Concentrations of metal ions (μg/g of tissue) in the livers of Swiss outbred mice treated with control vehicle or CQ (30 mg/kg) by oral gavage for 11 days. Data are presented as mean ± SEM, with p-value determined via Students t-test.

Liver				
Element	**Control conc.** (n = 9)	**CQ conc.** (n = 9)	**P-value**	**% Change from control** (if significant)
Sodium	1143 ± 46	1122 ± 31	0.72	
Magnesium	257 ± 8	274 ± 9	0.16	
Phosphorous	4548 ± 159	5109 ± 189	0.04	+ 12%
Potassium	3611 ± 89	3963 ± 109	0.02	+ 10%
Calcium	36.3 ± 2.6	37.6 ± 1.3	0.67	
Iron	96.2 ± 4.0	114.4 ± 4.1	0.005	+ 19%
Copper	5.98 ± 0.35	6.92 ± 0.64	0.22	
Zinc	33.7 ± 1.3	37.1 ± 1.7	0.14	

Table 6: Concentrations of metal ions (μg/g of tissue) in one subcortical hemisphere of Swiss outbred mice treated with control vehicle or CQ (30 mg/kg) by oral gavage for 11 days. Data are presented as mean ± SEM, with p-value determined via Students t-test.

Sub-cortical brain hemisphere				
Element	**Control conc.** (n = 9)	**CQ conc.** (n = 9)	**P-value**	**% Change from control** (if significant)
Sodium	3042 ± 168	2923 ± 197	0.64	
Magnesium	180 ± 5	176 ± 6	0.61	
Phosphorous	4930 ± 136	4757 ± 166	0.43	
Potassium	3298 ± 225	3324 ± 198	0.93	
Calcium	64.7 ± 5.5 (n = 8)	62.7 ± 7.6 (n = 8)	0.84	
Iron	23.2 ± 0.8 (n = 8)	19.5 ± 1.0	0.01	- 13%
Copper	4.21 ± 0.15	4.14 ± 0.19	0.78	
Zinc	14.7 ± 0.6	14.7 ± 0.4	0.93	

CQ-mediated metal ion redistribution does not alter P-gp or LRP1 expression

Since it has been shown previously that biometals copper and zinc are able to influence cell signalling pathways, including those that govern BBB transporter expression levels, it was hypothesised that CQ administration may result in increased sequestration of biometals in some barrier tissues, which may then elicit an effect upon the expression levels of important efflux transporter proteins, namely P-gp and LRP1. However, as could be expected from the ICP-MS results outlined above, the lack of CQ-mediated copper and zinc alterations in the barrier tissues assessed indicated that the hypothesised changes in transporter expression levels within these tissues was unlikely. As shown in Figures 3-5, no significant differences in P-gp or LRP1 expression were detected in the MEF, nor in the liver or kidney tissues, of Swiss outbred mice that were administered CQ by oral gavage for 11 days.

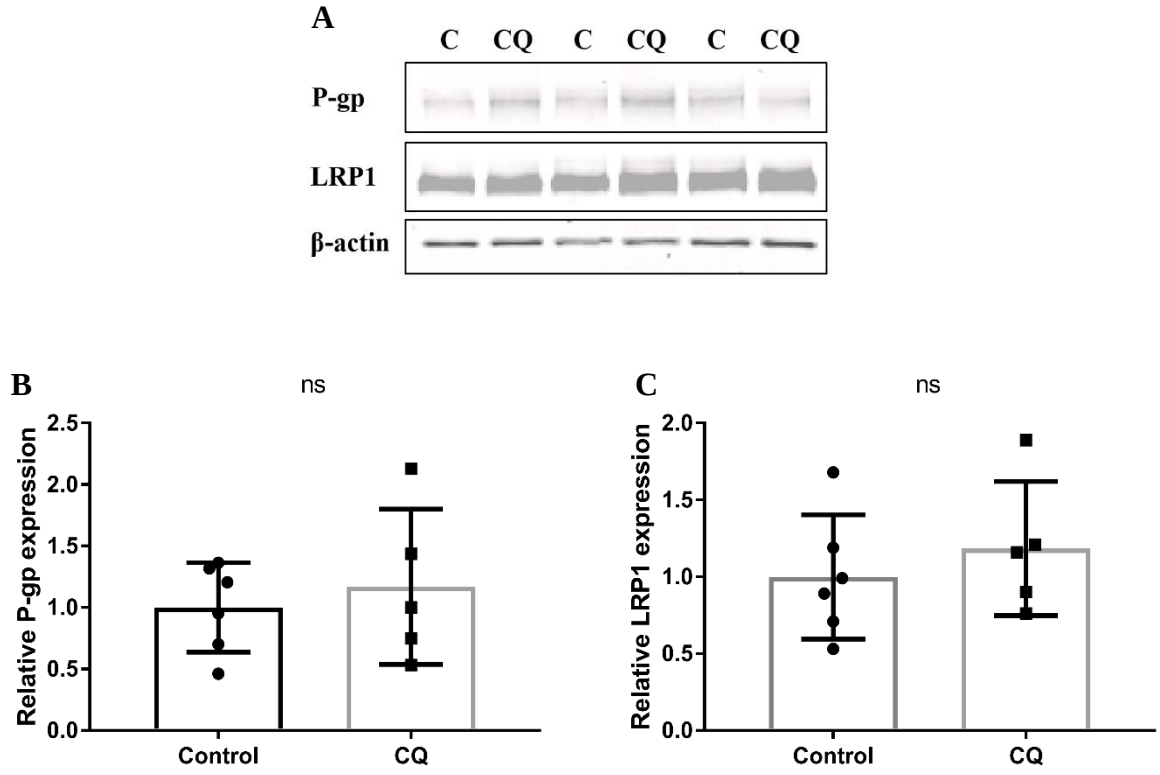

Figure 3: (A) Representative Western blot (WB) analyses of expression levels of P-gp and LRP1 in microvessel enriched fractions of mice treated with either vehicle (C) or clioquinol (CQ) (30 mg/kg once per day for 11 days). B) Graphical data of relative P-gp expression and C) relative LRP1 expression. Significance assessed by Students t-test (where n = 5-6, ns denotes no statistical significance). All data shown are individually plotted data points, with horizontal lines representing mean ± SD.

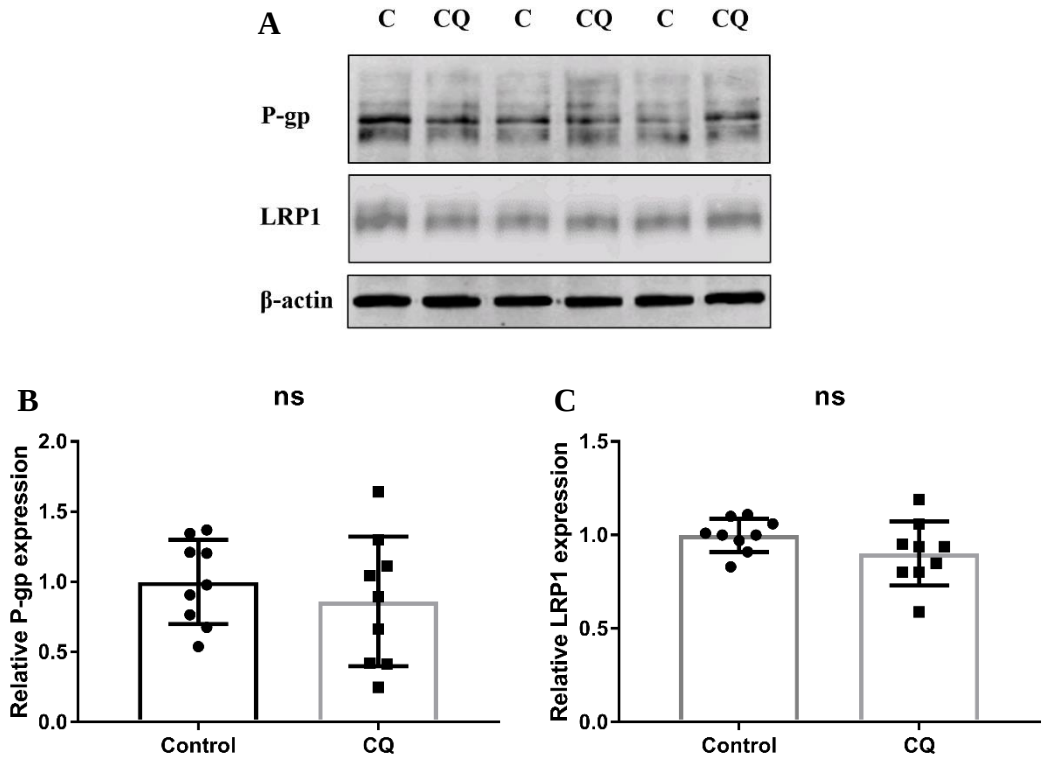

Figure 4: (A) Representative Western blot (WB) analyses of expression levels of P-gp and LRP1 in the livers of mice treated with either vehicle (C) or clioquinol (CQ) (30 mg/kg once per day for 11 days). B) Graphical data of relative P-gp expression and C) relative LRP1 expression. Significance assessed by Students t-test (where n = 9, ns denotes no statistical significance. All data shown are individually plotted data points, with horizontal lines representing mean ± SD.

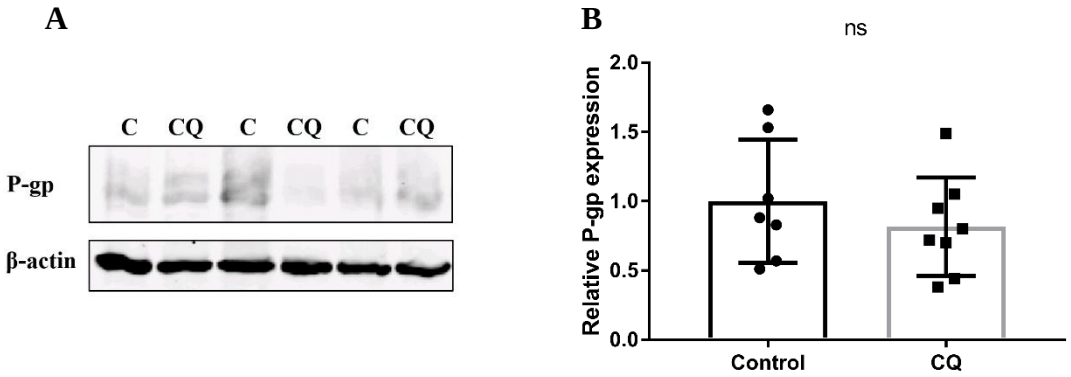

Figure 5: (A) Representative Western blot (WB) analyses of expression levels of P-gp in the kidneys of mice treated with either vehicle (C) or clioquinol (CQ) (30 mg/kg once per day for 11 days). B) Graphical data of relative P-gp expression. Significance assessed by Students t-test (where n = 7-9, ns denotes no statistical significance. All data shown are individually plotted data points, with horizontal lines representing mean ± SD.

CQ and Zn^{2+}/Cu^{2+} administration does not affect P-gp expression in primary mouse brain endothelial cells

The initial observation that prompted the work contained in this chapter (or study), was that CQ mediated biometal delivery to the human endothelial (hCMEC/D3) cell line was indeed able to cause a significant 1.7-fold upregulation of P-gp expression (Chapter 4). After observing that an 11 day treatment of CQ by oral gavage in Swiss outbred mice does not affect brain endothelial P-gp expression, thus opposing the relevance of our in vitro findings, the influence of CQ and biometals on P-gp expression on MBECs was measured, to determine whether the effect of CQ was species-specific. Primary MBECs were isolated from sacrificed Swiss outbred mice, and cultured in 96-well plates until reaching 70-80% confluency, at which point various treatments mimicking those outlined in earlier in vitro chapters (rifampicin at 50 μM, CQ + Zn^{2+} + Cu^{2+} at 0.5, 0.5 and 0.1 μM, and since we identified a copper driven mechanism, CQ + Cu^{2+} both at 0.1 μM, as an additional treatment) and were applied to the primary cells for 24 h, and in serum free media (excluding rifampicin treatment which was performed in normal serum containing media). The same in-cell western (ICW) protocol as was used in previous chapters was then applied, to measure any changes in P-gp expression resulting from these treatments, normalised to DAPI as a surrogate measure of cell number per well. The results summarised in Figures 6A-F indicate that MBECs do not respond in the same way to the presented treatments, as do hCMEC/D3 cells. Functioning as a positive control, a 24 h treatment with rifampicin (50 μM) resulted in a significant 1.2-fold upregulation of P-gp (Figures 6A and B), indicating a similar response to human derived cells (1.5-fold in hCMEC/D3s). Interestingly, a preliminary observation of primary MBECs exposed to the same treatment regime shown to cause a 1.7-fold upregulation in hCMEC/D3 cells (CQ, Zn^{2+}, Cu^{2+} at 0.5, 0.5 and 0.1 μM), suggested a 30% reduction in relative P-gp expression (Figures 6E and F), while treatment of MBECs with CQ + Cu^{2+} did not alter P-gp levels (Figures 6C and D).

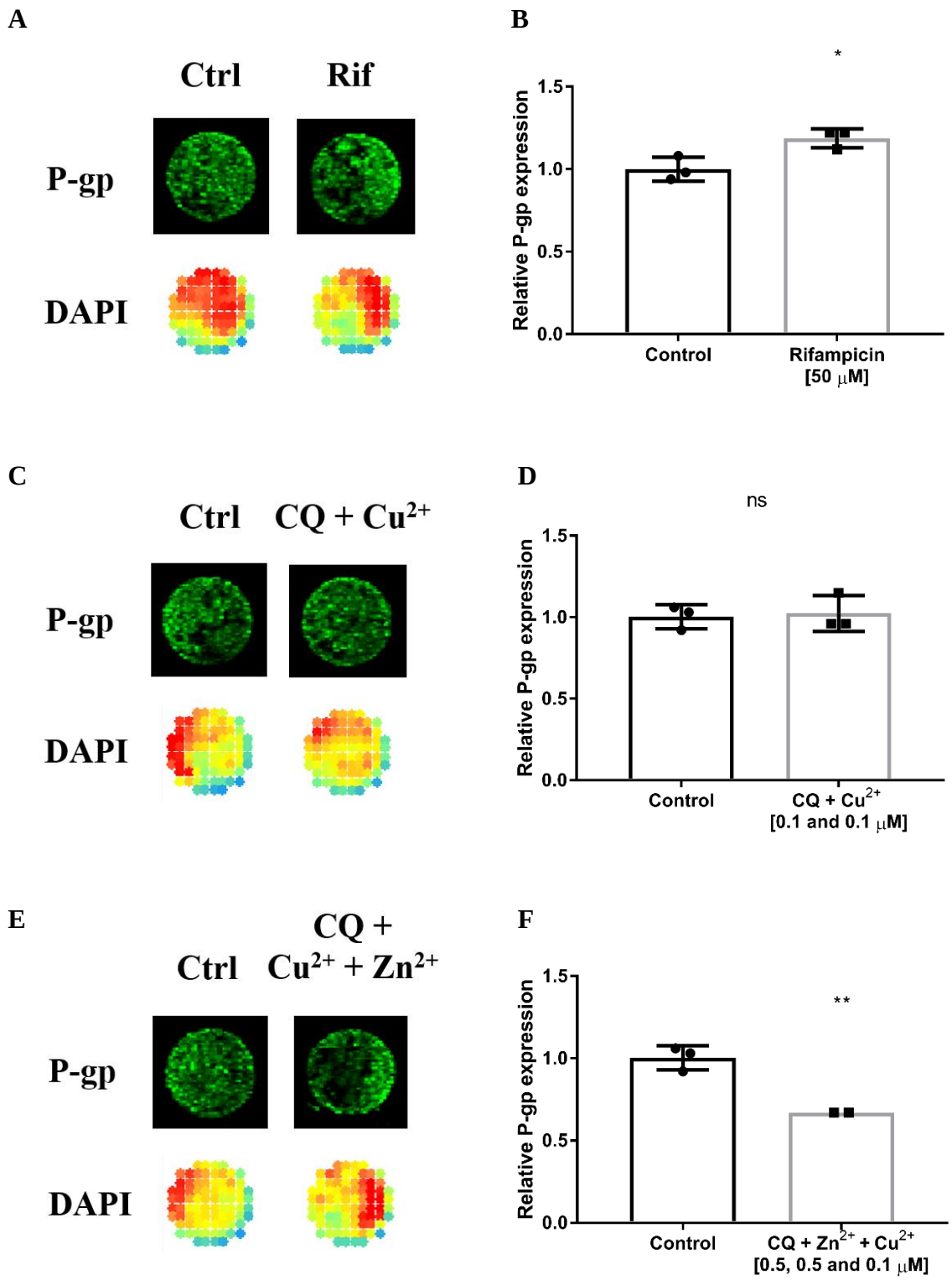

*Figure 6: Relative P-gp expression assessed by the in-cell western approach, in primary mouse brain endothelial cells (MBECs) isolated from Swiss outbred mice. A, C and E) Representative P-gp and DAPI signals following 24 h treatment with rifampicin (positive control), CQ + Cu^{2+} and CQ + Zn^{2+} + Cu^{2+}, respectively. B, D and F) Graphical representation of data produced in A, C and E. All data shown are individually plotted data points, with horizontal lines representing mean ± SD. Significance assessed by Students t-test, where n = 2-3; ns denotes no statistical significance; * denotes $p < 0.05$ and ** denotes $p < 0.01$.*

DISCUSSION

Previously, we had identified a potentially novel mechanism of action for the metal ionophore drug CQ, which when co-administered with copper at nanomolar concentrations, was able to produce a significant upregulation of the Aβ-trafficking transporter P-gp (Chapter 4). The main contention of this study was to observe whether or not the same effects manifest in the brain endothelium of an in vivo system, as well as other organs which might use biometals as an input for barrier transporter protein expression, in a manner analogous to that of the BBB. Thus the main aims of this study were: 1) to observe the ability of CQ to shuttle metal ions across the biological membranes of transporter interfaced tissues, and 2) to assess any resulting changes in the expression of the two main Aβ-trafficking transporters P-gp and LRP1 which may have resulted from altered metal ion levels within those tissues.

The study design used here possessed some definite limitations, which are addressed from the outset. Both the ICP-MS and WB were performed on homogenised sections of whole tissue (for example one whole lobe of kidney), and not on sub-organ regions of those tissues, limiting the ability to identify any localised sub-organ specific changes in the variables observed. Thus the values reported for changes in metal distribution and transporter expression are global organ values and not more specific sub-organ regions. Secondly, P-gp expression in the tissues assessed was diffuse and relatively low in comparison to the normalising protein β-actin, leading to noisier than optimal data production, and potentially obscuring the identification of any subtle changes in P-gp expression that might have manifested. P-gp expression has been shown to be diffuse in liver and kidney homogenates elsewhere (21, 22), indicating that the smeared bands shown herein are not errors in WB technique, but rather may represent P-gp in various states of post-translational glycolysation within these tissues, which are still able to

interact with the C219 antibody. Despite these limitations, many interpretations can be drawn from the data presented herein.

The most important anatomical region of interest regarding the AD-hypothesis of this study was the BBB, because it is across the brain endothelium where the most critical barrier for Aβ trafficking exists. The ICP-MS and WB results from the MEF assessed within this study provide a clear answer to this central hypothesis. In Swiss outbred mice, chronic administration of CQ (30 mg/kg for 11 days) did not increase copper levels within the MEF, nor did CQ affect the expression of P-gp or LRP1 within the same tissue. Since CQ did not increase copper concentrations in MEF however, this study does not indicate that P-gp expression is not modulated by enhanced delivery of copper to the brain endothelium, but rather that CQ is unable to meet this end. It is possible that an alternative ionophore could increase brain microvascular endothelial copper, and subsequently drive an increase in P-gp expression similar to that observed in the in vitro experiments presented in Chapter 4. Magnesium levels in the MEF however, were reduced by 12%. This finding may be significant, since Mg^{2+} functions as a concentration dependent auxiliary cofactor for the ATPase activity of the Aβ-trafficking transporter protein, P-gp (23). The observed 12% decrease of endothelial magnesium however, is probably too small to elicit a statistically significant impact on P-gp activity, which has been shown to respond logarithmically to Mg^{2+} concentration in vitro (23).

The observation of multiple changes in the mouse plasma biometal concentrations (increased zinc among others) may have been encouraging with regards to increasing BBB expression of P-gp and LRP1, however the plasma ion increases just mentioned did not translate to brain endothelial ion increases, and thus changes in P-gp and LRP1 expression did not manifest. There are several possible reasons for the failure to observe changes in endothelial transporter

expression. The first may be the species difference of the two models used in these studies. The PXR-activating rifampicin treatment employed here as a positive control, induced a modest yet significant 1.2-fold upregulation of P-gp (Figures 6A and B) in MBECs. While it has been reported that PXR sequence homology is sufficiently different in the mouse genome when compared to humans such that this system reacts less strongly to rifampicin in mouse cells when compared to cells derived from human (24), a modest yet significant increase in PXR signalling activation (approximately 1.2-fold) was reported elsewhere (24), which is in line with the modest P-gp increase observed in this study.

The preliminary observation of MBEC treatment with the established CQ + Zn^{2+} + Cu^{2+} regime appeared to actually reduce P-gp expression, and treatment with CQ + Cu^{2+} resulted in no difference. These results suggest that murine brain endothelial cells do not respond to biometal input in the same way as human brain endothelial cells in an in vitro setting, and as such a species difference can potentially explain the lack of effect seen in mice.

Another possibility is that the exposure of CQ to the brain endothelium is not sufficient to induce changes in vivo. CQ is a relatively hydrophobic small molecule, and when in vivo is normally highly protein bound (>99%) (17). It is for this reason that all of the in vitro experiments presented in earlier chapters were executed in serum free media. Whilst CQ is able to modestly penetrate the human and murine brains (25), the binding status of CQ to biological components whilst traversing the BBB, metallic or otherwise, is certainly unknown. This notion, combined with the absence of changes in biometal levels (zinc and copper) in MEF, indicates that CQ is most likely unable to deliver zinc or copper to the murine brain endothelium, and therefore transporter expression profiles remain unaltered. The same line of thinking can be extended to the other tissue compartments assessed for P-gp and LRP1

expression. Since no changes in copper levels were detected in the kidneys or livers of CQ treated mice, the absence of changes in P-gp and LRP1 expression in these tissues was expected and confirmed. This does not exclude the possibility however that an alternative ionophore drug that is able to deliver enhanced copper to the brain endothelium (or other tissue compartments) could resultantly induce an increase in P-gp expression.

One of the more interesting findings in this study was the CQ-induced increase of iron in the liver. As shown in figures 2A and B, iron levels were reduced by 13% in the murine subcortical brain region and increased by 19% in the mouse liver. This finding of CQ reducing brain iron load has been reported previously, with Kaur et al demonstrating a 30% decrease in iron from the substantia nigra of a pharmacologically induced mouse model of PD (mice treated with 1-methyl-4-phenyl-1,2,3,6-tetrahydropyridine) (26), and while assessing one hemisphere of the mouse subcortical brain region is far less precise a measure than that of the substantia nigra specifically, the two results are nonetheless concordant. What was until now unknown however, was that this iron load removed from the brain appears to be associated with an increase in iron in the liver, possibly due to the liver-mediated CQ catabolism, where CQ may inadvertently deliver iron as the drug itself accumulates via hepatic processes.

Prior to this study, the ionophoric effects of CQ have been studied almost exclusively with regard to Cu^{2+}, Zn^{2+} and Fe^{3+}, with little attention being allocated to any interactions between CQ and the other metal cations that are normally present and participate physiologically within biological systems. As detailed in the results section above, CQ when administered chronically to Swiss outbred mice, was able to induce changes in the tissue concentrations of not only zinc and iron, but also of the following metal ions: sodium (25% and 8% increases in the small intestines and plasma respectively), magnesium (12% reduction in MEF), phosphorous (12%

increases in both plasma and liver), potassium (19% reduction in the MEF and a 10% increase in liver), calcium (6% increase in plasma) and manganese (23% reduction in the kidneys). Whether or not CQ was able to redistribute these metals amongst biological compartments via the same direct ionophore effect that has been observed for zinc, copper and iron, cannot be determined from the data produced in this study, but speculation as to the feasibility of this mechanism is permissible. The effective ionic radii of all metals has been determined semi-empirically in the past, and the data can be called upon to make the assessment just described. Shannon estimated the ionic radii of Cu^{2+}, Zn^{2+}, Fe^{2+} and Fe^{3+} (the ions for which CQ binding has been previously demonstrated to occur with high affinity (27)) to be 73, 74, 61-78, and 55-64.5 pm, respectively (28). The effective ionic radii for both the mono-, di- and trivalent metal cations affected by CQ within this study were also estimated by Shannon (28), with the following values put forward: Na^{+} (102 pm), Mg^{2+} (72 pm), P^{3+} (44 pm), K^{+} (138 pm), Ca^{2+} (100 pm) and Mn^{2+} (67-83 pm)(28). Considering these radii along with the valence states of each ion, it is a feasible hypothesis that CQ is able to form coordination complexes with and thus facilitate ionophoric transport of Mg^{2+} and Mn^{2+} within biological systems. Coordination complexation between CQ and the remaining ions just described however, is less feasible, due to the constraints of size and electric charge which are likely imposed by the rigid chemical structure of CQ. It is possible that the remaining effects are secondary and related to the maintenance of ionic equilibrium, but understanding the exact nature of the physical processes imposed by CQ is a direction of future research. The potential consequences of the observed CQ-mediated in vivo metal redistribution are likely numerous and diverse, but when considering the general health of the animals treated with ionophores like CQ in this study and others, they are also likely to be subtle, at least in the short term.

In any case, to the best of our knowledge, the findings herein represent the first demonstration that CQ is able to effectively alter the distribution of the metal ions sodium, magnesium, phosphorous, potassium, calcium and manganese, in or out of the various compartments of a biological system, an effect which is normally prohibited by the ionic/hydrophobic repulsion of the charged ion/biological membrane interaction, but which is likely overcome by the hydrophobic shielding and thus ionophoric activity of the drug CQ. These observed effects are worthy of future consideration by researchers using ionophores for whatever means, who are intent on pursuing holistic interpretations of ionophore activity on whole-system physiology.

CONCLUSION

No significant changes in the expression of P-gp and LRP1 were observed in the MEFs of the brain endothelium, nor the liver or kidneys of Swiss outbred mice following 11 day CQ administration. We do report however, a range of subtle yet considerable redistributions of metal ions around the mouse body, including calcium, iron, magnesium, manganese, phosphorous potassium, sodium, and zinc, which we attribute to the ionophore effects of CQ. Finally, we observed a reduction in subcortical brain tissue iron load that was associated with an increase in iron within the murine liver, an effect which to the best of our knowledge was previously unknown. While most previous studies using ionophores have focussed on their effects within the brain, this study demonstrates that whole body metal status can be affected by administration of metal ionophores such as CQ, which may serve to inform future work using CQ or other ionophore drugs.

REFERENCES

1. Ding WQ, Lind SE. Metal ionophores - an emerging class of anticancer drugs. IUBMB Life. 2009;61(11):1013-1018.
2. Bourassa MW, Miller LM. Metal imaging in neurodegenerative diseases. Metallomics. 2012;4(8):721-738.
3. Lovell MA, Robertson JD, Teesdale WJ, Campbell JL, Markesbery WR. Copper, iron and zinc in Alzheimer's disease senile plaques. J Neurol Sci. 1998;158(1):47-52.
4. Suh SW, Jensen KB, Jensen MS, Silva DS, Kesslak PJ, Danscher G, Frederickson CJ. Histochemically-reactive zinc in amyloid plaques, angiopathy, and degenerating neurons of Alzheimer's diseased brains. Brain Res. 2000;852(2):274-278.
5. Dusek P, Roos PM, Litwin T, Schneider SA, Flaten TP, Aaseth J. The neurotoxicity of iron, copper and manganese in Parkinson's and Wilson's diseases. J Trace Elem Med Biol. 2015;31:193-203.
6. Whittaker MM, Whittaker JW. Cu(I)-dependent biogenesis of the galactose oxidase redox cofactor. J Biol Chem. 2003;278(24):22090-22101.
7. Tapiero H, Townsend DM, Tew KD. Trace elements in human physiology and pathology. Copper. Biomed Pharmacother. 2003;57(9):386-398.
8. Lynch SM, Colon W. Dominant role of copper in the kinetic stability of Cu/Zn superoxide dismutase. Biochem Biophys Res Commun. 2006;340(2):457-461.
9. Harris ZL, Klomp LW, Gitlin JD. Aceruloplasminemia: an inherited neurodegenerative disease with impairment of iron homeostasis. Am J Clin Nutr. 1998;67(5 Suppl):972S-977S.
10. Rucker RB, Kosonen T, Clegg MS, Mitchell AE, Rucker BR, Uriu-Hare JY, Keen CL. Copper, lysyl oxidase, and extracellular matrix protein cross-linking. Am J Clin Nutr. 1998;67(5 Suppl):996S-1002S.

11. Crouch PJ, Savva MS, Hung LW, Donnelly PS, Mot AI, Parker SJ, Greenough MA, Volitakis I, Adlard PA, Cherny RA, Masters CL, Bush AI, Barnham KJ, White AR. The Alzheimer's therapeutic PBT2 promotes amyloid-beta degradation and GSK3 phosphorylation via a metal chaperone activity. J Neurochem. 2011;119(1):220-230.
12. Beurel E, Grieco SF, Jope RS. Glycogen synthase kinase-3 (GSK3): regulation, actions, and diseases. Pharmacol Ther. 2015;148:114-131.
13. Harati R, Benech H, Villegier AS, Mabondzo A. P-glycoprotein, breast cancer resistance protein, organic anion transporter 3, and transporting peptide 1a4 during blood-brain barrier maturation: involvement of Wnt/beta-catenin and endothelin-1 signaling. Mol Pharm. 2013;10(5):1566-1580.
14. Liebner S, Corada M, Bangsow T, Babbage J, Taddei A, Czupalla CJ, Reis M, Felici A, Wolburg H, Fruttiger M, Taketo MM, von Melchner H, Plate KH, Gerhardt H, Dejana E. Wnt/beta-catenin signaling controls development of the blood-brain barrier. J Cell Biol. 2008;183(3):409-417.
15. Polakis P. Formation of the blood-brain barrier: Wnt signaling seals the deal. J Cell Biol. 2008;183(3):371-373.
16. Grossi C, Francese S, Casini A, Rosi MC, Luccarini I, Fiorentini A, Gabbiani C, Messori L, Moneti G, Casamenti F. Clioquinol decreases amyloid-beta burden and reduces working memory impairment in a transgenic mouse model of Alzheimer's disease. J Alzheimers Dis. 2009;17(2):423-440.
17. Adlard PA, Cherny RA, Finkelstein DI, Gautier E, Robb E, Cortes M, Volitakis I, Liu X, Smith JP, Perez K, Laughton K, Li QX, Charman SA, Nicolazzo JA, Wilkins S, Deleva K, Lynch T, Kok G, Ritchie CW, Tanzi RE, Cappai R, Masters CL, Barnham KJ, Bush AI. Rapid restoration of cognition in Alzheimer's transgenic mice with 8-

hydroxy quinoline analogs is associated with decreased interstitial Abeta. Neuron. 2008;59(1):43-55.

18. McInerney MP, Short JL, Nicolazzo JA. Neurovascular Alterations in Alzheimer's Disease: Transporter Expression Profiles and CNS Drug Access. AAPS J. 2017.

19. McInerney MP, Volitakis I, Bush AI, Banks WA, Short JL, Nicolazzo JA. Ionophore and biometal modulation of P-glycoprotein expression and function in human brain microvascular endothelial cells. Pharm Res. 2018;35(4):83.

20. Pan Y, Short JL, Choy KH, Zeng AX, Marriott PJ, Owada Y, Scanlon MJ, Porter CJ, Nicolazzo JA. Fatty acid-binding protein 5 at the blood-brain barrier regulates endogenous brain docosahexaenoic acid levels and cognitive function. J Neurosci. 2016;36(46):11755-11767.

21. Greiner B, Eichelbaum M, Fritz P, Kreichgauer HP, von Richter O, Zundler J, Kroemer HK. The role of intestinal P-glycoprotein in the interaction of digoxin and rifampin. J Clin Invest. 1999;104(2):147-153.

22. Abanda NN, Riches Z, Collier AC. Lobular distribution and variability in hepatic ATP binding cassette protein B1 (ABCB1, P-gp): ontogenetic differences and potential for toxicity. Pharmaceutics. 2017;9(1).

23. Urbatsch IL, Gimi K, Wilke-Mounts S, Senior AE. Investigation of the role of glutamine-471 and glutamine-1114 in the two catalytic sites of P-glycoprotein. Biochemistry. 2000;39(39):11921-11927.

24. Jones SA, Moore LB, Shenk JL, Wisely GB, Hamilton GA, McKee DD, Tomkinson NC, LeCluyse EL, Lambert MH, Willson TM, Kliewer SA, Moore JT. The pregnane X receptor: a promiscuous xenobiotic receptor that has diverged during evolution. Mol Endocrinol. 2000;14(1):27-39.

25. Opazo C, Luza S, Villemagne VL, Volitakis I, Rowe C, Barnham KJ, Strozyk D, Masters CL, Cherny RA, Bush AI. Radioiodinated clioquinol as a biomarker for beta-amyloid: Zn complexes in Alzheimer's disease. Aging Cell. 2006;5(1):69-79.

26. Kaur D, Yantiri F, Rajagopalan S, Kumar J, Mo JQ, Boonplueang R, Viswanath V, Jacobs R, Yang L, Beal MF, DiMonte D, Volitaskis I, Ellerby L, Cherny RA, Bush AI, Andersen JK. Genetic or pharmacological iron chelation prevents MPTP-induced neurotoxicity in vivo: a novel therapy for Parkinson's disease. Neuron. 2003;37(6):899-909.

27. Ferrada E, Arancibia V, Loeb B, Norambuena E, Olea-Azar C, Huidobro-Toro JP. Stoichiometry and conditional stability constants of Cu(II) or Zn(II) clioquinol complexes; implications for Alzheimer's and Huntington's disease therapy. Neurotoxicology. 2007;28(3):445-449.

28. Shannon RD. Revised effective ionic radii and systematic studies of interatomic distances in halides and chaleogenides Acta Crystallographica. 1976;A32(2):751-767.

Chapter 6:

Summary, Implications

&

Future Directions

SUMMARY

The work presented in this thesis is centrally concerned with the ability of the ionophore drug clioquinol (CQ), to increase the intracellular levels of biometals zinc and copper within the endothelium forming the blood-brain barrier (BBB), and subsequently increase the relative abundance of the xenobiotic efflux transporter, P-glycoprotein (P-gp). From a biomedical research perspective, the expression and activity of P-gp is of great importance to many fields. P-gp is heavily implicated in the denial of CNS access for many drugs, and attempts to override its role have been largely unsuccessful. P-gp, expressed at the luminal membrane of microvascular endothelial cells lining the BBB, functions to actively efflux a large range of drug molecules from the endothelial lipid bilayer back into the systemic circulation.

Furthermore, over the last two decades, P-gp, along with other BBB transporter proteins such as low density lipoprotein receptor-related protein 1 (LRP1), has been implicated in the development of Alzheimer's disease (AD). These proteins actively participate in the transport of the endogenously produced amyloid-beta peptide (Aβ) across the BBB as a means of clearing the brain of this toxic peptide. P-gp and LRP1 appear to both actively efflux Aβ from the brain to the blood, as well as preventing blood-to-brain penetration of systemically circulating Aβ. These actions combined prevent the accumulation of Aβ within the brain, which if left unbalanced, goes on to mediate neuronal toxicity and eventually precipitate the AD disease state. In recent times, much strong evidence has emerged to indicate that the downregulation of P-gp at the human BBB is a key pathophysiological event of AD, and that a corresponding reinstatement of P-gp expression to physiologically healthy levels may represent a viable therapeutic target for the treatment of AD. Understanding mechanisms which govern P-gp expression at the BBB, could be of crucial value to research focussing on CNS drug permeability, cancer and potentially in the treatment of AD.

An unexplored strategy for influencing P-gp expression at the BBB is the delivery of biometals to the endothelial cells that form the lumen facing layer of the brain microvasculature. Studies have shown previously that zinc and copper at optimal concentrations, are essential to endothelial barrier maintenance and integrity, and the current study was conducted with the intention of exploring and furthering such concepts, but with emphasis on the modulation of the important transporter, P-gp, in human cerebral microvascular endothelial (hCMEC/D3) cells. Zinc and copper uptake into endothelial cells however is dependent on the activity of transporters, and is a very regulated process. Therefore, to circumvent the endogenous mechanisms of biometal uptake, the ionophore agent CQ was used, with the intention of achieving higher zinc or copper concentrations than would manifest if using biometals alone.

Before testing this central hypothesis, several methods for assessing P-gp expression had to be tested and validated. Firstly, the BCA protein assay was assessed for accuracy and precision, and was found to be a satisfactory method for quantifying protein content in hCMEC/D3 cell lysates. Next, beginning with a semi-developed protocol, a western blot (WB) workflow was interrogated and finally validated over an iterative series of experiments. Although expensive in both time and materials, the final protocol was also found to be satisfactory, and was used multiple times throughout the remainder of the project.

Due to the desire to have an alternative protocol for probing P-gp expression in larger study designs, a higher-throughput method known as the in-cell western (ICW) was next trialled, developed and validated. Over many experimental iterations, the linearity and signal to noise ratio of the P-gp signal improved greatly, and the final protocol was assessed by the use of P-gp regulating agents, with the results compared to WB. Three separate treatment conditions (two upregulators and one down-regulator) were administered to hCMEC/D3 cells, and the

results indicated that relative P-gp abundance following treatment was the same whether measured by ICW or WB. Functional enhancement of P-gp activity using the rhodamine-123 (R123) substrate confirmed that observed upregulations in P-gp by the ICW method indeed produced enhanced P-gp functionality. Thus the ICW method was considered a validated method for P-gp quantification in hCMEC/D3 cells, and was used in later sections of the thesis. Before assessing the influence of CQ and biometals on P-gp expression in brain endothelial cells, the limits of toxicity had to be identified. Use of the 3-(4,5-dimethylthiazol-2-yl)-2,5-diphenyltetrazolium bromide (MTT) assay in conjunction with morphological assessments provided well characterised tolerances of the three chemical agents CQ, Zn^{2+} and Cu^{2+}, both alone and in combination, in hCMEC/D3 cells. Next, the central hypothesis of the thesis was tested in an in vitro setting. A complex eight-way study design involving CQ and the biometals Zn^{2+} and Cu^{2+}, both alone and in combination, revealed that only the combination of all three components produced a significant upregulation of P-gp expression in hCMEC/D3 cells. This result was confirmed by WB, and the functional enhancement that would follow upregulation of P-gp was confirmed using the R123 uptake assay. Inductively coupled plasma mass spectrometry (ICP-MS) revealed that the CQ/Zn^{2+}/Cu^{2+} treatment did not increase zinc levels in hCMEC/D3 cells, but that cytosolic copper levels were significantly enhanced. A time dependent analysis of copper uptake by ICP-MS revealed that CQ-mediated uptake of copper resulted in greater cellular copper concentrations than when Cu^{2+} was given alone, indicating that CQ was indeed able to enhance cytosolic uptake of copper. Thus it was found that increased cellular copper was associated with increased P-gp expression in hCMEC/D3 cells, indicating the possibility of a copper-driven mechanism.

Next, the validity of the findings above were assessed in an in vivo system. Swiss outbred mice were treated with a previously identified and clinically relevant dose of CQ by oral gavage for

an 11-day period. At the termination of the study, the mice were sacrificed before the brains and other peripheral organs (small intestine, liver, kidney and plasma) were isolated for metallomic and transporter expression (P-gp and LRP1) analysis. Microvessel enriched fractions (MEF) of the mouse cortices were obtained via centrifugation techniques, and probed directly for biometals and transporter expression. The 11-day treatment with CQ did not increase zinc or copper levels, nor P-gp or LRP1 expression levels in the MEF of the Swiss outbred mice, verifying the null hypothesis in this model. P-gp and LRP1 expression was also unchanged in the small intestine, liver and kidneys of the mice. Metallomic analysis however, revealed that CQ possessed considerable activity in the animals, redistributing the biometals sodium, magnesium, phosphorous, potassium, calcium and manganese into and out of each of the biological compartments assessed (MEF, small intestine, liver, kidney, plasma and subcortical brain tissue).

Finally, to probe the discrepancy between the in vitro and in vivo results, primary mouse brain endothelial cells (MBECs) were isolated from Swiss outbred mice, and cultured for several days before being administered with the same P-gp upregulating treatments identified above. Treatment with the positive control rifampicin (shown previously in the thesis to cause upregulation in hCMEC/D3 cells) elicited a similar response in MBECs, indicating that these cells could respond homeostatically to similar stimuli as cells derived from humans. But treatment of MBECs with either the CQ/Zn^{2+}/Cu^{2+} treatment, or an additional CQ/Cu^{2+} treatment, failed to induce P-gp upregulation. This latter finding allows for the possibility that MBECs may not respond to the same biometal regulation as do brain endothelial cells derived from humans, and is a possible source of the discrepancy between the in vitro and in vivo findings.

IMPLICATIONS

The work presented in this thesis has indicated that the ionophore drug CQ, in conjunction with copper and zinc, is able to induce an increase in the expression of the pharmaceutical and AD relevant xenobiotic efflux transporter, P-gp, in the immortalised human cerebral microvascular endothelial cell line. In an area that was previously unexplored, it is now apparent that biometals may play an important role in driving the expression of important transporters such as P-gp, and that ionophores such as CQ can potentially be used to modify this process. After further experimental inquiry, it may be determined that modifying biometal mediated P-gp signalling can pose as a therapeutic strategy in treatments attempting to modify disease states such as AD and cancer, as well as providing useful considerations for research areas concerned with CNS drug access. Before however these implications can be fully realised, directions of future research must be carefully pursued.

FUTURE DIRECTIONS

The work presented in this thesis opens up multiple avenues of research for further exploration. The most immediate research endeavour is to conduct experiments identifying the mechanism of action whereby CQ and biometal treatment causes P-gp upregulation in brain endothelial cells. Further experiments in this realm can also be used to confirm a copper driven mechanism, which could then be followed by experiments attempting to distinguish between the CQ/Cu^{2+} complex versus free Cu^{2+} as the active agent in catalysing P-gp upregulation. If it is found to be free Cu^{2+} which mediates P-gp upregulation, then the possibility of using alternative ionophore agents, perhaps with higher selectivity for Cu^{2+} over the other divalent biometals, emerges as an interesting strategy for instigating the Cu^{2+} driven P-gp upregulation in animal models.

Another imperative research question is to test if the CQ/biometal driven upregulation of P-gp translates to having any clinical value for applications such as AD, by first testing whether Aβ accumulation and efflux are affected in hCMEC/D3 cells following pre-treatment with the combination. Once the enhanced trafficking of Aβ via P-gp upregulation has been confirmed, reproducing these findings in an in vivo system could then be attempted. In light of the many biometals that were redistributed amongst the murine brain and periphery, if identified, Cu^{2+} and/or Zn^{2+} specific ionophores that are capable of delivering biometals to the brain endothelium specifically could be test the hypothesis more robustly.

Another area of possible research is to assess the impact of biometals on brain endothelial expression of other important transporters such as breast cancer resistance protein and multi-drug resistance protein 1, among others. Such experiments could characterise the extent to which biometal delivery can influence the signalling pathways that encode for ATP binding cassette transporters in general, and could bear important implications for BBB cell signalling pathways.

Thus while the data presented in this thesis have bared a significant contribution towards understanding the potential pathways of P-gp regulation at the BBB, the studies presented herein have also opened up new areas of research which can and will be investigated in the future. Many of these ideas are currently being explored in our laboratory, and future publications on these topics are keenly anticipated. Such studies will provide better understanding of the role of biometals in BBB function, and may potentially find application in the development of therapeutics for research settings such as AD and CNS drug access.

Appendix:

Copies of Published Manuscripts

The AAPS Journal (© 2017)
DOI: 10.1208/s12248-017-0077-5

Review Article

Theme: CNS Barriers in Health and Disease
Guest Editors: Marilyn E. Morris and Jean-Michel Scherrmann

Neurovascular Alterations in Alzheimer's Disease: Transporter Expression Profiles and CNS Drug Access

Mitchell P. McInerney,[1] Jennifer L. Short,[2] and Joseph A. Nicolazzo[1,3]

Received 26 January 2017; accepted 15 March 2017

Abstract. Despite a century of steady and incremental progress toward understanding the underlying biochemical mechanisms, Alzheimer's disease (AD) remains a complicated and enigmatic disease, and greater insight will be necessary before substantive clinical success is realised. Over the last decade in particular, a large body of work has highlighted the cerebral microvasculature as an anatomical region with an increasingly apparent role in the pathogenesis of AD. The causative interplay and temporal cascade that manifest between the brain vasculature and the wider disease progression of AD are not yet fully understood, and further inquiry is required to properly characterise these relationships. The purpose of this review is to highlight the recent advancements in research implicating neurovascular factors in AD, at both the molecular and anatomical levels. We begin with a brief introduction of the biochemical and genetic aspects of AD, before reviewing the essential concepts of the blood-brain barrier (BBB) and the neurovascular unit (NVU). In detail, we then examine the evidence demonstrating involvement of BBB dysfunction in AD pathogenesis, highlighting the importance of neurovascular components in AD. Lastly, we include within this review research that focuses on how altered properties of the BBB in AD impact upon CNS exposure of therapeutic agents and the potential clinical impact that this may have on people with this disease.

KEY WORDS: Alzheimer's disease; blood-brain barrier; CNS drug delivery; neurovascular unit; transporters.

INTRODUCTION

Alzheimer's Disease

The biomedical revolution of the last century afforded a steady increase in the average life expectancy in most of the western world (1). Since Alzheimer's disease (AD) is generally a disease of the elderly (2), a steady rise in AD diagnosis and mortality has accompanied the rise in life expectancy. According to the 2015 World Alzheimer Report, the prevalence of AD has been projected to increase exponentially, with diagnoses approximately doubling every 20 years, before reaching a figure as high as 131 million individuals across the world by 2050 (3), placing AD as one of the most central world-wide health concerns.

The manifestation of AD can be classified into one of two types: familial or sporadic, also known as autosomal dominant AD and late-onset AD, respectively. Untangling the genetic components and resulting phenotypes of AD is difficult, but currently familial AD is thought to represent between 1 and 5% of total AD cases (4). Familial AD has been demonstrated to involve specific genetic mutations, which precipitate AD symptoms much earlier in life (average of 46.2 years (5,6)). Sporadic AD, however, represents the remaining majority of cases, and symptoms occur much later in life, with an average age of symptom onset of 72 years (5,6). Whilst the root causes and temporal unfolding of the two segregated types of AD are quite different, the histochemical changes and resulting psychiatric phenotypes remain similar enough that both types are generally comprehended in unison. At a histochemical level, AD is known to involve multiple well-characterised pathogenic events and has been described as having a 'robust histological signature' that allows for straightforward post-mortem diagnosis (7). These pathophysiological 'hallmark features' include the formation of extra-neuronal senile plaques of which insoluble beta-amyloid (Aβ) peptides are the major component (8–10) and the presence of neurofibrillary tangles

[1] Drug Delivery, Disposition and Dynamics, Monash Institute of Pharmaceutical Sciences, Monash University, 381 Royal Parade, Parkville, VIC 3052, Australia.
[2] Drug Discovery Biology, Monash Institute of Pharmaceutical Sciences, Monash University, Parkville, 3052, VIC, Australia.
[3] To whom correspondence should be addressed. (e-mail: joseph.nicolazzo@monash.edu)

Published online: 01 May 2017

composed primarily of the hyper-phosphorylated tau protein (11–13). Other notable pathophysiological features include inflamed cerebral blood vessels also associated with Aβ deposits (14,15), elevated brain levels of soluble Aβ oligomers (16,17), increased oxidative stress within the brain (18) and a significantly reduced brain weight compared to healthy age-matched controls (19). But whilst much progress has been made in the biochemical characterisation of these events individually, the causative interplay between each, and how each fits within the wider temporal pathogenesis of AD, remains still largely enigmatic.

Current Understanding of Alzheimer's Disease Pathogenesis

Of all the pathogenic events described earlier, probably the most widely implicated and well characterised is the accumulation of the Aβ peptide in its various forms within the brain. The Aβ peptides are produced under normal physiological conditions in healthy individuals, and their presence is not indicative of a diseased state. Outlined in Fig. 1 is a schematic summary of the endogenous metabolic pathways of the Aβ peptides, which is augmented in several identified genetic mutations that result in the AD phenotype. Aβ is derived originally from a much larger transmembrane protein known as amyloid precursor protein (APP) (20–22). APP possesses intrinsic physiological functions, having been shown to be involved in synaptic formation and repair (23), but continually undergoes proteolytic cleavage by a group of secretases (α, β or γ), the identity of which governs the extent of Aβ production (Fig. 1). As shown in Fig. 1, APP can at first be hydrolytically cleaved by either α -or β-secretase. The resulting C83 or C99 fragments are then indiscriminately cleaved by γ-secretase in the same position, the latter of which results in the production of Aβ species (known as the amyloidogenic pathway). The Aβ peptide can exist in multiple isoforms, resulting from splice variant processing of the APP gene expression (24,25) and variable cleavage of APP by the promiscuous γ-secretase (26). As such, the current definition of the Aβ peptides has been extended to include all peptides ranging from 37 to 49 amino acids in length that share identical sequence homology with that of the initially identified $A\beta_{40–42}$ peptide (27). The two most abundant and pathologically relevant isoforms have been identified as $A\beta_{40}$ and $A\beta_{42}$, and these species constitute 90 and 5–10%, respectively, of the total Aβ produced in a non-AD human brain (28).

Genetic Causes and Risk Factors of Alzheimer's Disease

Much work probing for potential underlying genetic aspects of AD has occurred over the last two decades, and several landmark genes have been identified. Currently, there are several genetic mutations which are directly causative of familial AD which have been discussed elsewhere (29). A brief description of the main genetic risk factor identified for sporadic AD (apolipoprotein E) may aid in contextual framing of later sections. Strittmatter *et al.* (30) identified three allele variants of the gene encoding apolipoprotein E (APOE), namely ε2, ε3, and ε4, the latter of which is associated with an increased risk of developing sporadic AD (30,31). The exact role of APOE in its relationship with AD is not yet clear, but it has been found to be potentially involved in Aβ clearance across the blood-brain barrier (BBB) (discussed in detail in a later section), promotion of Aβ aggregation (31), direct Aβ proteolytic degradation (32), and astrocyte-mediated Aβ degradation (33). APOE allele status has also recently been shown to alter BBB permeability to large molecules in mice (34), and this finding is elaborated upon in later sections. APOE may participate in

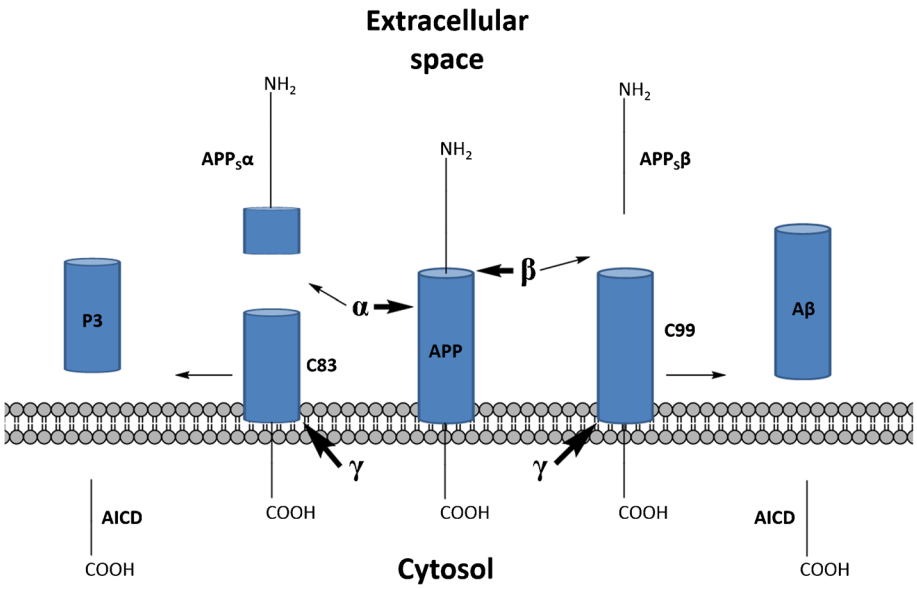

Fig. 1. Transmembrane spanning amyloid precursor protein (APP) undergoes variable proteolytic cleavage by α- or β-secretases to form either of the displayed fragments C83/$APP_s\alpha$ or C99/$APP_S\beta$, respectively. C83 and C99 fragments then undergo additional cleavage by γ-secretase, to form either the APP intracellular domain fragment (AICD) and non-pathogenic P3 fragments, or AICD and the AD centrally pathogenic peptide Aβ, respectively

some or indeed all of these mechanisms, whereby a partial loss-of-function mutation in the ε4 allele results in an APOE protein that is less effective in its amyloid related role(s), thereby allowing the accumulation of Aβ within the CNS. As work continues to attempt to identify new genes causative of AD, it is becoming increasingly apparent that straightforward genetic relationships will be unable to accurately describe sporadic AD, but that instead, clusters of genes may feed synergistically into the AD state, and this genetic heterogeneity will eventually explain the underlying biochemical basis of wider AD (29). Since each of the genetic mutations or polymorphisms identified for AD are associated with either increased Aβ production or an increased $A\beta_{42}/A\beta_{40}$ ratio and subsequently cause familial (or sporadic in the case of APOE status) AD, it is likely that both AD types, which share similar but not identical symptoms, are associated with elevated quantities of Aβ peptides within the CNS.

Aβ Cascade Hypothesis

Originally, it was thought that the Aβ-composed neuritic plaques were the main cause of neurodegeneration in AD. Subsequent investigations have compromised the simplicity of the Aβ hypothesis, by showing that Aβ plaque formation correlates poorly with the severity of dementia (35–37). Additionally, post-mortem analysis of some individuals who had lived well into their 90s with no display of clinically observable cognitive decline has sometimes revealed an extensive presence of mature neuritic plaques, suggesting that the plaques themselves may not be the primary cause of injury (7). Further examination indicated that approximately 20–40% of elderly people who appear cognitively normal possess Aβ plaques (38). These observations prompted investigations into the potentially toxic properties of soluble oligomeric species of Aβ. The amyloid cascade hypothesis was first proposed by Hardy and Higgins in 1992 (39). Briefly, it stated that it is the accumulation of oligomeric Aβ species within the CNS that is the central event in AD and that neuritic and fibrillar plaque deposition and tauopathic events are secondary processes and may result from the overaccumulation of Aβ species. This hypothesis has gained much support since its original proposal, and most current attempts at pharmacological interventions rest on this hypothesis. In 1999, it was found that the presence of soluble Aβ oligomers (Aβos) correlated well with synaptic loss and cognitive decline in human AD (16,17,40), pointing toward Aβos as a main culprit. Attempts to uncover the mechanisms underlying the neurotoxicity of Aβos are numerous and diverse, and whilst at present, it is widely accepted that Aβos do mediate neurodegeneration, it is still unclear which of the proposed mechanisms bare the most influence (41). As consensus for the Aβ hypothesis developed and consolidated over the 1990s and 2000s, the emphasis on AD research gradually pivoted toward identifying the mechanistic causality of Aβ accumulation within the CNS. Perhaps, one of the strongest hypotheses for the root cause of this accumulation, which has received a great deal of attention and experimental confirmation, is the neurovascular hypothesis of AD.

The Neurovascular Hypothesis of Alzheimer's Disease

The neurovascular hypothesis of AD was first put forward by Zlokovic *et al.* in 2005 (42,43). Briefly, it stated that a causative link between cerebrovascular dysregulation and brain Aβ accumulation may exist and may even be the root cause of Aβ accumulation in the CNS and therefore of sporadic AD. This hypothesis has made available the possibility of influencing new specific neurovascular targets via pharmacological intervention or other means, as a strategy for preventing Aβ accumulation early in the disease, or enhancing Aβ efflux and thus Aβ pool dissociation later in the disease—both as potential options for treating AD (43). Furthermore, it has been suggested that whilst the pathogenesis of AD is likely to arise from increased concentrations of Aβ in the CNS, this increase may manifest as a result of three key processes relating to the neurovasculature: (1) diminished or faulty degradation of Aβ species within the CNS, (2) impaired clearance of Aβ species from the CNS to the periphery, and (3) enhanced influx of peripheral Aβ species across the BBB. Substantial evidence supporting the neurovascular hypothesis has accumulated since 2005. In 2010, a landmark study was provided by Mawuenyega *et al.* (44), where the production-to-clearance ratios of $A\beta_{40}$ and $A\beta_{42}$ (P/C) were measured in 12 individuals suffering from sporadic AD and 12 healthy controls. Whilst the study reported near identical Aβ production rates for $A\beta_{40}$ and $A\beta_{42}$, the authors did find significantly altered clearance rates of both Aβ species between the two groups ($A\beta_{42}$ 7.6%/h for non-AD and 5.3%/h for AD individuals and $A\beta_{40}$ 7.0%/h for non-AD and 5.2%/h for AD individuals). Considering the Aβ production rate was found to be approximately 6.7%/h for both AD and control groups, this implies that the AD individuals in this study exhibited a P/C ratio of 1.35, compared to a P/C ratio of 0.95 for non-AD participants (44). This study provided substantial evidence of a reduced clearance capacity for Aβ species in the human AD state, which likely contributes to the accumulation of Aβ within the CNS. Subsequent investigations have identified multiple endogenous Aβ clearance mechanisms (summarised in Fig. 2), including astrocyte-mediated enzymatic degradation (45), Aβ removal via bulk flow of cerebrospinal fluid (CSF) (46), and active efflux across the BBB (detailed in later sections). The relative contributions of each of the described mechanisms are still under debate, but it has been estimated that active efflux of the Aβ peptide across the BBB accounts for between 25% (47) and 74% (48) of total Aβ clearance from the brain. Before detailing the discovered mechanisms of Aβ transport across the BBB, the currently evolving concepts of the BBB and the neurovascular unit (NVU) shall be discussed.

Structure and Function of the Blood-Brain Barrier

The BBB is anatomically defined by highly specialised brain microvascular endothelial cells (BMECs) that separate the brain parenchyma from the blood perfusing the brain. These BMECs possess several features otherwise absent in the endothelial cells of the peripheral vasculature (49). Amongst these features are the presence of tight junction proteins, namely the claudin, occludin, and junctional

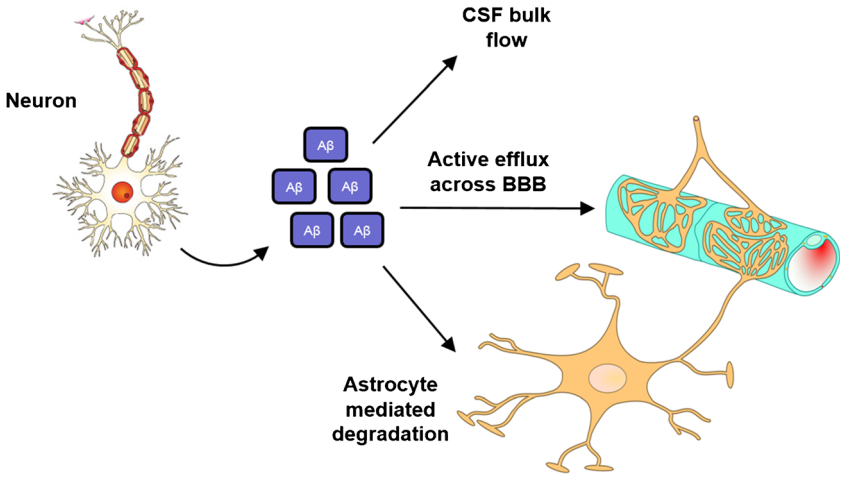

Fig. 2. Identified routes of clearance for the Aβ peptide. Aβ is continually cleaved from neurons and released into interstitial space, where it is cleared by several identified mechanisms: removal via the bulk flow of the cerebrospinal fluid (CSF), active efflux across the blood-brain barrier (BBB) via transport proteins and astrocyte-mediated enzymatic degradation

adhesion molecule proteins (50), which act in concert to establish an extracellular protein matrix that renders the paracellular route of blood-to-brain transmission impermeable to most molecules in the systemic circulation (51). BMECs do not possess the fenestrae found in peripheral vascular endothelial cells (52) but do exhibit a larger proportion of mitochondrial structures (53), to facilitate the rigorously maintained and energy-dependent transport processes that are constantly in flux at the BBB. A large range of transporter proteins are highly expressed at the BBB, in contrast to other tissue vasculature (54). Since the human brain weighs less than 2.4% of the total body weight, yet consumes ~20% of the body's glucose supply, it is fitting that glucose transporters belonging to the solute carrier superfamily (namely GLUT1) are highly expressed at the BBB relative to other tissues (55). Several important xenobiotic efflux transporters are also highly expressed at the BBB, including P-glycoprotein (P-gp; also known as ATP binding cassette sub-family B member 1, or ABCB1) where it plays a crucial role in the active efflux of a large range of substrates, which might otherwise affect the CNS via toxic mechanisms (56).

Despite the broad spectrum of substrates effluxed by P-gp, two other ATP-binding cassette efflux transporters, breast cancer resistance protein (BCRP—also known as ABCG2) and the multidrug resistance-associated proteins (MRPs), are considered equally as important in CNS defence and share significant overlap in substrate and inhibitor specificity (57). The breadth and overlap of substrate specificity between these three transporters perhaps indicate evolutionary redundancy and therefore the evolutionary importance of CNS protection from blood-borne xenobiotics. Also expressed at the BBB are a wide range of proteins belonging to the solute carrier superfamily. These membrane proteins selectively bind hydrophilic small molecule nutrients such as amino acids, vitamins, and hormones and shuttle them across the endothelial membrane, thus providing the CNS with its nutritional needs, without facilitating unfettered access to the bloodstream (58).

When taken together, the tight junction proteins and active influx and efflux transporters constitute a formidable barrier from which the brain receives with high selectivity the substances that it requires, whilst excluding substances with the potential for toxic insult. Whilst in the past, the BBB had been conceived of as a selective diffusion barrier that was largely static in nature, significant research in recent years has encouraged the viewpoint of the BBB as a much more dynamic and decisional interface, facilitating important communications between the peripheral circulation and the CNS (59), and it is becoming increasingly advantageous, both physiologically and in terms of disease states, to view the brain and BBB not as separate entities, but as one multifaceted and communicative entity, known as the NVU.

The Neurovascular Unit

Evidence accumulated over the last 20 years has indicated that the BBB is in constant communication with the various cell types surrounding it and that the absence of one or more of those cell types results in a property-altered BBB (60,61). Similar observations of these brain-cell interactions in other fields of inquiry prompted Lo *et al.* (62), in 2004, to coin the concept of the 'neurovascular unit' (NVU). As was predicted by the authors of that article (and as shown in Fig. 3), the concept of the NVU has gradually evolved to include not just endothelial cells, astrocytes, and neurons, but also pericytes, vascular smooth muscle cells, and glial cells, which constitute together a complex sensory and communicatory network. It is now observed that this grouping of cells acts together to temporally regulate barrier permeability, nutrient supply, angiogenesis, and the rate of cerebral blood flow (56). Neurons themselves are able to detect minute changes in the flux of nutrient and oxygen levels available to their disposal and accordingly react by relaying biochemical signalling to astrocytes or electrical signalling directly to the BBB via interneurons (63). Such signals can elicit an impressive variety of responses, including the upregulation of GLUT1 in response to glucose deprivation or hypoxia (64), release of matrix metalloproteinases for vascular remodelling following hypoxia or injury (65), coordination of angiogenesis

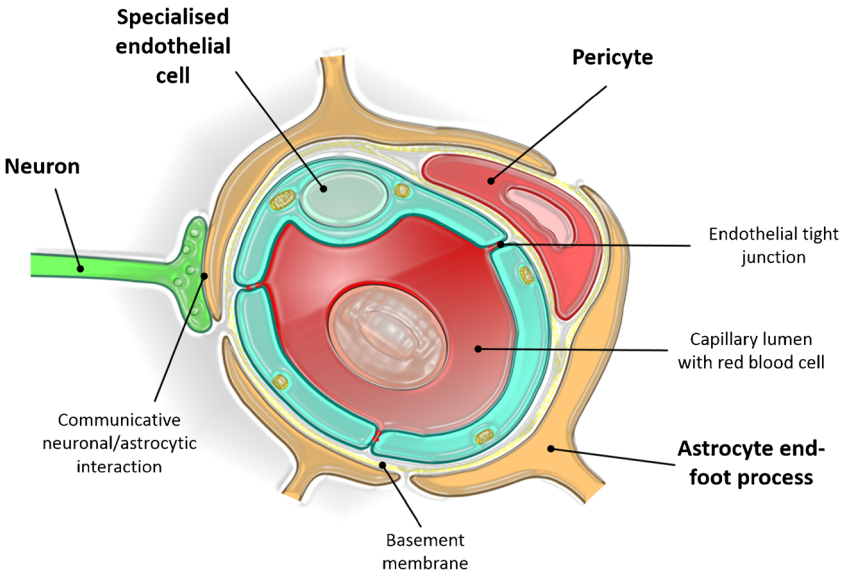

Fig. 3. The neurovascular unit (NVU) and its major cell-type components (*bold*) and relevant features (*non-bold*). The NVU is composed of neurons, specialised brain endothelial cells, pericytes and astrocytes. Features include tight junction protein matrices which limit paracellular diffusion of molecules, collagen fibrous basement membrane providing structural support and communicative junctions between neurons and astrocytes, facilitating direct and indirect information flow between the neuronal and vascular components

by stem cell factor secretion (66), brain water influx and efflux across the BBB (67) and pericyte-mediated modulation of BBB permeability (68). The flow of information between BMECs and the remainder of the NVU is not unidirectional, with strong evidence having been provided for endothelial input into astrocyte development and differentiation (69,70). BMECs can also affect and induce neurogenesis via secreted factors *in vitro* (71), further confirming the integration and co-dependency that is essential to the functional NVU.

This compilation of experiments highlighted earlier permits the emergence of a new way of conceptualising both the brain and the BBB. Older and more compartmentalised ways of envisioning the brain and neuronal circuitry as anatomically isolated components are gradually subsiding, instead giving way to the more integrated and networked concept of the NVU. As more and more brain diseases are discovered to involve brain vascular dysfunction (*i.e.* multiple sclerosis, stroke and HIV-1 infection) (72), it becomes increasingly apparent that the disease interventions of the future will most likely have incorporated this perspective of the integrated NVU, whilst resolving the currently mysterious disease states of today. AD is one such disease state that is benefiting from this view, and the alterations in the NVU and the BBB are discussed in the next section.

Evidence for Non-uniform Blood-Brain Barrier Dysfunction in Alzheimer's Disease

Despite the historical conception of the BBB as a static diffusion barrier that is homogenously impermeable to most molecules, the more modern viewpoint of a potentially vulnerable and non-uniform BBB is emerging. It is now being discovered that some anatomical regions of the NVU are leakier than others and that some of these brain regions share overlap with those areas most affected by AD. Pachter *et al.* (73) have shown that transporter-related and inflammation-related genes are expressed at different levels in arterioles *versus* capillaries, despite being derived from the same fundamental brain endothelial cell. The same group has also demonstrated heterogeneity with respect to tight junction protein expression in different regions of the brain endothelium (74), which would indicate that the BBB exists as a non-uniform barrier. An elegant study by Zhao and Pollack used several known P-gp substrates and an situ brain perfusion technique to measure the relative local cerebral perfusion flow rate, the vascular volume and P-gp efflux activity in different regions of the mouse brain (75). Whilst the authors' findings indicated that P-gp activity was relatively uniform across differing brain regions per unit capillary surface area, marked differences in perfusion flow rate and vascular volume were observed for the differing brain regions (200 ± 4 mL/min/100 g in the hippocampus, an AD-implicated brain region, *vs* 65 ± 45 mL/min/100 g in the pons (75) (a lower-order brain region, which does not have demonstrated involvement in AD (76)). Within the same study, the authors also assessed the differing brain uptake of three separate P-gp substrates (colchicine, quinidine and verapamil) in wild-type and P-gp-deficient mice. In wild-type mice, there was no correlation between regional vascular volume and drug disposition, whereas P-gp-deficient mice exhibited drug disposition that correlated strongly with vascular volume (75). These findings indicate the possibility that during the healthy stages of life, P-gp (and other efflux transporter) expression in the different brain regions is able to cope with the pharmacological and xenobiotic challenges presented, but that later in the ageing process, as BBB functionality begins to decrease (*e.g.* a reduction in P-gp expression per unit capillary surface area), those brain

regions exposed to relatively higher blood volumes and rates of perfusion may perhaps be those most vulnerable to xenobiotic or pharmacological insults. Whilst this natural age-mediated decline in BBB function is not on its own causative of AD, it may contribute to the likelihood of AD diagnosis and may also explain the heterogeneity of brain regions affected by AD.

As support for the neurovascular hypothesis has gradually increased, detailed studies assessing BBB leakage have emerged. Very recently, Van de Haar *et al.* (77) used dynamic contrast material-enhanced magnetic resonance to measure BBB leakage of the contrast agent gadobutrol in 16 patients diagnosed with early AD and 17 age-matched control subjects. After correction for vascular abnormalities, they found significant differences in cortex and general grey matter leakage rates between the two groups, indicating that the leakage may be AD-specific, rather than as a by-product of an underlying pathology. The images in this study did not imply region-specific BBB leakage, but rather a global elevation of leakage within the grey matter, and the authors pointed toward a global reduction of tight junction protein expression as the likely cause (77). Similar studies, however, have yielded alternative results. Using similar methods as previously mentioned, Wang *et al.* (78) observed a trend toward enhanced hippocampal leakage for patients diagnosed with mild cognitive impairment (MCI) compared to age-matched controls, a difference which ultimately did not reach statistical significance, but this failure to distinguish between the groups may have suffered from a low-power study design, combined with the expectedly small vascular changes that may be associated with MCI, as opposed to those of AD. More recently, Montagne *et al.* (79) showed a clear age-dependent decrease in hippocampal integrity, which was not observed in other brain regions. Interestingly, the findings held true amongst both cognitively normal and MCI cohorts, but the increase in permeability was on average more pronounced in individuals diagnosed with MCI (79). This particular study appears to bear two important implications: (1) the hippocampus may be a region of particular vulnerability during BBB breakdown and therefore a primary site of neurodegeneration (which is concordant with AD) and (2) that increased BBB leakage is likely a normal function of ageing, which is not on its own causative of diagnosable cognitive decline. Other studies have also shown that a range of brain insults, pharmacological or otherwise, are able to alter BBB permeability in a brain region-specific manner (80–82), indicating either a non-uniform response or a non-uniform vulnerability to those insults. Taken together, all the evidence highlighted earlier indicates increasingly that the interface between the brain and the rest of the body (*i.e.* the BBB) is pathologically altered in AD at an anatomical level. Enhanced leakage across the BBB could have multiple neurodegenerative consequences, such as increased permeability of inflammatory mediators, unchecked CNS immune infiltration and modified CNS disposition of drugs. But whether such increased leakiness of the BBB permits freer transit of Aβ peptides between the brain and blood is not yet clear, and in the next sections, the accumulation of the Aβ peptide and the currently hypothesised clearance mechanisms thereof are discussed within the context of the integrated NVU.

Evidence for Blood-Brain Barrier-Mediated Clearance of Aβ

As described earlier, strong evidence has indicated that it is Aβ clearance and not production which has gone awry in sporadic AD. Several routes of Aβ clearance have been identified, including astrocyte-mediated degradation, removal via CSF bulk flow and active efflux across the BBB. While it has been long understood that the Aβ peptide is cleared by efflux across the BBB, the relative contribution of this mechanism to total Aβ clearance has only recently been estimated. Using three separate Aβ assays to quantify venous to arterial ratios of endogenous Aβ peptides in cognitively healthy subjects, Roberts *et al.* (47) concluded that approximately 25% of brain-derived Aβ peptides are cleared via BBB transit. Shibata *et al.* (48) attempted to quantify the same relative contributions in wild-type C57BL/6 mice. Using fractional clearance rates of iodinated Aβ, after 60 nM cannula injections and at various time points, the authors estimated that 74% of Aβ clearance was BBB mediated in this mouse model (48). A more recent study by Qosa *et al.* (83) attempted to quantify Aβ clearance mechanisms, also using C57BL/6 mice. The authors found that of the total $A\beta_{40}$ cleared from the brain over the 30-min interval measured, approximately 38% was degraded within the CNS and that the remaining 62% was effluxed across the BBB. The apparent disparity between these results (25% of brain Aβ cleared across the BBB in humans *versus* 62–74% in mice) underscores inherent differences in Aβ trafficking between these two species and casts considerable doubt over the validity of mouse models in Aβ trafficking studies. In any case, a large effort attempting to identify and characterise the specific transporters involved in BBB-mediated trafficking of the Aβ peptide has ensued over the last decade, and the findings (summarised in Fig. 4) shall now be discussed in detail.

Low-Density Lipoprotein Receptor-Related Protein Mediates Aβ Efflux

Of particular relevance to AD amongst the transport proteins expressed at the BBB is low-density lipoprotein receptor-related protein (LRP-1). The initially identified role of LRP-1 was receptor-mediated endocytotic transport of low-density lipoproteins such as cholesterol, to facilitate neuronal consumption of vital steroids. Recently, however, it has been shown that amongst other processes (such as lipid homeostasis, intracellular signalling and apoptotic cellular debris processing), LRP-1 participates in the active transcytosis of Aβ across the BBB (48,84,85). Furthermore, a soluble (*i.e.* non membrane bound) version of LRP-1 (sLRP) has been found to bind more than 70% of plasma Aβ in individuals without dementia and is also involved in chaperoning plasma Aβ across the hepatocyte membrane, thereby facilitating its delivery to the central site of degradation (86). In line with genetic studies demonstrating a link between APOE and AD risk, several research groups have found the APOE4 allele to interfere with LRP-1-mediated Aβ transport across the BBB (87,88). The results, as interpreted by Deane *et al.* (87), indicated that the APOE protein may mediate LRP-1 brain-to-blood transport of Aβ and that the ε4 allele, being much less efficient at this process,

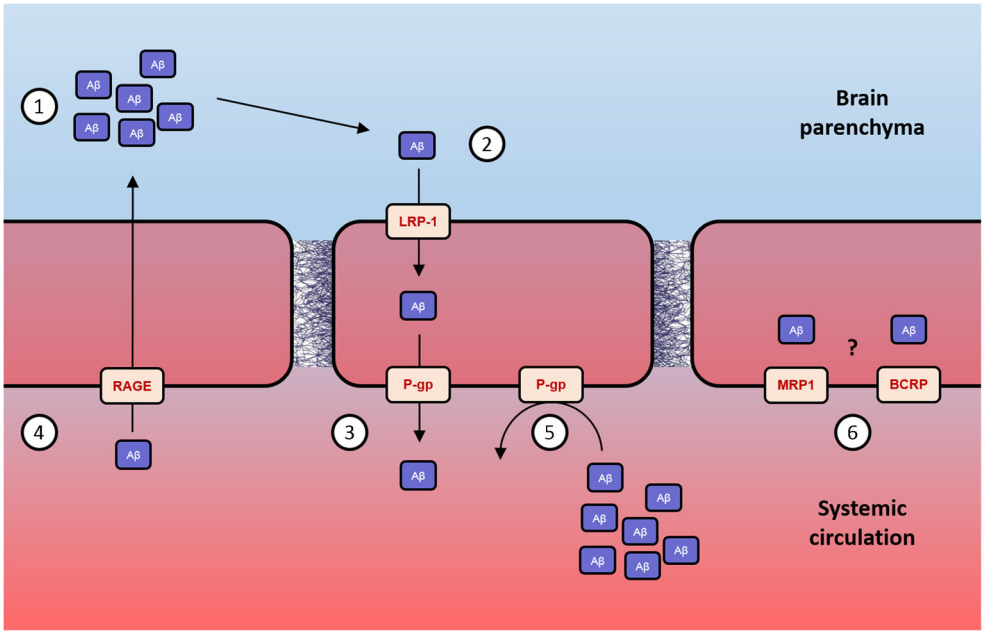

Fig. 4. Clearance mechanism currently understood as involved in Aβ trafficking across the blood-brain barrier (BBB): (*1*) dissociated pool of oligomeric Aβ in the interstitial fluid of the brain, which accumulates to toxic levels in AD, (*2*) LRP-1 traffics Aβ peptides from dissociated pool into brain endothelium, (*3*) P-gp effluxes Aβ peptides from endothelial lipid-bilayer membrane into systemic circulation, (*4*) RAGE facilitates receptor-mediated endocytosis of blood-borne Aβ peptides, back into the brain interstitial fluid, (*5*) P-gp prevents the relatively higher concentrated (compared to brain ISF) blood-borne Aβ from crossing the BBB by active efflux from the lipid bilayer membrane and (*6*) the possible involvement of MRP1 and/or BCRP in Aβ efflux under either normal conditions or potentially in later stages of AD or AD mouse models, after homeostatic transporter regulation responses (i.e. BCRP upregulation following disease-mediated downregulation of P-gp)

incidentally redirects Aβ trafficking through the very low-density lipoprotein (VLDL) receptor pathway. The VLDL receptor transcytosis of Aβ has a clearance rate approximately 25-fold slower than that of LRP-1 (89), which may explain the mechanism by which possession of the APOE4 allele acts as an important AD risk factor. LRP-1 knockout mice do not survive the embryonic life stage and therefore could not be utilised to study the effects of LRP-1 in AD. Instead, the research group headed by Banks *et al.* (90) developed an LRP-1-specific antisense oligonucleotide cocktail, which was then administered directly to the brains of mice to knockdown the expression of the BBB transport protein, without affecting hepatic LRP-1. They found that chronic administration (1 week) of the cocktail reduced brain microvascular expression of LRP-1 by 50% and that this resulted in an increase of approximately 30% of immunoreactive $A\beta_{40–42}$ within the brain (90). Furthermore, the same mice were tested for hippocampal-related cognition via several methods and were found to exhibit behaviour indicative of an impaired memory, which was statistically significant compared to mice not dosed with the LRP-1-specific antisense oligonucleotide cocktail (90). These studies clearly demonstrate that LRP-1 is implicated in Aβ trafficking across the mouse BBB. Qosa *et al.* (83) treated animals with both a known P-gp inhibitor and an LRP-1 antibody and found that the BBB-mediated efflux of $A\beta_{40}$ was reduced from the previously established value of 62, to 31 and 39% respectively, providing more evidence of BBB transporter involvement of Aβ clearance. Finally, a group of geneticists looked for associations between genetic mutations in LRP-1 and AD incidence, onset and severity. Chalmers *et al.* (91) found no evidence of links between particular alleles or singular nucleotide polymorphisms, which seems to indicate that the involvement of LRP-1 in AD is governed either environmentally or by an uncovered genetic mechanism occurring downstream of LRP-1 expression.

P-glycoprotein Contributes to Blood-Brain Barrier Aβ Efflux

P-gp was first ascribed its identity in 1976 (P denoting resistance to drug permeability), by its discoverers Juliano and Ling, who were the first to recognise this protein as a major culprit of the multi-drug-resistant exhibiting phenotype presented by Chinese hamster ovary cells (92). Since this discovery, a large portion of research has ensued, eventually elucidating the character of P-gp, which is now known as a very active ATP-dependent efflux pump for a broad range of substrates. P-gp is highly expressed in the liver, kidneys and small intestines and in endothelial cells forming the BBB (93–96). The primary function of P-gp in each of these tissues is the active efflux of xenobiotics (including natural diet derived toxins as well as exogenous drugs) from the intracellular space out into the lumen of the respective tissues (97). Considering the broad range of substrates that are affected by P-gp function, this transporter has a very important role in the protection of the CNS—especially with respect to human pharmacological efforts targeting the CNS—which has

prompted some researchers to refer to P-gp as 'the gatekeeper' of blood-to-brain compound transport (98). However, despite this perceived importance, it should also be noted that a P-gp knockout mouse model is surprisingly non-lethal (99), which has subsequently been shown to be due to the considerable substrate overlap shared by other members of the ABC superfamily (100). P-gp-deficient mice do however exhibit the phenotypical properties of an enhanced accumulation of administered drugs within the brain, which is accompanied by an exacerbated sensitivity to the toxic profiles of those drugs accumulated (101).

The role of P-gp in brain-to-blood transport of the Aβ peptide has been thoroughly explored, yielding mostly concordant conclusions. Lam *et al.* (102) were the first to demonstrate that pharmacological blockade of P-gp in P-gp-transfected HEK293 cells resulted in reduced Aβ secretion and that Aβ was able to compete for binding and efflux against other known P-gp substrates. Cirrito *et al.* (103) used a P-gp-deficient mouse model to demonstrate a reduction in brain clearance of exogenously administered $A\beta_{42}$ from 16% in wild-type mice to 6% in P-gp-null mice. Additionally, the same study showed an enhanced accumulation of exogenously administered Aβ in the mouse hippocampus and an elevated concentration of endogenous Aβ in the brain interstitial fluid of wild-type mice dosed with a P-gp inhibitor (103). Kuhnke *et al.* (104) provided additional evidence for a role for P-gp-mediated Aβ transport in MDR-1 gene-transfected porcine epithelial cells and inverted membrane vesicles. More recently, Wang *et al.* (105) have shown that P-gp-deficient mice exhibit greater radiolabelled Aβ accumulation after intravenous administration compared to wild-type counterparts and that after these mice were cross bred Tg2576 APP mice, a similar accumulation of (endogenously produced) Aβ was observed. In tandem, these findings indicate a role for P-gp in facilitating both brain-to-blood Aβ efflux, as well as the prevention of blood-to-brain transit of the same peptide.

Further evidence for P-gp involvement in human and sporadic AD was provided by Vogelgesang *et al.* (106), in 2002. This group analysed the apparent expression levels of P-gp in 243 deceased human subjects via semi-quantitative immunohistochemistry and found an inverse correlation between P-gp status and the frequency of Aβ deposition in the medial temporal lobe. This study suggested that an absence or reduction of normal P-gp production, by whatever causal means, may permit the inefficient clearance of Aβ peptides from brain-to-blood in humans diagnosed with AD. More recently, a smaller but similar study by Chiu *et al.* (107) has provided concordant evidence to that of Vogelgesang *et al.*, by showing a decrease in P-gp expression as a function of age in both normal and AD-diagnosed brains. Another study by Wijesura *et al.* (108) also appeared to confirm the previous findings, whereby immunohistochemistry on human brain slices revealed a reduced abundance of P-gp, but not BCRP or MRP4, in those samples associated with diagnosed AD. Finally, another recent study demonstrating the likely role for P-gp in AD used a radiolabelled P-gp substrate (^{11}C–verapamil) to demonstrate reduced P-gp functionality (as opposed to post-mortem expression analysis), in living humans diagnosed with mild AD, when compared to age-matched controls (109).

Similar findings of reduced P-gp have also been demonstrated in mouse models of AD. Hartz *et al.* (110) employed freshly isolated mouse brain capillaries and, upon administering fluorescently labelled Aβ followed by quantitative fluorescence detection analysis, found that administration of either P-gp or LRP-1 inhibitors reduced transport of fluorescent Aβ to approximately 50% of those capillaries that were untreated. This same group also used a fluorescent marker of P-gp activity to demonstrate a 70% decrease in P-gp activity and western blotting to show a 60% decrease in P-gp expression, in an APP transgenic (Tg) mouse model of AD (110). This latter finding prompted the questioning of a straightforward causal relationship between reduced P-gp expression and reduced brain-to-blood Aβ transport, and it was hypothesised that mild elevations of Aβ concentrations can inhibit P-gp expression, setting off a degenerative cycle of peptide accumulation and a reduced capacity for removal of that peptide.

Quite apart from the many studies implicating P-gp in Aβ transport, there have also been several attempts to demonstrate that the Aβ peptide itself downregulates P-gp, via interference with the Wnt/β-catenin signalling pathway, or alternatively proposed mechanisms (111–114). Unfortunately, however, whilst carefully executed, many of these experiments have been conducted with Aβ concentrations ranging between 100 and 500 nM, which, upon examination, may be several orders of magnitude above concentrations that would be physiologically relevant in the human body. Some have suggested that a distinction should be drawn between total Aβ found in a human brain, and the proportion of that total that is currently water solubilised and thus freely available for interaction with the endothelium, and therefore associated signalling and expression systems. In 1999, an elegant study by Lue *et al.* (16) revealed that indeed the soluble component of total brain Aβ provided for a much more robust correlates of local toxicity and that those soluble Aβ concentrations were significantly lower than what many research groups use in experiments attempting to identify toxic Aβ mechanisms. Using post-mortem brain tissue from healthy, borderline and clinically diagnosed AD individuals and centrifugation techniques to separate soluble from insoluble Aβ fragments, this group found that soluble $A\beta_{40}$ concentrations ranged between 1.9 and 66.5 pg/g of brain tissue for healthy controls to AD-diagnosed individuals, respectively, and between 0 and 15.5 pg/g in the same subjects for $A\beta_{42,}$ within the entorhinal cortex (16). Very similar concentration ranges were also observed in the superior frontal gyrus within the same study. Taking into account that different regions of the brain consist of between 70 and 100% water, and the molecular weight of an Aβ monomer is approximately 4.5 kDa, it would follow that soluble and therefore biologically available Aβ would, in molar terms, range between 0.6 and 21 pM, in the healthy and AD-afflicted brains, respectively. On the luminal face of the BMECs, the Aβ concentrations presented to the endothelium appear to be higher than those of the brain parenchyma that were just described. Currently, Aβ quantification techniques and subsequent attempts at correlation suffer from an absence of universal standardisation, and a seemingly wide range of values are reported in the literature. A recent review by Toledo *et al.* (115) summarised the reports of total plasma $A\beta_{40}$ levels as falling between 214 and 985 pg/mL (or 68–

312 pM) and total plasma $A\beta_{42}$ ranging between 36 and 140 pg/mL (or 11–44 pM). Similar to Lue *et al.*, a 2014 study conducted by Sotolongo-Grau *et al.* (116) attempted to stratify 'directly accessible' Aβ from total plasma Aβ concentrations. The group observed a blood-plasma concentration range of directly accessible $A\beta_{40}$ of 39–50 pg/mL (or 12–16 pM) across healthy controls and those diagnosed with AD, respectively (116). The same methods identified $A\beta_{42}$ levels maintained at a flat 13 pg/mL (or 4 pM) in plasma, regardless of AD status. Other recent studies attempting to identify new AD biomarkers have identified the same low to mid-picomolar range for the differing Aβ species (117) but demonstrated also that CSF Aβ levels are considerably higher, manifesting in the low nanomolar range (118). These findings again indicate that biologically available Aβ concentrations occur in the low-picomolar range at the abluminal face of the cerebral microvasculature, and in the mid to high-picomolar range, at the luminal face of the BBB. Therefore, some of the experiments described earlier, which have employed the Aβ peptide at concentrations of 100 nM or higher in attempt to observe the potentially toxic effects on transporter systems, may have exposed the biological models used within to unreasonably high concentrations. Since Aβ is known most essentially as a very toxic molecule, the concentrations used earlier cast doubt over the validity of the P-gp downregulation effects of Aβ, and it is likely that other mechanisms may be held responsible for the reduction in P-gp (and possibly LRP-1) expression. In any case, future studies attempting to identify the directionality of the causative relationship between toxic Aβ accumulation and altered transporter expression should include a careful selection of Aβ concentrations, with the previous information in mind.

Additional Transporters Implicated in Blood-Brain Barrier-Mediated Trafficking of Aβ

The receptor for advanced glycation end products (RAGE) has been shown to play a role in blood-to-brain re-uptake of Aβ species (119). RAGE is upregulated in the AD brain and has been shown to mediate Aβ deposition into the cell membranes of neurons and microglia, thus allowing Aβ to bypass normal physiological antioxidant mechanisms and inflict oxidative damage upon those cells (120). Krohn *et al.* (121) engineered several mouse strains with alternative ABC transporter knockouts (other than P-gp). They found that 6-month-old mice lacking the gene encoding for multi-drug resistance-associated protein (MRP1 also referred to as ABCC1) appeared to exhibit an almost 13-fold higher accumulation of Aβ species in the brain (121). This finding may, however, require further validation but suggests that MRP1 may be involved in Aβ trafficking. Tai *et al.* (122) were the first to show that BCRP may too have involvement in prevention of apical to basolateral BBB transmission of Aβ. Whilst this study was suggestive, several other groups attempted to confirm the findings in subsequent years. The general trend seems to be that BCRP is playing a minor role in Aβ efflux, which may become more important when P-gp is knocked down under experimental conditions (123). While P-gp expression has indeed been shown to be downregulated in both AD and cerebral amyloid angiopathy (CAA) in post-mortem brain analyses (99,124), it has also been shown that BCRP expression is upregulated, potentially in response to P-gp downregulation or by linked signalling mechanisms (124). These findings illustrate the complex and dynamic nature of proteostasis amongst the BBB transporters and highlight the difficulty in identifying the key variations between normal brain and AD brain Aβ trafficking. Figure 4 comprises a schematic diagram which summarises current understanding of transporters implicated Aβ trafficking in AD, including P-gp, LRP-1, BCRP, RAGE and MRP1, along with their directionality and anatomical orientation.

The accumulated evidence discussed earlier suggests quite strongly that AD involves pathophysiological changes in the BBB at a molecular level. Although it is likely that other BBB-related pathogenic mechanisms may be found to contribute to AD, the observed changes in LRP-1 or P-gp expression, alone or in combination, would appear to bear consequences sizeable enough to accommodate the significant accumulation of Aβ within the CNS over time, which may ultimately result in the AD phenotype. The alterations in transporter expression profiles that occur in both natural ageing and in AD as described earlier are also likely to greatly affect CNS exposure to drug molecules, which will be described in a later section.

Blood-Brain Barrier Function in Preventing Apical to Basolateral Diffusion of Aβ

With regard to BBB implication in the pathogenesis of AD, most of the research focus has been on impaired clearance mechanisms which normally traffic Aβ in the brain-to-blood direction. This focus follows a logical trajectory, since the most AD-relevant pathological changes occur within the brain. In recent times, however, much evidence has emerged suggesting that there may be also be a protective role for the BBB in preventing blood-borne Aβ from entering the brain and that this mechanism may also be impaired in the early stages of the AD progression. This concept has been explored with various models, yielding unsurprisingly, differing conclusions. Clifford *et al.* (125) showed that FITC-conjugated $A\beta_{40–42}$ are unable to cross a healthy mouse brain endothelium, until those animals are pretreated with pertussis toxin, a known instigator of BBB breakdown, after which the noxious peptides begin to accumulate in neurons of AD-associated brain regions. Tai *et al.* (122) used a human cerebromicrovascular endothelial cell line (hCMEC/D3) to show that inhibition of P-gp (and BCRP) increased apical-to-basolateral but not basolateral-to-apical permeability of iodinated-Aβ (I-$A\beta_{40}$), concluding that both proteins may function in preventing blood-borne Aβ from traversing the BBB.

Maness *et al.* (126) demonstrated that I-$A\beta_{42}$ can penetrate the mouse BBB when administered peripherally and that pre-complexing the peptide with aluminium, which has been shown to be associated with AD (127), enhances this uptake (128). Similar experiments have confirmed apical-to-basolateral diffusion of I-$A\beta_{42}$ in other laboratories (129), a process which is apparently exacerbated by induced cerebral ischemia, which has been suggested (130) and elaborated upon (131) as a causative risk factor for AD in the past. Some of the discrepancies arising from these studies may be partially explained by the type of labelling

used in the experiments; for example, it may be possible that FITC-conjugated Aβ cannot traverse the BBB of a live animal due to substrate recognition of the FITC moiety by an efflux transporter or by altering the confirmation and thus polar interactions between the Aβ peptide and brain endothelial membranes.

In line with the findings of Lue *et al.* (1999) and Sotolongo-Grau *et al.* (2014), it may be that Aβ concentrations in the periphery are higher than that of soluble and freely available Aβ in the brain parenchyma, which suggests that a concentration gradient would promote both receptor-mediated uptake and passive diffusion of the Aβ peptide in the blood-to-brain direction. If such a gradient does indeed exist, then the roles for P-gp, RAGE, BCRP and MRP1 in Aβ trafficking or the prevention thereof become even more prominent in the overall understanding of AD. Such a gradient would also emphasise the importance of peripheral Aβ clearance mechanisms, namely hepatic catabolism (132–134), which may also become impaired during ageing, and could drive the Aβ gradient to an even less favourable position. Interestingly, one study explored the relationship between hepatic Aβ catabolism and clearance across the BBB. Marques *et al.* (135) demonstrated that by ligating the livers of healthy rats (which dramatically slowed the peripheral clearance of I-Aβ_{40}), the brain-to-blood clearance rate of I-Aβ_{40} following brain injection was significantly reduced by 40.7%, in comparison to rats receiving sham surgery. These concepts have been further explored under the peripheral sink hypothesis of AD, but as is often the case for AD, the experiments have produced some conflicting results (135–137).

NEUROVASCULAR IMPAIRMENT IN ALZHEIMER'S DISEASE: IMPACT ON CNS DRUG AND BIOMOLECULE DISTRIBUTION

As discussed in previous sections, AD appears to be accompanied by both anatomical and molecular changes at the BBB. Since the BBB exists primarily to protect the brain from xenobiotic entities within the systemic circulation, the consequences of these changes are expected to be unfavourable for general CNS health, regardless of cognitive status. Despite the speculated impact that these changes would have on CNS drug delivery, inflammatory mediator and xenobiotic exposure, exploration of the consequences of an AD-compromised BBB has been limited. Since small polar molecules, small lipophilic molecules, endogenous biologics and biological therapeutics each traverse the BBB via different mechanisms, it would be useful to consider the changes in BBB permeability to these different mechanisms separately.

Permeability Alterations in Alzheimer's Disease Mouse Models

Many AD mouse models have been used to assess potential AD-related changes in both drug and biomolecule permeability and distribution, but conflicting results have emerged. The studies, summarised in Table I, include seven different AD mouse models, four studies using live human imaging or human post-mortem tissue analysis and a wide range of permeant molecules used for assessing BBB permeability. Much of this data has been well summarised recently (138), and therefore, the most recent studies in Table I will be discussed, after reiterating the findings of the previous review. Mehta *et al.* described the inherent complexity of reaching conclusions about AD-related alterations in BBB permeability. Since differing molecule types exhibit varying mechanisms of BBB transit, it follows that each mechanism would be affected by AD pathogenesis in a different way, which averts the validity of any global statements about a hyperpermeable BBB observed in AD. The apparent changes occurring in the cerebrovasculature during human AD are diverse and intertwined; they include but are probably not limited to thickening of the basement membrane (139,140), alterations in transporter expression profiles (141), reduced and less tightly regulated cerebral blood flow (142–144) and disruption of tight junction expression and integrity (145). Each of these effects will impact upon the uptake of small drug-like molecules or the penetration of systemic proteins in very different ways. This is perhaps one of the main causes of the apparent discordance in experiments probing AD-related BBB hyperpermeability, produced by different laboratories. Recently, some important studies have emerged that have both reinforced and strongly challenged the increasingly widespread view that AD implicates a leaky BBB, and these shall now be discussed.

In 2012, Bell *et al.* (34) elegantly demonstrated one of the downstream effects of APOE4 allele possession, by using targeted replacement of mouse APOE genotypes with the three human variants. Using both imaging agent leakage and CNS exposure to systemic and neurotoxic proteins for quantification, the authors demonstrated convincingly that mouse possession of the human APOE4 allele resulted in a significantly leakier BBB. Evidence was then provided to suggest that in comparison with the alternative alleles, APOE4 possession results in ineffective APOE/LRP-1 binding, an interaction which normally suppresses cytokine production (146). The increased cytokine activity prompts upregulation of the matrix metalloproteinases in pericytes and subsequent tight junction catabolism (34), ultimately resulting in increased permeability to larger molecules. Whilst this study did not involve an AD-specific mouse model, it does highlight a potential causative link between APOE genotype and AD susceptibility, centring on BBB permeability. In contrast to this study, however, a very comprehensive publication by Bien-Ly *et al.* (147) in 2015 provided perfect opposition to both the findings of Bell *et al.* and the current consensus that widespread BBB disruption is implicated in AD. Using three separate mouse models (PS2-APP, tau Tg and an APOE4 knock-in model, as used by Bell *et al.* 2012), this group found no alterations in brain penetration of the multiple antibodies and dextran molecules employed as tracers within the study and concluded that no evidence of a compromised BBB emerged within their work (147). The apparent discrepancy between laboratories may arise from several variables. The relative timeframes as well as the nature and size of tracer molecules employed in these experiments would likely have a strong impact on the ability to resolve differences between the models being tested. Amongst the conflicting publications just described, as well as many others appearing in Table I, timeframes ranging from 1 to 24 h, and biological molecules ranging in size from 3 to 40 kDa and in nature from semi-synthetic to endogenous biological, are all used to demonstrate relative BBB

Table I. Summary of Studies Assessing AD-Related CNS Exposure to Different Molecules, with Highlighted Rows Representing Studies of the Human AD State

Permeant assessed	**Species/mouse model**	**Technique for assessing permeability**	**Result**	**Reference**
Large biological or bio-conjugated molecules				
IgG	APP/PS1	Extravasation of endogenous IgG	Increased permeability	Takechi 2008 (155)
[^{131}I]albumin	APP/PS1	Brain uptake after systemic administration	Decreased permeability	Poduslo 2001 (156)
Fibrinogen and IgG	Human brain slices	Immununohisto-chemistry	Increased permeability	Ryu 2009 (157)
Anti-transferrin receptor antibody	PS2-APP, tau Tg and hAPOE4 knock-in mice	ELISA on tissue lysates after IV injection	No change in any mouse model	Bien-Ly 2015 (147)
Texas-red conjugated bovine serum albumin and Evans blue	Tg2576	Brain extravasation assessed	Increased permeability	Ujiie 2003 (158)
TMR-Dextran (40 kDa imaging agent)	Targeted replacement of mouse APO with human APOE2, 3 or 4	Imaging and associated protein quantification	Increased permeability assessed by both imaging agent and protein distribution, in APOE4 carrying mice	Bell 2012 (34)
Albumin	Human	CSF to serum ratios	Increased ratios	Janelidze 2017 (154)
Small biomolecules				
[^{14}C]sucrose	3 x Tg (AD)	Brain uptake after 60 second perfusion	Decreased permeability	Bourasset 2009 (159)
[^{14}C]sucrose	3 x Tg (AD)	Hippocampal-to-perfusion ratio after 4 minute perfusion	No change	Mehta 2013 (160)
Urea, creatinine	Human	CSF to serum ratio	Increased permeability for urea and decreased for creatinine	Daiello 2016 (153)

Exogenous small molecules				
Gadobutrol (coordination complexed imaging agent)	Human	Live imaging after IV administration	Patients registered as cognitively impaired (AD or MCI) had increased permeability	Van de Haar 2016 (77)
Diazepam	3 x Tg AD at 11 months of age	Brain transport coefficient	No difference	Bourasset 2009 (159)
Clioquinol	Tg2576 mice	Brain uptake and brain:plasma ratios	Increased uptake and ratios at some but not all time points	Opazo 2006 (161)
PBT2	Tg2576 mice	Brain:plasma ratio at 120 minutes post-dose	No difference	Adlard 2008 (162)
Memantine	3 x Tg AD at 18-20 months of age	Brain-to-perfusate ratios over 4 minute period	Reduced permeability in transgenic animals	Mehta 2013 (160)

AD Alzheimer's disease, *APO* apolipoprotein, *APOE2, 3, 4* apolipoprotein E2, E3, E4, *CSF* cerebrospinal fluid, *MCI* mild cognitive impairment, *Tg* transgenic, TMR Tetramethylrhodamine, APP/PS1 mouse model possessing the human transgenes for both the Swedish APP and presenilin-1 mutations, PS2-APP mouse model possessing the human transgenes for both the presenilin-2 and Swedish APP mutations.

permeability. It is well known within the pharmaceutical sciences that even a subtle change within the molecular structure of a particular compound or endogenous biological entity can have profound implications with regard to the adsorption, distribution, metabolism, excretion and toxicity of that molecule within a biological system (148–151). Therefore, it is not then surprising that such disparate yet equally valid results emerge whilst probing AD-altered cerebrovasculature, with a structurally diverse set of compounds. Another potential factor confounding these discrepancies is the age of the animals that are being tested. An interesting and recent study by Do *et al.* (152) characterised the transporter expression levels in the brain endothelium of AD transgenic mouse models during ageing. Using 3xTg AD mice (considered as a model that closely mimics human AD pathology due to the presence of both amyloid and tau pathologies) sacrificed at either 3, 6 or 18 months of age, Do *et al.* (152) employed centrifugation techniques to enrich brain fractions for microvessel content, before western blotting lysates for a variety of transporters that may be involved in Aβ trafficking. The authors found that the expression of RAGE consistently increased, and organic anion transporter protein 1A4 (OATP1A4) consistently decreased, as a function of age. In the same mice, ABCG4 was elevated at the 3-month time point but reduced to control levels at the two remaining time points tested, whereas both ABCB1 (P-gp) and ABCG2 (BCRP) were increased only at 18 months but remained the same as control at the first two time points assessed. The cholesterol efflux transporter ABCA1 was found to be significantly upregulated (compared to control animals) at all three time points but interestingly was found to be increased by the largest magnitude at the 6-month time point (3-fold higher) in comparison to the two adjacent time points measured. Finally, LRP-1 levels were assessed only at the 18-month time point and were significantly reduced compared to controls. In each of the non-transgenic littermate control groups, the expression levels of the proteins probed did not change with ageing, indicating that the expression levels of the transporters probed do not fluctuate under normal, disease-free ageing conditions. Therefore, this elegant study by Do *et al.* has demonstrated some largely underappreciated facts—that the homeostatic consequences of human gene knock-in into mice occur as a dynamic process as ageing progresses and that the profile of transporter expression levels changes over time, as the need to combat pernicious accumulation of Aβ mounts. Applied to a more general setting, the results of Do *et al.* indicate that during the temporal unfolding of pathology, the profile of BBB transporter expressions within an individual will evolve over time, which implies that one insult, pharmacological or otherwise, may produce a remarkably differing impact upon CNS health, depending on the disease status of the animal or indeed human being assessed.

Permeability Alterations in Human Alzheimer's Disease

Aside from AD mouse models, recent experiments accomplished in live humans have substantiated strong evidence for a compromised BBB in the human AD state. In 2016, Van de Haar *et al.* (77) used gadobutrol to characterise subtle changes in BBB leakage by dynamic contrast material-enhanced magnetic

resonance. Their pilot study included seven patients diagnosed with AD, nine diagnosed with mild cognitive impairment (MCI) and 17 healthy control subjects. Two key findings emerged from the study; patients with MCI and AD both possessed significantly more tissues in the white and grey matter associated with BBB leakage than age-matched healthy controls and that BBB leakage in grey matter regions correlated well with mini-mental state examination scores (77). Considering the relatively low number of subjects involved in the study, combined with the subtlety of changes in BBB leakage expected for MCI patients, these findings are somewhat remarkable. Gadobutrol is a relatively small molecule (604.7 Da) that consists of a gadolinium ion surrounded by a synthetic macrocycle, which is thought to cross the BBB by the paracellular route (77). Therefore, the enhanced permeability of gadobutrol is indicative of a leakier BBB by virtue of reduced tight junction protein abundance. Also recently, Daiello *et al.* (153) put forward an interesting study quantifying the relative distributions of the endogenous biological molecules creatinine, urea and albumin, by measuring the CSF-to-serum ratios (C/S) in humans diagnosed with MCI or AD, compared to healthy volunteer subjects. The C/S ratios indicated increased, decreased and unchanged permeability for urea, creatinine and albumin, respectively (153). This study in particular demonstrates quite usefully a source of discrepancy between analogous experiments attempting to quantify or indeed disprove global changes in BBB permeability associated with AD. Within the same set of individuals, the probing of only one molecule to assess BBB permeability would lead to vastly different conclusions, depending on the molecule chosen for the assessment (*e.g.* creatinine *versus* urea). Most recently, Janelidze *et al.* (154) quantified the C/S ratios of albumin in a large cohort of 1015 people that included healthy controls and a range of diagnosed dementia patients in a longitudinal study. The study reported increased albumin ratios in groups that had been diagnosed with AD, dementia with Lewy bodies, Parkinson's disease dementia, subcortical vascular dementia and frontotemporal dementia, but not in people diagnosed with MCI, nor for a special cohort of individuals that had been diagnosed with MCI at the commencement of the study but had progressed to AD later (154). This latter finding casts some doubt on the neurovascular hypothesis, whereby dysfunction in the cerebral vasculature should demonstrably predict the acquisition of AD.

The widespread usage of transgenic AD mouse models to assess BBB permeability to various molecules may not accurately reflect the human AD state, most primarily because the knock-in of human proteins such as APP would likely affect the efflux transporter and tight junction expression profiles of such genetically modified animals. The mouse brain may respond homeostatically to the presence of foreign proteins, by significantly upregulating any proteins implicated in the metabolism and transport of the foreign protein introduced (such as knocked-in APP). Since many metabolic and transporter proteins possess multiple functions and often produce or transport products that feed into adjacent metabolic and transport networks, the networked effects and final consequences of multiple-gene inserted mouse models may be simply too numerous, diverse and unpredictable, for these models to pose as useful reflections of the human AD state. Furthermore, non-uniformity in the type of AD mouse model employed, the age at which measurements are made, the timeframe over which the experiments are conducted and the type of molecule employed to probe BBB leakage, will always produce discordant results with regard to global statements of BBB permeability in AD. AD research in general surely does suffer from an ill-fitting superimposition of well-intentioned mouse models upon the human AD condition, generating a relationship from which experimental dissonance continually springs. Therefore, it is anticipated by many that as information-rich and higher-resolution imaging techniques are developed and begin to reach technical maturity, alongside the identification of accurate and descriptive biomarker clusters, the necessary information for treating the human AD state will emerge from human studies alone, eventually making redundant the use of rodent models in AD research entirely.

It is worth noting that when focussing only on studies assessing the permeability of molecules across the BBB in the human AD state, a general trend toward increased permeability can be observed. Of such studies (highlighted in Table I), a total of six molecules have been assessed (albumin, fibrinogen, IgG, urea, creatinine and gadobutrol), and increased permeability was reported for five of those six. Most of these studies have been conducted in very recent times, have used state-of-the-art techniques, have involved many prudent and carefully selected attempts to eliminate confounding variables, and most importantly, were executed in human biological systems. When focussing only on human experiments, the evidence in totality points strongly in the direction of an altered and hyper-permeable BBB in the human AD state, but once more, whether this observation represents a cause or a consequence of AD pathological events is yet to be resolved. The potential risk that people with AD may be unintentionally subjected to toxic concentrations of normally therapeutic pharmaceuticals may indeed exist, if CNS exposure is truly increased in this patient population. Further studies are then, definitely warranted, to fully characterise the nature of AD-affected distributions of the various molecule types, especially for those already used widely in clinical practice amongst the elderly population.

CONCLUSIONS

Enough evidence has now accumulated to put beyond doubt that the BBB is an anatomical region implicated in the pathogenic cascade of sporadic AD. But once more, whether BBB impairment manifests as a cause or as a consequence of AD is still unknown. New technologies and methods may, however, have the power to change the current situation. The recent development of non-invasive and highly sensitive brain and BBB imaging techniques, as well as the anticipated identification of accurate biomarkers or biomarker clusters for AD in the near future, will eventually culminate in a robust temporal characterisation of the wider AD pathogenesis. Such an achievement will highlight the most plausible targets for treating AD biochemically, which may or may not be associated specifically with the neurovasculature. Regardless of the cause/consequence status of BBB impairment in AD, the implications of an AD-affected BBB are clinically relevant, and most of the evidence presented herein indicates definite changes in the distribution of molecules, biological or otherwise, across the periphery/CNS axis. It is unlikely that these distributions will all correlate well with one another, since multiple routes for BBB penetration exist for structurally differing molecules, and future

understanding of AD-altered BBB permeability may involve more complex or more numerous interactions than are currently understood.

ACKNOWLEDGEMENTS

Mitchell P. McInerney is supported by an Australian Government Research Training Program Scholarship.

REFERENCES

1. Vaupel JW. Biodemography of human ageing. Nature. 2010;464:536–42.
2. Guerreiro R, Bras J. The age factor in Alzheimer's disease. Genome Med. 2015;7:106.
3. Prince M, Wimo A, Guerchet M, Ali GC, Wu YT, Prina M, World Alzheimer Report. The global impact of dementia: an analysis of prevalence, incidence, cost and trends. London: Global Observatory for Ageing and Dementia Care–King's College; 2015.
4. Strobel G. What is early onset familial Alzheimer disease (eFAD). Alzforum: Retrieved 05.01.2017 [cited 2017]; Available from: http://www.alzforum.org/early-onset-familial-ad/overview/what-early-onset-familial-alzheimer-disease-efad.
5. Waring SC, Doody RS, Pavlik VN, Massman PJ, Chan W. Survival among patients with dementia from a large multi-ethnic population. Alzheimer Dis Assoc Disord. 2005;19:178–83.
6. Ryman DC, Acosta-Baena N, Aisen PS, Bird T, Danek A, Fox NC, et al. Symptom onset in autosomal dominant Alzheimer disease: a systematic review and meta-analysis. Neurology. 2014;83:253–60.
7. Selkoe DJ. Alzheimer's disease. 2011;CSH Perspect Bio:a004457-a
8. Alzhiemer A. Über einen eigenartigen schweren Erkrankungsprozeß der Hirnrinde. Neurologisches Centralblatt. 1906;23:1129–36.
9. Glenner GG, Wong CW. Alzheimer's disease: initial report of the purification and characterization of a novel cerebrovascular amyloid protein. Biochem Biophys Res Commun. 1984;120:885–90.
10. Masters CL, Simms G, Weinman NA, Multhaup G, McDonald BL, Beyreuther K. Amyloid plaque core protein in Alzheimer disease and Down syndrome. Proc Natl Acad Sci USA. 1985;82:4245–9.
11. Nukina N, Ihara Y. One of the antigenic determinants of paired helical filaments is related to tau protein. J Biochem. 1986;99:1541–4.
12. Kenneth S, Kosik CLJ, Selkoe DJ. Microtubule-associated protein tau is a major antigenic component of paired helical filaments in Alzheimer disease. Proc Natl Acad Sci USA. 1986;83:4044–8.
13. Inge Grundke-Iqbal KI, Tung Y-C, Quinlan M, Wisniewski HM, Binder LI. Abnormal phosphorylation of the microtubule-associated protein tau in Alzheimer cytoskeletal pathology. Proc Natl Acad Sci USA. 1986;83:4913–7.
14. Akiyama H, Barger S, Barnum S, Bradt B, Bauer J, Cole GM, et al. Inflammation and Alzheimer's disease. Neurobiol Aging. 2000;21:383–421.
15. Swardfager W, Lanctot K, Rothenburg L, Wong A, Cappell J, Herrmann N. A meta-analysis of cytokines in Alzheimer's disease. Biol Psychiatry. 2010;68:930–41.
16. Lue LF, Kuo YM, Roher AE, Brachova L, Shen Y, Sue L, et al. Soluble amyloid beta peptide concentration as a predictor of synaptic change in Alzheimer's disease. Am J Pathol. 1999;155:853–62.
17. McLean CA, Cherny RA, Fraser FW, Fuller SJ, Smith MJ, Beyreuther K, et al. Soluble pool of Abeta amyloid as a determinant of severity of neurodegeneration in Alzheimer's disease. Ann Neurol. 1999;46:860–6.
18. Markesbery WR. Oxidative stress hypothesis in Alzheimer's disease. Free Radic Biol Med. 1997;23:134–47.
19. Uylings HBM, de Brabander JM. Neuronal changes in normal human aging and Alzheimer's disease. Brain Cogn. 2002;49:268–76.
20. Scheuner D, Eckman C, Jensen M, Song X, Citron M, Suzuki N, et al. Secreted amyloid beta-protein similar to that in the senile plaques of Alzheimer's disease is increased in vivo by the presenilin 1 and 2 and APP mutations linked to familial Alzheimer's disease. Nat Med. 1996;2:864–70.
21. Sherrington R, Rogaev EI, Liang Y, Rogaeva EA, Levesque G, Ikeda M, et al. Cloning of a gene bearing missense mutations in early-onset familial Alzheimer's disease. Nature. 1995;375:754–60.
22. Haass C, Selkoe DJ. Cellular processing of beta-amyloid precursor protein and the genesis of amyloid beta-peptide. Cell. 1993;75:1039–42.
23. Priller C, Bauer T, Mitteregger G, Krebs B, Kretzschmar HA, Herms J. Synapse formation and function is modulated by the amyloid precursor protein. J Neurosci. 2006;26:7212–21.
24. Weidemann A, Konig G, Bunke D, Fischer P, Salbaum JM, Masters CL, et al. Identification, biogenesis, and localization of precursors of Alzheimer's disease A4 amyloid protein. Cell. 1989;57:115–26.
25. Rohan de Silva HA, Jen A, Wickenden C, Jen LS, Wilkinson SL, Patel AJ. Cell-specific expression of beta-amyloid precursor protein isoform mRNAs and proteins in neurons and astrocytes. Brain Res Mol Brain Res. 1997;47:147–56.
26. Hartmann T, Bieger SC, Bruhl B, Tienari PJ, Ida N, Allsop D, et al. Distinct sites of intracellular production for Alzheimer's disease Aβ40/42 amyloid peptides. Nat Med. 1997;3:1016–20.
27. Dries DR, Yu G. Assembly, maturation and trafficking of the gamma-secretase complex in Alzheimer's disease. Curr Alzheimer Res. 2008;5:132–46.
28. Walsh DM, Selkoe DJ. A beta oligomers—a decade of discovery. J Neurochem. 2007;101:1172–84.
29. Ringman JM, Goate A, Masters CL, Cairns NJ, Danek A, Graff-Radford N, et al. Genetic heterogeneity in Alzheimer disease and implications for treatment strategies. Curr Neurol Neurosci Rep. 2014;14:499.
30. Strittmatter WJ, Saunders AM, Schmechel D, Pericak-Vance M, Enghild J, Salvesen GS, et al. Apolipoprotein E: high-avidity binding to beta-amyloid and increased frequency of type 4 allele in late-onset familial Alzheimer disease. Proc Natl Acad Sci USA. 1993;90:1977–81
31. Schmechel DE, Saunders AM, Strittmatter WJ, Crain BJ, Hulette CM, Joo SH, et al. Increased amyloid beta-peptide deposition in cerebral cortex as a consequence of apolipoprotein E genotype in late-onset Alzheimer disease. Proc Natl Acad Sci U S A. 1993;90:9649–53.
32. Jiang Q, Lee CY, Mandrekar S, Wilkinson B, Cramer P, Zelcer N, et al. ApoE promotes the proteolytic degradation of Abeta. Neuron. 2008;58:681–93.
33. Koistinaho M, Lin S, Wu X, Esterman M, Koger D, Hanson J, et al. Apolipoprotein E promotes astrocyte colocalization and degradation of deposited amyloid-beta peptides. Nat Med. 2004;10:719–26.
34. Bell RD, Winkler EA, Singh I, Sagare AP, Deane R, Wu Z, et al. Apolipoprotein E controls cerebrovascular integrity via cyclophilin a. Nature. 2012;485:512–6.
35. Arriagada PV, Marzloff K, Hyman BT. Distribution of Alzheimer-type pathologic changes in nondemented elderly individuals matches the pattern in Alzheimer's disease. Neurology. 1992;42:1681–8.
36. Serrano-Pozo A, Frosch MP, Masliah E, Hyman BT. Neuropathological alterations in Alzheimer disease. Cold Spring Harb Perspect Med. 2011;1:a006189.
37. Nagy Z, Esiri MM, Jobst KA, Morris JH, King EMF, McDonald B, et al. Relative roles of plaques and tangles in the dementia of Alzheimer's disease: correlations using three sets of neuropathological criteria. Dement Geriatr Cogn Disord. 1995;6:21–31.
38. Jack Jr CR, Knopman DS, Jagust WJ, Shaw LM, Aisen PS, Weiner MW, et al. Hypothetical model of dynamic biomarkers of the Alzheimer's pathological cascade. Lancet Neurol. 2010;9:119–28.

39. Hardy JA, Higgins GA. Alzheimer's disease: the amyloid cascade hypothesis. Science. 1992;256:184–5.
40. Wang J, Dickson DW, Trojanowski JQ, Lee VM. The levels of soluble versus insoluble brain Abeta distinguish Alzheimer's disease from normal and pathologic aging. Exp Neurol. 1999;158:328–37.
41. Kayed R, Lasagna-Reeves CA. Molecular mechanisms of amyloid oligomers toxicity. J Alzheimers Dis. 2013;33(Suppl 1):S67–78.
42. Zlokovic BV. Neurovascular mechanisms of Alzheimer's neurodegeneration. Trends Neurosci. 2005;28:202–8.
43. Zlokovic BV, Deane R, Sallstrom J, Chow N, Miano JM. Neurovascular pathways and Alzheimer amyloid beta-peptide. Brain Pathol. 2005;15:78–83.
44. Mawuenyega KG, Sigurdson W, Ovod V, Munsell L, Kasten T, Morris JC, et al. Decreased clearance of CNS beta-amyloid in Alzheimer's disease. Science. 2010;330:1774.
45. Thal DR. The role of astrocytes in amyloid β-protein toxicity and clearance. Exp Neurol. 2012;236:1–5.
46. Iliff JJ, Wang M, Liao Y, Plogg BA, Peng W, Gundersen GA, et al. A paravascular pathway facilitates CSF flow through the brain parenchyma and the clearance of interstitial solutes, including amyloid β. Sci Transl Med. 2012;4:147ra11.
47. Roberts KF, Elbert DL, Kasten TP, Patterson BW, Sigurdson WC, Connors RE, et al. Amyloid-β efflux from the central nervous system into the plasma. Ann Neurol. 2014;76:837–44.
48. Shibata M, Yamada S, Kumar SR, Calero M, Bading J, Frangione B, et al. Clearance of Alzheimer's amyloid-ss(1-40) peptide from brain by LDL receptor-related protein-1 at the blood-brain barrier. J Clin Invest. 2000;106:1489–99.
49. Hawkins BT, Davis TP. The blood-brain barrier/ neurovascular unit in health and disease. Pharmacol Rev. 2005;57:173–85.
50. Kniesel U, Wolburg H. Tight junctions of the blood-brain barrier. Cell Mol Neurobiol. 2000;20:57–76.
51. Nicolazzo JA, Charman SA, Charman WN. Methods to assess drug permeability across the blood-brain barrier. J Pharm Pharmacol. 2006;58:281–93.
52. Fenstermacher J, Gross P, Sposito N, Acuff V, Pettersen S, Gruber K. Structural and functional variations in capillary systems within the brain. Ann N Y Acad Sci. 1988;529:21–30.
53. Oldendorf WH, Cornford ME, Brown WJ. The large apparent work capability of the blood-brain barrier: a study of the mitochondrial content of capillary endothelial cells in brain and other tissues of the rat. Ann Neurol. 1977;1:409–17.
54. Shawahna R, Decleves X, Scherrmann JM. Hurdles with using in vitro models to predict human blood-brain barrier drug permeability: a special focus on transporters and metabolizing enzymes. Curr Drug Metab. 2013;14:120–36.
55. Erickson MA, Banks WA. Blood-brain barrier dysfunction as a cause and consequence of Alzheimer's disease. J Cereb Blood Flow Metab. 2013;33:1500–13.
56. Zlokovic BV. Neurovascular pathways to neurodegeneration in Alzheimer's disease and other disorders. Nat Rev Neurosci. 2011;12:723–38.
57. Matsson P, Pedersen JM, Norinder U, Bergstrom CA, Artursson P. Identification of novel specific and general inhibitors of the three major human ATP-binding cassette transporters P-gp, BCRP and MRP2 among registered drugs. Pharm Res. 2009;26:1816–31.
58. Campos-Bedolla P, Walter FR, Veszelka S, Deli MA. Role of the blood-brain barrier in the nutrition of the central nervous system. Arch Med Res. 2014;45:610–38.
59. Banks WA. Brain meets body: the blood-brain barrier as an endocrine interface. Endocrinology. 2012;153:4111–9.
60. Beuckmann CT, Dernbach K, Hakvoort A, Galla HJ. A new astrocytic cell line which is able to induce a blood-brain barrier property in cultured brain capillary endothelial cells. Cytotechnology. 1997;24:11–7.
61. Zlokovic BV. The blood-brain barrier in health and chronic neurodegenerative disorders. Neuron. 2008;57:178–201.
62. Lo EH, Broderick JP, Moskowitz MA. tPA and proteolysis in the neurovascular unit. Stroke. 2004;35:354–6.
63. Muoio V, Persson PB, Sendeski MM. The neurovascular unit—concept review. Acta Physiol. 2014;210:790–8.
64. Boado RJ, Pardridge WM. Glucose deprivation and hypoxia increase the expression of the GLUT1 glucose transporter via a specific mRNA cis-acting regulatory element. J Neurochem. 2002;80:552–4.
65. Boroujerdi A, Welser-Alves JV, Milner R. Matrix metalloproteinase-9 mediates post-hypoxic vascular pruning of cerebral blood vessels by degrading laminin and claudin-5. Angiogenesis. 2015;18:255–64.
66. Sun L, Hui AM, Su Q, Vortmeyer A, Kotliarov Y, Pastorino S, et al. Neuronal and glioma-derived stem cell factor induces angiogenesis within the brain. Cancer Cell. 2006;9:287–300.
67. Mae M, Armulik A, Betsholtz C. Getting to know the cast—cellular interactions and signaling at the neurovascular unit. Curr Pharm Des. 2011;17:2750–4.
68. Thanabalasundaram G, Pieper C, Lischper M, Galla HJ. Regulation of the blood-brain barrier integrity by pericytes via matrix metalloproteinases mediated activation of vascular endothelial growth factor in vitro. Brain Res. 2010;1347:1–10.
69. Estrada C, Bready JV, Berliner JA, Pardridge WM, Cancilla PA. Astrocyte growth stimulation by a soluble factor produced by cerebral endothelial cells in vitro. J Neuropathol Exp Neurol. 1990;49:539–49.
70. Mi H, Haeberle H, Barres BA. Induction of astrocyte differentiation by endothelial cells. J Neurosci. 2001;21:1538–47.
71. Plane JM, Andjelkovic AV, Keep RF, Parent JM. Intact and injured endothelial cells differentially modulate postnatal murine forebrain neural stem cells. Neurobiol Dis. 2010;37:218–27.
72. Karamanos Y, Gosselet F, Dehouck MP, Cecchelli R. Blood-brain barrier proteomics: towards the understanding of neurodegenerative diseases. Arch Med Res. 2014;45:730–7.
73. Macdonald JA, Murugesan N, Pachter JS. Endothelial cell heterogeneity of blood-brain barrier gene expression along the cerebral microvasculature. J Neurosci Res. 2010;88:1457–74.
74. Paul D, Cowan AE, Ge S, Pachter JS. Novel 3D analysis of Claudin-5 reveals significant endothelial heterogeneity among CNS microvessels. Microvasc Res. 2013;86:1–10.
75. Zhao R, Pollack GM. Regional differences in capillary density, perfusion rate, and P-glycoprotein activity: a quantitative analysis of regional drug exposure in the brain. Biochem Pharmacol. 2009;78:1052–9.
76. Mrzilkova J, Zach P, Bartos A, Tintera J, Ripova D. Volumetric analysis of the pons, cerebellum and hippocampi in patients with Alzheimer's disease. Dement Geriatr Cogn Disord. 2012;34:224–34.
77. van de Haar HJ, Burgmans S, Jansen JF, van Osch MJ, van Buchem MA, Muller M, et al. Blood-brain barrier leakage in patients with early Alzheimer disease. Radiology. 2016;281:527–35.
78. Wang H, Golob EJ, Su MY. Vascular volume and blood-brain barrier permeability measured by dynamic contrast enhanced MRI in hippocampus and cerebellum of patients with MCI and normal controls. J Magn Reson Imaging. 2006;24:695–700.
79. Montagne A, Barnes SR, Sweeney MD, Halliday MR, Sagare AP, Zhao Z, et al. Blood-brain barrier breakdown in the aging human hippocampus. Neuron. 2015;85:296–302.
80. Suzuki R, Nitsch C, Fujiwara K, Klatzo I. Regional changes in cerebral blood flow and blood-brain barrier permeability during epileptiform seizures and in acute hypertension in rabbits. J Cereb Blood Flow Metab. 1984;4:96–102.
81. Phares TW, Kean RB, Mikheeva T, Hooper DC. Regional differences in blood-brain barrier permeability changes and inflammation in the apathogenic clearance of virus from the central nervous system. J Immunol. 2006;176:7666–75.
82. Brown RC, Egleton RD, Davis TP. Mannitol opening of the blood-brain barrier: regional variation in the permeability of sucrose, but not 86Rb+ or albumin. Brain Res. 2004;1014:221–7.
83. Qosa H, Abuasal BS, Romero IA, Weksler B, Couraud PO, Keller JN, et al. Differences in amyloid-β clearance across mouse and human blood-brain barrier models: kinetic analysis and mechanistic modeling. Neuropharmacology. 2014;79C:668–78.

84. Deane R, Sagare A, Zlokovic BV. The role of the cell surface LRP and soluble LRP in blood-brain barrier Abeta clearance in Alzheimer's disease. Curr Pharm Des. 2008;14:1601–5.
85. Deane R, Wu Z, Sagare A, Davis J, Du Yan S, Hamm K, et al. LRP/amyloid beta-peptide interaction mediates differential brain efflux of Abeta isoforms. Neuron. 2004;43:333–44.
86. Sagare A, Deane R, Bell RD, Johnson B, Hamm K, Pendu R, et al. Clearance of amyloid-beta by circulating lipoprotein receptors. Nat Med. 2007;13:1029–31.
87. Deane R, Sagare A, Hamm K, Parisi M, Lane S, Finn MB, et al. apoE isoform-specific disruption of amyloid beta peptide clearance from mouse brain. J Clin Invest. 2008;118:4002–13.
88. Bachmeier C, Paris D, Beaulieu-Abdelahad D, Mouzon B, Mullan M, Crawford F. A multifaceted role for apoE in the clearance of beta-amyloid across the blood-brain barrier. Neurodegener Dis. 2013;11:13–21.
89. Li Y, Lu W, Marzolo MP, Bu G. Differential functions of members of the low density lipoprotein receptor family suggested by their distinct endocytosis rates. J Biol Chem. 2001;276:18000–6.
90. Jaeger LB, Dohgu S, Hwang MC, Farr SA, Murphy MP, Fleegal-DeMotta MA, et al. Testing the neurovascular hypothesis of Alzheimer's disease: LRP-1 antisense reduces blood-brain barrier clearance, increases brain levels of amyloid-β protein, and impairs cognition. J Alzheimers Dis. 2009;17:553–70.
91. Chalmers KA, Barker R, Passmore PA, Panza F, Seripa D, Solfrizzi V, et al. LRP-1 variation is not associated with risk of Alzheimer's disease. Int J Mol Epidemiol Genet. 2010;1:104–13.
92. Juliano RL, Ling V. A surface glycoprotein modulating drug permeability in Chinese hamster ovary cell mutants. Biochim Biophys Acta. 1976;455:152–62.
93. Cordon-Cardo C, O'Brien JP, Casals D, Rittman-Grauer L, Biedler JL, Melamed MR, et al. Multidrug-resistance gene (P-glycoprotein) is expressed by endothelial cells at blood-brain barrier sites. Proc Natl Acad Sci USA. 1989;86:695–8.
94. Chin JE, Soffir R, Noonan KE, Choi K, Roninson IB. Structure and expression of the human MDR (P-glycoprotein) gene family. Mol Cell Biol. 1989;9:3808–20.
95. Thiebaut F, Tsuruo T, Hamada H, Gottesman MM, Pastan I, Willingham MC. Cellular localization of the multidrug-resistance gene product P-glycoprotein in normal human tissues. Proc Natl Acad Sci USA. 1987;84:7735–8.
96. Fojo AT, Ueda K, Slamon DJ, Poplack DG, Gottesman MM, Pastan I. Expression of a multidrug-resistance gene in human tumors and tissues. Proc Natl Acad Sci USA. 1987;84:265–9.
97. Callaghan R. Providing a molecular mechanism for P-glycoprotein; why would I bother? Biochem Soc Trans. 2015;43:995–1002.
98. Nicolazzo JA, Banks WA. Decreased blood-brain barrier expression of P-glycoprotein in Alzheimer's disease: impact on pathogenesis and brain access of therapeutic agents. Ther Deliv. 2011;2:841–4.
99. Schinkel AH, Mol CA, Wagenaar E, van Deemter L, Smit JJ, Borst P. Multidrug resistance and the role of P-glycoprotein knockout mice. Eur J Cancer. 1995;31A:1295–8.
100. Lagas JS, Vlaming ML, Schinkel AH. Pharmacokinetic assessment of multiple ATP-binding cassette transporters: the power of combination knockout mice. Mol Interv. 2009;9:136–45.
101. Borst P, Schinkel AH. P-glycoprotein ABCB1: a major player in drug handling by mammals. J Clin Invest. 2013;123:4131–3.
102. Lam FC, Liu R, Lu P, Shapiro AB, Renoir JM, Sharom FJ, et al. Beta-amyloid efflux mediated by p-glycoprotein. J Neurochem. 2001;76:1121–8.
103. Cirrito JR, Deane R, Fagan AM, Spinner ML, Parsadanian M, Finn MB, et al. P-glycoprotein deficiency at the blood-brain barrier increases amyloid-beta deposition in an Alzheimer disease mouse model. J Clin Invest. 2005;115:3285–90.
104. Kuhnke D, Jedlitschky G, Grube M, Krohn M, Jucker M, Mosyagin I, et al. MDR1-P-glycoprotein (ABCB1) mediates transport of Alzheimer's amyloid-beta peptides—implications for the mechanisms of Abeta clearance at the blood-brain barrier. Brain Pathol. 2007;17:347–53.
105. Wang W, Bodles-Brakhop AM, Barger SW. A role for P-glycoprotein in clearance of Alzheimer amyloid β-peptide from the brain. Curr Alzheimer Res. 2016;13:615–20.
106. Vogelgesang S, Cascorbi I, Schroeder E, Pahnke J, Kroemer HK, Siegmund W, et al. Deposition of Alzheimer's beta-amyloid is inversely correlated with P-glycoprotein expression in the brains of elderly non-demented humans. Pharmacogenetics. 2002;12:535–41.
107. Chiu C, Miller MC, Monahan R, Osgood DP, Stopa EG, Silverberg GD. P-glycoprotein expression and amyloid accumulation in human aging and Alzheimer's disease: preliminary observations. Neurobiol Aging. 2015;36:2475–82.
108. Wijesuriya HC, Bullock JY, Faull RL, Hladky SB, Barrand MA. ABC efflux transporters in brain vasculature of Alzheimer's subjects. Brain Res. 2010;1358:228–38.
109. Deo AK, Borson S, Link JM, Domino K, Eary JF, Ke B, et al. Activity of P-glycoprotein, a β-Amyloid transporter at the blood-brain barrier, is compromised in patients with mild Alzheimer disease. J Nucl Med. 2014;55:1106–11.
110. Hartz AM, Miller DS, Bauer B. Restoring blood-brain barrier P-glycoprotein reduces brain amyloid-beta in a mouse model of Alzheimer's disease. Mol Pharmacol. 2010;77:715–23.
111. Hartz AM, Zhong Y, Wolf A, LeVine H 3rd, Miller DS, Bauer B. Aβ40 reduces P-glycoprotein at the blood-brain barrier through the ubiquitin-proteasome pathway. J Neurosci. 2016;36:1930–41.
112. Park R, Kook SY, Park JC, Mook-Jung I. Aβ1-42 reduces P-glycoprotein in the blood-brain barrier through RAGE-NF-kappaB signaling. Cell Death Dis. 2014;5:e1299.
113. Qosa H, LeVine 3rd H, Keller JN, Kaddoumi A. Mixed oligomers and monomeric amyloid-β disrupts endothelial cells integrity and reduces monomeric amyloid-beta transport across hCMEC/D3 cell line as an in vitro blood-brain barrier model. Biochim Biophys Acta. 1842;2014:1806–15.
114. Magdesian MH, Carvalho MM, Mendes FA, Saraiva LM, Juliano MA, Juliano L, et al. Amyloid-beta binds to the extracellular cysteine-rich domain of Frizzled and inhibits Wnt/beta-catenin signaling. J Biol Chem. 2008;283:9359–68.
115. Toledo JB, Shaw LM, Trojanowski JQ. Plasma amyloid beta measurements—a desired but elusive Alzheimer's disease biomarker. Alzheimers Res Ther. 2013;5:8.
116. Sotolongo-Grau O, Pesini P, Valero S, Lafuente A, Buendia M, Perez-Grijalba V, et al. Association between cell-bound blood amyloid-β(1-40) levels and hippocampus volume. Alzheimers Res Ther. 2014;6:56.
117. Rembach A, Faux NG, Watt AD, Pertile KK, Rumble RL, Trounson BO, et al. Changes in plasma amyloid beta in a longitudinal study of aging and Alzheimer's disease. Alzheimers Dement. 2014;10:53–61.
118. Janelidze S, Stomrud E, Palmqvist S, Zetterberg H, van Westen D, Jeromin A, et al. Plasma β-amyloid in Alzheimer's disease and vascular disease. Sci Rep. 2016;6:26801.
119. Deane R, Du Yan S, Submamaryan RK, LaRue B, Jovanovic S, Hogg E, et al. RAGE mediates amyloid-beta peptide transport across the blood-brain barrier and accumulation in brain. Nat Med. 2003;9:907–13.
120. Yan SD, Chen X, Fu J, Chen M, Zhu H, Roher A, et al. RAGE and amyloid-beta peptide neurotoxicity in Alzheimer's disease. Nature. 1996;382:685–91.
121. Krohn M, Lange C, Hofrichter J, Scheffler K, Stenzel J, Steffen J, et al. Cerebral amyloid-β proteostasis is regulated by the membrane transport protein ABCC1 in mice. J Clin Invest. 2011;121:3924–31.
122. Tai LM, Loughlin AJ, Male DK, Romero IA. P-glycoprotein and breast cancer resistance protein restrict apical-to-basolateral permeability of human brain endothelium to amyloid-beta. J Cereb Blood Flow Metab. 2009;29:1079–83.
123. Do TM, Noel-Hudson MS, Ribes S, Besengez C, Smirnova M, Cisternino S, et al. ABCG2- and ABCG4-mediated efflux of amyloid-β peptide 1-40 at the mouse blood-brain barrier. J Alzheimers Dis. 2012;30:155–66.
124. Xiong H, Callaghan D, Jones A, Bai J, Rasquinha I, Smith C, et al. ABCG2 is upregulated in Alzheimer's brain with cerebral amyloid angiopathy and may act as a gatekeeper at

the blood-brain barrier for Abeta(1-40) peptides. J Neurosci. 2009;29:5463–75.
125. Clifford PM, Zarrabi S, Siu G, Kinsler KJ, Kosciuk MC, Venkataraman V, et al. Abeta peptides can enter the brain through a defective blood-brain barrier and bind selectively to neurons. Brain Res. 2007;1142:223–36.
126. Maness LM, Banks WA, Podlisny MB, Selkoe DJ, Kastin AJ. Passage of human amyloid beta-protein 1-40 across the murine blood-brain barrier. Life Sci. 1994;55:1643–50.
127. Martyn CN, Barker DJ, Osmond C, Harris EC, Edwardson JA, Lacey RF. Geographical relation between Alzheimer's disease and aluminum in drinking water. Lancet. 1989;1:59–62.
128. Banks WA, Niehoff ML, Drago D, Zatta P. Aluminum complexing enhances amyloid beta protein penetration of blood-brain barrier. Brain Res. 2006;1116:215–21.
129. Pluta R, Barcikowska M, Januszewski S, Misicka A, Lipkowski AW. Evidence of blood-brain barrier permeability/leakage for circulating human Alzheimer's beta-amyloid-(1-42)-peptide. Neuroreport. 1996;7:1261–5.
130. Kalaria RN. The role of cerebral ischemia in Alzheimer's disease. Neurobiol Aging. 2000;21:321–30.
131. Pluta R, Jablonski M, Ulamek-Koziol M, Kocki J, Brzozowska J, Januszewski S, et al. Sporadic Alzheimer's disease begins as episodes of brain ischemia and ischemically dysregulated Alzheimer's disease genes. Mol Neurobiol. 2013;48:500–15.
132. Tamaki C, Ohtsuki S, Iwatsubo T, Hashimoto T, Yamada K, Yabuki C, et al. Major involvement of low-density lipoprotein receptor-related protein 1 in the clearance of plasma free amyloid beta-peptide by the liver. Pharm Res. 2006;23:1407–16.
133. Hone E, Martins IJ, Fonte J, Martins RN. Apolipoprotein E influences amyloid-beta clearance from the murine periphery. J Alzheimers Dis. 2003;5:1–8.
134. Ghiso J, Shayo M, Calero M, Ng D, Tomidokoro Y, Gandy S, et al. Systemic catabolism of Alzheimer's Abeta40 and Abeta42. J Biol Chem. 2004;279:45897–908.
135. Marques MA, Kulstad JJ, Savard CE, Green PS, Lee SP, Craft S, et al. Peripheral amyloid-beta levels regulate amyloid-beta clearance from the central nervous system. J Alzheimers Dis. 2009;16:325–9.
136. Henderson SJ, Andersson C, Narwal R, Janson J, Goldschmidt TJ, Appelkvist P, et al. Sustained peripheral depletion of amyloid-β with a novel form of neprilysin does not affect central levels of amyloid-β. Brain. 2014;137:553–64.
137. Georgievska B, Gustavsson S, Lundkvist J, Neelissen J, Eketjall S, Ramberg V, et al. Revisiting the peripheral sink hypothesis: inhibiting BACE1 activity in the periphery does not alter β-amyloid levels in the CNS. J Neurochem. 2015;132:477–86.
138. Mehta DC, Short JL, Hilmer SN, Nicolazzo JA. Drug access to the central nervous system in Alzheimer's disease: preclinical and clinical insights. Pharm Res. 2015;32:819–39.
139. Claudio L. Ultrastructural features of the blood-brain barrier in biopsy tissue from Alzheimer's disease patients. Acta Neuropathol. 1996;91:6–14.
140. Farkas E, De Jong GI, de Vos RA, Jansen Steur EN, Luiten PG. Pathological features of cerebral cortical capillaries are doubled in Alzheimer's disease and Parkinson's disease. Acta Neuropathol. 2000;100:395–402.
141. Abuznait AH, Kaddoumi A. Role of ABC transporters in the pathogenesis of Alzheimer's disease. ACS Chem Neurosci. 2012;3:820–31.
142. Schuff N, Matsumoto S, Kmiecik J, Studholme C, Du A, Ezekiel F, et al. Cerebral blood flow in ischemic vascular dementia and Alzheimer's disease, measured by arterial spin-labeling magnetic resonance imaging. Alzheimers Dement. 2009;5:454–62.
143. den Abeelen AS, Lagro J, van Beek AH, Claassen JA. Impaired cerebral autoregulation and vasomotor reactivity in sporadic Alzheimer's disease. Curr Alzheimer Res. 2014;11:11–7.
144. Leeuwis AE, Benedictus MR, Kuijer JP, Binnewijzend MA, Hooghiemstra AM, Verfaillie SC, et al. Lower cerebral blood flow is associated with impairment in multiple cognitive domains in Alzheimer's disease. Alzheimers Dement. 2016
145. Spulber S, Bogdanovic N, Romanitan MO, Bajenaru OA, Popescu BO. Claudin expression profile separates Alzheimer's disease cases from normal aging and from vascular dementia cases. J Neurol Sci. 2012;322:184–6.
146. Kawamura A, Baitsch D, Telgmann R, Feuerborn R, Weissen-Plenz G, Hagedorn C, et al. Apolipoprotein E interrupts interleukin-1beta signaling in vascular smooth muscle cells. Arterioscler Thromb Vasc Biol. 2007;27:1610–7.
147. Bien-Ly N, Boswell CA, Jeet S, Beach TG, Hoyte K, Luk W, et al. Lack of widespread BBB disruption in Alzheimer's disease models: focus on therapeutic antibodies. Neuron. 2015;88:289–97.
148. Kragh-Hansen U, Minchiotti L, Galliano M, Peters Jr T. Human serum albumin isoforms: genetic and molecular aspects and functional consequences. Biochim Biophys Acta. 1830;2013:5405–17.
149. Terp BN, Cooper DN, Christensen IT, Jorgensen FS, Bross P, Gregersen N, et al. Assessing the relative importance of the biophysical properties of amino acid substitutions associated with human genetic disease. Hum Mutat. 2002;20:98–109.
150. Yang Y, Engkvist O, Llinas A, Chen H. Beyond size, ionization state, and lipophilicity: influence of molecular topology on absorption, distribution, metabolism, excretion, and toxicity for druglike compounds. J Med Chem. 2012;55:3667–77.
151. Palm K, Luthman K, Ungell AL, Strandlund G, Artursson P. Correlation of drug absorption with molecular surface properties. J Pharm Sci. 1996;85:32–9.
152. Do TM, Dodacki A, Alata W, Calon F, Nicolic S, Scherrmann JM, et al. Age-dependent regulation of the blood-brain barrier influx/efflux equilibrium of Amyloid-β peptide in a mouse model of Alzheimer's disease (3xTg-AD). J Alzheimers Dis. 2016;49:287–300.
153. Daiello LA, Stopa EG, Ott BR, de la Monte S, Johanson CE. CNS molecular gradients in mild cognitive impairment and Alzheimer's disease: implications for blood-brain barrier permeability. Alzheimers Dement. 2016;12:P1149.
154. Janelidze S, Hertze J, Nagga K, Nilsson K, Nilsson C, Wennstrom M, et al. Increased blood-brain barrier permeability is associated with dementia and diabetes but not amyloid pathology or APOE genotype. Neurobiol Aging. 2016;51:104–12.
155. Takechi R, Galloway S, Pallebage-Gamarallage MM, Mamo JC. Chylomicron amyloid-beta in the aetiology of Alzheimer's disease. Atheroscler Suppl. 2008;9:19–25.
156. Poduslo JF, Curran GL, Wengenack TM, Malester B, Duff K. Permeability of proteins at the blood-brain barrier in the normal adult mouse and double transgenic mouse model of Alzheimer's disease. Neurobiol Dis. 2001;8:555–67.
157. Ryu JK, McLarnon JG. A leaky blood-brain barrier, fibrinogen infiltration and microglial reactivity in inflamed Alzheimer's disease brain. J Cell Mol Med. 2009;13:2911–25.
158. Ujiie M, Dickstein DL, Carlow DA, Jefferies WA. Blood-brain barrier permeability precedes senile plaque formation in an Alzheimer disease model. Microcirculation. 2003;10:463–70.
159. Bourasset F, Ouellet M, Tremblay C, Julien C, Do TM, Oddo S, et al. Reduction of the cerebrovascular volume in a transgenic mouse model of Alzheimer's disease. Neuropharmacology. 2009;56:808–13.
160. Mehta DC, Short JL, Nicolazzo JA. Altered brain uptake of therapeutics in a triple transgenic mouse model of Alzheimer's disease. Pharm Res. 2013;30:2868–79.
161. Opazo C, Luza S, Villemagne VL, Volitakis I, Rowe C, Barnham KJ, et al. Radioiodinated clioquinol as a biomarker for beta-amyloid: Zn complexes in Alzheimer's disease. Aging Cell. 2006;5:69–79.
162. Adlard PA, Cherny RA, Finkelstein DI, Gautier E, Robb E, Cortes M, et al. Rapid restoration of cognition in Alzheimer's transgenic mice with 8-hydroxy quinoline analogs is associated with decreased interstitial Abeta. Neuron. 2008;59:43–55.

Journal of Pharmaceutical Sciences 106 (2017) 2614-2624

Contents lists available at ScienceDirect

Journal of Pharmaceutical Sciences

journal homepage: www.jpharmsci.org

Pharmacokinetics, Pharmacodynamics and Drug Transport and Metabolism

Development and Validation of an In-Cell Western for Quantifying P-Glycoprotein Expression in Human Brain Microvascular Endothelial (hCMEC/D3) Cells

Mitchell P. McInerney [1], Yijun Pan [1], Jennifer L. Short [2], Joseph A. Nicolazzo [1, *]

[1] Drug Delivery, Disposition and Dynamics, Monash Institute of Pharmaceutical Sciences, Monash University, Parkville, VIC, Australia
[2] Drug Discovery Biology, Monash Institute of Pharmaceutical Sciences, Monash University, Parkville, VIC, Australia

ARTICLE INFO

Article history:
Received 19 October 2016
Revised 6 December 2016
Accepted 7 December 2016
Available online 5 January 2017

Keywords:
P-glycoprotein
membrane transporter
blood-brain barrier
cell culture
ABC transporters
drug resistance
efflux pumps
endothelial

ABSTRACT

An in-cell western (ICW) protocol detecting the relative expression of P-glycoprotein (P-gp) in human cerebro-microvascular endothelial cells (hCMEC/D3) was developed and optimized, with the intention of improving throughput relative to western blotting (WB). For validation of the ICW protocol, hCMEC/D3 cells were incubated with known P-gp upregulators (10 μM rifampicin and 5 μM SR12813) and treated with siRNA targeted against MDR1, before measuring changes in P-gp expression, using both ICW and WB in parallel. To confirm a relationship between the detected P-gp expression and function, the uptake of the P-gp substrate rhodamine-123 was assessed following SR12813 treatment. Rifampicin and SR12813 significantly upregulated P-gp expression (1.5-fold and 1.9-fold, respectively) compared to control, as assessed by the ICW protocol. WB analysis of the same treatments revealed 1.4-fold and 1.5-fold upregulations. MDR1 siRNA reduced P-gp abundance by 20% and 35% when assessed by ICW and WB, respectively. SR12813 treatment reduced rhodamine-123 uptake by 18%, indicating that the observed changes in P-gp expression by ICW were associated with comparable functional changes. The correlation of P-gp upregulation by WB, rhodamine-123 uptake, and the ICW protocol provide validation of a new ICW method as an alternative method for quantification of P-gp in hCMEC/D3 cells.

Introduction

P-glycoprotein (P-gp) is a physiologically important efflux pump responsible for protecting many cell types and organs from the excessive accumulation of a broad spectrum of potentially harmful xenobiotics.[1] P-gp is expressed at relatively low levels in most mammalian tissues, but it appears most abundantly in intestinal epithelial cells; kidney proximal tubules; liver bile ductules, and the brain endothelial cells that line the cerebrovasculature and comprise the blood-brain barrier (BBB).[2-5] Within the aforementioned tissues, the prominent presence of P-gp is considered integral to the maintenance of normal physiological function.[2-5] In cancerous cells, however, the expression of P-gp is often highly upregulated in response to previous exposure to cytotoxic treatments, and the resulting cells are characterized as multidrug resistant, by virtue of the enhanced P-gp-mediated efflux activity, which effectively limits the access of drugs to their intracellular targets.[6] Within cancer research, this upregulated function has engendered a status for P-gp as a formidable barrier to delivering cytotoxic drugs to their sites of action *in vivo*.[7]

P-gp is also considered a hindrance for drugs targeting the central nervous system (CNS).[8,9] P-gp, sometimes referred to as "the gatekeeper" of the brain,[10] greatly limits the access of many CNS-acting drugs to their therapeutic targets, through the active efflux of a wide range of drugs from the lipid membrane of brain endothelial cells, back into the systemic circulation.[11] Thus the modulation of P-gp expression and function has been a strategy considered for enhancing the CNS delivery of drugs which are P-gp substrates, although with only limited success achieved thus far.[7,12] To further highlight the importance of P-gp, it is becoming increasingly apparent that P-gp expression and function may play an important role in several neurological disease states, including

Abbreviations used: BBB, blood-brain barrier; hCMEC/D3, human cerebro-microvascular endothelial cell line; ICW, in-cell western; IR, infrared; MDR1, multi-drug resistance gene, encoding for P-glycoprotein; P-gp, P-glycoprotein; R123, rhodamine-123; WB, western blot/western blotting.

* *Correspondence to:* Joseph A. Nicolazzo (Telephone: +61-3-9903-9605; Fax: +61-3-9903-9583).
E-mail address: joseph.nicolazzo@monash.edu (J.A. Nicolazzo).

http://dx.doi.org/10.1016/j.xphs.2016.12.017

Alzheimer's disease[13-16] and Parkinson's disease,[17,18] among others.[19] Therefore, methods for assessing the relative quantities of P-gp which might result from physiological or pathological processes, or after pharmacological interventions, are of great use to many research areas that focus on the BBB. Currently, the method most commonly employed for quantifying P-gp abundance is western blotting (WB).

WB as a method of protein quantification has been indispensable to the life sciences since its inception in 1979. The combination of both the apparent simplicity and the relative inexpensiveness of the technique quickly established the role of WB as the preferred or most widely used method of protein quantification. Certainly this method facilitated the rapid expansion of data accumulated throughout the 1980s and 1990s, greatly enhancing knowledge and understanding of the processes underlying cellular signaling, communication, metabolism, transport, and structure. Particularly pertinent to the pharmaceutical sciences is the ability of WB to measure changes in protein expression resulting from pharmacological interventions in various cell types. The employment of WB to answer such research questions is extremely useful and widespread; yet despite this ubiquity, WB possesses several key drawbacks. The most prominent of these drawbacks is that WB may be considered a low throughput method. The need to generally harvest >10 μg of protein for analysis often necessitates the use of 6-well plates, and the average 2-day processing time delays the researcher's ability to optimize experimental protocols and proceed with experiments whose parameters rely on the results from previous experiments. These factors may also limit the set of experimental conditions that are explored, that is, 1-2 time points and/or concentrations of pharmacological intervention are often tested, since the labor time required to investigate alternatives increases linearly with each extra data point desired.

An alternative method known as the in-cell western (ICW) is beginning to occupy a place within the literature. The ICW protocol is based on the same principles as WB; primary and secondary antibodies are still used to signal and quantify the protein of interest, but the antibodies bind to the target of interest in its native form (not sodium dodecyl sulfate treated) and *in situ* (within cellular matrices in 96-well plates). Most importantly, the ICW protocol can be performed on 96-well plates, a format which provides moderate but still significant benefits, when compared to WB. The smaller scale of ICW reduces the quantity of consumables used within an experiment, and also enhances the throughput and therefore the effective rate of a researcher's investigations.

The aim of this study is to develop and validate an ICW western protocol for the relative quantification of P-gp, as a moderately improved alternative to WB, in immortalized human cerebral microvascular endothelial cells (hCMEC/D3), a cell line which closely models the human BBB.[20] As a part of the validation process, the auto-fluorescent capacities of several 96-well plate types were assessed, to aid appropriate plate selection and thus minimize the impact of experimental artifacts. Next, the linearity of the P-gp signal and 4′,6-diamidino-2-phenylindole (DAPI) nuclear stain (to be later used for normalization of the P-gp signal) was assessed as a function of increasing cell density. For further validation of the responsiveness of the P-gp ICW, hCMEC/D3 cells were exposed to 2 known upregulators of P-gp (rifampicin, SR12813) as well as small interfering ribonucleic acid (siRNA) against MDR1 (the gene encoding P-gp), and P-gp expression was assessed by the new ICW protocol and WB in parallel. Finally, to confirm the link between ICW-measured changes in P-gp and apparent P-gp functionality at the cellular membrane, cellular accumulation of the P-gp-specific substrate rhodamine-123 (R123) was assessed after exposure to one of the treatments used in this study, SR12813.

Materials and Methods

Materials

DAPI, Triton X-100, Tween-20, paraformaldehyde, sodium chloride, potassium chloride, disodium phosphate, R123, SR12813, rifampicin, potassium phosphate, and Corning black polystyrene tissue culture (TC)–treated 96-well plates were all purchased from Sigma-Aldrich (St. Louis, MO). Tris buffer salt (TRIZMA base), sodium dodecyl sulfate, ammonium persulfate, N,N,N′,N′-tetramethylethylenediamine, trypan blue, glycerol, Hank's balanced salt solution (HBSS), trypsin–ethylenediaminetetraacetic acid solution 0.25% in HBSS, and Dulbecco's sterile phosphate buffered saline (PBS) were all purchased from Sigma Life Sciences (St. Louis, MO). Forty percent acrylamide/bis solution was purchased from Bio-Rad Laboratories (Hercules, CA). Valspodar (PSC833) was a gift from Novartis (Basel, Switzerland). Odyssey blocking buffer and the IR dye 800CW goat anti-mouse IgG antibody were both purchased from Millennium Science (Mulgrave, Australia). cOmplete Tablets Mini EASY pack protease inhibitors were purchased from Roche Diagnostics GmbH (Mannheim, Germany), and 0.2 μm pore-sized nitrocellulose membrane roll was purchased from GE Life Sciences (Rydalmere, Australia). The C219 P-gp antibody was purchased from Australian Biosearch (Balcatta, Australia). Corning Costar transparent 96-well plates were purchased from Invitro (Noble Park North, Australia). Fluorescein goat anti-mouse IgM antibody was purchased from Vector Laboratories (Burlingame, CA). Black polystyrene ViewPlate-96 F TC 96-well plates were purchased from Perkin Elmer, and Pierce BCA protein assay kit and Pierce IP lysis buffer were purchased from Thermo Fisher Scientific (Scoresby, Australia). The hCMEC/D3 cells were generously provided by Dr. Pierre-Olivier Couraud (INSERM, Paris, France). Both Clonetics endothelial basal medium 2 (EBM2) basal media and Clonetics EGM-2 single quots growth factor kits were purchased from Lonza (Walkersville, MD). Collagen type I was purchased from Corning Discovery Labware (Bedford, MD). Normal transparent 6 and 96-well plates were purchased from Corning Incorporated (Corning, NY). HiPerFect transfection reagent, 4 × GeneSolution siRNA for ABCB1 (SI03040156, SI03028116, SI00018732, and SI00018718), AllStars Negative Control siRNA (SI03650318), and the RNeasy Plus Mini Kit were purchased from Qiagen (Hilden, Germany).

Selection of Appropriate 96-Well Plate for ICW

Inherent properties of 96-well plates can greatly influence the values produced by certain assays. Edge effects as well as autofluorescence (a concept which can be applied to infrared [IR] and other light sources as well) occur to varying degrees on different plate types, and the type of plastic used can also influence the spread of light to and from adjacent wells. The type of plate used in any one assay is crucial and should always be thoroughly explored in the planned experimental context before commencing studies. Therefore, an experiment was conducted whereby 3 different plate types (Corning, Costar, and Perkin Elmer) containing no reagents were scanned on the LiCor Odyssey IR imager, without reagents but using the same settings under which the experimental data would later be analyzed. Briefly, all 3 plate types were thoroughly wiped clean with 80% (vol/vol) ethanol, as well as the glass surface of the Odyssey imager. The plates were then individually placed within the imager, and the imager software was set to the microplate2 setting with a 3.0-mm focus offset, a medium image quality with 169 μm resolution, and the light intensity from the 800 nm channel was set to 10. The entire plate was scanned and a 96-well plate ICW grid was applied to the constructed image, with care taken to align the grid such that only light emanating from the individual wells was integrated. The integrated intensity of IR light from each well

was exported from the Odyssey software, and plotted as a function of its row position within the 96-well plate.

Seeding/Splitting of the hCMEC/D3 Cell Line

Vials of the hCMEC/D3 cell line were kept cryogenically frozen in liquid nitrogen in a solution comprised of 5% (vol/vol) dimethyl sulfoxide (DMSO) in heat inactivated fetal bovine serum solution. One milliliter vials containing ~2 million cells were dispensed into T-75 flasks containing 14 mL of EBM2 media, which had been pre-coated with 3 mL of a 0.1 mg/mL solution of collagen type I and incubated for 1 h, before being washed with 10 mL of PBS to remove excess collagen. Two hours after seeding, the DMSO containing EBM2 media was removed and replaced with freshly warmed media. EBM2 was supplemented with the following: 0.01% (vol/vol) ascorbic acid, 0.01% (vol/vol) gentamicin/amphotericin, 0.01% (vol/vol) hydrocortisone, 0.025% (vol/vol) epidermal growth factor, 0.025% (vol/vol) insulin-like growth factor, 0.025% (vol/vol) vascular endothelial growth factor, 0.1% (vol/vol) b-splice variant fibroblast growth factor, 10 mM 4-(2-hydroxyethyl)-1-piperazineethanesulfonic acid, 1% (vol/vol) penicillin/streptomycin, and 2.5% (vol/vol) fetal bovine serum.

Signal-to-Noise Ratio Optimization

Once it had become apparent that the initially observed signal-to-noise ratio was far from optimal, several iterations of the initially trialed ICW protocol were executed. hCMEC/D3 cells were plated onto a Corning black polystyrene TC-treated 96-well plate at 35,000 cells/cm^2 and left to grow for 48 h (to mimic future experimental conditions), by which point the cells had reached 80%-90% confluency. While the above conditions remained the same throughout the iterative process, the following variables were explored with the intent of optimization: varying primary and secondary antibody concentrations; times of primary and secondary antibody incubation; intensity of light source within the LiCor Odyssey IR scanner; presence and concentration of surfactants to lower non-specific antibody binding; and the addition of extra rinse steps at the very end of the protocol. Each of these variables was fine tuned to generate an optimal signal-to-noise ratio, and the final protocol is described in the next section.

Construction of Standard Curves for IR P-gp Signal and Cell Number (Normalization)

The first ICW experiments were designed to assess the construction of the standard curves of both the IR P-gp signal derived from hCMEC/D3 cells and the fluorescent nuclear stain DAPI, the latter to be used to normalize the data to the total number of cells. To construct the standard curves, hCMEC/D3 cells (passage 30-35) were seeded onto collagen type I-coated Corning 96-well plates at varying seeding densities, ranging from 5000 to 35,000 cells/well (to facilitate observation of a standard curve). Cells were allowed to settle for either 2 h before commencing the ICW protocol such that no cell growth had occurred and thus the linearity of the seeding density was preserved, or for 24 h to assess the ability of the DAPI stain to respond to cell growth. After the appropriate time interval, the ICW protocol was applied. As shown in Figure 2a, the initial P-gp ICW trial yielded data of poor quality and a signal of low magnitude. As such, the protocol was iteratively improved to reach the final protocol described herein. EBM2 media was removed from all wells and the cells were briefly rinsed with 150 μL of PBS. The PBS was discarded and replaced with 150 μL of fixing solution (4% wt/vol paraformaldehyde in PBS), and the plate was left to stand without agitation at room temperature for 20 min. After 20 min, the fixing solution was discarded and the cells were permeabilized by 4 consecutive 5-min rinses with 200 μL of cell permeabilization solution (0.1% Triton X-100 in PBS) under moderate shaking at room temperature. A final rinse using 210 μL of PBS was included to remove any residual surfactant. A 150-μL aliquot of LiCor PBS blocking buffer™ was applied to each well and the plate was left on gentle agitation for 1 h at room temperature. The blocking buffer was then discarded and replaced with 50 μL of the same blocking buffer, now containing a 1:50 dilution of the C219 P-gp antibody or blocking buffer alone (to be used as secondary antibody controls). The plate was then left under gentle shaking overnight in a cool room (4°C). All wells were then subjected to 4 consecutive 200-μL washes under gentle shaking with PBS-T (0.1% vol/vol Tween-20 in PBS). After the fourth rinse, each well was incubated with 50 μL of blocking buffer containing 0.5% (vol/vol) Tween-20, 1 μg/mL DAPI, and LiCor goat anti-mouse (secondary) antibody (1:2000). Immediately after application of the secondary antibody, the plate was wrapped in aluminum foil and placed on gentle agitation at room temperature for 1 h. Finally, after DAPI/secondary antibody incubation, the plate was subjected to 5 more 5-min rinses with 200 μL of PBS-T at room temperature, followed by 2 final rinses with PBS (in place of PBS-T) to remove residual surfactant (the increased number of final rinses greatly reduces non-specific secondary antibody binding). The plate was then carefully aligned on the Odyssey imager (such that only light emanating from the individual wells was recorded) and scanned using the settings previously described.

To remove the intrinsic IR auto-fluorescence associated with the plates, an average of the IR signal was calculated from cell-free wells, and this average was subtracted from all other cell-containing wells. Next an average of control wells that had undergone incubation with secondary antibody only (primary antibody omitted) was calculated, and this value was also subtracted from all remaining data points, to account for non-specific binding of the secondary antibody. These 2 subtractions were performed as separate steps, to facilitate the calculation of the percentage contributions from both specific and non-specific secondary antibody binding to P-gp, after the exclusion of plate-intrinsic IR auto-fluorescence.

The plate was then scanned in a Perkin Elmer fluorescence spectrophotometer with an excitation wavelength of 495 nm and emission wavelength of 515 nm, and the scan mode was set to well area scan mode with 100 flashes spaced 0.72 mm apart, round scan mode, and fluorescence emission measurements occurring at the bottom of the wells. The plates always included wells which contained only collagen, and an average of these wells was subtracted from all other fluorescent data points to remove any non-specific fluorescence not associated with DAPI staining. For experiments where P-gp expression was measured following exposure to a known modulator of P-gp expression, the data were expressed as a fold change in comparison to the average of control wells, according to Equation 1:

$$\text{Fold change} = \frac{IR_t - IR_b}{F_t - F_b} \Bigg/ \frac{\sum_{i=1}^{n} \left(\frac{IR_c - IR_b}{F_c - F_b} \right)}{n} \quad (1)$$

where IR_t is the IR signal from treatment wells; IR_b the IR signal from control wells treated with secondary antibody only (P-gp signal background subtraction); F_t the fluorescent signal from treatment wells; F_b the fluorescent signal from empty wells containing collagen only (DAPI background subtraction); IR_c the IR signal from control wells; F_c the fluorescent signal from control wells; and n the number of control replicates.

Imaging of IR Antibody Signal Origin

Due to the generally hydrophobic nature of many antibodies and proteins, non-specific binding between the antibodies utilized in

this protocol and serum proteins used in blocking buffers must be assessed, in order to determine an appropriate signal origin. In short, close range visualization of the signal being measured at the cellular level would be desirable to build confidence that the future data generated were indeed a reflection of P-gp abundance, rather than experimental artifact. Therefore, an imaging experiment was conducted to visualize hCMEC/D3 cells at the cellular level, to observe the signal origin, using the following experimental protocol. Briefly, untreated hCMEC/D3 cells were cultured in a 96-well plate until reaching ~90% confluency, at which point the media was removed, and the cells were rinsed with 200 μL of PBS followed by fixation in paraformaldehyde as described above. Next, the ICW protocol was followed as described above, except for the secondary antibody incubation. To facilitate imaging by confocal fluorescence microscopy, the IR-conjugated secondary antibody was replaced in this experiment with a goat anti-mouse secondary antibody conjugated to fluorescein isothiocyanate (FITC), at a concentration of 20 μg/mL. All other parameters of the ICW protocol remained the same. Images were captured on a Perkin Elmer Operetta high throughput imager using Harmony version 3.5.2 and a 20× UPlanApo NA0.8 objective. DAPI fluorescence was collected using a 380/40 excitation and 445/70 emission filter, and fluorescein fluorescence using a 475/30 excitation and 525/50 emission filter.

Validation of P-gp ICW by Comparison to WB Following Treatment With P-gp Regulators

Once the changeable parameters of the ICW protocol were optimized and a desirable signal-to-noise ratio had been achieved, the impact of known modulators of P-gp expression were compared using the novel ICW protocol and a traditional WB technique. hCMEC/D3 cells were seeded at 35,000 cells/cm^2 onto collagenated 6 (WB) or black Corning 96 (ICW) well plates. Approximately 24 h after seeding, when cells had reached 30%-50% confluency, the media was removed and replaced with treatment media containing either 0.1% DMSO (control), 10 μM rifampicin, or 5 μM SR12813, all as separate experiments. In each of these experiments cells were incubated in treatment media for 72 h, at which point the treatment media was removed and cells were briefly rinsed in 2 mL or 200 μL of PBS (6-well or 96-well plate) and then immediately lysed for WB analysis or fixed with 4% paraformaldehyde for 20 min, as per the ICW protocol. The remainder of the ICW protocol was then carried out as described in the previous sections, and the WB analysis was executed using the technique described below. To each well, 200 μL of a solution containing a 6:1 ratio of Pierce IP lysis buffer and a 7 times concentrated solution of cOmplete protease inhibitor cocktail, respectively, was added to each well. Cells were then lysed in this solution for 15 min at 4°C, after which each well was scraped to ensure full detachment of cells. The solution from each well was transferred to a pre-cooled Eppendorf tube and spun at 14,000 relative centrifugal force for 5 min before supernatant collection and protein content analysis via the Pierce BCA protein assay kit using bovine serum albumin as a standard. WB was carried out by loading a 10% acrylamide, 1-mm hand-cast gel with varying volumes of lysate/laemmli (5:1 ratio) buffer resulting in 15 μg of protein being loaded into each lane. Electrophoresis was executed at 60 V for 30 min followed by 1.5 h at 150 V. Electrophoresed gels along with extra thick blot paper and 0.2-μm pore-sized nitrocellulose membranes were allowed to equilibrate in transfer buffer containing 20% (vol/vol) methanol for 30 min before transfer. Transfer was executed using semi-dry consumables and the Turbo-blot transfer system (Bio-rad, Gladesville, Australia) set to 40 min at 25 V and 1.0 A. Transfer membranes were then rinsed briefly in tris-buffered saline tween 20 (TBS-T) and then incubated in ~20 mL of LiCor™ blocking buffer at room temperature for 1 h. Membranes were again rinsed briefly in TBS-T and then incubated with a 1:500 dilution of the C219 antibody in TBS-T overnight. The β-actin antibody was added to incubation solution for only the final 20 min of the overnight primary antibody incubation step, to avoid saturation of the actin signal, at a dilution of 1:10,000. Following 4 × 10 min membrane washes in TBS-T, the membranes were incubated in LiCor™ goat anti-mouse secondary antibodies for 2 h at room temperature followed by the same washing regime as above. Membranes were scanned on the LiCor Odyssey IR imaging instrument, and densitometric analysis was executed via the ImageJ software. Data were normalized to β-actin signal and expressed as fold changes compared to controls.

P-gp Knockdown by siRNA Transfection

To confirm that the ICW was able to detect changes in P-gp abundance, the hCMEC/D3 cell line was treated with siRNA against MDR1. Briefly, cells were seeded at densities of 35,000 cells/cm^2 on collagenated plastic, and left to grow for 48 h. On the day of transfection (48 h after seeding), a solution containing 4 separate 5-nM siRNA complexes (with the target sequences: ACCGGACATCCCAGTGCTTCA, AACATTCGCTATGGCCGTGAA, GACAGAAAGCTTAGTACCAAA, and ATCGAGTCACTGCCTAATAAA) was mixed with 3% (vol/vol) HiPerFect Transfection reagent in serum-free EBM2 media, and allowed to incubate at room temperature for 10 min to allow siRNA transfection complexes to form. These solutions were then delivered to the cells dropwise (200 or 20 μL/well for 6-well and 96-well plates, respectively), and the cells were left to incubate with these complexes for 8 min. After 8 min, each well received 1.8 or 0.18 mL of serum-containing EBM2 media (6-well or 96-well plates), and then left to incubate at 37°C for 48 h. After this 48-h siRNA incubation period, cells were either fixed for ICW or lysed for PCR or WB analysis. Additional wells were treated with a scrambled siRNA sequence for use as a negative control, against which the statistical comparisons were made. Before assessing the above siRNA protocol for P-gp knockdown, identical procedures were executed on 96-well plates for cell viability analysis via the MTT assay. The MTT assay included 4 groups: (1) control, (2) transfection reagent alone, (3) P-gp siRNA + transfection reagent, and (4) scrambled siRNA + transfection reagent, and was executed as follows. After the 48-h transfection complex incubation period, all treatment/media solutions were discarded, and the cells were washed twice with 150 μL of warm PBS. All wells were then treated with 160 μL of FBS-free EBM2 media which contained 6.25% (vol/vol) of an 8-mg/mL MTT reagent solution. The plates were then wrapped in aluminum foil and left to incubate for a further 4 h. After the 4-h incubation with the MTT reagent, the solution was discarded, and 150 μL of DMSO was added to each well. The plates were then briefly shaken and incubated with DMSO for a further 30 min to dissolve the MTT crystals. Once more the plates were briefly shaken, and then absorbance at 540 nm was recorded. Blank wells which had undergone all the above procedures except in the absence of cells were also present on the plate, an average of which was taken and subtracted from each individual reading recorded. The absorbances were then normalized against the average of the control values, to be expressed comparatively as % viability when compared to the control group.

Verification of MDR1 Gene Downregulation by PCR

Total RNA from mock and siRNA transfected hCMEC/D3 cells was isolated using an RNeasy Plus Mini Kit (Qiagen). Each PCR reaction mixture (25 μL) contained 12.5 μL iScript™ 2X probes RT-PCR reaction mix, 0.5 μL iScript™ reverse transcriptase, 0.695 μL of Taqman® primer/probe, 100 ng of RNA (in 5 μL), and 6.305 μL nuclease-free water. Measurement of gene expression by

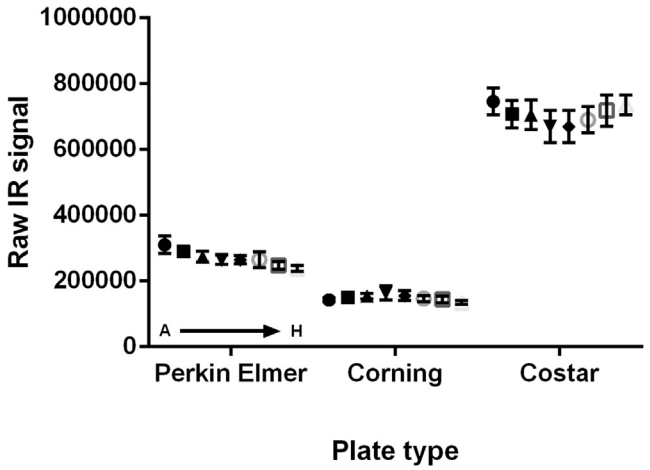

Figure 1. IR signal from 8 rows (a-h, displayed on graph from left to right for each plate type) of 3 different plate types when scanned on the LiCor Odyssey imager with the same scanning settings used in all subsequent experiments (microplate2 setting, 3-mm focus offset, scan intensity = 10). Left: Black polystyrene ViewPlate-96 F TC (Perkin Elmer); middle: Black TC-treated, clear flat bottom wells (Corning); right: transparent, clear flat bottom 96-well plates, sterile but untreated (Costar). The Corning plate exhibited superior inter-row consistency and low auto-fluorescence among the plate types tested. Data are presented as mean ± SD (n = 12 wells/row).

quantitative analysis was carried out in a CFX96 system (Bio-Rad). Thermocycling was performed at 50°C for 10 min, 95°C for 5 min, followed by 50 cycles of 95°C for 15 s and 60°C for 30 s. The threshold cycles (Ct) were calculated automatically using the CFX manager software. To determine relative gene expression between scrambled siRNA and P-gp-directed siRNA transfected cells, the fold change method ($2^{-\Delta\Delta Ct}$) was employed using Equations 2 and 3, with glyceraldehyde 3-phosphate dehydrogenase and β-actin employed as reference genes. The geometric mean of the Ct values for the 2 reference genes (Ct reference) were used in the calculation:

$$\Delta Ct = Ct_{(P-gp)} - Ct_{(reference)} \quad (2)$$

$$\Delta\Delta Ct = \Delta Ct_{(siRNA\ transfected\ cells)} - \Delta Ct_{(scrambled\ siRNA\ cells)} \quad (3)$$

Verification of P-gp Upregulation by Functional P-gp Assay

For assessment of functional upregulation of P-gp, hCMEC/D3 cells were seeded onto 24-well plates at a density of 35,000 cells/cm^2. Approximately 24 h later, when cells had reached 30%-50% confluency, the media was removed and replaced with 500 μL of media with 0.1% DMSO (control), or media containing the known P-gp upregulator, SR12813 (5 μM), before being left to incubate for 72 h. The relatively higher increase in P-gp expression observed by SR12813 (relative to rifampicin) guided the selection of this molecule for functional analysis. After the 72-h growth period, the accumulation experimental protocol was commenced, based on the protocol developed by Tai et al.[15] Initially, the drug solutions were removed and all wells were rinsed twice with 500 μL of pre-warmed PBS, before being re-incubated for 15 min on a shaker platform in transport buffer (10 mM 4-(2-hydroxyethyl)-1-piperazineethanesulfonic acid in HBSS, pH 7.40) again containing 0.1% (vol/vol) DMSO or 5 μM SR12813. In addition, a subset of control and drug treated cells were incubated with 5 μM PSC833 (a P-gp inhibitor). After 15 min, the wells were then rinsed once more with 500 μL/well of transport buffer, which was then replaced with 500 μL of transport buffer containing 5 μM of the known P-gp substrate R123, in addition to the 5 μM SR12813 ± 5 μM PSC833. Cells were then left on gentle shaking inside an incubator for 60 min. After 60 min, each well was rinsed 3 times with 500 μL/well of ice-cold transport buffer, before being immediately lysed with ice-cold lysis solution (1% Triton X-100 in

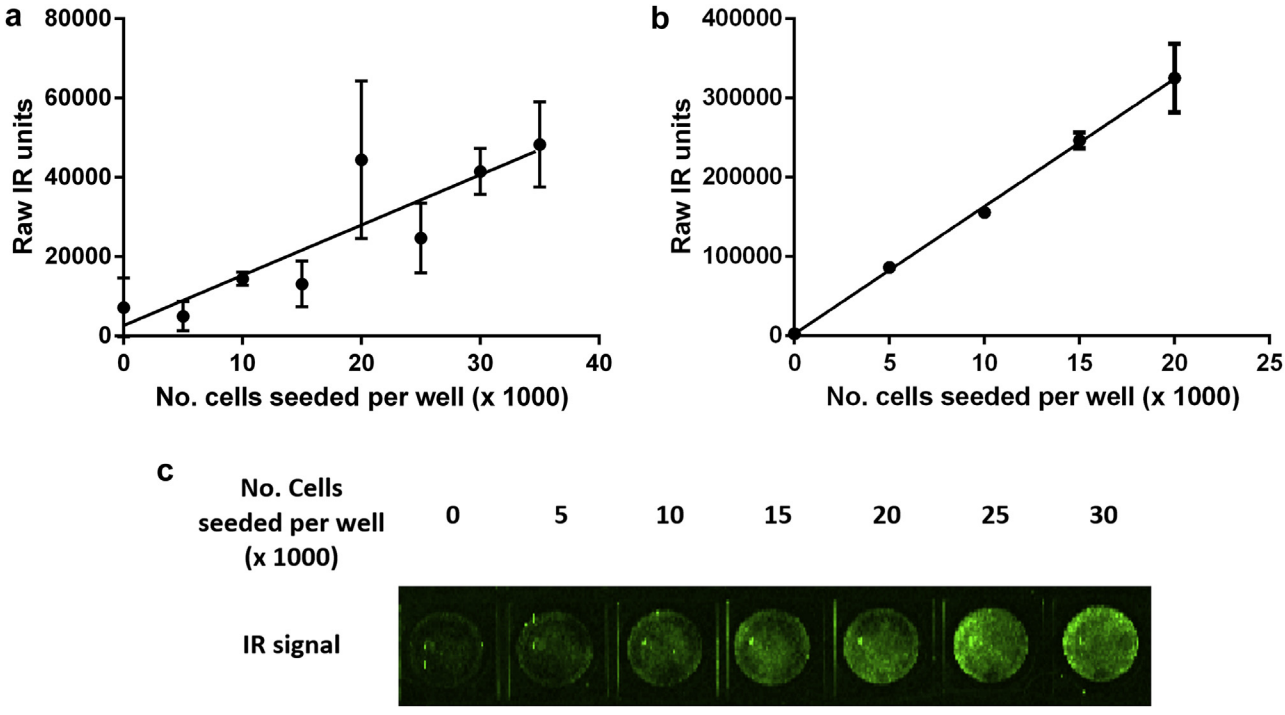

Figure 2. Iterative improvement of experimental protocol of ICW for P-gp in hCMEC/D3 cells: IR signal from P-gp as a function of known number of hCMEC/D3 cells seeded in (a) initial trial with signal:noise of only 10% and an R^2 = 0.64 and (b) final protocol with a signal:noise ratio of 98% and an R^2 of 0.98. Data are mean ± SD where n = 3. (c) Representative image of P-gp signal generated with increasing number of hCMEC/D3 cells by this developed and optimized ICW protocol.

Milli-Q water), for 15 min with gentle agitation at 4°C. After 15 min, the fluorescence of R123 in each individual well was measured using an Enspire fluorescence spectrophotometer (PerkinElmer, Waltham, MA), with an excitation wavelength of 511 nm and an emission wavelength of 534 nm. The unknown concentrations of R123 were determined by comparison to standard solutions of known concentrations of R123 which were prepared in the same matrix (1% Triton X-100 in Milli-Q) and on the same day as the accumulation experiment and pipetted into and scanned in a 24-well plate. Immediately after fluorescence was measured, two 20-μL aliquots from each well were removed and dispensed onto a non-sterile 96-well plate for protein content analysis. This new 96-well plate was then processed and compared to a freshly prepared standard curve for protein quantification using the BCA protein kit and bovine serum albumin as a standard. The accumulation of R123 was then expressed as nmol of R123 per μg of total protein per well.

Statistical Analysis

All statistical analyses were executed using the GraphPad Prism 6 software. All data are presented as mean ± SD and the number of biological replicates is in most cases conveyed by representation by individual data points on each graph. For experiments comparing differences between 2 groups only, a Student's t-test was used, and for all experiments considering 3 or more groups, statistical differences were assessed by a one-way ANOVA, using a *post hoc* Tukey's test, unless otherwise stated.

Results

Selection of Appropriate 96-Well Plate for ICW

The first experiment assessed the magnitude and consistency of light interference and plate auto-fluorescence in several plate types to help guide plate selection. As shown in Figure 1, the row to row variation in inherent signal magnitude was surprisingly marked in both Perkin Elmer and Costar plates, highlighting their incompatibility with the assay. The Corning plates appeared to provide superior properties and thus this plate type was selected for further use in the development and optimization of the ICW protocol.

Construction of Standard Curves for IR P-gp Signal and Cell Number (Normalization) and Signal-to-Noise Ratio Optimization

The new ICW assay was trialed for signal detection for both the IR P-gp signal and the normalizing DAPI signal. Figures 2a and 2b show a standard curve of the IR P-gp signal as a function of increasing cell density in the initial trial (Fig. 2a) and then after a series of incremental changes in experimental protocol (Fig. 2b), including alterations in primary and secondary antibody concentrations, the addition of surfactant during secondary antibody incubation, the temporal extension of primary antibody incubation, alteration of light intensity settings, and the addition of multiple rinsing steps at the end of the protocol. In the initial trial experiment, the signal contribution to overall IR light was found to be only 10%, but after the optimization process this ratio reached >98%. Also improved was the linearity of the standard curve, which was initially calculated to have an R^2 of 0.64 (Fig. 2a), but which reached 0.98 in the final protocol (Fig. 2b), indicating a high degree of linearity. As shown in the *y*-axis of Figures 2a and 2b, signal magnitude was also enhanced approximately 8-fold, in the center of the final linear dynamic range, as a result of the optimization process. Figure 2c exemplifies the typical IR signal readout, where a fairly homogenous distribution of light emanates from each well, in this case increasing with cell density from left to right.

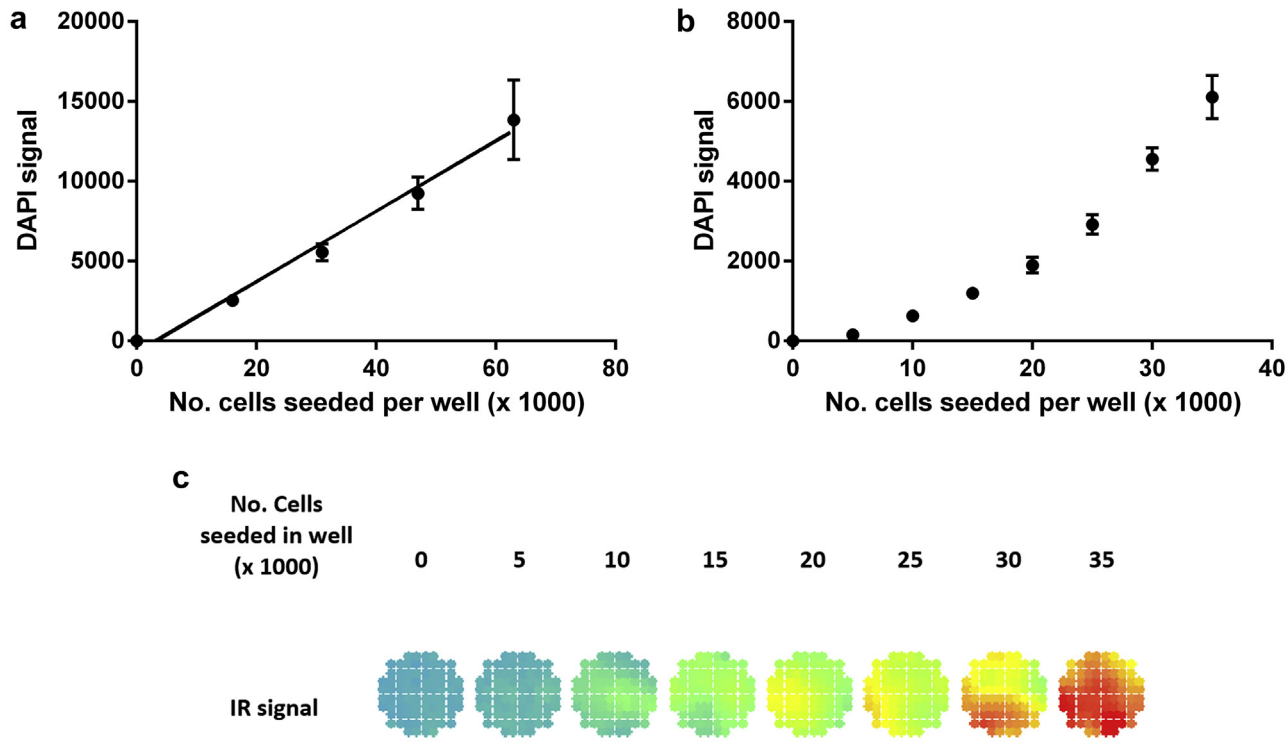

Figure 3. Linearity of DAPI signal as a function of number of hCMEC/D3 cells seeded. (a) Linear signal obtained when cells are fixed 4 h post seeding ($R^2 = 0.94$), and (b) exponential signal obtained when cells are fixed 24 h after seeding, at which point significant cell growth reveals differences in proliferation rates for different seeding densities. Data are mean ± SD where $n = 3$. (c) Representative image of DAPI heat map with increasing number of hCMEC/D3 cells generated by Perkin Elmer software.

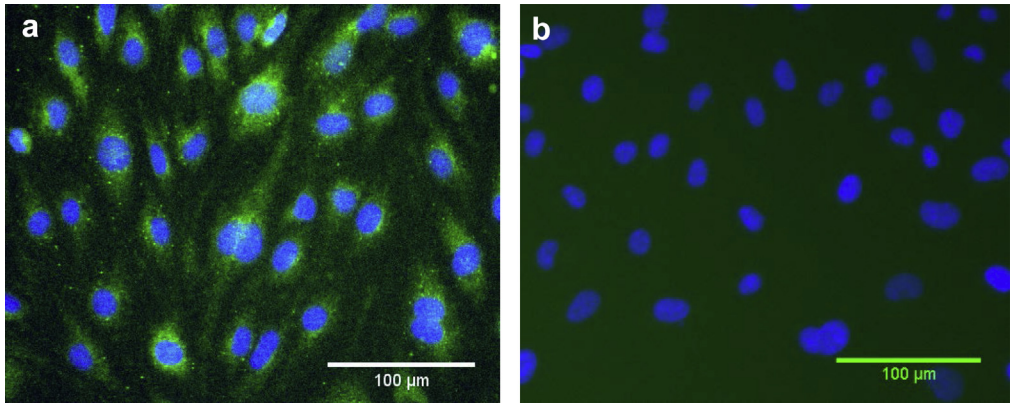

Figure 4. (a) hCMEC/D3 cells stained with FITC conjugated to C219 antibody for P-gp (green) and DAPI binding to DNA in cell nucleus (blue); (b) image generated same as above but in the absence of C219 P-gp antibody, showing vastly reduced green channel signal. Images demonstrate that the majority of the FITC signal originates from cell surfaces and organelles rather than inter-cell background regions and that non-specific secondary antibody binding is largely absent when the P-gp primary antibody is omitted from the protocol.

The same iterative process described above was applied simultaneously to the DAPI signal intended for use to normalize the P-gp signal to the number of cells in each well. The DAPI signal appeared to be quite consistent and robust in the first iteration, and did not require any further optimization. Figures 3a and 3b show the DAPI signal plotted as a function of increasing number of cells seeded into individual wells, either immediately after the completion of cell plating (4 h post plating) or after allowing for significant cell growth (24 h post plating). The difference between the profiles shown here (linear vs. exponential/sigmoidal) demonstrates an aspect of sensitivity in the assay. Figure 3a indicates that the DAPI signal reflects the intended linear increase in the number of cells with increasing cell density, and Figure 3b indicates that a relatively low cell density can retard cellular proliferation, due to the lower concentration of cell signaling factors within the growth setting, as has been demonstrated previously.[21] Figure 3c shows a DAPI heat map where increasingly red colors represent increasing cell density as detected by DAPI fluorescence.

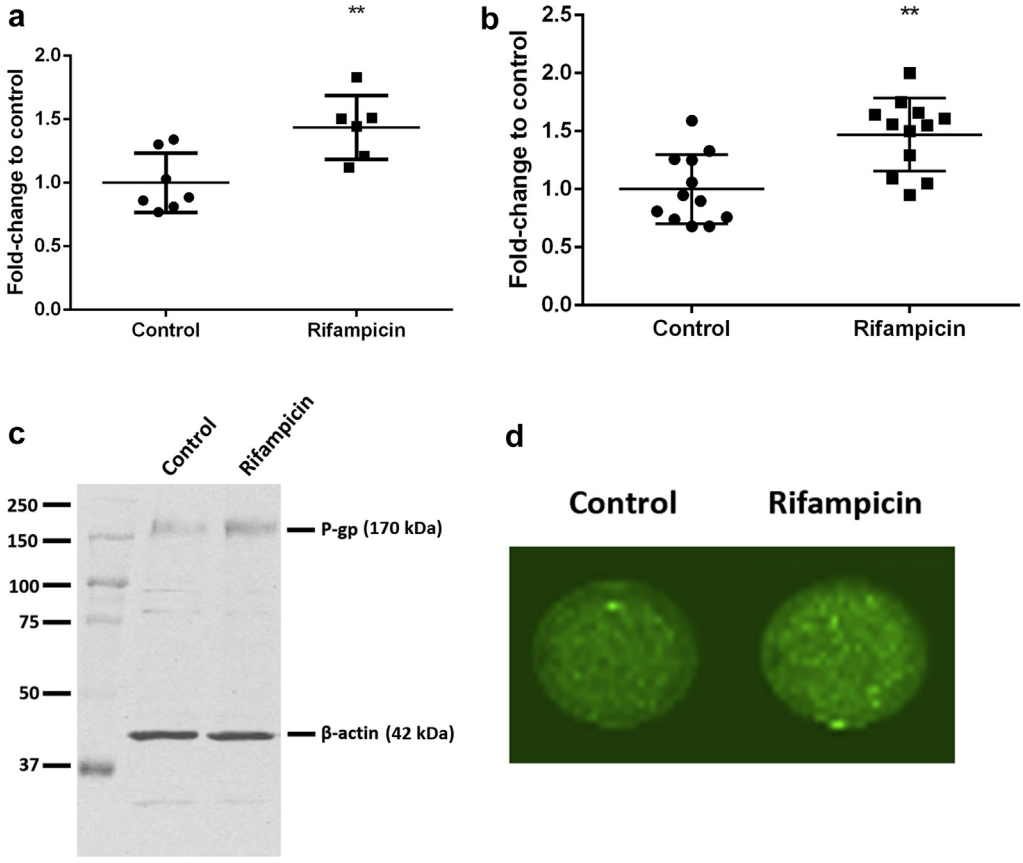

Figure 5. Use of known P-gp upregulator rifampicin for validation of P-gp ICW protocol. (a) 72 h treatment with 10 µM rifampicin led to a 1.4-fold upregulation when assessed by WB ($n = 6$-7); (b) the same treatment as above led to a 1.5-fold upregulation when assessed by ICW ($n = 12$); (c) representative western blot; and (d) representative image of IR P-gp signal from control well (left) and 10 µM rifampicin. Data shown are mean ± SD where $^{**}p < 0.01$, when compared to control via an unpaired t-test.

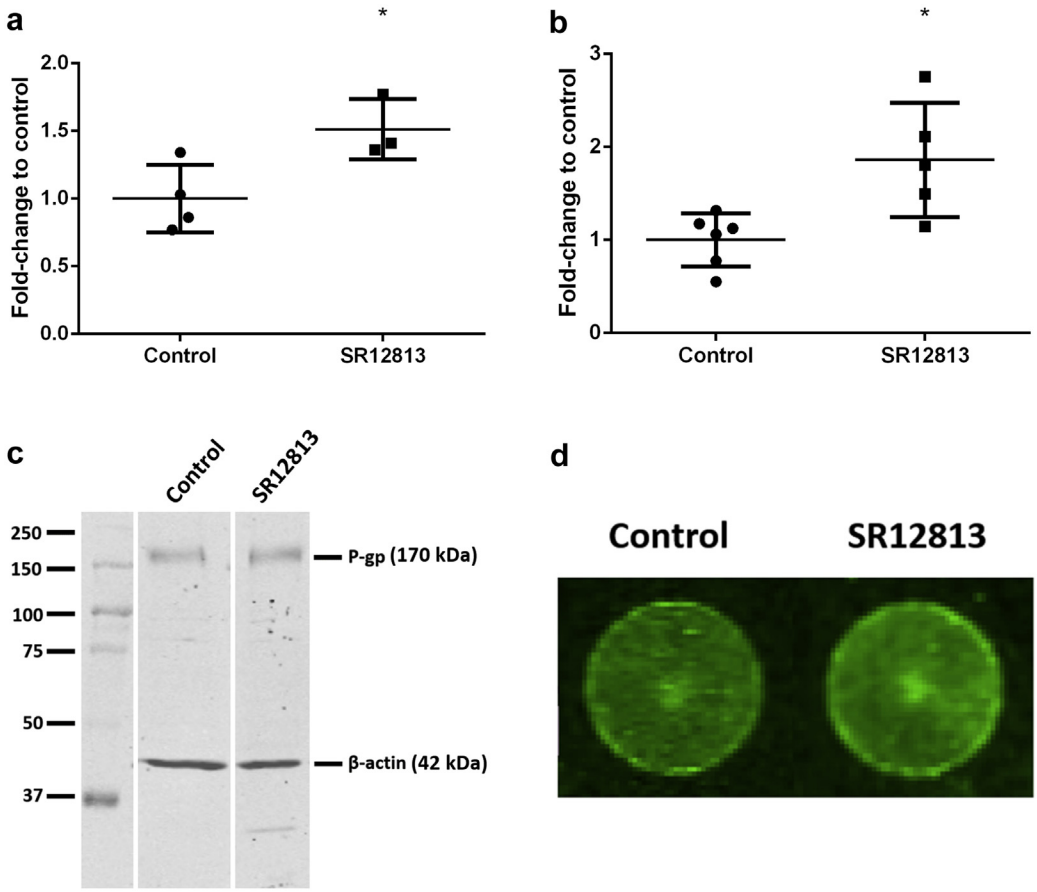

Figure 6. Use of known P-gp upregulator SR12813 for validation of P-gp ICW protocol. (a) 72 h treatment with 5 μM SR12813 led to a 1.5-fold upregulation as assessed by WB (n = 3-4); (b) 72 h treatment with 5 μM SR12813 led to a 1.9-fold upregulation as assessed by ICW (n = 5-6); (c) representative western blot; and (d) representative image of IR P-gp signal from control well (left) and well treated with 5 μM SR12813 (right). Data shown are mean ± SD where $^*p < 0.05$, when compared to control via an unpaired t-test.

Imaging of IR Antibody Signal Origin in hCMEC/D3 Cells

Once satisfactory standard curves relating hCMEC/D3 seeding density to the P-gp and DAPI signals had been obtained, it was necessary to confirm that the signal associated with both P-gp and DAPI was arising from the appropriate cellular origins. Therefore, an experiment utilizing the now established ICW protocol was executed with the IR emitting secondary antibody being substituted for the fluorescent FITC-conjugated secondary antibody to facilitate visualization by confocal fluorescence microscopy. As can be seen in Figure 4a, the green channel (FITC) displays an appreciable P-gp signal dispersed among the cell surface, and some trans-Golgi apparatus and endoplasmic reticulum staining, all above a visibly present but low background stain. The DAPI signal, shown in blue, correlated spatially with the FITC signal in an expected manner. Figure 4b shows an image taken under the same conditions but in the absence of primary antibody incubation. The very low level of green fluorescence in this image demonstrates the requirement of the P-gp antibody, supporting antibody specificity under the conditions of this assay.

Validation of P-gp ICW by Comparison to WB Using Known P-gp Regulators

The next phase of the ICW validation involved treating hCMEC/D3 cells with compounds which were shown previously in the literature to cause an upregulation in P-gp expression and to compare these results to those obtained using the traditional WB procedure. Figures 5a and 5b show the increased expression of P-gp by 1.4-fold and 1.5-fold after a 72 h treatment with rifampicin, when assessed by WB and ICW, respectively. Figure 5c illustrates a representative blot from this experiment, and Figure 5d represents the raw IR signal from one control well and one rifampicin treated well. Figures 6a and 6b show a 1.5-fold and 1.9-fold upregulation of P-gp following a 72-h SR12813 treatment, as assessed by WB and ICW, respectively. Representative examples of the WB and ICW results are depicted in Figures 6c and 6d respectively, where the intensity of the IR signal is visibly enhanced upon treatment of the hCMEC/D3 cell line with 5-μM SR12813. This close approximation to WB analysis by the new ICW protocol indicated that this new ICW assay was able to detect similar fold changes in P-gp expression as the traditional WB approach, but with the potential for moderate improvements in throughput.

P-gp Knockdown by siRNA Transfection

As an extra measure of confirmation that the ICW IR signal originated with P-gp, siRNA directed against P-gp was transfected into the hCMEC/D3 cell line. Initially, a cell viability assay (MTT) was utilized to ensure that the transfection reagents and siRNA samples did not interfere with cellular density and metabolism. The MTT results, shown in Figure 7a, indicate that the transfection regime used herein did not appear to harm the normal functioning of the cells. As shown in Figure 7b, treating immortalized human brain endothelial cells with 4 separate siRNA target sequences resulted in a 55% reduction in available MDR1 mRNA, as assessed by PCR.

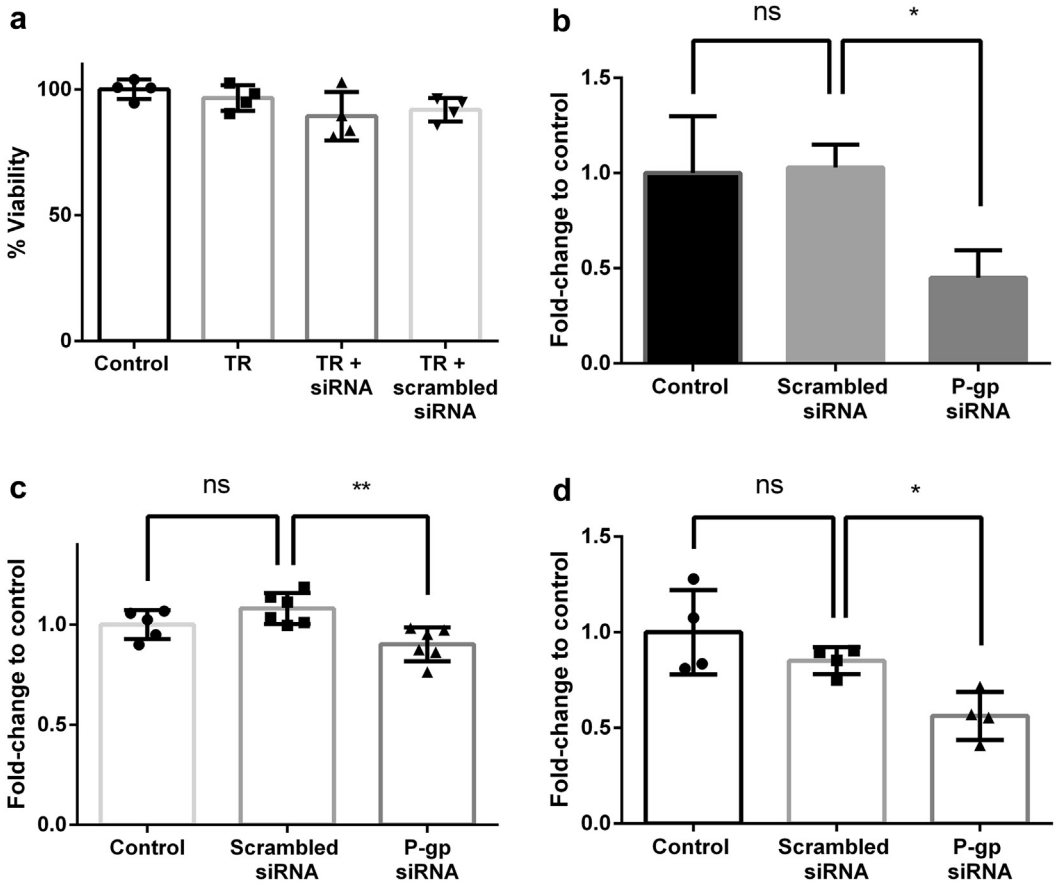

Figure 7. Resulting cell viability and knockdown of P-gp at the gene and protein level, after 48 h treatment with transfection reagent + siRNA directed against MDR1 or scrambled siRNA. (a) Cell viability assay demonstrating no significant differences observed in MTT metabolism between control, transfection reagent (TR), transfection reagent + P-gp siRNA; and transfection reagent + scrambled siRNA. (b) PCR assessment shows a 55% reduction in MDR1 mRNA expression between scrambled and P-gp siRNA treated groups ($n = 3$). (c) ICW assessment shows a 20% reduction in P-gp expression relative to scrambled siRNA control. (d) WB assessment shows a 35% reduction in P-gp expression relative to the scrambled siRNA control. All data were expressed as mean ± SD and assessed by one-way ANOVA with a *post hoc* Tukey's test, where $^{*}p < 0.05$ and $^{**}p < 0.01$.

When cells were treated with a non-specific target sequence, no significant alterations in MDR1 mRNA were found (Fig. 7b). This alteration in MDR1 mRNA by siRNA transfection was next analyzed via ICW. The P-gp siRNA transfection treatment produced a 20% reduction in P-gp expression when compared to the scrambled siRNA transfected control (Fig. 7c). The same experiment performed in 6-well plates to allow for WB analysis showed a 35% decrease in P-gp abundance in the siRNA-mediated knockdown group alone, compared to the scrambled siRNA sequence (Fig. 7d).

Verification of P-gp Upregulation by Functional P-gp Assay

In order to confirm that the observed upregulation of P-gp by ICW correlated appropriately with enhanced P-gp functionality, SR12813 treatment shown to produce the largest alteration in P-gp abundance was selected for use in a follow-on experiment. As shown in Figure 8, treatment of the hCMEC/D3 cell line with 5-μM SR12813 decreased R123 accumulation by 18%, while the negative control subset of cells incubated with the P-gp inhibitor PSC833 increased R123 accumulation by 80%.

Discussion

The WB protocol is a very useful method for protein quantification, but at times it can restrain the researcher's rate of decision making and scope of inquiry, by necessitating increased labor per each extra data point desired. Here we attempt to demonstrate the validity of a different method (ICW), with the aim of moderately increasing throughput. Before confidence in this new method could be experienced, the method needed first to be trialed, developed, and validated as an accurate and sensitive method for measuring P-gp abundance using hCMEC/D3 cells as a model of human brain endothelial cells, cells which express P-gp at a similar magnitude to human brain microvessels.[22]

During the development phase of assay preparation, multiple parameters were altered in an effort to improve the signal-to-noise ratio and magnitude. Changes in primary and secondary antibody concentration were altered to find an optimal balance between signal magnitude and the cost-effectiveness of the assay. Initially (first iteration), the primary and secondary antibody dilutions were set to an arbitrary starting point of 1:50 and 1:200, respectively, which yielded the poor signal-to-noise ratio of only 10% (Fig. 2a). An antibody optimization experiment indicated that the signal-to-noise ratio improved to 67%, when the primary and secondary dilutions were instead set to 1:20 and 1:2000, indicating that much of the noise in the initial iteration was due to non-specific binding of the concentrated secondary antibody. In another effort to reduce the initially high background, which is often caused by non-specific binding of secondary antibody, the concentration of Tween-20 in the secondary antibody buffer was increased from 0.1% to 0.5% (vol/vol). This increase in surfactant concentration reduced the background level of IR detection and increased again the signal-to-noise ratio to 87%, indicating that the provision of a hydrophobic alternative to that of the cellular matrix improved the signal-to-noise ratio by absorbing much

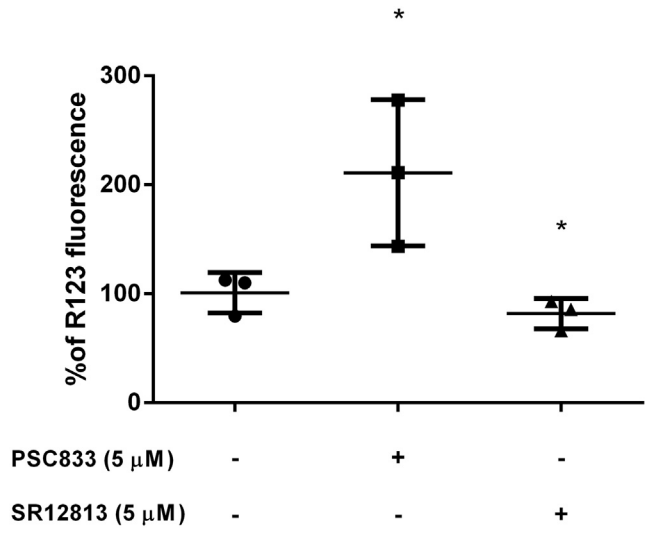

Figure 8. Accumulated R123 fluorescence normalized by milligram of protein and expressed as a % relative to the control after 72 h treatment with SR12813. Accumulation during incubation with PSC833 (P-gp inhibitor) causes an 80% increase in accumulated R123, relative to control ($p < 0.01$, positive control) and pre-incubation with SR12813 for 72 h reduced accumulation of R123 by 18% (*$p < 0.05$, all data were expressed as mean ± SD and assessed by one-way ANOVA with a *post hoc* Tukey's test).

of the non-specific secondary antibody binding. The final improvement in background reduction involved the addition of multiple extra rinsing steps after secondary antibody incubation. The initial trial (Fig. 2a) included only 3 post-secondary antibody rinses with PBS-T. Toward the end of the development process, the protocol was updated to 5 consecutive rinses in 200 μL of PBS-T, followed by 2 additional rinses with PBS to remove any residual surfactant which might interfere with light transmission. The addition of these final rinse steps increased the signal-to-noise ratio to its final value of 98%, which was considered satisfactory. The standard curves of both the IR P-gp signal and the DAPI nuclear stain (Figs. 2b and 3a, respectively) produced by using the final iteration of the ICW protocol showed a high degree of linearity with R^2 values of 0.94 and 0.98, respectively, over the range tested (5000-20,000 cells/well). Therefore, we define the detection limits of this assay between these seeding densities, which do capture the normal working densities for hCMEC/D3 cells. A typical cell seeding density for hCMEC/D3 cells into 96-well plates would approximate between 10,000 and 15,000 cells/well. When looking at the standard curves of both these signals, such seeding densities are well within the linear dynamic range of both the IR P-gp and DAPI standard curves. Future experiments utilizing the new ICW, however, would presumably interrogate P-gp regulation between 2 and 5 days after seeding, where cell density may have increased by a factor of 2-3 by that point in time. Producing linear standard curves under such conditions (after 2-5 days of growth) is however not possible, due to the nature of *in vitro* cell culture, where cell growth and expansion are hindered by the physical space of the wells. Therefore, the standard curves here served to show that both the P-gp and DAPI signals were in fact able to respond to increasing abundances of P-gp and nuclei, and that those signals were not saturable as near as possible to future experimental conditions.

During the development phase, we intentionally chose to use the nuclear DAPI stain for P-gp normalization rather than a "housekeeping protein," in order to avoid some of the apparent issues associated with this practice. It has been well reported in the literature that house-keeping protein expression levels fluctuate more than was previously understood, and that their high expression levels lead to saturated signals.[23-26] Since each cell can possess only one nucleus, DAPI reflects quite accurately the number of nuclei and therefore the number of cells within a given well, which ultimately is the intended purpose of normalization. It is this rationale combined with the robust and highly linear response from the DAPI molecule which validates this choice.

One of the main concerns when validating a new ICW is genuine signal origin. Unlike WB, there is no attached information about the size of the protein signal in the ICW result. Additionally, unwanted interactions between secondary antibody and the experimental reagents (blocking buffer, collagen, plastic, etc.) may occur and contribute to the observed signal, where the researcher may be unaware of such effects. To investigate the potential for these issues, cellular imaging in both the presence and absence of primary P-gp antibody was performed after execution of the final ICW protocol. In the hCMEC/D3 cell line, expression of matured P-gp should be observed at the cellular and lysosomal membranes,[27] as well as P-gp undergoing intracellular trafficking at the trans-Golgi apparatus and the endoplasmic reticulum.[27] Although the wide-field imaging system used in this study was not powerful enough to distinguish accurately between these various localizations and relative magnitudes of P-gp expression, it was successfully demonstrated that the signal obtained after ICW protocol did originate from the hCMEC/D3 cell body and not from intercellular space, with a high-concentration green channel light emphasizing the spindle-like shape of endothelial cells, over a much lower and homogenously distributed background stain (Fig. 4a). Furthermore, when a similar image was generated with an identical protocol but in the absence of the C219 P-gp primary antibody (Fig. 4b), the previously observed cell body staining was absent, above the same homogenous but low background. Therefore, these images served to build confidence that the observed signal was mostly genuine and specific for P-gp.

Once a seemingly satisfactory protocol had been developed, it was necessary to determine whether it was able to detect changes in P-gp expression resulting from pharmacological intervention, assessed side by side with the current standard technique of WB. Several treatments shown to alter P-gp expression in other laboratories were identified in the literature, and replication of these results was undertaken as evidence that the new assay was able to detect changes in P-gp abundance at a similar level of confidence to that of WB. Bendayan et al have worked extensively with P-gp inhibitors and upregulators, using WB to observe changes in P-gp expression. Bendayan et al had shown previously that known agonists of human pregnane X receptor were able to initiate an upregulation in P-gp abundance in hCMEC/D3 cells, as assessed by WB. A 2013 publication by this group showed that 72-h treatment with rifampicin or SR12813 caused a 1.9-fold and 2.2-fold increase in P-gp abundance, respectively, as assessed by WB.[28] When the studies were replicated via the ICW protocol, increases in P-gp abundance were indeed observed, albeit sometimes to a more modest degree. For each of the treatments trialed (rifampicin, SR12813, and siRNA targeted against MDR1), both methods produced approximately the same fold changes between WB and ICW, indicating that the ICW is able to produce results in concordance with those obtained using WB, whether those fold changes reflect increases or decreases in P-gp abundance.

It can be useful for researchers to distinguish between total cellular P-gp regulation and the portion of membrane-bound P-gp pertaining to cellular efflux specifically. Within this framework, the ICW is intended not as a standalone tool, but rather to be employed in parallel with functional R123 experiments to better understand the nature and relationship of the detected alterations. It is important to note, however, that the changes in P-gp abundance measured by either WB or ICW are not expected to correlate linearly with functional changes in P-gp by the R123 assay, for which there are several reasons. First, changes measured by WB or ICW represent total P-gp in the whole cell, whereas the functional R123

assay measures the activity of only the membrane component of cellular P-gp. Additionally, P-gp activity may be at or near the point of saturation when presented with the R123 concentrations typically used in P-gp function experiments, a feature which is necessary to achieve satisfactory R123 signal detection levels. Furthermore, R123 has been shown to be effluxed by transporters other than P-gp,[29] further hindering a straightforward relationship between P-gp expression and apparent function. Therefore, the 1.9-fold upregulation of P-gp by SR12813 corresponding to an 18% reduction of R123 accumulation appears as expected and appropriate, within the context of routine findings in our laboratory among others,[28,30] as well as confirming a link between observed P-gp expression by ICW and functional enhancement of P-gp activity.

In total, the validation process in this study included comparisons of pharmacologically treated samples between ICW and WB; siRNA knockdown of P-gp gene transcription; fluorescent images indicating appropriate P-gp signal origin; and finally correlation of observed P-gp expression by ICW with functional upregulation, as demonstrated by the fluorescent P-gp substrate R123. Taken together, the findings of this newly developed ICW protocol appear to provide a valid alternative for the detection of relative P-gp abundance in hCMEC/D3 cells. The 96-well plate format may allow researchers to assess the impact of interventions at multiple time points, or perform multiple experiments in parallel within the one plate, while requiring no additional labor time than is required by the processing of one WB. Therefore, the ICW method for assessing P-gp expression presented herein represents a viable alternative to WB, which can offer a modest but useful improvement in the rate of progress for researchers probing P-gp regulation and abundance.

Conclusion

This study has developed and validated a new ICW method for quantifying the expression of P-gp in hCMEC/D3 cells. The method facilitates a moderate improvement in throughput when compared to WB, and can occupy a place within standard protocols of the laboratories focused on P-gp regulation.

Acknowledgments

This project was funded by the National Health and Medical Research Council of Australia (grant 1048855) and the Bethlehem Griffiths Research Foundation.

References

1. Silva R, Vilas-Boas V, Carmo H, et al. Modulation of P-glycoprotein efflux pump: induction and activation as a therapeutic strategy. *Pharmacol Ther*. 2015;149:1-123.
2. Cordon-Cardo C, O'Brien JP, Casals D, et al. Multidrug-resistance gene (P-glycoprotein) is expressed by endothelial cells at blood-brain barrier sites. *Proc Natl Acad Sci U S A*. 1989;86:695-698.
3. Chin JE, Soffir R, Noonan KE, Choi K, Roninson IB. Structure and expression of the human MDR (P-glycoprotein) gene family. *Mol Cell Biol*. 1989;9:3808-3820.
4. Thiebaut F, Tsuruo T, Hamada H, Gottesman MM, Pastan I, Willingham MC. Cellular localization of the multidrug-resistance gene product P-glycoprotein in normal human tissues. *Proc Natl Acad Sci U S A*. 1987;84:7735-7738.
5. Fojo AT, Ueda K, Slamon DJ, Poplack DG, Gottesman MM, Pastan I. Expression of a multidrug-resistance gene in human tumors and tissues. *Proc Natl Acad Sci U S A*. 1987;84:265-269.
6. Ambudkar SV, Dey S, Hrycyna CA, Ramachandra M, Pastan I, Gottesman MM. Biochemical, cellular, and pharmacological aspects of the multidrug transporter. *Annu Rev Pharmacol Toxicol*. 1999;39:361-398.
7. Binkhathlan Z, Lavasanifar A. P-glycoprotein inhibition as a therapeutic approach for overcoming multidrug resistance in cancer: current status and future perspectives. *Curr Cancer Drug Targets*. 2013;13:326-346.
8. Davis TP, Sanchez-Covarubias L, Tome ME. P-glycoprotein trafficking as a therapeutic target to optimize CNS drug delivery. *Adv Pharmacol*. 2014;71:25-44.
9. McCaffrey G, Davis TP. Physiology and pathophysiology of the blood-brain barrier: P-glycoprotein and occludin trafficking as therapeutic targets to optimize central nervous system drug delivery. *J Investig Med*. 2012;60:1131-1140.
10. Schinkel AH. P-glycoprotein, a gatekeeper in the blood-brain barrier. *Adv Drug Deliv Rev*. 1999;36:179-194.
11. Callaghan R. Providing a molecular mechanism for P-glycoprotein; why would I bother? *Biochem Soc Trans*. 2015;43:995-1002.
12. Miller DS, Bauer B, Hartz AM. Modulation of P-glycoprotein at the blood-brain barrier: opportunities to improve central nervous system pharmacotherapy. *Pharmacol Rev*. 2008;60(2):196-209.
13. Kuhnke D, Jedlitschky G, Grube M, et al. MDR1-P-glycoprotein (ABCB1) mediates transport of Alzheimer's amyloid-beta peptides—implications for the mechanisms of Abeta clearance at the blood-brain barrier. *Brain Pathol*. 2007;17:347-353.
14. Lam FC, Liu R, Lu P, et al. beta-Amyloid efflux mediated by p-glycoprotein. *J Neurochem*. 2001;76:1121-1128.
15. Tai LM, Loughlin AJ, Male DK, Romero IA. P-glycoprotein and breast cancer resistance protein restrict apical-to-basolateral permeability of human brain endothelium to amyloid-beta. *J Cereb Blood Flow Metab*. 2009;29:1079-1083.
16. Vogelgesang S, Cascorbi I, Schroeder E, et al. Deposition of Alzheimer's beta-amyloid is inversely correlated with P-glycoprotein expression in the brains of elderly non-demented humans. *Pharmacogenetics*. 2002;12:535-541.
17. Liu X, Ma T, Qu B, Ji Y, Liu Z. Pesticide-induced gene mutations and Parkinson disease risk: a meta-analysis. *Genet Test Mol Biomarkers*. 2013;17:826-832.
18. Westerlund M, Belin AC, Olson L, Galter D. Expression of multi-drug resistance 1 mRNA in human and rodent tissues: reduced levels in Parkinson patients. *Cell Tissue Res*. 2008;334:179-185.
19. Qosa H, Miller DS, Pasinelli P, Trotti D. Regulation of ABC efflux transporters at blood-brain barrier in health and neurological disorders. *Brain Res*. 2015;1628:298-316.
20. Weksler BB, Subileau EA, Perriere N, et al. Blood-brain barrier-specific properties of a human adult brain endothelial cell line. *FASEB J*. 2005;19:1872-1874.
21. Todaro GJ, Green H. Quantitative studies of the growth of mouse embryo cells in culture and their development into established lines. *J Cell Biol*. 1963;17:299-313.
22. Ohtsuki S, Ikeda C, Uchida Y, et al. Quantitative targeted absolute proteomic analysis of transporters, receptors and junction proteins for validation of human cerebral microvascular endothelial cell line hCMEC/D3 as a human blood-brain barrier model. *Mol Pharm*. 2013;10:289-296.
23. Ferguson RE, Carroll HP, Harris A, Maher ER, Selby PJ, Banks RE. Housekeeping proteins: a preliminary study illustrating some limitations as useful references in protein expression studies. *Proteomics*. 2005;5:566-571.
24. Gorr TA, Vogel J. Western blotting revisited: critical perusal of underappreciated technical issues. *Proteomics Clin Appl*. 2015;9:396-405.
25. Welinder C, Ekblad L. Coomassie staining as loading control in Western blot analysis. *J Proteome Res*. 2011;10:1416-1419.
26. Li R, Shen Y. An old method facing a new challenge: re-visiting housekeeping proteins as internal reference control for neuroscience research. *Life Sci*. 2013;92:747-751.
27. Fu D, Arias IM. Intracellular trafficking of P-glycoprotein. *Int J Biochem Cell Biol*. 2012;44:461-464.
28. Chan GN, Patel R, Cummins CL, Bendayan R. Induction of P-glycoprotein by antiretroviral drugs in human brain microvessel endothelial cells. *Antimicrob Agents Chemother*. 2013;57:4481-4488.
29. van der Sandt IC, Blom-Roosemalen MC, de Boer AG, Breimer DD. Specificity of doxorubicin versus rhodamine-123 in assessing P-glycoprotein functionality in the LLC-PK1, LLC-PK1:MDR1 and Caco-2 cell lines. *Eur J Pharm Sci*. 2000;11:207-214.
30. Tai LM, Reddy PS, Lopez-Ramirez MA, et al. Polarized P-glycoprotein expression by the immortalised human brain endothelial cell line, hCMEC/D3, restricts apical-to-basolateral permeability to rhodamine 123. *Brain Res*. 2009;1292:14-24.

Pharm Res
https://doi.org/10.1007/s11095-018-2377-6

RESEARCH PAPER

Ionophore and Biometal Modulation of P-glycoprotein Expression and Function in Human Brain Microvascular Endothelial Cells

Mitchell P. McInerney[1] • Irene Volitakis[2] • Ashley I. Bush[2] • William A. Banks[3,4] • Jennifer L. Short[5] • Joseph A. Nicolazzo[1]

Received: 8 January 2018 / Accepted: 26 February 2018

ABSTRACT

Purpose Biometals such as zinc and copper have been shown to affect tight junction expression and subsequently blood-brain barrier (BBB) integrity. Whether these biometals also influence the expression and function of BBB transporters such as P-glycoprotein (P-gp) however is currently unknown.

Methods Using the immortalised human cerebral microvascular endothelial (hCMEC/D3) cell line, an in-cell western assay (alongside western blotting) assessed relative P-gp expression after treatment with the metal ionophore clioquinol and biometals zinc and copper. The fluorescent P-gp substrate rhodamine-123 was employed to observe functional modulation, and inductively coupled plasma mass spectrometry (ICP-MS) provided information on biometal trafficking.

Results A 24-h treatment with clioquinol, zinc and copper (0.5, 0.5 and 0.1 μM) induced a significant upregulation of P-gp (1.7-fold) assessed by in-cell western and this was confirmed with western blotting (1.8-fold increase). This same treatment resulted in a 23% decrease in rhodamine-123 accumulation over a 1 h incubation. ICP-MS demonstrated that while t8his combination treatment had no effect on intracellular zinc concentrations, the treatment significantly enhanced bioavailable copper (4.6-fold).

Conclusions Enhanced delivery of copper to human brain microvascular endothelial cells is associated with enhanced expression and function of the important efflux pump P-gp, which may provide therapeutic opportunities for P-gp modulation.

KEY WORDS blood-brain barrier · clioquinol · ionophore · P-glycoprotein · transporter

ABBREVIATIONS

Aβ	Amyloid beta peptide
AD	Alzheimer's disease
APS	Ammonium persulfate
BBB	Blood-brain barrier
BMEC	Brain microvascular endothelial cells
CNS	Central nervous system
CQ	Clioquinol
DAPI	4′,6-diamidino-2-phenylindole
EBM2	Endothelial basal medium 2
EDTA	Ethylenediaminetetraacetic acid
HBSS	Hank's balanced salt solution
hCMEC/D3	Immortalised human cerebral microvascular endothelial cell line
ICP-MS	Inductively coupled plasma mass spectrometry
ICW	In-cell western
IR	Infra-red
MTT	3-(4,5-dimethylthiazol-2-yl)-2,5-diphenyltetrazolium bromide
P-gp	P-glycoprotein
PBS	Phosphate buffered saline
PSC833	Valspodar
R123	Rhodamine-123
SDS	Sodium dodecyl sulfate
TEMED	Tetramethylethylenediamine

✉ Joseph A. Nicolazzo
joseph.nicolazzo@monash.edu

[1] Drug Delivery, Disposition and Dynamics, Monash Institute of Pharmaceutical Sciences, Monash University, 381 Royal Parade Parkville, VIC, 3052, Australia

[2] The Florey Institute of Neuroscience and Mental Health, Parkville, VIC Australia

[3] Division of Gerontology and Geriatric Medicine, Department of Medicine, University of Washington School of Medicine Seattle, Washington, USA

[4] Geriatrics Research Education and Clinical Center, Veterans Affairs Puget Sound Health Care System, Seattle, Washington, USA

[5] Drug Discovery Biology, Monash Institute of Pharmaceutical Sciences Monash University, Parkville, VIC, Australia

Published online: 05 March 2018

TRIS	Tris(hydroxymethyl)aminomethane
WB	Western blot

INTRODUCTION

The blood-brain barrier (BBB) is a dynamic interface which separates the brain parenchyma from the systemic circulation, and serves to protect the brain from xenobiotic insult, whilst simultaneously permitting a high influx of central nervous system (CNS)-essential nutrients (1). To facilitate these needs, a large range of transporter proteins are expressed within the specialised endothelial cells that line the lumen of the BBB (2). Over decades of transporter characterisation research, one of these transporters, P-glycoprotein (P-gp), has emerged as of particular interest in both drug discovery efforts and the pathophysiology of some disease states. P-gp is expressed on the luminal face of the brain endothelium (3), where from the lipid milieu of plasma membrane bilayer it actively effluxes xenobiotics (4), pharmaceuticals and endogenously produced substrates. The existence of P-gp at the BBB has hindered the success of many attempts at brain-targeted drug discovery, whereby many otherwise pharmacologically sound molecular entities are denied CNS access, by virtue of P-gp activity (5). P-gp is also associated with a pathological role in tumorigenesis, where sustained upregulation of P-gp can be a key defensive feature, preventing cellular access of chemotherapeutic agents (6).

It is also becoming increasingly apparent that P-gp plays a pivotal role in the prevention of some disease states, such as that of Alzheimer's disease (AD) (7). In AD, the noxious amyloid-beta (Aβ) which is thought to be responsible for downstream neurodegeneration, is steadily produced by neurons, and cleared from the brain by several mechanisms to prevent accumulation (8). Active efflux of Aβ across blood-brain barrier (BBB) represents one of the main clearance mechanisms of Aβ from the brain parenchyma (9–11), and P-gp appears to play a role in both brain-to-blood efflux of Aβ, as well as in preventing blood-borne Aβ from diffusing or endocytosing back into the brain (12,13). Although the timelines and causes of the observed reductions are not yet fully understood (7), waning P-gp expression has been observed within the pathophysiological cascade of AD, which likely corresponds to a reduced capacity for healthy Aβ trafficking (14,15). Thus it has been suggested that approaches to increase the expression or activity of P-gp by pharmacological means may aid in the treatment of AD, by restoring BBB efflux mechanisms of Aβ trafficking, and subsequently halting the accumulation of Aβ within the CNS (16,17).

Since P-gp activity is of such interest to CNS-drug access, oncology and AD research, understanding the various biological inputs for P-gp expression is of importance. One potential mechanism for upregulating P-gp is the redistribution of biometals within brain endothelial cells, which has been shown previously to contribute to BBB integrity in a positive manner. Whilst this area is relatively unexplored, some encouraging studies have been conducted. Zinc ions have been shown for example to protect BBB diffusion integrity in juvenile rats (18), and elsewhere Zn^{2+} was demonstrated as essential in maintaining cultured porcine endothelial barrier function (19). More recently, additional studies have also shown that in primary brain microvascular endothelial cells (BMECs), copper at low concentrations increases cell viability and proliferation (20), and that copper alongside vascular endothelial growth factor is a stimulatory driver of angiogenesis in the rat vascular endothelium (21). Thus it was hypothesised that enhanced delivery of zinc or copper ions to human BMECs might facilitate the upregulation of the key AD-related efflux transporter, P-gp.

A set of pharmacological tools available for enhancing the delivery of biometals to cell interiors are a class of drugs known as the ionophores. One of the early ionophores, clioquinol (CQ), has been shown previously to enhance the delivery of both copper and zinc ions across cell membranes and into the cytosol of neurons, where these ions are then freed to influence cell signalling pathways in a positive manner, with respect to AD (22). Additionally, a nine week treatment of CQ in APP2576 transgenic mice (a mouse model of familial AD that overexpresses a mutant form of amyloid precursor protein, resulting in elevated levels of both soluble and plaque entombed Aβ), produced a 49% reduction in Aβ brain deposition (23). Since CQ was able to ameliorate the AD phenotype in this mouse model via the redistribution of metal ions within the brain, it is possible that CQ may have the potential to traffic plasma-bound biometals in or out of the brain endothelium en route to the brain, with the potential of influencing BBB transporter expression profiles along the way. Therefore, it was hypothesised that by enhancing brain endothelial cell levels of Cu^{2+} and Zn^{2+}, CQ may be able to upregulate P-gp expression and function at the BBB. Herein we used a recently developed and validated in-cell western (ICW) approach, which provides higher throughput and is less labour and consumable intensive than other methods such as western blotting (24), to assess whether CQ can shuttle metal ions into immortalised human cerebral microvascular endothelial cells (hCMEC/D3), resulting in upregulation of P-gp expression and function. The outcomes of these studies have the potential to provide insight into fundamental mechanisms governing the regulation of the important BBB efflux transporter P-gp, with implications for both CNS drug delivery and Aβ clearance from the brain.

MATERIALS AND METHODS

Materials

4′,6-diamidino-2-phenylindole (DAPI), 3-(4,5-dimethylthiazol-2-yl)-2,5-diphenyltetrazolium bromide (MTT reagent), triton X-100, Tween-20, paraformaldehyde, sodium chloride, potassium chloride, disodium phosphate, rhodamine-123 (R123), potassium phosphate and Corning black polystyrene TC-treated 96 well plates were all purchased from Sigma Aldrich (St Louis, MO). TRIS buffer salt (TRIZMA base), sodium dodecyl sulphate (SDS), ammonium persulfate (APS), N,N,N′,N′-tetramethylethylenediamine (TEMED), trypan blue, glycerol, Trypsin-ethylenediaminetetraacetic acid (EDTA) solution 0.25% in Hank's balanced saline solution (HBSS) and Dulbecco's sterile phosphate buffered saline (PBS) were all purchased from Sigma Life Sciences (St Louis, MO). 40% acrylamide/bis solution was purchased from Bio-Rad Laboratories (Hercules, CA). Valspodar (PSC833) was a gift from Novartis (Basel, Switzerland). Odyssey PBS blocking buffer and the goat-anti-mouse secondary antibody were both purchased from Millennium Science (Mulgrave, Victoria, Australia). cOmplete Tablets Mini EASY pack protease inhibitors were purchased from Roche Diagnostics GmbH (Mannheim, Germany). Nitrocellulose membrane (0.2 μm pore-sized) was purchased from GE Life Sciences (Rydalmere, New South Wales, Australia). The C219 P-glycoprotein antibody was purchased from Australian Biosearch (Balcatta, Western Australia, Australia). Corning Costar transparent 96 well plates were purchased from Invitro (Noble Park North, Victoria, Australia). Fluorescein was purchased from Vector laboratories (Burlingame, CA). Black polystyrene ViewPlateR-96 F TC from Perkin Elmer, the Pierce IP lysis buffer and the BCA protein assay kit were all purchased from Thermo Fisher Scientific (Scoresby, VIC, Australia). Both Clonetics EBM-2 basal media and Clonetics EGM-2 single quots growth factor kits were purchased from Lonza (Walkersville, MD). Collagen type I was purchased from Corning Discovery Labware (Bedford, MD). Heat inactivated fetal bovine serum (FBS) was purchased from Life Technologies (Mulgrave, Victoria, Australia). 6 and 96-well plates were purchased from Corning Incorporated (Corning, NY). The purified water used in all experiments was obtained from a Millipore unit and filtered through a Q-pod fitted with a 0.22 μm membrane filter.

Seeding/Splitting of the hCMEC/D3 Cell Line

The immortalized human brain microvascular endothelial cell line (hCMEC/D3) was generously provided by Dr. Pierre-Olivier Couraud (INSERM, Paris, France). The EBM2 media which was used for all cell culture experiments, was prepared by supplementation with the following prior to commencement of the studies: 0.01% (*v*/v) ascorbic acid, 0.01% (v/v) gentamicin/amphotericin, 0.01% (v/v) hydrocortisone, 0.025% (*v*/v) epidermal growth factor, 0.025% (*v*/v) insulin-like growth factor, 0.025% (v/v) vascular endothelial growth factor, 0.1% (v/v), b-splice variant fibroblast growth factor, 10 mM HEPES, and 1% (*v*/v) penicillin/streptomycin and 2.5% (v/v) FBS. Vials of the hCMEC/D3 cell line were kept cryogenically frozen in liquid nitrogen in a solution comprised of 5% (v/v) DMSO in FBS solution. 1 mL vials containing approximately 2 million cells were dispensed into T-75 flasks containing 14 mL of EBM2 media, which had been precoated with 3 mL of a 0.1 mg/mL solution of Collagen type I and incubated for 1 h, before being washed with 10 mL of PBS to remove excess collagen. 2 h after seeding of the hCMEC/D3 cells, the initial media was aspirated off and the cells washed twice with warm PBS, before being replaced with fresh and warm EBM2 media. The media was then changed every 2 days until the flasks reached approximately 90–100% confluency, at which point they were split into new flasks or plates for subsequent experiments. All experiments involving cells being treated with CQ and/or metal ions Zn^{2+} and Cu^{2+}, involved the following preparation: cells were left to grow in EBM2 growth media until they had reached 70–80% confluency. At the commencement of treatment, in order to remove trace FBS from wells and thus prevent extensive protein binding by CQ, the media was always removed and the cells were rinsed twice with PBS, before the addition of FBS-free EBM2 media with or without CQ and/or Zn^{2+} and Cu^{2+}, in which the cells were incubated until the experimental endpoint. The cells were always stored in an incubator that was kept continuously at 37°C, with an air composition of 95% O_2 and 5% CO_2. All experiments performed using the hCMEC/D3 cell line occurred between passage 30 to 35.

Identification of Combinatorial CQ/Zn^{2+}/Cu^{2+} Toxicity in hCMEC/D3 Cells via Morphological Assessment and Cell Viability (MTT) Assay

hCMEC/D3 cells were seeded onto 96 well plates, at a density of 30,000 cells cm^{-2} and allowed to grow until reaching approximately 70–80% confluency. Cells were then washed twice with 150 uL of PBS and then re-nourished with 150 μL of FBS-free EBM2 media containing CQ, $ZnCl_2$ and $CuCl_2$ at increasing concentrations first individually, and in subsequent experiments, in combination. The 96-well plates were then returned to the incubator for 24 h, after which, the plates were transported to a temperature and humidity controlled chamber housing a microscope and camera for morphological assessment. The microscope used was the Nikon Ti-E from Nikon, Japan. The camera used to generate the images was a Photometrics Coolsnap Myo from Photometrics, USA. The 10 x objective lens used was Version 3.22 from Nikon. One image per treatment well

was captured before all treatment/media solutions were discarded, and the cells were washed twice with 160 µL of warm PBS. All wells were then treated with 160 µL of FBS free EBM2 media which additionally contained 6.25% (*v*/v) of an 8 mg/mL MTT reagent solution and then re-incubated for a further 4 h. After the 4 h incubation with the MTT reagent, the solution was aspirated off and 150 µL of DMSO was added to each well. The plates were then agitated for 30 s and then incubated with DMSO for a further 30 min. Again the plates were shaken for 30 s, and then absorbance at 540 nm was recorded on a Perkin Elmer absorbance spectrophotometer (Waltham, MA). Blank samples which had undergone all the above procedures except in the absence of cells were also present on the plate, an average of which was taken and subtracted from each individual reading recorded. The absorbance values were then normalized against the average of the control values, to be expressed comparatively as % viability when compared to the control group. Statistical comparisons of the datasets was performed using Dunnett's multiple comparisons test.

Influence of CQ/Zn^{2+}/Cu^{2+}Combinations on P-gp Expression Using an In-Cell Western Approach

hCMEC/D3 cells were seeded onto 96-well collagen-coated plates at a density of 30,000 cells/cm^2 and left to grow in 150 µL of EBM2 growth media until they had reached 70–80% confluency. Cells were then treated with individual and combinatorial treatments of CQ, $ZnCl_2$ and $CuCl_2$ in FBS free media for 24 h, after which the treatment solutions were discarded, and the expression of P-gp quantified by the previously reported ICW technique (24). Briefly, 150 µL of fixing solution (4% (*w*/*v*) paraformaldehyde in PBS) was transferred to each well, and the plate was left at room temperature for 20 min. The fixing solution was then discarded and cells were rinsed four times with 200 µL of cell permeabilisation solution (0.1% w/v Triton X-100 in PBS) under mild shaking. A final rinse using 210 µL of PBS was included to remove the detergent. Next, 150 µL of *Licor* PBS blocking buffer was added to each well and the plate was left to stir for 1 h at room temperature. The PBS blocking buffer solution was then removed, and 50 µL of PBS blocking buffer solution containing either a 1:50 dilution of the C219 P-gp antibody or no additional reagents (to be later used as secondary antibody controls) was added. The plate was then left overnight on gentle agitation at 4°C. The following day, each well was rinsed again four times with 200 µL of Tween washing solution (0.1% (*v*/v) Tween-20 in PBS, (PBS-T)). After removal of the last rinse, each well received 50 µL of PBS blocking buffer containing 0.5% (v/v) Tween-20, 1 µg/mL DAPI, and a 1:2000 dilution of *Licor* goat-anti-mouse (secondary) antibody. During secondary antibody incubation the plate was wrapped in aluminium foil and agitated gently at room temperature for 1 h. After this final incubation the plate was subjected to seven more 5 min rinses with 200 µL of PBS-T in each well, and the final two of these rinses using PBS to remove residual surfactant. The plate was then scanned on an *Odyssey* imager using the 'microplate2' setting with a 3 mm focus offset and the scan intensity of the 800 channel set to 5. After scanning, an ICW grid was applied to the obtained image within the *Odyssey* software, and the integrated intensity of IR signal from each well was then exported. The average of the IR signal of control wells that had not received P-gp primary antibody incubation was calculated and subtracted from all sample wells, to remove signal coming from non-specific binding of secondary antibody. The plate was then scanned in a *Perkin Elmer* fluorescence spectrophotometer with an excitation/emission wavelengths of 358 and 461 nm respectively. Wells treated only with collagen were used to calculate fluorescent background and subtracted from all other wells to discount any non-specific fluorescence. The remaining P-gp signal of treatment wells was then divided by the remaining DAPI signal, and finally expressed as fold change compared to the average of the control wells (not dissimilar to WB), according to Eq. 1:

$$Fold\ change = \frac{IR_t - IR_b}{F_t - F_b} \Big/ \frac{\sum_{i=1}^{n} \left(\frac{IR_c - IR_b}{F_c - F_b} \right)}{n} \quad (1)$$

where IR_t = the IR signal from treatment wells; IR_b = the infra-red signal from control wells treated with secondary antibody only (P-gp signal background subtraction); F_t = the fluorescence signal from treatment wells; F_b = the fluorescence signal from empty wells containing collagen only (DAPI background subtraction); IR_c = the IR signal from control wells; F_c = the fluorescence signal from control wells and n = the number of control replicates.

Confirmation of CQ/Zn^{2+}/Cu^{2+}Mediated Upregulation of P-gp Using Western Blotting

hCMEC/D3 cells were seeded onto 6-well collagen-coated plates at a density of 30,000 cells/cm^2 and left to grow in 2 mL of EBM2 growth media until they had reached 70–80% confluency. Cells were then treated with CQ, $ZnCl_2$ and $CuCl_2$ (0.5, 0.5 and 0.1 µM) in FBS free media for 24 h. Immediately after the 24 h incubation period, treatment solutions were discarded and to each well, 200 µL of a solution containing a 6:1 ratio of *Pierce IP* lysis buffer and a 7×–concentrated solution of cOmplete Tablets Mini EASY pack protease inhibitors, was dispensed into each well. Cells were then lysed in this solution for 15 min at 4°C, after which each well was scraped to ensure full detachment of cells. The solution from each well was transferred to a pre-cooled Eppendorf tube and spun at 14,000 rcf for 5 min before supernatant collection and protein content analysis via the *Pierce* BCA

protein assay kit using bovine serum albumin (BSA) as a standard. Western blotting was carried out by loading a 10% acrylamide 1 mm hand-cast gel with varying volumes of lysate/Laemlli (5:1 ratio) buffer resulting in 15 μg of total cellular protein being loaded into each lane. Electrophoresis was executed at 60 V for 30 min followed by 1.5 h at 150 V. Electrophoresed gels along with extra thick blot paper and 0.2 μm pore-sized nitrocellulose membranes were allowed to equilibrate in transfer buffer containing 10% (*v*/v) methanol for 30 min before transfer. Transfer was executed using semi-dry consumables and the Turbo-blot transfer system (*Bio-rad*, Gladesville, New South Wales, Australia) set to 40 min at 25 V and 1.0 A. Transferred membranes were then rinsed briefly in TBS-T and then incubated in ~20 mL of *Licor* blocking buffer at room temperature for 1 h. Membranes were again rinsed briefly in TBS-T and then incubated with a 1:500 dilution of the C219 antibody in TBS-T overnight. The β-actin antibody was added to the incubation solution for only the final 20 min of the overnight primary antibody incubation step, to avoid saturation of the actin signal at a dilution of 1:10,000. Following 4 × 10 min membrane washes in TBS-T, the membranes were incubated in *Licor* goat-anti-mouse secondary antibodies for 2 h at room temperature followed by the same washing regime as above. Membranes were scanned on the *Licor Odyssey* imaging instrument, and densitometric analysis was executed via the *ImageJ* software. Densitometric P-gp signals were normalised to β-actin signals and expressed as relative fold-changes to controls.

Influence of CQ/Zn^{2+}/Cu^{2+} on P-gp Function Assessed by R123 Trafficking

hCMEC/D3 cells were seeded onto two separate 24-well collagen-coated plates at a density of 30,000 cells/cm^2 and left to grow in 500 μL of EBM2 growth media until they had reached 70–80% confluency. Plate 1 was used for the analysis of R123 uptake and plate 2, processed in parallel until the final 10 min of experimentation, was used for the determination of R123 efflux. Upon reaching 70–80% confluency, cells were treated with either (1) no treatment (control) or (2) 0.5 μM CQ, 0.1 μM Zn^{2+} and 0.1 μM Cu^{2+}. Each of these treatment conditions contained 0.1% DMSO and each were administered in an identical fashion to replicates occurring on both plates. After a 24 h incubation, the uptake/efflux experimental protocol was commenced; all solutions were removed and the wells were rinsed twice with 500 μL of pre-warmed PBS. Following rinsing, the cells were then re-incubated in transport buffer (10 mM HEPES in HBSS, pH = 7.40), or transport buffer containing 5 μM PSC833 (a known P-gp inhibitor), for 15 min on a shaker platform. After 15 min the wells were rinsed once with 500 μL/well of transport buffer, which was then replaced with 500 μL of transport buffer (± 5 μM PSC833) with the addition of 5 μM of the known P-gp substrate R123. Both plates (still effectively identical at this stage) were then left on gentle shaking inside an incubator for 60 min. After 60 min, the experimental processing of the two plates diverged; plate 1 (R123 uptake) was rinsed three times with 500 μL per well of ice-cold transport buffer before being immediately lysed with ice-cold transport lysis solution (1% *v*/v Triton X-100 in MilliQ water), for 20 min and on gentle agitation at 4°C. After 20 min, the fluorescence of R123 in each individual well was measured using an *Enspire* fluorescence spectrophotometer (PerkinElmer, Waltham, MA), with an excitation wavelength of 511 nm and an emission wavelength of 534 nm. The unknown concentrations of R123 were determined by comparison to standard solutions of known R123 concentrations which were prepared in the same matrix (1% *v*/v Triton X-100 in milliQ water) on the day of the uptake experiments. Immediately after the fluorescence was measured, two 20 μL aliquots from each well were removed and dispensed onto a non-sterile 96 well plate for protein content analysis. This new 96-well plate was then processed and compared to a freshly prepared standard curve for protein quantification using a BCA protein kit and BSA dissolved in the same matrix used as standards, and these values were later used to normalise R123 content in individual wells. The wells in plate 2 (R123 efflux) were then also rinsed three times with 500 μL per well of ice-cold transport buffer, before being re-incubated in transport buffer (± 5 μM PSC833) for a further 10 min, again on gentle agitation. After this 10 min period, all wells in the plate were subjected to the same lysing protocol as described for plate 1, before the measurement of R123 fluorescence and determination of protein content (described above). The experiment was executed in such a way that both plates 1 and 2 received identical treatments with respect to time, excluding the 10 min efflux phase (plate 2 only). The R123 fluorescence values from the accumulation plates were first normalised by well specific protein content, and then expressed as a percentage relative to the control replicates. The data from the efflux plates were expressed as the percentage of R123 remaining after efflux, relative to the accumulation control wells.

Assessment of hCMEC/D3 Cellular Translocation of Zn^{2+} and Cu^{2+} by CQ Treatment

To identify whether treatment of hCMEC/D3 cells with CQ and different metal combinations resulted in enhanced cellular uptake of metals, the concentrations of Cu and Zn were measured by inductively coupled plasma mass spectrometry (ICP-MS). hCMEC/D3 cells were seeded onto two separate 24-well collagen-coated plates at a density of 30,000 cells/cm^2 and left to grow in 500 μL of EBM2 growth media until they had reached 70–80% confluency. Cells were then treated with the same treatment regime as was used for assessing P-gp

expression above (individual and combinatorial treatments of CQ, Zn^{2+} and Cu^{2+}) in FBS free media for 24 h. After 24 h of treatment (or alternative time points as illustrated in results figures), the media was removed and cells were rinsed twice with sterile PBS to wash out any plastic-bound metal ions, before the addition of 250 µL per well of 1% Triton X-100 in PBS. Lysis was carried out exactly as was described for western blotting (including protein quantification for normalisation), except for the omission of the cellular-debris removing centrifuge step, but including the removal of a 20 µL aliquot for protein quantification by the BCA assay, to later be used for normalising data against well-to-well variability in cell density. Samples were stored at −80°C until analysis by ICP-MS. After freeze-drying the samples, each lyophilised cell crude extract was resuspended by adding 30 µL of concentrated nitric acid 65% (Suprapur Merck, Darmstadt, Germany) and allowed to digest for 6 h at room temperature. The samples were heated at 90°C for 20 min using a heating block to complete the digestion. The reduced volume after digestion was ~20 µL. Each sample was made up to 1.150 mL by the addition of 1.130 mL of 1% (*v*/v) of nitric acid diluent. Measurements were made with an Agilent 7700 series ICP-MS instrument (Agilent Technologies, Santa Clara, CA) under routine multi-element operating conditions using a Helium Reaction Gas Cell. The instrument was calibrated using 0, 5, 10, 50, 100 and 500 ppb of certified multi-element ICP-MS standard calibration solutions (ICP-MS-CAL2–1, ICP-MS-CAL-3 and ICP-MS-CAL-4, AccuStandard, New Haven, CT) for a range of elements. A certified internal standard solution containing 200 ppb of Yttrium (Y89) as an internal control (ICP-MS-IS-MIX1–1, Accustandard, New Haven, CT) was used for internal calibration. For each individual treatment tested, wells containing no cells were also incubated in treatment solutions, and underwent the same procedure as just described, such that background signal caused by treatment/plastic contamination was quantified, and averages of these controls were subtracted from actual experimental metal concentrations. The remaining metal concentrations were then multiplied by the lysis volume (230 µL) to reach a molar quantity of metal ions, and then normalised by the protein content of each well measured during lysis, and resultantly expressed as nmol (metal)/mg of protein, according to Eq. 2:

$$Normalised\ [metal] = \frac{([cellular\ metal] - [blank\ metal]) \times V}{protein} \quad (2)$$

where [cellular metal] = the metal concentrations in treated cell samples determined by ICP-MS, [blank metal] = the metal concentrations in samples derived from wells which received treatment but contained no cells, V = the volume of lysis buffer after the removal of protein content sample (0.00023 L), and protein = protein mass per well determined by the BCA assay, used here to normalise against well-to-well variability in cell density.

Statistical Comparisons

All data were visualised and statistically analysed using the Prism Graphpad Version 7 software. All comparisons between two groups were assessed by Student's t-test, whilst all experiments involving more than two groups, were assessed by one-way analysis of variance (ANOVA), with multiple comparisons assessed by Dunnett's test, or Tukey's test in the case of ICP-MS. Differences between groups were considered significant if the generated *p* values fell below 0.05.

RESULTS

Identification of Combinatorial CQ/Zn^{2+}/Cu^{2+} Limits of Toxicity in hCMEC/D3 Cells

Before the chemical agents CQ/Zn^{2+}/Cu^{2+} could be assessed for modulation of P-gp, the toxicity of each agent individually and in combination against the hCMEC/D3 cell line had to first be assessed, so as to not unintentionally deliver toxic concentrations and induce P-gp upregulation by generic cellular defence mechanisms. Toxicity in this regard was assessed via the use of the MTT reagent alongside morphological assessment of the cells via microscopy. Each component of CQ, Zn^{2+} and Cu^{2+} was assessed over the concentration range of 0.1 to 10 µM. As shown in Fig. 1a and c, low concentrations of both CQ (0.1 and 0.5 µM) and Cu^{2+} (0.1 µM) actually stimulated metabolism of the MTT reagent (proxy for cell viability), causing 36 and 23% increases in formazan production, respectively. On these same figures it is observed that the highest concentrations of CQ and Cu^{2+} which did not induce detectable toxicity were 0.5 and 1 µM respectively. Figure 1b shows cell viability following Zn^{2+} treatment, and indicates that the cells tolerated the addition of Zn^{2+} up to a concentration of 1 µM.

Representative images from the morphological assessment are shown in Fig. 1d, e, f and are concordant with the results generated by the MTT assay, whereby cells treated with 0.5 µM of CQ (Fig. 1e) appear as normal compared to control cells, but in contrast those treated with 10 µM of CQ (Fig. 1f) exhibit visible pathological morphology. The same procedures were executed for treatment combinations of all three chemical agents (CQ/Zn^{2+}/Cu^{2+}), and the highest concentrations tolerated by the hCMEC/D3 cell line were 0.5, 0.5 and 0.1 µM for CQ/Zn^{2+}/Cu^{2+} in combination, respectively. Therefore these concentrations were chosen for the further experiments below regarding P-gp regulation, function and biometal trafficking.

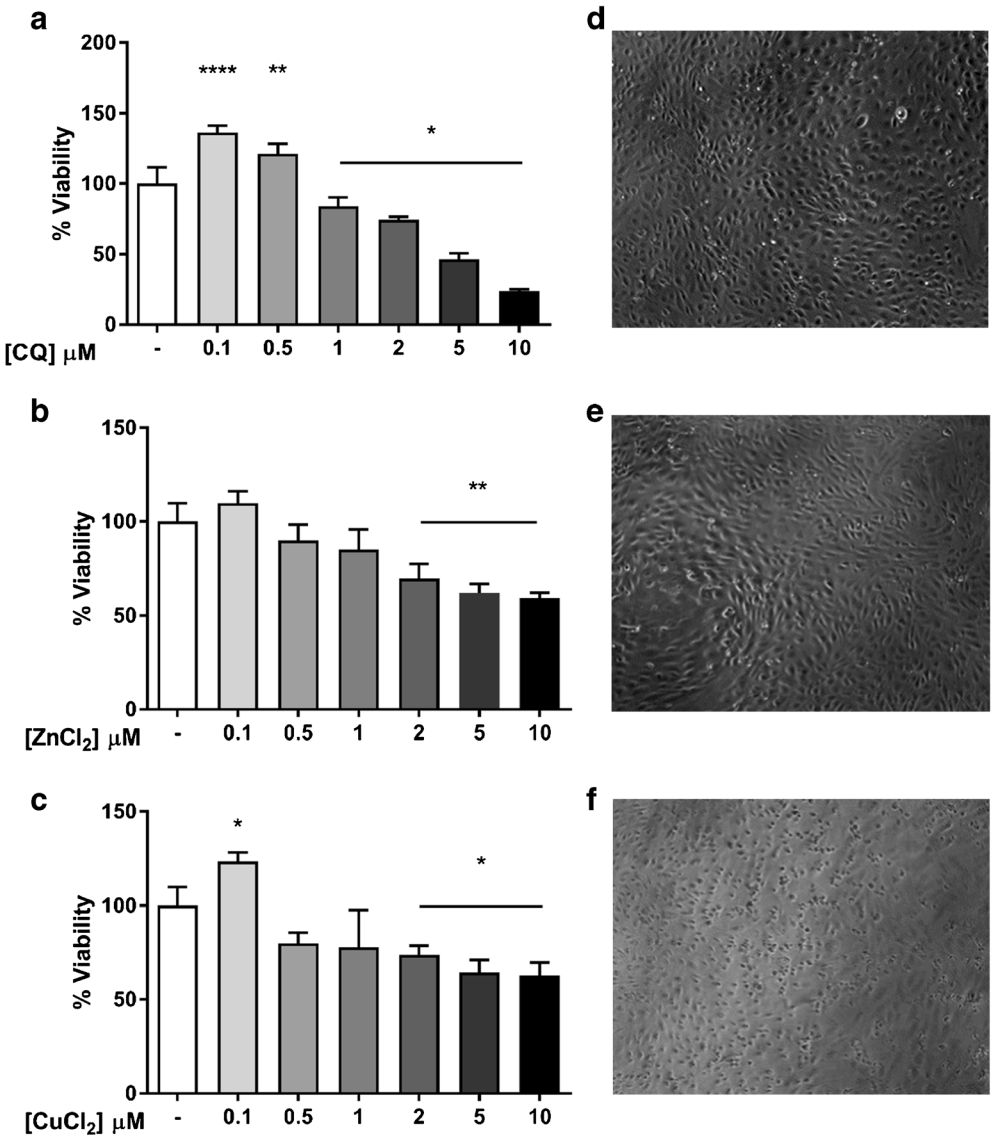

Fig. 1 Cell viability as assessed by cellular metabolism of the MTT reagent following treatment of hCMEC/D3 cells with increasing concentrations of the chemical agents CQ (**a**), Zn^{2+} (**b**) and Cu^{2+} (**c**). Lower concentrations of CQ and Cu^{2+} (0.5 and 0.1 μM respectively) increase cell viability whilst higher concentrations induce decreases in cell viability. Figures (**d**-**f**) are microscopic images of hCMEC/D3 cells used for morphological assessments of the following treatments (**d**) control indicating benchmark for normal morphology, (**e**) 0.5 μM CQ - normal morphology and thus indicating no toxicity and (**f**) 10 μM CQ - altered morphology indicating toxicity of treatment. All data shown were assessed by Dunnett's test, and bars represent mean ± SD where n = 3 and * denotes $p < 0.05$.

P-gp Expression in hCMEC/D3 Cells is Increased with Exposure to CQ/Zn^{2+}/Cu^{2+} Combination

A recently developed ICW protocol (24) was implemented to first assess whether CQ and the metal ions Zn^{2+} and Cu^{2+}, alone or in combination, were able to enhance P-gp expression in hCMEC/D3 cells. The highest non-toxic concentrations that were tolerated by the hCMEC/D3 cell line (both alone and in combination) were identified as 0.5 μM CQ, 0.5 μM Zn^{2+} and 0.1 μM Cu^{2+} via the MTT assay and morphological assessment. As shown in Fig. 2a and b, the only treatment group to significantly increase P-gp expression relative to control group after analysis via a Dunnett's one-way ANOVA, was the combination of all three components: CQ (0.5 μM), Zn^{2+} (0.5 μM) and Cu^{2+} (0.1 μM), which produced a 1.7-fold increase in P-gp abundance ($p = 0.0045$). Since each of the components (CQ, Zn^{2+} and Cu^{2+}) when tested alone had no significant effect on P-gp expression, this result indicated that the presence of CQ and both metal ions may be required for significant upregulation of P-gp. The influence of this treatment group on P-gp expression was then assessed by western blotting, to confirm the observed upregulation, and as shown in Fig. 2c, d, this combination produced a significant 1.8-fold upregulation of P-gp abundance ($p = 0.043$), similar to that observed with the ICW approach. All further studies assessing the influence of CQ/Zn^{2+}/Cu^{2+}on hCMEC/D3 dynamics were undertaken with this particular combination.

Functional Trafficking of the P-gp Substrate R123 is Enhanced Following CQ/Zn^{2+}/Cu^{2+} Treatment

Since P-gp is expressed and subsequently localised in two distinct regions of brain endothelial cells, namely, the outer cell membrane and the lysosomal membrane (25), an assay

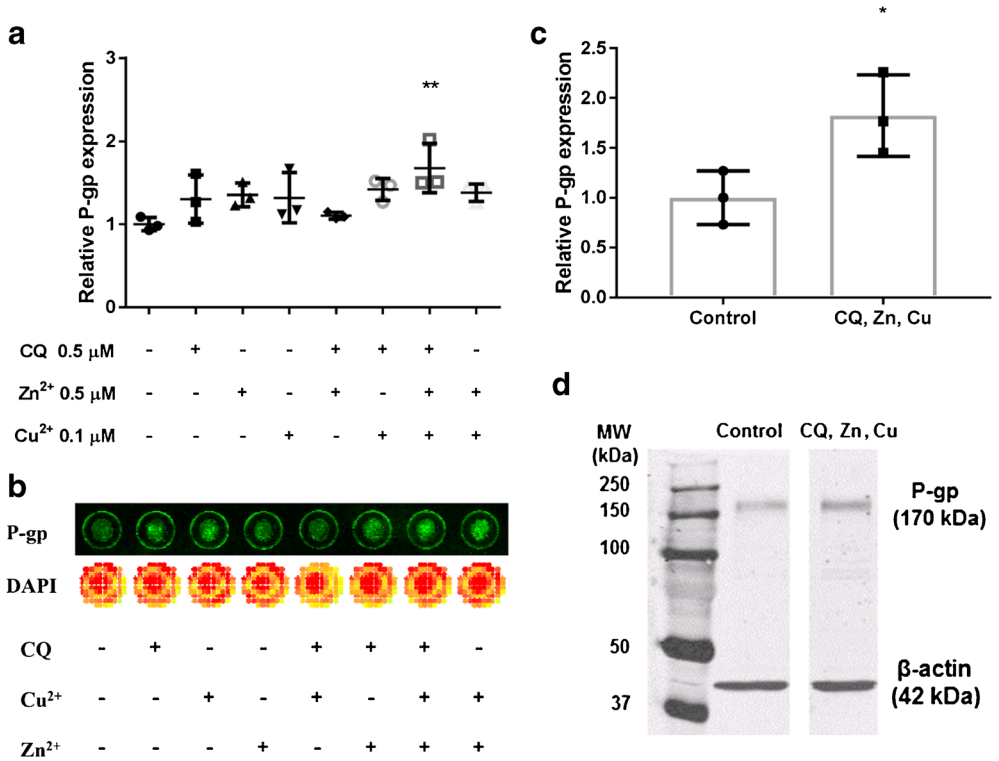

Fig. 2 Combinatorial assessment of P-gp upregulation after 24 h treatment with the chemical agents CQ (0.5 μM), Zn^{2+} (0.5 μM) and Cu^{2+} (0.1 μM). (**a**) Quantification of relative P-gp expression as assessed by the recently developed ICW protocol. Statistical significance was assessed by a two-way ANOVA (Dunnett's test where n = 3 and ** denotes $p < 0.01$). (**b**) Representative image of ICW results showing raw infrared P-gp signal (above) and cell number normalising DAPI heat map (below), indicating differential P-gp expression above homogenous inter-well cell distribution. (**c**) Quantification of relative P-gp expression between control and ICW-validated combination of CQ, Zn^{2+} and Cu^{2+} as assessed by western blotting. Statistical significance was assessed by a Students t-test (where n = 3 and * denotes $p < 0.05$). (**d**) Representative western blot for P-gp and β-actin of control versus combination of CQ, Zn^{2+} and Cu^{2+}. All data shown are individually plotted data points with bars representing mean ± SD.

utilising the known P-gp substrate R123 was used concomitantly, to ensure that any increase in P-gp expression resulted in increased cellular efflux capacity. Figure 3a illustrates the relative cytosolic accumulation of R123 after a 1 h incubation with the substrate in the presence or absence of the known P-gp inhibitor PSC833. The presence of PSC833 induced a 36% increase in R123 accumulation, whilst pre-incubation for 24 h with CQ (0.5 μM), Zn^{2+} (0.5 μM) and Cu^{2+} (0.1 μM) produced a 23% decrease in R123 accumulation. The inhibitory effect of PSC833 on R123 accumulation was offset by pre-incubation with CQ (0.5 μM), Zn^{2+} (0.5 μM) and Cu^{2+} (0.1 μM). After the accumulation phase, cells were presented with empty transport buffer (± PSC833) and allowed to efflux the substrate for 10 min before additional measurements were made, to demonstrate substrate flux in a bidirectional capacity. As shown in Fig. 3b, 32% of the initial R123 load remained in control cells, whilst PSC833 incubated cells retained 56% of the initial substrate load due to P-gp inhibition. The cells pre-treated with the $CQ/Zn^{2+}/Cu^{2+}$ combination however, retained significantly less R123 than control cells (23%), signifying a functional enhancement of P-gp activity in both reducing cellular accumulation of and increased efflux capacity of the R123 substrate. These findings indicate that the induction of P-gp was effective in a bidirectional capacity.

CQ Increases Intracellular Copper but Not Zinc, Measured by Inductively-Coupled Plasma Mass Spectrometry

As a part of identifying the mechanism by which CQ and metal ions were able to facilitate upregulation of P-gp, ICP-MS was employed to measure changes in cellular metal levels (zinc and copper) resulting from the same treatment regime as was assessed for P-gp upregulation above. Despite the complex experimental design and notable intra-treatment noise, three treatment groups (Cu^{2+}, CQ/Cu^{2+} and $CQ/Zn^{2+}/Cu^{2+}$) produced significant increases in cytosolic copper levels when compared to the control group via Tukey's test (Fig. 4a). No significant differences between the Cu^{2+} treatment and the P-gp upregulating combination ($CQ/Zn^{2+}/Cu^{2+}$) treatment groups were determined ($p = 0.12$, bars 4 and 7), however this comparison was hindered by the large study design, and was resolved in subsequent experiments. The same ICP-MS analyses

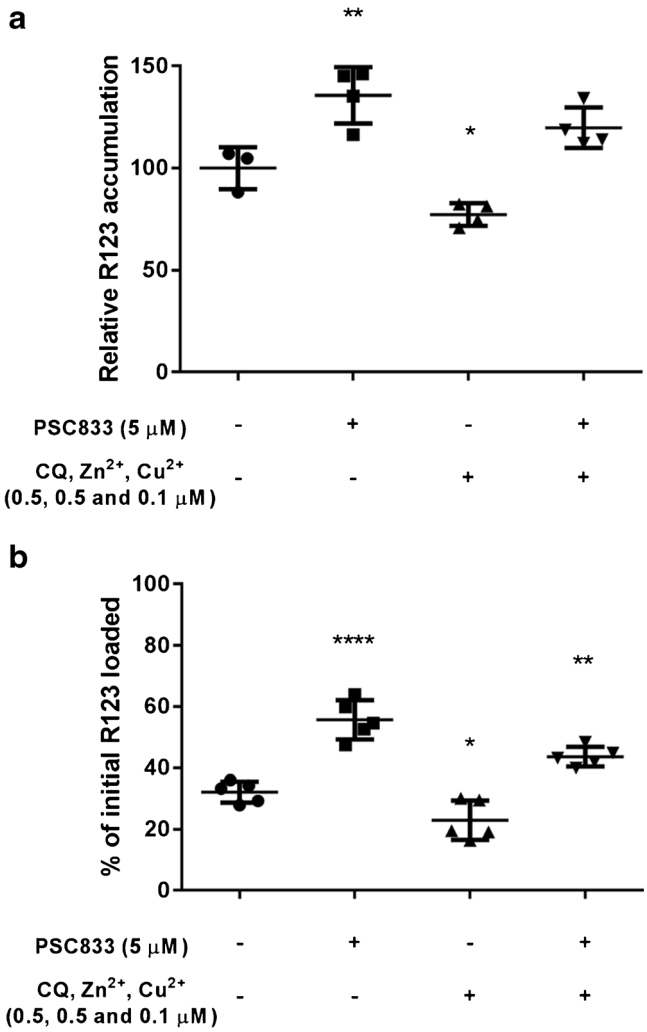

Fig. 3 Functional P-gp upregulation assessed by use of the known fluorescent P-gp substrate Rhodamine-123 (R123), normalised to well protein content via BCA protein assay. (**a**) Relative R123 accumulation is significantly increased (+36%) by assay co-incubation with the known P-gp inhibitor PSC833, and significantly decreased (−23%) after 24 h preincubation with the chemical agents CQ (0.5 μM), Zn^{2+} (0.5 μM) and Cu^{2+} (0.1 μM), assessed by two-way ANOVA (Dunnett's test where n = 3–4, * denotes $p < 0.05$ and ** denotes $p < 0.01$). (**b**) Percentage of initial R123 loaded remaining after 10 min of substrate efflux. Control cells retained 36%, cells coincubated with PSC833 retained significantly more R123 (56%, where **** denotes $p < 0.0001$) and cells receiving 24 h preincubation with the chemical agents CQ (0.5 μM), Zn^{2+} (0.5 μM) and Cu^{2+} (0.1 μM) retained significantly less R123 (23%), as assessed by two-way ANOVA (Dunnett's test where n = 5). All data shown are individually plotted data points with bars representing mean ± SD.

albeit for zinc is depicted in Fig. 4b. None of the eight treatment groups were able to significantly increase cytosolic zinc levels, suggesting that the observed effects of the CQ/Zn^{2+}/Cu^{2+} enhancing P-gp expression and function, are unlikely to be mediated by effects by Zn^{2+}, but rather by Cu^{2+}.

To gain further insight into CQ-mediated mechanisms of P-gp upregulation, the kinetics of free versus CQ-mediated copper uptake into hCMEC/D3 cells were assessed in parallel. Figure 5 shows free copper (in blue) increasing marginally over time, whilst CQ-mediated copper uptake (shown in red) resulted in a significantly larger copper increase, but only the final time point assessed (24 h). Taken together, this set of ICP-MS experiments indicate that whilst endogenous copper uptake mechanisms are apparent in hCMEC/D3 cells, CQ administered in combination with copper can enhance the delivery of copper to intracellular regions, as was hypothesised, presumably via the metal ionophore activity described above, although the significant increases of cytosolic copper mediated by this ionophore are only visible after 24 h.

DISCUSSION

P-gp plays an important role in many life science applications and disease states, and understanding the biological inputs modulating the expression and activity of P-gp is a valuable endeavour. Whilst it has been shown that biometals such as zinc and copper can influence the barrier like properties of the endothelium (18–21), the effects of metal ions on barrier transporter proteins such as P-gp are relatively unknown. This study attempted to identify whether enhanced uptake of either of the biometals zinc or copper by ionophoric delivery via the use of CQ could result in modulation of P-gp expression and/or activity.

To investigate this aim, the relative expression of P-gp was measured in an ICW assay, performed in the immortalised hCMEC/D3 cell line. This ICW approach has been validated previously by comparing modulated P-gp expression results with those derived from WB, after treatment with several known P-gp regulating compounds (24). The results from the ICW in this study indicated that only the combination of

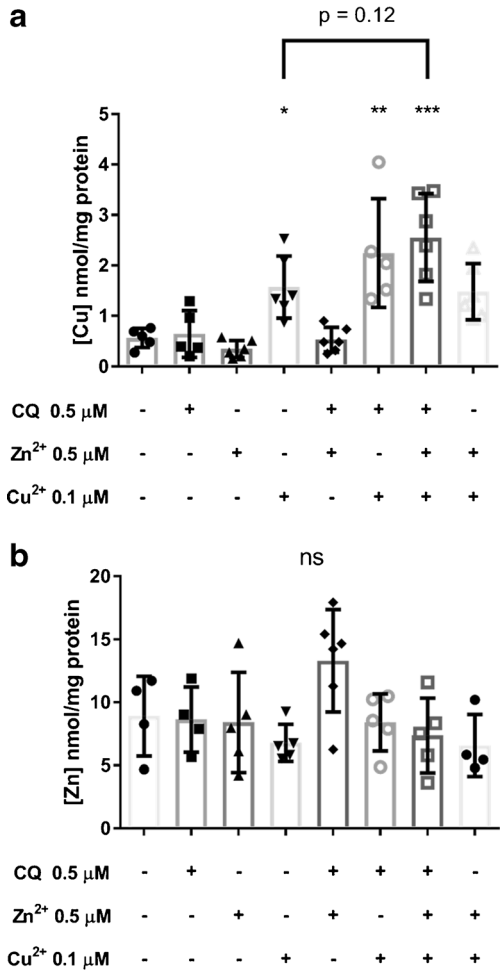

Fig. 4 Combinatorial assessment of metal ion accumulation assessed by inductively coupled plasma mass spectrometry, normalised to well protein content via BCA protein assay, after 24 h treatment by the chemical agents CQ (0.5 μM), Zn^{2+} (0.5 μM) and Cu^{2+} (0.1 μM). (**a**) Intracellular Cu levels are significantly increased by 0.1 μM Cu in isolation (bar 4 where * denotes $p < 0.05$), or by combination with CQ (bar 6 where ** denotes $p < 0.01$) or by combination with CQ and Zn (bar 7 where *** denotes $p < 0.001$), as assessed by two-way ANOVA (Dunnett's test where n = 5–6). Additional two-way ANOVA analysis via Tukey's test indicates near significant difference ($p = 0.12$) between treatment groups with Cu^{2+} alone (bar 4) and in combination with CQ and Zn (bar 7), indicating that CQ may enhance Cu uptake. (**b**) All treatment groups failed to increase intracellular Zn levels including CQ + Zn group (bar 5 where $p = 0.15$) as assessed by two-way ANOVA (Dunnett's test where n = 5–6). All data shown are individually plotted data points with bars representing mean ± SD.

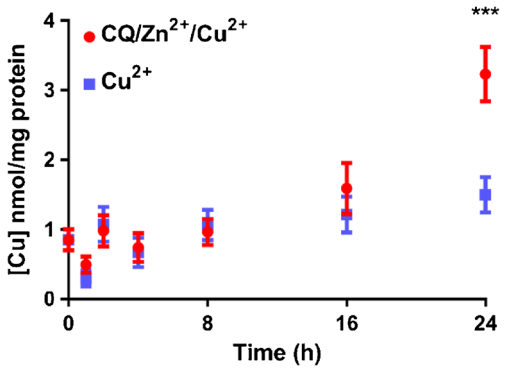

Fig. 5 Time-dependent assessment of intracellular Cu levels via inductively coupled plasma mass spectrometry, normalised to well protein content via BCA protein assay, after 1, 2, 4, 8, 16 or 24 h treatment with the chemical agents Cu^{2+} (0.1 μM) alone (shown in blue) or with combination shown to induce P-gp upregulation: CQ (0.5 μM), Zn^{2+} (0.5 μM) and Cu^{2+} (0.1 μM) (shown in red). No significant differences in copper accumulation between the two treatment groups are resolved until the final time-point of 24 h, (where *** denotes $p < 0.001$). Statistical comparisons were made between time matched groups via Student's t-test, and all data shown represent mean ± SEM where n = 3–6.

CQ, Zn^{2+} and Cu^{2+} (0.5, 0.5 and 0.1 μM) produced a statistically significant upregulation (1.7-fold) of P-gp expression. Use of the fluorescent P-gp substrate R123 showed that treating hCMEC/D3 cells for 24 h with the combination just described induced a reduction in R123 accumulation, and an increase in post-R123-loading efflux, indicating that the activity of P-gp had been functionally enhanced. This effect of P-gp functional enhancement was negated when cells were co-treated with the known P-gp inhibitor PSC833, indicating specific modulation of P-gp. These results were also confirmed by WB, which indicated a concordant 1.8-fold increase in P-gp expression. Previous studies have demonstrated links between biometal treatment and BBB integrity, barrier function, endothelial viability and angiogenesis in both *in vitro*, as well as murine and porcine *in vivo* systems (18–21). Since it has been shown elsewhere that tight junction proteins essential for barrier formation and function, and the expression for transporters like P-gp are both under the influence of similar signalling pathways (26,27), these findings of enhanced expression and function of P-gp via biometal delivery are consistent with the other experimental evidence available.

Investigation of biometal uptake into the endothelial cell line by ICP-MS revealed that despite the combination of CQ/Zn^{2+}/Cu^{2+} being required to achieve significant upregulation of P-gp, cytosolic zinc levels were not affected in the experimental paradigm used (Fig. 4b), indicating that zinc may not play a major role in the observed endothelial upregulation of P-gp. Treatment with copper alone (0.1 μM $CuCl_2$) was able to significantly increase levels of cytosolic copper from approximately 0.6 ± 0.2 nmol/mg of protein to 1.6 ± 0.6 nmol/mg of protein (Fig. 4a), but this increase did not appear to drive an increase in P-gp expression in the experimental paradigm that was explored (Fig. 1a). Under normal physiological conditions, BBB uptake of zinc and copper are mediated and regulated by endogenous biometal transporter proteins, divalent metal transporter 1 (DMT1; both zinc and copper) (28), and copper transporter 1 (CTR1; copper only) (28). The rate and extent of copper uptake however, is mediated by CTR1 expression, which has been shown to become downregulated by endothelial cells in the presence of relatively higher extracellular concentrations of copper, by a process of internalisation and recycling of the CTR1 transporter (29). Cytosolic protein-

mediated copper storage mechanisms also function within cells, to limit the biologically available copper and thus prevent toxicity (30). Therefore, therapeutically enhanced delivery of copper to cellular interiors might be required to drive the desired copper-mediated protein signalling and expression, such as the upregulation of P-gp. The use of the ionophore compound CQ appears to have achieved this aim. As assessed by ICP-MS, treatment of hCMEC/D3 cells with CQ/Cu^{2+} and CQ/Zn^{2+}/Cu^{2+} increased cytosolic copper to 2.2 ± 1.1 and 2.6 ± 0.9 nmol/mg of protein respectively (Fig. 4a). Whilst these average increases (compared to the 0.1 μM Cu^{2+} treatment group value of 1.6 ± 0.6 nmol/mg of protein) did not reach statistical significance due to the large study design, subsequent experiments were able to resolve this difference. When time-dependent copper uptake in hCMEC/D3 cells was measured in a separate experiment as shown in Fig. 5, CQ-mediated copper delivery was observed as significantly enhanced at the 24-h time point when compared to uptake of free copper alone, but not in earlier time-point measurements (3.2 ± 1 *vs* 1.5 ± 0.6 nmol/mg of protein respectively). This experiment demonstrates that while endogenous endothelial copper uptake is rate and extent limited, copper delivery to cell interiors can be enhanced by the use of biometal ionophores such as CQ.

Whilst encouraging, the data presented herein are subject to some limitations. Firstly, due to the high proportion of protein binding (31), it was required for CQ to be administered to cells in serum free media, which represents a divergence from physiological conditions, where proteins appear ubiquitously in all biological fluids and will most likely interact with CQ *in vivo*. Additionally, the lysis protocol used for the generation of the ICP-MS data was designed intentionally to leave the cells largely intact, and thus to observe and quantify only cytosolic and cytosolically protein-bound biometals in our analysis. As a result, any biometals that were taken up by the cells and immediately utilised for cellular processes such as incorporation into plasma membrane bound proteins, etc. may not have been measured in our experiments, potentially leading to an underestimation of biometal uptake, in the case of both endogenous and CQ-mediated copper uptake.

Despite these limitations, we find that the data presented in this study provides firm ground upon which to base further experiments. Most obvious is the need to identify the mechanism by which increased intracellular copper is able to drive P-gp expression. Copper interacts with a host of cell proteins (32), some of which may be upstream of P-gp expression signalling mechanisms. Cu^{2+} has also been shown to inhibit glycogen synthase kinase 3 (22), a signalling molecule which has been demonstrated to be an integral part of the Wnt/β-catenin signalling pathway that serves as one input for P-gp expression (33,34), and which has been reported to be functional in hCMEC/D3 cells (34). Another possibility is the stabilisation of P-gp at the plasma membrane. Normally, P-gp exhibits the presence of a divalent magnesium ion, the concentration of which influences marginal control over P-gp stability and activity, but which is not essential for P-gp activity (35). An increase of Cu^{2+} ion influx through the plasma membrane might have the potential to displace Mg^{2+} ions, subsequently stabilising P-gp at the plasma membrane. Studies to elucidate the mechanism of CQ/Cu^{2+} mediated upregulation of P-gp are currently underway, alongside investigations in animal models, to interrogate the broader context of the *in vitro* findings observed within this study.

These studies have highlighted that CQ together with biometals, can increase the expression and function of P-gp in BBB phenotypical cells. It is possible, therefore, that part of the Aβ-lowering effects of CQ reported previously (23,36) may result from increased BBB efflux of Aβ, since Aβ is a substrate of P-gp, although further studies to confirm this hypothesis are required to be undertaken. Furthermore, this study has revealed a potential role of Cu^{2+} in regulating the expression and function of P-gp at the BBB, which is a novel finding. Given that P-gp is a major hindrance to the CNS entry of many therapeutic agents intended to reach the brain, it is possible that intentional manipulation of brain endothelial cell Cu^{2+} levels could be exploited to reduce P-gp expression and enhance CNS delivery of drugs which are substrates of P-gp. In addition, drugs such as CQ which modulate the brain endothelial cell levels of Cu^{2+} have the potential to result in interactions with drugs which are substrates of P-gp, as the enhanced P-gp expression mediated by CQ could reduce the CNS entry of drugs with high affinity to P-gp.

CONCLUSION

When co-administered with copper at nanomolar concentrations, CQ is able to produce significant upregulation of P-gp, in an immortalised human cerebral microvascular endothelial cell line. Enhanced P-gp expression appears to be associated with increased intracellular copper uptake, and future studies will interrogate the mechanism mediating the increase of this important efflux transporter, along with the biological relevance of these findings within *in vivo* systems.

ACKNOWLEDGMENTS AND DISCLOSURES

The studies completed within this publication were funded by the following sources; NHMRC Project APP1048855; the Mason Foundation and the Bethlehem Griffiths Research Foundation. Mitchell P. McInerney is supported by an Australian Government Research Training Program Scholarship.

REFERENCES

1. Hawkins BT, Davis TP. The blood-brain barrier/neurovascular unit in health and disease. Pharmacol Rev. 2005;57(2):173–85.
2. Zlokovic BV. Neurovascular pathways to neurodegeneration in Alzheimer's disease and other disorders. Nat Rev Neurosci. 2011;12(12):723–38.
3. Tatsuta T, Naito M, Oh-hara T, Sugawara I, Tsuruo T. Functional involvement of P-glycoprotein in blood-brain barrier. J Biol Chem. 1992;267(28):20383–91.
4. Callaghan R. Providing a molecular mechanism for P-glycoprotein; why would I bother? Biochem Soc Trans. 2015;43(5):995–1002.
5. Punitha AD, Srivastava AK. CNS drug targeting: have we travelled in right path? J Drug Target. 2013;21(9):787–800.
6. Fletcher JI, Williams RT, Henderson MJ, Norris MD, Haber M. ABC transporters as mediators of drug resistance and contributors to cancer cell biology. Drug Resist Updat. 2016;26:1–9.
7. McInerney MP, Short JL, Nicolazzo JA. Neurovascular alterations in Alzheimer's disease: transporter expression profiles and CNS drug access. AAPS J. 2017;19(4):940–56.
8. Selkoe DJ. Alzheimer's Disease. Cold Spring Harb Perspect Biol. 2011;3(7):a004457–7.
9. Roberts KF, Elbert DL, Kasten TP, Patterson BW, Sigurdson WC, Connors RE, *et al.* Amyloid-beta efflux from the central nervous system into the plasma. Ann Neurol. 2014;76(6):837–44.
10. Shibata M, Yamada S, Kumar SR, Calero M, Bading J, Frangione B, *et al.* Clearance of Alzheimer's amyloid-ss(1-40) peptide from brain by LDL receptor-related protein-1 at the blood-brain barrier. J Clin Invest. 2000;106(12):1489–99.
11. Qosa H, Abuasal BS, Romero IA, Weksler B, Couraud PO, Keller JN, *et al.* Differences in amyloid-beta clearance across mouse and human blood-brain barrier models: Kinetic analysis and mechanistic modeling. Neuropharmacology. 2014;79C:668–78.
12. Cirrito JR, Deane R, Fagan AM, Spinner ML, Parsadanian M, Finn MB, *et al.* P-glycoprotein deficiency at the blood-brain barrier increases amyloid-beta deposition in an Alzheimer disease mouse model. J Clin Invest. 2005;115(11):3285–90.
13. Wang W, Bodles-Brakhop AM, Barger SW. A role for P-glycoprotein in clearance of Alzheimer amyloid beta-peptide from the brain. Curr Alzheimer Res. 2016;13(6):615–20.
14. Vogelgesang S, Cascorbi I, Schroeder E, Pahnke J, Kroemer HK, Siegmund W, *et al.* Deposition of Alzheimer's beta-amyloid is inversely correlated with P-glycoprotein expression in the brains of elderly non-demented humans. Pharmacogenetics. 2002;12(7):535–41.
15. Deo AK, Borson S, Link JM, Domino K, Eary JF, Ke B, *et al.* Activity of P-glycoprotein, a beta-Amyloid transporter at the blood-brain barrier, is compromised in patients with mild Alzheimer disease. J Nucl Med. 2014;55(7):1106–11.
16. Miller DS, Bauer B, Hartz AM. Modulation of P-glycoprotein at the blood-brain barrier: opportunities to improve central nervous system pharmacotherapy. Pharmacol Rev. 2008;60(2):196–209.
17. Abuznait AH, Kaddoumi A. Role of ABC transporters in the pathogenesis of Alzheimer's disease. ACS Chem Neurosci. 2012;3(11):820–31.
18. Song Y, Xue Y, Liu X, Wang P, Liu L. Effects of acute exposure to aluminum on blood-brain barrier and the protection of zinc. Neurosci Lett. 2008;445(1):42–6.
19. Hennig B, Wang Y, Ramasamy S, McClain CJ. Zinc deficiency alters barrier function of cultured porcine endothelial cells. J Nutr. 1992;122(6):1242–7.
20. Wang J, Chen J, Tang Z, Li Y, Hu L, Pan J. The effects of copper on brain microvascular endothelial cells and claudin via apoptosis and oxidative stress. Biol Trace Elem Res. 2016;174(1):132–41.
21. Li QF, Ding XQ, Kang YJ. Copper promotion of angiogenesis in isolated rat aortic ring: role of vascular endothelial growth factor. J Nutr Biochem. 2014;25(1):44–9.
22. Crouch PJ, Savva MS, Hung LW, Donnelly PS, Mot AI, Parker SJ, *et al.* The Alzheimer's therapeutic PBT2 promotes amyloid-beta degradation and GSK3 phosphorylation via a metal chaperone activity. J Neurochem. 2011;119(1):220–30.
23. Cherny RA, Atwood CS, Xilinas ME, Gray DN, Jones WD, McLean CA, *et al.* Treatment with a copper-zinc chelator markedly and rapidly inhibits beta-amyloid accumulation in Alzheimer's disease transgenic mice. Neuron. 2001;30(3):665–76.
24. McInerney MP, Pan Y, Short JL, Nicolazzo JA. Development and validation of an in-cell western for quantifying P-glycoprotein expression in human brain microvascular endothelial (hCMEC/D3) cells. J Pharm Sci. 2017;106(9):2614–24.
25. Fu D, Arias IM. Intracellular trafficking of P-glycoprotein. Int J Biochem Cell Biol. 2012;44(3):461–4.
26. Liebner S, Corada M, Bangsow T, Babbage J, Taddei A, Czupalla CJ, Reis M, Felici A, Wolburg H, Fruttiger M, Taketo MM, von Melchner H, Plate KH, Gerhardt H, Dejana E. Wnt/beta-catenin signaling controls development of the blood-brain barrier. J Cell Biol 2008;183(3):409–417.
27. Tran KA, Zhang X, Predescu D, Huang X, Machado RF, Gothert JR, *et al.* Endothelial beta-catenin signaling is required for maintaining adult blood-brain barrier integrity and central nervous system homeostasis. Circulation. 2016;133(2):177–86.
28. Zheng W, Monnot AD. Regulation of brain iron and copper homeostasis by brain barrier systems: implication in neurodegenerative diseases. Pharmacol Ther. 2012;133(2):177–88.
29. Clifford RJ, Maryon EB, Kaplan JH. Dynamic internalization and recycling of a metal ion transporter: Cu homeostasis and CTR1, the human Cu(+) uptake system. J Cell Sci. 2016;129(8):1711–21.
30. Tapiero H, Townsend DM, Tew KD. Trace elements in human physiology and pathology. Copper Biomed Pharmacother. 2003;57(9):386–98.
31. Adlard PA, Cherny RA, Finkelstein DI, Gautier E, Robb E, Cortes M, *et al.* Rapid restoration of cognition in Alzheimer's transgenic mice with 8-hydroxy quinoline analogs is associated with decreased interstitial Abeta. Neuron. 2008;59(1):43–55.
32. Hordyjewska A, Popiolek L, Kocot J. The many "faces" of copper in medicine and treatment. Biometals. 2014;27(4):611–21.
33. Shen DY, Zhang W, Zeng X, Liu CQ. Inhibition of Wnt/beta-catenin signaling downregulates P-glycoprotein and reverses multidrug resistance of cholangiocarcinoma. Cancer Sci. 2013;104(10):1303–8.
34. Lim JC, Kania KD, Wijesuriya H, Chawla S, Sethi JK, Pulaski L, *et al.* Activation of beta-catenin signalling by GSK-3 inhibition increases P-glycoprotein expression in brain endothelial cells. J Neurochem. 2008;106(4):1855–65.
35. Urbatsch IL, Gimi K, Wilke-Mounts S, Senior AE. Investigation of the role of glutamine-471 and glutamine-1114 in the two catalytic sites of P-glycoprotein. Biochemistry. 2000;39(39):11921–7.
36. Grossi C, Francese S, Casini A, Rosi MC, Luccarini I, Fiorentini A, *et al.* Clioquinol decreases amyloid-beta burden and reduces working memory impairment in a transgenic mouse model of Alzheimer's disease. J Alzheimers Dis. 2009;17(2):423–40.